National Library of Canada
Bibliotheque nationale du Canada

Canadian Theses Service
Service des thèses canadiennes

Ottawa, Canada
K1A 0N4

NOTICE

The quality of this microform is heavily dependent upon the quality of the original thesis submitted for microfilming. Every effort has been made to ensure the highest quality of reproduction possible.

If pages are missing, contact the university which granted the degree.

Some pages may have indistinct print especially if the original pages were typed with a poor typewriter ribbon or if the university sent us an inferior photocopy.

Reproduction in full or in part of this microform is governed by the Canadian Copyright Act, R.S.C. 1970, c. C-30, and subsequent amendments.

AVIS

La qualité de cette microforme dépend grandement de la qualité de la thèse soumise au microfilmage. Nous avons tout fait pour assurer une qualité supérieure de reproduction.

S'il manque des pages, veuillez communiquer avec l'université qui a conféré le grade.

La qualité d'impression de certaines pages peut laisser à désirer, surtout si les pages originales ont été dactylographiées à l'aide d'un ruban usé ou si l'université nous a fait parvenir une photocopie de qualité inférieure.

La reproduction, même partielle, de cette microforme est soumise à la Loi canadienne sur le droit d'auteur, SRC 1970, c. C-30, et ses amendements subséquents.

NL-339 (r. 88/04) c

Canada

THE ROLE OF STRUCTURAL FORCES IN MEMBRANE TRANSPORT : CELLULOSE MEMBRANES

By
André Y. Tremblay

A THESIS PRESENTED TO THE UNIVERSITY OF OTTAWA
IN PARTIAL FULFILLMENT OF THE
THE REQUIREMENTS FOR THE DEGREE OF
DOCTOR OF PHILOSOPHY

© André-Yves Tremblay, Ottawa, Canada, 1989

National Library of Canada
Bibliothèque nationale du Canada

Canadian Theses Service
Service des thèses canadiennes

Ottawa, Canada
K1A 0N4

The author has granted an irrevocable non-exclusive licence allowing the National Library of Canada to reproduce, loan, distribute or sell copies of his/her thesis by any means and in any form or format, making this thesis available to interested persons.

The author retains ownership of the copyright in his/her thesis. Neither the thesis nor substantial extracts from it may be printed or otherwise reproduced without his/her permission.

L'auteur a accordé une licence irrévocable et non exclusive permettant à la Bibliothèque nationale du Canada de reproduire, prêter, distribuer ou vendre des copies de sa thèse de quelque manière et sous quelque forme que ce soit pour mettre des exemplaires de cette thèse à la disposition des personnes intéressées.

L'auteur conserve la propriété du droit d'auteur qui protège sa thèse. Ni la thèse ni des extraits substantiels de celle-ci ne doivent être imprimés ou autrement reproduits sans son autorisation.

ISBN 0-315-59990-1

Canada

UNIVERSITÉ D'OTTAWA
UNIVERSITY OF OTTAWA

© Copyright 1989
by
André Y. Trembiay

Abstract

The phenomena governing Transition RO/UF (nanofiltration) membrane transport have been critically studied. The residuals and predicted pore sizes of 965 individual permeation runs performed on 70 cellulose membranes were used to discriminate between several restricted transport models and various solute-solvent-membrane material interactions.

Solute-membrane interactions were found to be mediated by the presence of structured solvent at the surface of the membrane. Two new interaction parameters, Ψ_{DP} and κ' describing structural solvent forces at the surface of a membrane have been quantified. For solvent mediated interactions, the potential energy of a solute molecule $\phi'_{DP}(\underline{d})$ at a distance $\underline{d}$ from the membrane surface can be obtained by combining Ψ_{DP} and κ' and the Stokes-Einstein radius a_s of the solute as follows;

$$\phi'_{DP}(\underline{d}) = -\Psi_{DP}\, a_s\, e^{-\kappa'(\underline{d}-a_s)}$$

A method to evaluate Ψ_{DP} from simple permeation experiments and κ' from direct force measurements is given. This approach permits the decoupling of solute size and solute-membrane material interactions in predicting separation. The inverse of κ' was found to be approximately equal to the diameter of a solvent molecule.

A linear correlation was obtained between the square root of Ψ_{DP} and the solubility parameter δ_{SP} for all solutes tested in this work. The slope of this correlation reflects the ability of the membrane material to structure water dipoles at a solid-liquid interface. The ordinate's intercept of this correlation was equal to the solubility parameter of the solvent which implies that steric solute interactions ($\Psi_{DP} \rightarrow 0$) occur when δ_{SP} of the solute approaches that of the solvent. The results of this study indicate that a solute molecule can penetrate hydrated layers of solvent at

the surface of a material to different extents depending on its size and solvent compatibility. These findings are assumed to be applicable to reverse osmosis transport and indicate that if a membrane material is to be used in RO it must be capable of structuring solvent molecules at its surface.

Several parametric studies were performed using the surface force pore flow (SFPF) model to determine the exact shape of the velocity profile in the membrane pore under conditions of solute adsorption and rejection. These studies were performed at various feed concentrations and values of λ for polyethylene glycol, of molecular weight 1000, and casein.

The shape of the solute separation vs. solute radius curve was studied parametrically as a function of pressure for four restricted transport models. The shape of this curve was also determined, using a radially dependent pore model (RDPM), for adsorptive and repulsive van der Waals interactions, electrical double layer (DLVO) interactions, increased viscosity in the membrane pore and effects of chain permeability and the shape of the interacting surface.

Morphological reasons are given for the general inability to reduce the pore radius of cellulose membranes below 1.5 nm. Viscometric measurements performed on cellulose casting solutions indicate that the dissolved elements of the solution exist as rigid, rod-like structures. It is proposed, that the pore size of cellulose membranes be limited by the regular occurrence of indentations on the protofibril surface and by stacking limitations, enhanced by the geometry of the protofibrils. This interpretation is conform with the folded ribbon model of a cellulose protofibril described in the literature.

A mes parents et Marlene

Acknowledgements

I am indebted to the Division of Chemistry of the National Research Council of Canada for the stimulating research environment and excellent facilities it has provided throughout these years. My most sincere words of appreciation to Dr. C.E. Capes of the NRC for supporting this project.

Many thanks to my advisors Drs. S. Sourirajan and F.D.F. Talbot for providing me with the right amount of guidance and independence to produce a very personal piece of work. Particular appreciation is expressed to Dr. T. Matsuura for many helpful discussions and his careful review of the manuscript. I would like to acknowledge the assistance of Drs. J. Murray and J. Roovers.

Special thanks to my colleagues in the Chemical Engineering Section of the NRC whose help and friendship greatly contributed to this work.

Finally, I wish to thank my friends for their understanding and encouragement.

Nomenclature

Descriptors

A	Solute
B	Solvent
M	Membrane material
1	Bulk feed solution, see Figure 0.1
2	Boundary layer, see Figure 0.1
3	Bulk permeate solution, see Figure 0.1

Alphabetic

a_s	Stokes Einstein radius (nm)
A_0, A_1	Constants defined by Equation 2.56
A_{AM}	Hamaker constant (J)
$\underline{B}$	van der Waals interaction constant in the SFPF model (m^3)
$b(r)$	Friction function in the SFPF and MD-SFPF models (dim)
C_{Ai}	Concentration of solute in; $i = 1$ Bulk solution, $i = 2$ Boundary Layer (Pore entrance), $i = 3$ Permeate, see Figure 0.1 (mol/m^3)
C'_{A3}	Concentration at the pore outlet for a given pore radius R, see Figure 0.1 (mol/m^3)
$c_A(r,z)$	Concentration of solute at position (r,z) in the pore (mol/m^3)
$C_A(\rho)$	Solute concentration at the pore outlet = $c_{A3}(\rho)/C_{A2}$ (dim)
c°_A	Bulk solute concentration (mol/m^3)
$\underline{C}$	Lennard-Jones interaction constant (m^{12})

d	distance separating two surfaces, see Figure 0.2 (m, nm)
$\underline{d}$	distance from the center of a molecule to the membrane surface, see Figure 0.2 (m, nm)
$D_\infty = D_{AB}$	Bulk solution diffusion coefficient (m^2/sec)
e	Protonic charge (C)
e_i	Residual of the solute separation = $f_{\text{exptl}} - f_{\text{calc}}$
ΔE	Heat of vaporization (J mol^{-1})
f	Observed separation based on the bulk solution conc. (dim)
f'	True solute separation based on the boundary layer conc. (dim)
$f_{\text{calc}}(R)$	Calculated separation for a given pore radius (dim)
f_{exptl}	Experimental separation (dim or %)
f_∞	Molecular friction coefficient (N·sec/m)
F_A	Driving force of solute A due to the chemical potential gradient (N)
F_{AB}	Friction force between solute A and solvent B (N)
F_{AM}	Friction force between solute A and the membrane surface (N)
$G(\lambda,\rho)$	Lag coefficient (dim)
$\overline{G}$	Center-line approximation for $G(\lambda,\rho)$ (dim)
ΔH_{MIX}	Ethalpy of mixing (J mol^{-1})
$J_A(r) = N_A(r)$	Molar flux of solute, (mol/m^2 o sec)
K'_A	Partition coefficient between the interfacial solution and the bulk solution (dim)
$K(\lambda,\rho)$	Enhanced friction (dim)
$\overline{K}^{-1}$	Center-line approximation for $K^{-1}(\lambda,\rho)$ (dim)
k	Boltzmann constant (J/K)
$\langle N_i \rangle$	Radially averaged molar flux of component i, (mol/m^2)
P, P_g	Operating or gauge pressure for atmospheric permeate discharge (kPa, Pa, atm)
P_i	Pore inlet pressure (kPa, Pa, atm)
P_o	Pore outlet pressure (kPa, Pa, atm)
ΔP	Effective trans-membrane pressure (kPa)
Pe	Pore Peclet number = $\chi\langle V\rangle\delta/\zeta D_\infty$ (dim)
Q_B	Average Pore flowrate (m^3/sec)

R_{avg}	Average pore size (m, nm)
R_{well}	Radius of confinement of solute molecules (m, nm)
$\overline{R}_a$	Geometric mean pore size (m, nm)
R	Effective or hydrodynamic membrane pore radius (nm).
$\underline{R}$	Gas constant (J/mol K).
r	Radial distance (nm)
SS_{Resid}	Sum of squares of the residuals
t_{ads}	Thickness of an adsorbed solvent layer containing pure solvent (nm)
t_i	Interfacial water thickness (nm)
$u_A = U_A$	Solute velocity with respect to the pore wall (m/sec)
$u_{Aw}(R)$	Solute velocity at the pore wall (m/sec)
$V = u_B$	Fluid velocity inside the pore (m/sec)
V'_A, V'_B	Molar volume of the component in solution (m^3 mol^{-1})
$\langle V \rangle$	Average fluid velocity inside the pore (m/sec)
x'	Dimensionless distance away from the membrane surface defined by Equation 2.52
$Y(R)$	Pore size distribution function
z	Axial distance from the pore inlet, in cylindrical coordinate (nm)

Greek Letters

$\alpha(\rho)$	Fluid velocity in the pore, SFPF and MD-SFPF models $= u_B(r)\delta/D_{AB}$ (dim)
$\alpha'(\rho)$	Fluid velocity in the pore, RDPM model $= Gu_B(r)\delta/K_{-1}D_{AB}$ (dim)
α''	Reciprocal of the coil permeability
$\beta_1(\rho)$	Solution viscosity $= \eta/\chi_{AB}R^2C_{A2}$ (dim)
$\beta_2(\rho)$	Operating pressure $= (P_i - P_o)/\underline{R}TC_{A2}$ (dim)
η	Solution viscosity (kg $m^{-1}sec^{-1}$)
η_0	Solution viscosity at zero shear rate (kg $m^{-1}sec^{-1}$)
δ	Pore length (nm)

$\varphi(\lambda)$	Rejection coefficient = $C'_{A3}(R)/C_{A2}$ (dim)
Φ_M	Electrostatic potential of the membrane surface (Volts)
Φ_A	Electrostatic potential of the solute (Volts)
γ	Surface tension (N/m)
χ	Lag coefficient (dim)
$\chi_{AM}(r)$	Proportionality constant defined by Equation A.21 (J·sec/m^2·mol)
$\chi_{AB}(r)$	Proportionality constant defined by Equation A.25 (J·sec/m^2·mol)
ϵ	Dielectric constant (dim)
κ	Reciprocal Debye length given by Equation 2.55 (nm^{-1})
κ'	Reciprocal decay period of the structural solvent force (nm^{-1})
λ	Ratio of the solute radius to the pore radius = a_s/R (dim)
μ	Chemical potential (J/mol)
μ°	Chemical potential at a reference concentration (J/mol)
π	Osmotic pressure (kPa, Pa)
θ	Wetting angle (degree)
ρ	Radial distance = r/R (dim)
σ	Mean deviation of the log-normal pore size distribution
ϕ_A, ϕ_B	Volume fraction of the component in solution
$\phi(\rho)$	Potential function at a distance (1-ρ) from the pore wall = $\phi'(r)/\underline{RT}$ (dim)
$\phi'(r)$	Potential function for a force interacting with the solute at a distance (R-r) from the pore wall (J/mol).
ξ	Enhanced friction (dim)
Ψ_{DLVO}	Potential constant in the double layer (DLVO) interaction defined in Equation 2.54
Ψ_{DP}	Potential constant in the dipole (DP) interaction defined in Equation 2.57

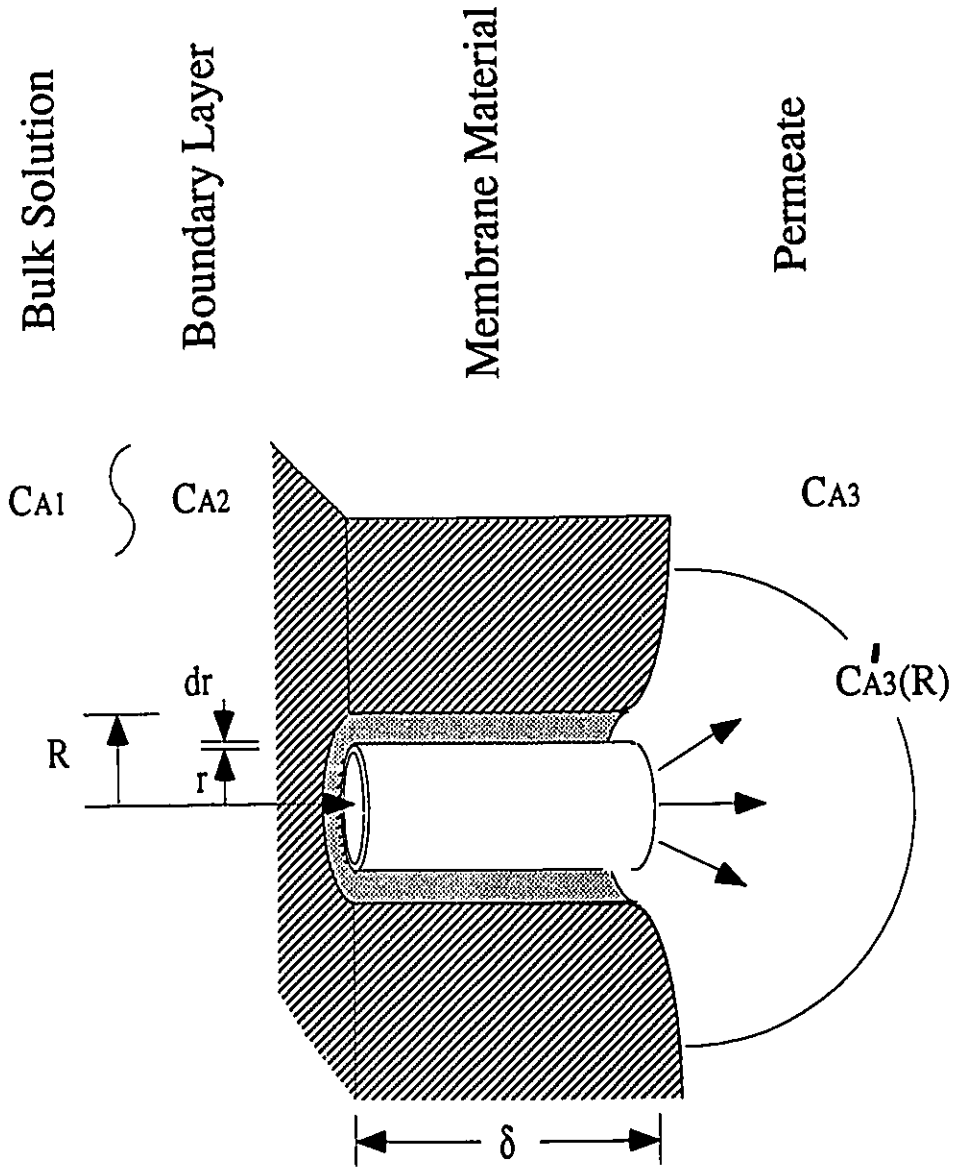

Figure 0.1: Pore through the selective layer of a membrane.

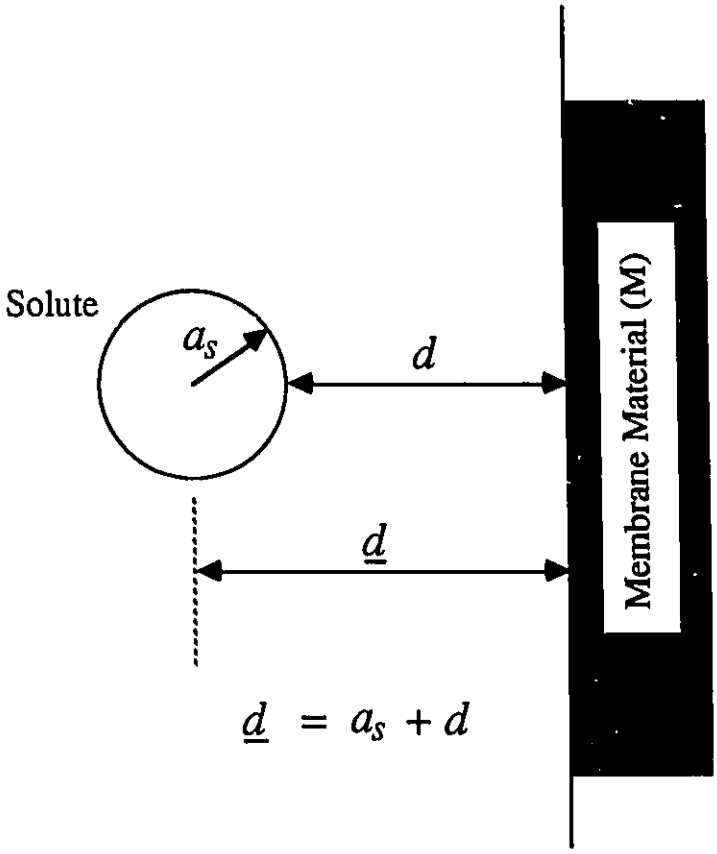

Figure 0.2: Definition of d and $\underline{d}$.

Contents

List of Figures

List of Tables

Chapter 1

Introduction

Synthetic membrane separations constitute an expanding market which is expected to grow well into the 21^{st} century. New applications are emerging as the awareness of this technology increases and as novel materials become available.

The areas of pervaporation and non-aqueous separations lack selective membranes which can resist solvent degradation. Most reverse osmosis (RO) and ultrafiltration (UF) membranes are made from polymers which swell and/or dissolve in the presence of organic liquids. Materials which offer stability to organics lack the proper surface characteristics in order to be selective towards one or several solution components. Inorganic membrane materials offer a substantial resistance to solvent degradation but have lower permeabilities and a higher cost per unit area compared to polymeric membranes of equivalent pore size.

Cellulose remains in a class of its own as a potential RO membrane material. It is highly stable in organic media and extremely hydrophilic offering a potential selectivity and a resistance to fouling unequalled by many presently available polymers. The hydrophilic properties of cellulose make it ideal for the separation and fractionation of materials in biotechnology where membranes having controlled pore sizes and very narrow pore size distributions are needed to perform the difficult downstream processing of solutions containing proteins, sugars, amino acids, or low molecular weight components of nucleic acids. The hydrophilicity of cellulose reduces membrane fouling which is a serious problem encountered in using this separation process in biotechnology.

The separation of aqueous ethanol solutions and organic liquids by RO holds great promise as an alternative to higher energy consuming separation processes such as distillation. Ethanol for example, produced by fermentation, is usually dehydrated by distillation, an inefficient process which consumes the energy equivalent to a large fraction of the product ethanol [1,2].

The main conclusions of a study performed by the Bend Research Group [1] on the feasibility of a countercurrent RO separation process as applied to the separation of ethanol and water are the need for membranes having higher ethanol-water selectivities and a greater structural resistance to ethanol solutions. State of the art RO membranes used in desalination exhibit decreasing ethanol-water selectivities with increasing ethanol concentration in the feed stream. These membranes are non selective towards either component at ethanol concentrations of 50 to 60 vol. % [1].

Matsuura et al. [3] have shown that cellulose is a very promising membrane material for the separation of aqueous ethanol solutions. In the case of a cellulose membrane, it was predicted from Gas Chromatography (GC) measurements that an average pore diameter of 1.51 nm is needed to obtain 90% ethanol separation from a 10 wt.% ethanol solution, while average pore diameters of less than 0.95 nm are needed for all other commercially available membrane materials [3].

The main problem in using cellulose as a membrane material is the general inability to obtain a suitable porous morphology with an average pore radius equal to or less than 1.5 nm. One of the objectives of this work is to reduce the pore size of cellulose membranes, and if this should prove impossible, explain why the 1.5 nm limitation exists. A novel solvent system for cellulose will be used to produce a variety of cellulose membranes and several post treatments will be performed to reduce the pore size of these membranes.

Understanding the mechanism of RO and UF membrane transport is very important to select the best materials in order to produce membranes with increased selectivities and permeabilities. This knowledge is vital if the field of membrane technology is to become competitive with existing unit operations such as distillation, solvent exchange, cryogenic separations and centrifugation, to name a few processes which are in turn being optimized in the face of competing technologies.

To this day the phenomena governing RO transport in aqueous systems remains the subject of much controversy. Soltanieh and Gill [4] have clearly demonstrated that models which have a linear dependence on driving forces (pressure and concentration), such as the solution-diffusion model, can describe solvent transport through RO membranes but fail to describe solute transport. They have quantitatively shown that solute flux is not linearly dependent on these driving forces and that convective flow has a significant effect on solute transport. The result of their analysis is that pore flow contributions cannot be neglected in RO transport [4].

The fact that independently measured diffusion coefficients for a given membrane material are an order of magnitude lower than those measured in RO experiments [4], casts a serious doubt on the use of a purely diffusive model to explain RO transport. The solution-diffusion-imperfection model was developed to account for this discrepancy [5]. In this model, imperfections in the selective layer of the membrane are used to account for convective flow contributions to solute transport. From a rigorous modelling point of view this involves a substantial change to the initial model brought about by a lack of fit to experimental data. Performing such an activity without a general look at other possible models is not a proper fitting procedure.

The Preferential Sorption-Capillary Flow model proposed by Sourirajan [6] and the Surface Force-Pore Flow (SFPF) model of Matsuura [7] both consider that solute and solvent transport are partially governed by surface phenomena and fluid transport under pressure through capillary pores. In these models, it is proposed that solute is rejected in the vicinity of the membrane material producing an enriched layer of solvent at the solution-membrane interface. Separation can occur if the pore radii of the membrane are equal to or less than the thickness of the solvent enriched layer. In such a case, membrane pores are filled with solvent which preferentially permeates through the membrane. These models predict that RO transport can be easily explained as a consequence of reducing the porosity of UF membranes. This is a particularly interesting concept since cellulose acetate RO membranes are made by heat treating or shrinking UF membranes to reduce their pore size [6].

The nature of the solute-membrane interactions and shape of the concentration profile must be determined if such models are to be used to describe solute transport through the small pores of RO membranes. The shape of this profile will depend on the type of solute-solvent-membrane interaction occuring at the surface of the

membrane material.

High Performance Liquid Chromatography (HPLC) has been used to evaluate the magnitude of surface interactions [7]. This bulk measurement method cannot discriminate between the types of possible interactions since it does not provide distance or position related information with respect to a surface. Membrane permeation data contains this positional information but the results are confounded with the unknown value of the membrane pore size. Attempts will be made to determine the nature and quantify the magnitude of these interaction forces by performing experiments with a polydisperse solute containing molecules of various sizes. Such experiments can provide information on the pore size of the membrane. In this analysis, a certain type of interaction is assumed and the concentration profile inside a membrane pore incorporated into a prospective radially dependent pore model. These assumptions can then be verified by fitting the transport model to membrane permeation data.

Reverse osmosis membranes cannot be used for this type of study since most polydisperse solutes used in membrane characterization are rejected at levels of 90% or more by these membranes. This limits experimental accuracy to 5 discrete intervals of 2% (based on a separation accuracy of $\pm 1\%$) which is clearly insufficient to perform model discrimination. Membranes having pore sizes in the "Transition" region between RO and UF have the sieving characteristics of UF membranes and some of the interfacial interaction properties of RO membranes. The lower limit of porosity of 1.5 nm for cellulose membranes falls in this Transition RO/UF range and is ideally suited to study the nature and extent of the surface interactions which determine RO transport.

The presence of solvent at the surface of the membrane plays an important role in the transport of solute through the small pores of RO membranes but plays a minor role in the transport of solute through UF membranes. This behavior is illustrated in Figure 1.1 where it is easily seen that variations in the pore size of a membrane affects the type of mechanisms whose contribution dominates solute transport through the membrane.

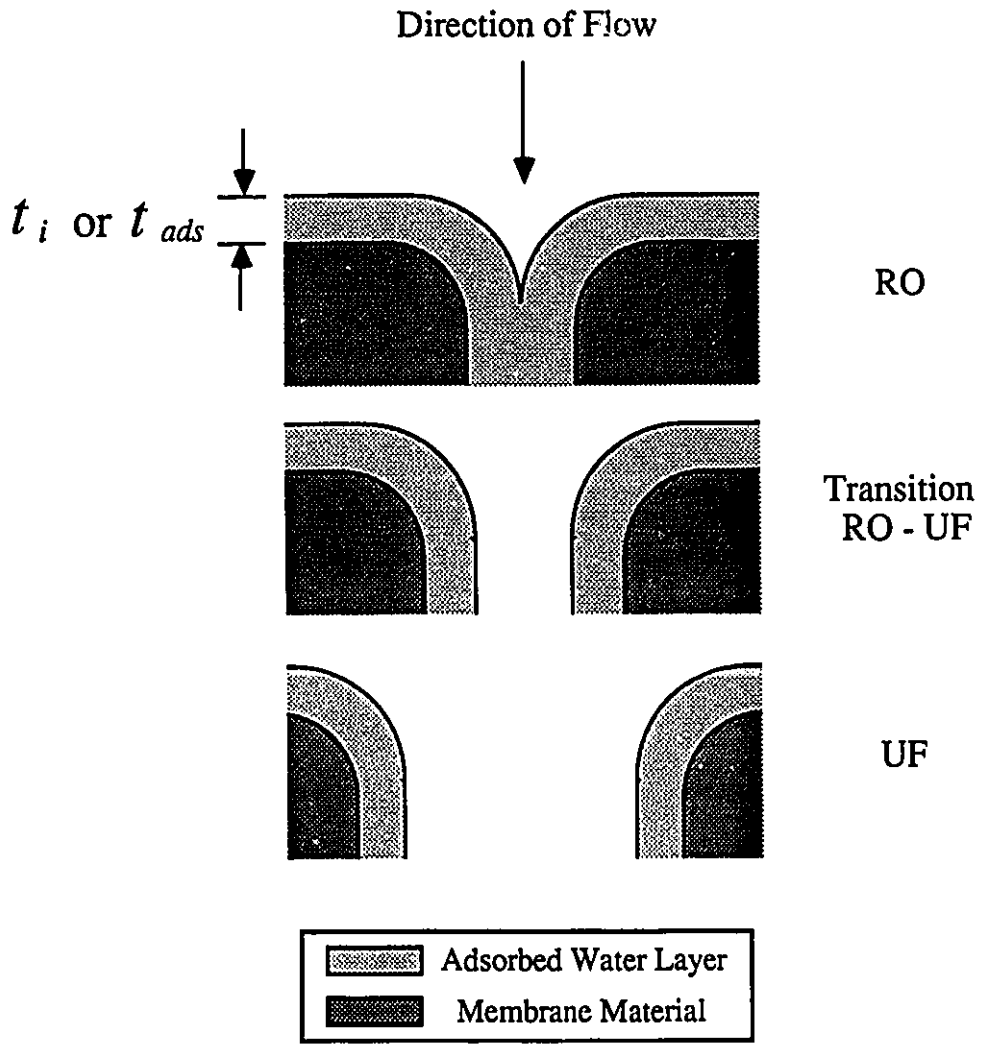

Figure 1.1: Preferential sorption of solvent for RO, Transition, and UF membranes, based on the value of t_i = 1.17 nm for water-cellulose as determined by gas chromatography [7].

Attempts will be made to demonstrate that interfacial molecular interactions cannot be ignored in explaining solute transport in this range of pore sizes and that a sufficiently large number of observations can be used to discriminate between the possible interactions occurring at the membrane surface. This study will also show that models describing the restricted flow of solutes through molecular sized pores can be used to quantitatively evaluate the pore size of Transition RO/UF and UF membranes.

The objectives of this research are as follows:

1. Determine the nature and quantify surface interactions at a membrane interface for pore sizes slightly larger than those found in RO membranes.

2. Compare different restricted transport models used in membrane characterization.

3. Study membranes cast from a novel solvent for cellulose.

4. Attempt to reduce the pore size of cellulose membranes.

5. Demonstrate the feasibility and use of automation in membrane characterization.

6. Attempt to explain why a lower limit of pore size exists for cellulose membranes.

Models proposed by physiologists for the restricted transport of solutes through pores of similar dimension as those of the solute molecules will be discussed and compared to current membrane transport models. Difficulties encountered with the convergence of these models and limitations in the predictions will also be discussed.

The automated testing equipment developed in the course of this work is tailor made for membrane characterization and is an important feature in the routine evaluation of membrane pore size. Although the only type of membrane material used in this work is cellulose, the characterization methods and automation procedures developed in this study are applicable to other membrane materials and systems.

This work is a contribution in the three areas of membrane characterization, the study of cellulose membrane morphology and the use of robotics in membrane testing. These three unrelated topics are discussed sequentially and as independent parts in the text, this format might be disputable but is a direct consequence of the multidisciplinary nature of this field.

Chapter 2

Fundamentals of Membrane Characterization

Membrane porosity and solute-membrane surface interactions are major factors affecting the performance of pressure driven membrane separation processes. These characteristics determine whether a membrane can separate salt from water (RO), dialyze a salt and protein mixture (UF) or fractionate low molecular weight organics (Transition RO/UF[1]). Typical RO membranes can separate sodium chloride from water and have pore radii below 1.5 nm. Transition membranes have pores between 1.5 and 2.5 nm and can separate molecules in the 500 to 10,000 molecular weight range. UF membranes are commonly used to separate larger molecules such as proteins and macromolecules and have pore sizes ranging from 2.5 to 20.0 nm.

The lack of good testing standards and the time consuming nature of membrane characterization experiments have led to the general omission of pore size measurements from the synthetic membrane literature. The routine evaluation and reporting of membrane pore sizes and solute-membrane surface interactions would increase the understanding of membrane separation processes and ultimately help in the design and selection of better membrane materials to answer the challenging separations which face this process.

[1]Transition membranes are also termed nanofiltration membranes. This designation refers to the pore size of the membrane and is somewhat confusing since RO and UF membranes have pores in the nanometer range. The term "Transition RO/UF" membrane, used in this work, is a more accurate, but less popular, description of a membrane which exhibits the characteristics of both RO and UF membranes.

The purpose of this chapter is to present and compare several methods used in evaluating the pore size of synthetic membranes. Some historical notes and a brief discussion of various membrane characterization techniques have been included. Four restricted transport models describing solute separation as a function of pore radius are summarized in this section with detailed derivations given in Appendix A. Simplified equations describing the two limiting cases of diffusive and convective flow are derived for all models.

The first restricted transport model is a simple radially averaged pore model (RAPM) proposed by physiologists such as Pappenheimer *et al.* [8], Renkin [9], Verniory *et al.* [10,11] and Anderson *et al.* [12]. The second model is the radially dependent Surface Force Pore Flow approach of Matsuura and Sourirajan (SFPF) [7]. The third model is a modified version of the SFPF model (MD-SFPF), it is similar to the SFPF model but uses the same boundary condition at the pore exit as the RAPM model [13]. The fourth and final model is based on the radially dependent approach of the SFPF models but uses the basic hydrodynamic considerations advanced in the RAPM model and is termed Radially Dependent Pore Model (RDPM).

Several possible solute-membrane and solvent-membrane interactions such as van der Waals forces, electrical double layer, and hydration, or structural forces have been quantified for use with the radially dependent models. Other possible effects such as solute chain permeability, increased viscosity within the pore, central confinement of solute molecules, and the presence of a distribution of pore sizes in the selective layer of the membrane were all studied and quantified with respect to these transport models. The equations describing solute separation for all four models, in convective and diffusive flow, have been summarized in Table 2.1

The significance of these fundamental derivations on solute separations will be studied parametrically in this Chapter. These models will be used to determine the pore size of the cellulose membranes produced in this work and the nature and significance of solute-membrane and solute-solvent-membrane interactions for the polyethylene glycol (PEG)-water-cellulose system used in this study.

2.1 Review of Characterization Methods

Early qualitative studies on membrane transport by Dutrochet (1826), Brücke (1840) and Fick (1855) [14,15,16] were centered on explaining the phenomenon of osmosis. These workers did not attempt to evaluate the pore size of the membranes used in their studies. It was only in the later half of the 19^{th} century that quantitative studies on the pore size of natural and synthetic membranes were initiated.

Guérout and Becquerel (1872) [17] determined the pore size of natural and synthetic UF membranes by combining measurements of their thickness, void fraction, and pure water flux at a given pressure. Membrane pores were modeled as an array of capillaries running perpendicular to the surface of the membrane. The pore sizes obtained in their work, were within an order of magnitude of presently accepted values. Eighty two years later, Renkin reported that this purely hydraulic method tends to underpredict the actual pore size of a membrane by a factor of 1/2 [9].

Unfortunately, this simple method can only be applied to homogeneous membranes which have a constant porosity throughout the thickness of the membrane. Most commercial synthetic membranes are asymmetric in nature, where a dense selective layer, 0.02 to 0.5 μm thick, covers a more porous support layer having a thickness of 10 to 30 μm. The average pore size of the selective layer can be up to two orders of magnitude smaller than that of the support layer.

In a second characterization method, a wet membrane is subjected to pressurized air, the pressure at which small bubbles start to appear at the surface of the membrane is used to calculate the pore size of the membrane. This procedure was first suggested by Barus (1894) who noticed in one of his meteorological experiments that extremely large pressures were needed to pass air through a porcelain septum submerged in water [18]. For a wet membrane, the minimum pore radius R which allows the permeation of air at a pressure P was determined by Barus using the following equation,

$$R = 2\gamma \cos\theta / P, \tag{2.1}$$

where γ is the surface tension and θ the wetting angle of the fluid inside the pore.

From Equation 2.1; for water with $\theta = 0$ and the pore radii expected in this work (1.0 nm to 3.0 nm), pressures of 14.38 and 4.79 MPa (1420 and 473 atm) are needed for gas permeation. A porous cellulose structure would collapse at such pressures and the pore size of the membrane would eventually be altered under the test conditions. This method is often used to characterize microfiltration (MF) membranes which have pores in the μm range. Typical air pressures of 0.1 and 1 MPa (1 and 10 atm) are used to characterize such membranes.

The first systematic and quantitative study on the pore size of UF membranes was performed by Bechhold in 1906 [19,20,21]. He characterized a series of graded UF membranes by the pure water permeation and bubble point methods. Bechhold coined the word ultrafiltration and was the first to point out the role of adsorption in membrane separation [22].

Membrane characterization using solutes of different sizes was first performed by Manegold (1927) [23] and later by Ferry (1936) [24]. Ferry used simple geometric arguments to describe the restricted transport of solutes through membrane pores. He then calculated a sieving constant and a pore size for several synthetic and natural membranes.

The direct measurement of large pore UF membranes became possible with developments in electron microscopy. Unfortunately, to this day, methods such as Scanning Electron Micrography (SEM) and Transmission Electron Micrography (TEM) are of limited use in the routine evaluation of pore sizes. The resolution of these micrographic methods depends on the wavelength of the electron beam used in the technique where high beam intensities are needed in order to increase resolution. Most polymers used as membrane materials are destroyed by the intensity of this electron beam at resolutions of 5.0 nm or less.

In the SEM technique, this material degradation problem is solved by making a carbon or gold replica of the surface of a fractured sample [25]. This replica or imprint of the surface can then be observed at high beam intensities. This imaging technique is limited to the two dimensional observation of the surface of a fractured sample and cannot provide an in depth evaluation of pore radius for three dimensional porous media.

In the TEM technique the electron beam must pass through the sample causing severe material degradation. Since three dimensional replicas of a membrane material are impossible to produce, it can be concluded that due to material degradation problems, electron micrography techniques can only be used for membranes having very large pores typically greater than those found in UF membranes and for inorganic membranes which have a greater resistance to degradation than their polymeric equivalents. A considerable amount of pore shrinkage can also occur during the freeze drying procedure used in preparing the sample, which imposes a further limitation on these techniques.

Velicangil *et al.* [26] have determined that membrane pore radii obtained from electron microscope measurements are overestimated by a factor of 3, compared to those obtained from hydrodynamic methods. This suggests that the pore radius observed by solute permeation is the actual hydraulic radius which results from the combined hydration of the membrane and the shear forces acting on the solvent in the pore. This would indicate that an *in situ* pore measurement obtained from a hydrodynamic method would be a more useful tool to predict membrane performance.

Gas adsorption-desorption methods such as B.E.T. are of limited use due to the asymmetric nature of the membrane and the possible shrinkage of the porous network during sample preparation as in the SEM and TEM methods.

A qualitative estimate of pore size can be obtained from Molecular Weight Cut-Off measurements. This value represents the lowest molecular weight which exhibits 90% rejection by the membrane. This single measurement is difficult to use since it depends on the nature and magnitude of solute-membrane interactions. A considerable amount of frustration can be experienced in selecting commercial membranes based on molecular weight cut-off values. Membrane manufacturers perform these measurements with proteins and dextrans which have different interactions with the membrane material. The measurements are also performed at different concentrations and under different conditions of mass transfer in the boundary layer at the surface of the membrane. Separations for solutes other than those tested are often difficult to predict based on molecular weight cut-off measurements.

The pore size of a membrane can be determined by measuring the exclusion of solute molecules from membrane pores. This information can be related to the pore

radius of the membrane by a simple sieving model [27]. Such an approach does not account for solute-membrane interactions or the restricted transport of solutes in pores which have approximately the same dimension as those of the solute molecules. These models are limited in their ability to estimate the pore size of a membrane.

Some methods of characterization involve the permeation of a polydisperse solute of known molecular weight distribution through a membrane. The permeate is compared to the feed solution and the pore size of the membrane determined. This is a very rapid procedure since only one experiment is necessary to obtain the pore size of the membrane. However, some major problems exist in using this method to characterize membranes. Solute size, a_s, cannot be accurately determined since it must be measured by Size Exclusion Chromatography (SEC). This method relies on the porosity of chromatographic support to perform the separation of solute based on size. Unfortunately the affinity of a solute for the support material plays an important role in performing the separation. The columns are usually used with a universal calibration curve which does not account for interactions with the membrane material and provides a very rough idea of solute size which limits their use where information on the precise size of the solute is desired.

The shear dependent aggregation of solutes in SEC is different from that of a membrane. In SEC, transport in and out of a pore is strictly diffusion controlled whereas in the case of a membrane pore it is both convective and diffusive. The ability of an aggregate to withstand shear deformation will be different in both cases. The presence of high molecular weight fractions in the test mixture can affect the permeation characteristics of low molecular weight solutes. It would be difficult to account for such an effect.

SEC can only be used as a characterization method for solutions containing at least 1% solution. This is mainly due to limits in detection. At such a concentration, the effects of concentration polarization at the surface of the membrane cannot be neglected which involves the coupling of a second model defining the mass transfer at the membrane surface which adds a further complication since both models are now coupled. SEC has a reproducibility of 3 to 5% which is unsuitable as an analytical method in the determination of pore sizes. It is for these reasons that methods involving the permeation of solutions containing polydisperse probe solutes were not considered in this work.

From a transport point of view, the relevant pore size of a membrane is its hydrodynamic pore radius. This is the radius of a pore once the membrane is hydrated or swollen with solvent. Hydrodynamic characterization techniques provide an *in situ* method which is more useful and representative of membrane pores under normal operating conditions. In this method, dilute solutions of selected "probe" solutes are permeated through a membrane, the size of such solutes are chosen to be selectively rejected by the membrane. Ideally, "probe" solutes are chosen to be relatively neutral with respect to the membrane surface, *i.e.* they are not strongly rejected or adsorbed by the membrane material. In such cases solute-membrane interactions are purely steric and simple to model. In practice the distribution or concentration of solute molecules close to the surface of the membrane differs from that of the bulk solution. This effect can arise from solute-membrane interactions or solvent mediated interactions. In such cases, the accuracy of model predictions will depend on the decoupling of solute-membrane or solute-solvent-membrane interactions and pore size.

Most hydrodynamic methods are based on the restricted transport of solutes through pores whose radii are comparable to that of a solute molecule. The restricted transport of solutes through sub-micron sized pores has been studied for over 130 years. Fick commented on the restricted diffusion of solutes in dialysis experiments using colloidon (cellulose nitrate) membranes in 1855 [14]. Early work, on restricted transport, involved corrections to Stokes' Law in settling experiments where the particle diameters were comparable to that of the settling chamber [28,29,30]. Faxén (1922) derived a viscous drag factor from theoretical considerations for spherical particles confined to the central axis of a pore [31]. Based on geometrical arguments, Ferry obtained a rejection coefficient between the concentration inside a pore to that of the bulk solution [24].

Much of the current research on hindered transport stems from key papers by Pappenheimer, Renkin and Borrero (1951) [8], Pappenheimer (1953) [32] and Renkin (1954) [9] who introduced hydrodynamic terms to describe the restricted transport of a solute through pores of molecular dimension. A renewed interest in this area occurred in the early 1970's with the arrival of track-etched membranes [33]. Theories of restricted transport could be tested for the first time since these membranes were symmetric and had pores of known dimension with a narrow size distribution.

Several excellent reviews are available on the subject of restricted transport in membranes, such as Ferry's classic review [22], Solomon [34] on biological membranes, Bean [35], and recently Deen [36].

The dynamic viscosity of water between two molecularly smooth mica surfaces has been measured directly down to surface separations of 1.85 nm and found to be identical to that of bulk water $\eta = 0.98 \cdot 10^{-3}$ kg $\cdot$ m^{-1}sec^{-1} [37]. This implies that bulk solution measurements are valid down to pore radii of 0.93 nm. It is also calculated, by extrapolation, that the plane of slip lies within one molecular layer of the surface [37], which implies that for pure water permeation, Poiseuille flow can exist in very small pores of RO membranes.

Finally, by a simple process of elimination, the hydrodynamic methods which use "probe" solutes are the preferred tool to determine the pore size of membranes having pores smaller than those found in UF membranes. This characterization method was selected to determine the pore size of all membranes produced in this work and is described in greater detail in following sections.

2.2 Membrane Characterization using Probe Solutes

As discussed in the previous section, the pore size of a synthetic membrane can be determined by the selective permeation of dilute solutions containing "probe" solutes of known molecular size. In most characterization studies, the pore radius R and the radius of the "probe" solute a_s are of comparable magnitudes. The transport of solute molecules through the pore is restricted by the presence of the pore wall which causes an effect of retardation on solute permeation. This effect can be quantified by a suitable restricted transport model. This type of model is used to calculate a rejection coefficient between the solute concentration at the pore outlet $C'_{A3}(R)$ to that of the pore inlet C_{A2} expressed as a function of known bulk solution properties such as viscosity, density, osmotic pressure, along with the diffusivity and size of the "probe" solute. This ratio is then related to the true solute separation of a membrane, f', as follows,

$$f' = 1 - \frac{C'_{A3}(R)}{C_{A2}}. \tag{2.2}$$

For an iso-porous [2] membrane the concentration of solution at the exit of all membrane pores is identical to that of the permeate $C'_{A3}(R) = C_{A3}$, where C_{A3} is the observed permeate concentration for the entire membrane. If there exists a distribution in the size of the pores at the membrane surface then $C'_{A3}(R) \neq C_{A3}$ and $C'_{A3}(R)$ must be averaged over the entire distribution to predict the permeate concentration C_{A3}. The averaging procedure for a membrane having a distribution of pore sizes is described in Appendix A.

The effects of concentration polarization were neglected in this study (see Appendix B). In such cases, the bulk solution concentration C_{A1} is assumed equal to the concentration at the entrance of the pore, $C_{A1} \approx C_{A2}$.

For an iso-porous membrane, the observed separation f is defined as

$$f = 1 - \frac{C'_{A3}(R)}{C_{A1}} \tag{2.3}$$

and is approximately equal to the true separation of the membrane $f' \approx f$.

[2] Pores in the selective layer of the membrane have equal radii, R is constant.

The experimental separation f_{exptl} is determined by measuring the solute concentration in the the feed and permeate solutions and is calculated as follows,

$$f_{\text{exptl}} = 1 - \frac{\text{measured permeate conc.}}{\text{measured feed conc.}}. \tag{2.4}$$

In practice, several permeation experiments are performed using solutes of different sizes. The size of these solutes are selected to span the entire range of possible values for the observed separation (0-100%). The experimental separation for each probe solute (i) is determined using Equation 2.4, and the calculated or predicted separation $f_{\text{calc}}(R)$ for this solute is obtained from the restricted transport model. The parameters of the model, such as the pore radius R and various solute-membrane interactions, are obtained by minimizing the sum of squares of residuals defined as

$$\text{SS}_{\text{Resid}} = \sum_{i=1}^{n} (f_{\text{exptl}} - f_{\text{calc}})_i^2. \tag{2.5}$$

Since the separation of solute by a membrane has a limit of 100%, experimental plots of separation vs. solute radius appear to be nonlinear and a general, non derivative, optimization technique known as the Simplex method was used to minimize the sum of squares of residuals SS_{Resid}. This optimization technique was developed by Spendley *et al.* [38] and later by Nedler and Mead [39]. The simplex is a geometric figure consisting, in N dimensions, $N + 1$ points (or vertices) and all their interconnecting points where N is the number of unknowns. This figure can expand or contract to find the minimum value of the SS_{Resid}. The subroutine called AMOEBA found in Reference [40] was used in all optimizations performed in this work.

The mathematical expressions to evaluate $C'_{A3}(R)/C_{A2}$ and the assumptions involved in obtaining these equations are summarized in the next sections for four different restricted transport models. Detailed derivations of the RAPM, SFPF and MD-SFPF models have been included in Appendix A.

2.2.1 The simple case of a radially averaged pore model (RAPM)

In the radially averaged model proposed by Verniory *et al.* [10] and Anderson and Quinn [12], membrane pores are modeled as an array of capillaries running perpendicular to the surface of the membrane, only steric solute-membrane interactions are considered and the velocity profile in the pore is assumed to be parabolic. The fluid velocity V, inside a pore of radius R, at any dimensionless radial position $\rho = r/R$ is expressed as

$$V = 2\langle V\rangle(1-\rho^2). \tag{2.6}$$

A radially averaged rejection coefficient between the concentration at the pore outlet to that of the pore inlet is given by

$$\frac{C'_{A3}(R)}{C_{A2}} = \frac{\chi}{1-e^{-Pe}(1-\chi)}, \tag{2.7}$$

where,

$$Pe = \frac{\chi}{\xi D_\infty}\left[\frac{R^2\,\Delta P}{8\eta}\right]. \tag{2.8}$$

The boundary conditions for solute concentration $c_A(r,z)$ at the pore entrance $z=0$ and pore exit $z=\delta$ are given by

$$c_A(r,0) = C_{A2}, \tag{2.9}$$

$$c_A(r,\delta) = C'_{A3}(R). \tag{2.10}$$

The radially averaged "enhanced friction", ξ, represents the ratio of the pore friction coefficient to the bulk friction coefficient and the radially averaged "lag coefficient", χ, accounts for the retarding effect of the pore wall and they are expressed as functions of λ , the ratio of the solute radius a_s to the pore radius R, ($\lambda = a_s/R$). These values are determined from centerline approximations of the radially dependent values K^{-1} and G (see Appendix A) as follows,

$$\xi = \Phi(1 - 2.1044\lambda + 2.089\lambda^3 - 0.948\lambda^5), \tag{2.11}$$

$$\chi = \Phi(2-\Phi)(1 - 2/3\lambda^2 - 0.163\lambda^3), \tag{2.12}$$

$$\Phi = (1-\lambda)^2. \tag{2.13}$$

This model represents the simplest form of restricted transport for steric interactions and has been included in this discussion for comparison with other radially dependent models.

For large values of Pe (convective flow) Equation 2.7 becomes,

$$\frac{C'_{A3}(R)}{C_{A2}} = \chi. \tag{2.14}$$

For small values of Pe, (diffusive flow) Equation 2.7 becomes,

$$\frac{C'_{A3}(R)}{C_{A2}} = \frac{\xi(1+Pe)}{\xi+Pe}. \tag{2.15}$$

2.2.2 The surface force pore flow model (SFPF)

Introduced in the late 1970's, the SFPF model provides an added degree of flexibility in describing restricted transport through porous media. The broad lines of this model resemble those advanced in the finely porous model proposed by Merten [41]. The SFPF remains original in its approach since the exact shape of the velocity profile can be determined as a function of radial solution properties and solute-membrane interactions can be quantified using High Performance Liquid Chromatography (HPLC).

As in the RAPM, the membrane is modeled by an array of pores running perpendicular to the surface of the membrane. A radially dependent rejection coefficient is expressed as a ratio of the radial concentration at the pore outlet to that at the pore entrance,

$$\frac{c_{A3}(r)}{C_{A2}} = \frac{\exp\left[\frac{u_B(r)\delta}{D_{AB}}\right]}{1 + \frac{b(r)}{e^{-\phi'(r)/\underline{R}T}}\left(\exp\left[\frac{u_B(r)\delta}{D_{AB}}\right] - 1\right)}. \tag{2.16}$$

The boundary conditions for solute concentration $c_A(r,z)$ at the pore entrance $z = 0$ and pore exit $z = \delta$ are given by

$$c_A(r,0) = C_{A2}e^{-\phi'(r)/\underline{R}T}, \tag{2.17}$$

$$c_A(r,\delta) = c_{A3}(r)e^{-\phi'(r)/\underline{R}T}. \tag{2.18}$$

The overall concentration at the outlet of the pore is determined by taking the radial average of this concentration as follows,

$$C'_{A3}(R) = \frac{\int_0^R c_{A3}(r)u_B(r)rdr}{\int_0^R u_B(r)rdr}. \tag{2.19}$$

In dimensionless terms, Equation 2.16 becomes,

$$C_A(\rho) = \frac{c_{A3}(\rho)}{C_{A2}} = \frac{\exp(\alpha(\rho))}{1 + \frac{b(\rho)}{e^{-\phi(\rho)}}(\exp(\alpha(\rho)) - 1)}, \tag{2.20}$$

where $\rho = r/R$ and $\alpha = u_B(r)\delta/D_{AB}$.

The radially averaged value of the friction coefficient $b(\rho)$ is used in this model where $b(\lambda) = b(r)|_{r=0}$. The values of $b(\lambda)$ were determined by an empirical correlation based on the friction of solute molecules translating through a narrow pore and are defined by the following equations,

$$\mathrm{b}(\lambda) = \begin{cases} [1 - 2.104\lambda + 2.09\lambda^3 - 0.95\lambda^5]^{-1} & \text{when} \quad \lambda \leq 0.22, \\ [44.57 - 416.2\lambda + 934.9\lambda^2 + 302.4\lambda^3] & \text{when} \quad 1 > \lambda > 0.22. \end{cases} \tag{2.21}$$

The assumption of a parabolic velocity profile is not necessary in this approach and the exact velocity profile can be obtained by solving the following differential equation,

$$\frac{d^2\alpha(\rho)}{d\rho^2} + \frac{1}{\rho}\frac{d\alpha(\rho)}{d\rho} + \frac{\beta_2}{\beta_1} + \frac{1}{\beta_1}(1 - e^{-\phi(\rho)}) \quad (C_A(\rho) - 1) - \frac{(b(\rho) - 1)\alpha(\rho)C_A(\rho)}{\beta_1} = 0. \tag{2.22}$$

Once the exact velocity profile is determined, the concentration at the pore outlet is obtained by taking the radial average of $C_A(\rho)$ as follows,

$$\frac{C'_{A3}(R)}{C_{A2}} = \frac{\int_0^1 \left[\dfrac{e^{\alpha}}{1 + \frac{b(\lambda)}{e^{-\phi(\rho)}}(e^{\alpha} - 1)}\right] \alpha\rho d\rho}{\int_0^1 \alpha\rho d\rho}. \tag{2.23}$$

For large values of α (convective flow) Equation 2.23 becomes,

$$\frac{C'_{A3}(R)}{C_{A2}} = \frac{\int_0^1 \dfrac{e^{-\phi}}{b(\lambda)}\alpha\rho d\rho}{\int_0^1 \alpha\rho d\rho}. \tag{2.24}$$

For small values of α, (diffusive flow) Equation 2.23 becomes,

$$\frac{C'_{A3}(R)}{C_{A2}} = \frac{\int_0^1 \left[\dfrac{1 + \alpha}{1 + \frac{b(\lambda)}{e^{-\phi}}\alpha}\right] \alpha\rho d\rho}{\int_0^1 \alpha\rho d\rho}. \tag{2.25}$$

2.2.3 A modified version of the SFPF model, (MD-SFPF).

The SFPF model has recently been modified to account for inconsistencies in the choice of the boundary conditions at the entrance and exit of the pore [13]. However, the model obtained by Mehdizadeh and Dickson [13], for dilute solutions of non-electrolytes, is identical to that obtained by deriving the SFPF model with the boundary condition defined by Equation 2.27 (see Appendix A). The boundary condition selected in the MD-SFPF model is similar to that used in the derivation of the RAPM model. Accounting for solute-membrane interactions, Equations 2.9 and 2.10 become,

$$c_A(r,0) = C_{A2}e^{-\phi'(r)/\underline{R}T}, \tag{2.26}$$

$$c_A(r,\delta) = C'_{A3}(R)e^{-\phi'(r)/\underline{R}T}. \tag{2.27}$$

Deriving the expression $C'_{A3}(R)/C_{A2}$ for the MD-SFPF model and omitting the steps which led to Equation A.45, with the new boundary conditions, the analog of Equation A.45 is obtained,

$$\ln\left[\frac{C'_{A3}(R)e^{-\phi'(r)/\underline{R}T} - \dfrac{J_A(r)b(r)}{u_B(r)}}{C_{A2}e^{-\phi'(r)/\underline{R}T} - \dfrac{J_A(r)b(r)}{u_B(r)}}\right] = \frac{u_B(r)}{D_{AB}}\delta. \tag{2.28}$$

For reasons of clarity, substitute for the two dimensionless quantities, $\alpha(\rho) = u_B(r)\delta/D_{AB}$ and $\phi(\rho) = \phi'(r)/\underline{R}T$, Equation 2.28 becomes,

$$\left[C'_{A3}(R)e^{-\phi} - c_{A3}(r)b(r)\right] = \left[C_{A2}e^{-\phi} - c_{A3}(r)b(r)\right]\cdot e^{\alpha}. \tag{2.29}$$

Taking logarithms of both sides and rearranging,

$$\frac{c_{A3}(r)}{C_{A2}} = \frac{1}{b(r)\,(e^{\alpha}-1)}\left[e^{\alpha}e^{-\phi} - \frac{C'_{A3}(R)}{C_{A2}}e^{-\phi}\right]. \tag{2.30}$$

As in Equation 2.19 the concentration at the pore outlet can be determined by taking the radial average of $c_{A3}(r)$

$$C'_{A3}(R) = \frac{\int_0^R c_{A3}(r)u_B(r)rdr}{\int_0^R u_B(r)rdr}. \tag{2.19}$$

Substituting Equation 2.30 into Equation 2.19,

$$\frac{C'_{A3}(R)}{C_{A2}} = \frac{\int_0^1 \left[\frac{e^{-\phi}e^{\alpha} - \frac{C'_{A3}(R)}{C_{A2}}e^{-\phi}}{b(r)(e^{\alpha}-1)} \right] \alpha\rho d\rho}{\int_0^1 \alpha\rho d\rho}. \tag{2.31}$$

Equation 2.31 can be rearranged as follows,

$$\frac{C'_{A3}(R)}{C_{A2}} = \frac{\int_0^1 \frac{e^{-\phi}}{b(r)(1-e^{-\alpha})}\alpha\rho d\rho}{\int_0^1 \left[1 + \frac{e^{-\phi}}{b(r)(e^{\alpha}-1)} \right] \alpha\rho d\rho}. \tag{2.32}$$

Since the centerline approximations for $b(r)$ is available, $b(r) = b(\lambda)$, Equation 2.32 becomes,

$$\frac{C'_{A3}(R)}{C_{A2}} = \frac{\int_0^1 \frac{e^{-\phi}}{b(\lambda)(1-e^{-\alpha})}\alpha\rho d\rho}{\int_0^1 \left[1 + \frac{e^{-\phi}}{b(\lambda)(e^{\alpha}-1)} \right] \alpha\rho d\rho}. \tag{2.33}$$

For large values of α (convective flow) Equation 2.33 becomes,

$$\frac{C'_{A3}(R)}{C_{A2}} = \frac{\int_0^1 \frac{e^{-\phi}}{b(\lambda)}\alpha\rho d\rho}{\int_0^1 \alpha\rho d\rho}. \tag{2.34}$$

For small values of α, (diffusive flow) Equation 2.33 becomes,

$$\frac{C'_{A3}(R)}{C_{A2}} = \frac{\int_0^1 \frac{e^{-\phi}}{b(\lambda)}(1+\alpha)\rho d\rho}{\int_0^1 \left[\alpha + \frac{e^{-\phi}}{b(\lambda)} \right] \rho d\rho}. \tag{2.35}$$

2.2.4 A radially dependent pore model (RDPM)

A variation of these restricted transport models was obtained by combining the ideas advanced in the RAPM and the SFPF models. Looking at Equations A.36 from the SFPF model and 2.36 from the RAPM (see below), notice that they can be split into both diffusive and convective terms. The difference between these equations is that in the SFPF and MD-SFPF models one factor ($1/b(r)$) is used for both components, K^{-1} and G. In the SFPF model, this leads to the definition of a dimensionless velocity $\alpha(\rho) = u_B(r)\delta/D_{AB}$ which does not account for the lower diffusivity of a solute confined by the pore wall.

$$J_A(r) = -\frac{1}{b(r)} D_{AB} \left[\frac{\partial c_A(r,z)}{\partial z}\bigg|_{r=r} \right] + \frac{1}{b(r)} c_A(r,z) u_B(r). \qquad (A.36)$$

$$J_A(r) = -K^{-1} D_{AB} \left[\frac{\partial c_A(r,z)}{\partial z}\bigg|_{r=r} \right] + G \cdot c_A(r,z) u_B(r). \qquad (2.36)$$

As seen in Figure 2.1, the center-line approximations for K^{-1} and G are quite different from those of $b(\lambda)$ given by Equation 2.21. This point with respect to Ferry's and Pappenheimer's work is discussed extensively by Been [12] and Du Bois [10].

The value of $b(\lambda)$ is derived from Faxen's equation [31] for $\lambda < 0.22$ and from a fit to experimental data obtained from RO experiments. This is somewhat different from using Faxen's equation for all values of λ. The ability of the correlation $b(\lambda)$ to predict the pore size of a membrane will be determined from the data generated in this work. However for the derivations included in this restricted transport model, K^{-1} and G were treated separately.

Brenner and Gaydos [42] introduced the concept that the translational Brownian movement of a sphere in a quiescent fluid is not a scalar as in unbounded fluids but a symmetric second rank tensor or dyadic. The centerline values of K^{-1} and G as proposed in Reference [12] are reported to be valid for the range $0< \lambda <0.4$ but provide unreasonable estimates in the range $0.4< \lambda <1.0$. The correlation used by Bungay and Brenner [43] is more suitable for the entire range of λ as seen in Figure 2.1. These correlations, given in Reference [43], were used to estimate the values of K^{-1} and G throughout this work.

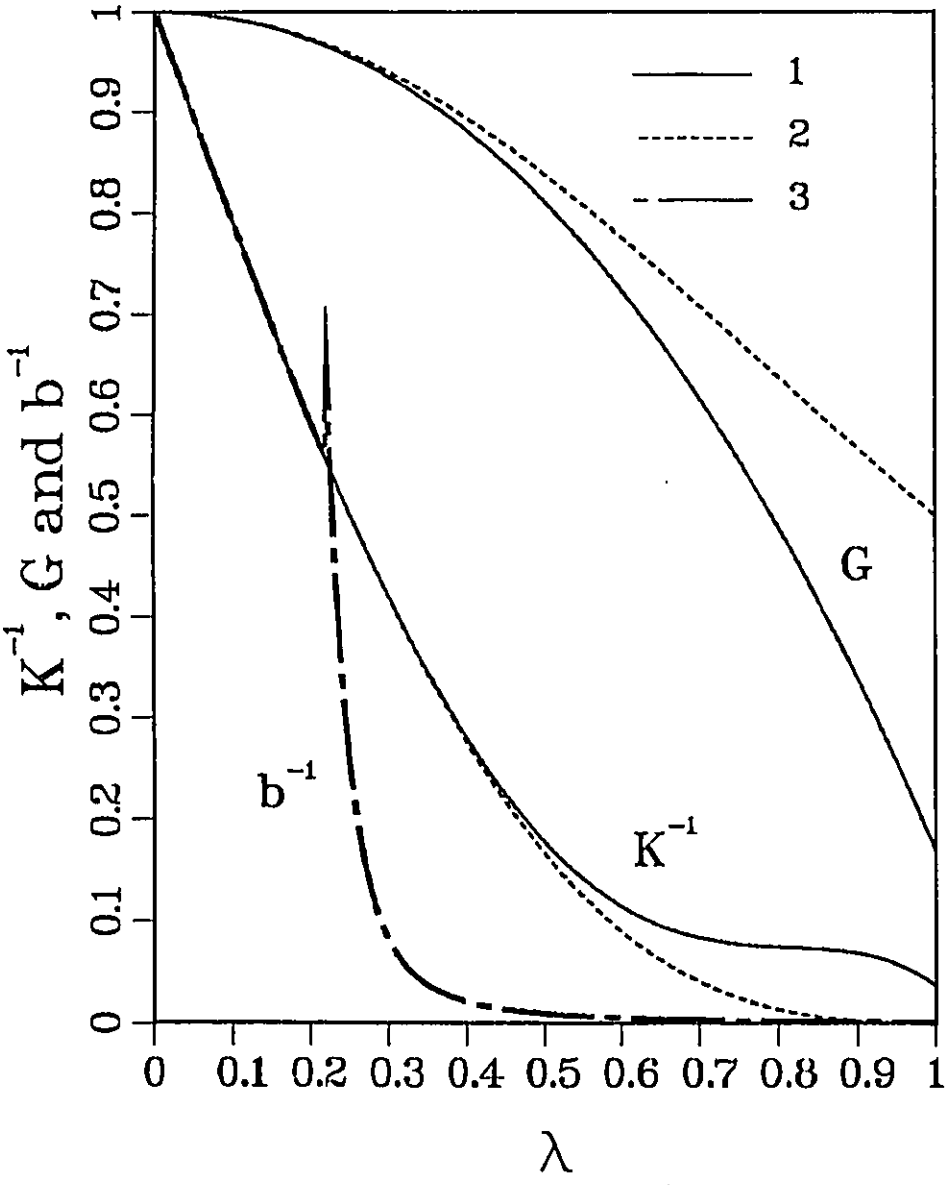

Figure 2.1: Plot of the radially dependent quantities K^{-1}, G and b^{-1} vs. λ from, 1) Anderson and Quinn [12], 2) Bungay and Brenner [43], 3) Matsuura and Sourirajan [7].

Since center-line approximations for the values K^{-1} and G are available [12,43] and offer good approximations for the radial values. They were included in the derivation of a radially dependent pore model RDPM.

As to the selection of a boundary condition at the pore outlet, it is generally well accepted that an unstirred layer of permeate exists on the low pressure side of the membrane. The presence of such a layer was speculated as early as 1877 by Pfeffer [44]. Since there is no cross flow on the permeate side of the membrane, it is reasonable to assume that the thickness of such a layer would be of the order or perhaps greater than that of the boundary layer on the high pressure side of the membrane, whose thickness is in the μm range. The thickness of this layer is several orders of magnitude greater than the pore diameter of UF and RO membranes. Assuming that little mixing occurs at the outlet of the pore, an average concentration $C'_{A3}(R)$, (see Figure 0.1), can be defined inside the unstirred layer a sufficient distance away from the pore exit.

The following boundary conditions are obtained,

$$c_A(r,0) = C_{A2}e^{-\phi'(r)/\underline{R}T}, \tag{2.26}$$

$$c_A(r,\delta) = C'_{A3}(R)e^{-\phi'(r)/\underline{R}T}, \tag{2.27}$$

which can be used to derive the radially dependent model RDPM.

The derivations of this model parallel those of the SFPF and MD-SFPF models and are summarized below. Repeating the operations which led to Equation A.45 using Equation 2.36 as a starting point and the boundary conditions defined by Equations 2.26 and 2.27, the analogue of Equation A.45 is obtained,

$$\ln\left[\frac{C'_{A3}(R)e^{-\phi'(r)/\underline{R}T} - \frac{J_A}{Gu_B}}{C_{A2}e^{-\phi'(r)/\underline{R}T} - \frac{J_A}{Gu_B}}\right] = \frac{Gu_B}{K^{-1}D_{AB}}\delta. \tag{2.37}$$

For reasons of clarity substitute the two dimensionless quantities,
$\alpha'(\rho) = Gu_B\delta/K^{-1}D_{AB}$ and $\phi(\rho) = \phi'(r)/\underline{R}T$, Equation 2.37 becomes,

$$\left[C'_{A3}e^{-\phi} - \frac{c_{A3}}{G}\right] = \left[C_{A2}e^{-\phi} - \frac{c_{A3}}{G}\right]\cdot e^{\alpha'}. \tag{2.38}$$

Taking logarithms of both sides and rearranging,

$$\frac{c_{A3}(r)}{C_{A2}} = \frac{G}{\left(e^{\alpha'}-1\right)}\left[e^{\alpha'}e^{-\phi} - \frac{C'_{A3}(R)}{C_{A2}}e^{-\phi}\right]. \tag{2.39}$$

As in Equation 2.19 the concentration at the pore outlet is determined by taking the radial average of $c_{A3}(r)$,

$$C'_{A3}(R) = \frac{\int_0^R c_{A3}(r)u_B(r)rdr}{\int_0^R u_B(r)rdr}. \tag{2.19}$$

Substituting Equation 2.39 into Equation 2.19,

$$\frac{C'_{A3}(R)}{C_{A2}} = \frac{\int_0^1 \left[\frac{e^{-\phi}e^{\alpha'} - \frac{C'_{A3}(R)}{C_{A2}}e^{-\phi}}{\frac{1}{G}(e^{\alpha'}-1)}\right]\frac{K^{-1}}{G}\alpha'\rho d\rho}{\int_0^1 \frac{K^{-1}}{G}\alpha'\rho d\rho}. \tag{2.40}$$

Equation 2.40 can be rearranged as follows,

$$\frac{C'_{A3}(R)}{C_{A2}} = \frac{\int_0^1 \frac{Ge^{-\phi}}{\left(1-e^{-\alpha'}\right)}\frac{K^{-1}}{G}\alpha'\rho d\rho}{\int_0^1 \left[1+\frac{Ge^{-\phi}}{(e^{\alpha'}-1)}\right]\frac{K^{-1}}{G}\alpha'\rho d\rho}. \tag{2.41}$$

Since the centerline approximations $K^{-1}(\lambda,0)$ and $G(\lambda,0)$ are independent of ρ, from Equation 2.41,

$$\frac{C'_{A3}(R)}{C_{A2}} = \frac{\int_0^1 \frac{Ge^{-\phi}}{\left(1-e^{-\alpha'}\right)}\alpha'\rho d\rho}{\int_0^1 \left[1+\frac{Ge^{-\phi}}{(e^{\alpha'}-1)}\right]\alpha'\rho d\rho}. \tag{2.42}$$

For large values of α' (convective flow) Equation 2.42 becomes,

$$\frac{C'_{A3}(R)}{C_{A2}} = \frac{\int_0^1 Ge^{-\phi}\alpha'\rho d\rho}{\int_0^1 \alpha'\rho d\rho}. \tag{2.43}$$

For small values of α', (diffusive flow) Equation 2.42 becomes,

$$\frac{C'_{A3}(R)}{C_{A2}} = \frac{\int_0^1 Ge^{-\phi}(1+\alpha')\rho d\rho}{\int_0^1 \left[\alpha' + Ge^{-\phi}\right]\rho d\rho}. \tag{2.44}$$

2.2.5 Determining the shape of the velocity profile.

One of the interesting features of the SFPF model is its ability to predict the shape of the velocity profile $u_B(r)$. The value of $u_B(r)$ is determined by performing a momentum balance on two coaxial cylinders of radius r and $(r + dr)$ shown in Figure 0.1. This balance is described in detail in Reference [7], and leads to the following differential equation,

$$\frac{d^2u_B(r)}{dr^2} + \frac{1}{r}\frac{du_B(r)}{dr} - \frac{1}{\eta}\frac{[P(r,\delta) - P(r,0)]}{\delta} - \frac{\chi_{AM}(r)c_{A3}(r)u_B(r)}{\eta} = 0. \quad (2.45)$$

The expression for the pressure gradient in the pore as a function of r is obtained from Equation 4-62 in Reference [7],

$$P(r,\delta) - P(r,0) = -(P_i - P_0) - \underline{R}T\left[c_{A3}(r) - C_{A2}\right] \cdot \left[1 - e^{-\phi'(r)/\underline{R}T}\right]. \quad (2.46)$$

Inserting Equation 2.46 into 2.45,

$$\frac{d^2u_B(r)}{dr^2} + \frac{1}{r}\frac{du_B(r)}{dr} + \frac{1}{\eta}\frac{(P_i - P_o)}{\delta} + \frac{1}{\eta}\frac{RT}{\delta}(c_{A3}(r) - C_{A2})(1 - e^{-\phi'(r)/\underline{R}T})$$
$$-\frac{(b(r)-1)\chi_{AB}(r)c_{A3}(r)u_B(r)}{\eta} = 0. \quad (2.47)$$

The velocity profile as a function of r can be determined by solving Equation 2.47 numerically, subject to the following boundary conditions,

$$\begin{aligned} \text{at r} = 0, \quad \frac{du_B(r)}{dr} &= 0\,, \\ \text{at r} = \text{R}, \quad u_B(r) &= 0\,. \end{aligned}$$

In dimensionless terms equation 2.47 becomes,

$$\frac{d^2\alpha(\rho)}{d\rho^2} + \frac{1}{\rho}\frac{d\alpha(\rho)}{d\rho} + \frac{\beta_2}{\beta_1} + \frac{1}{\beta_1}(1 - e^{-\phi(\rho)})(C_A(\rho) - 1) - \frac{(b(\rho)-1)\alpha(\rho)C_A(\rho)}{\beta_1} = 0.$$

(2.22)

The velocity profile can be determined numerically by the Runge-Kutta procedure [40]. In this calculation scheme, an initial guess of the dimensionless velocity at the center of the pore $\alpha(0)$, is provided from calculations based on Poiseuille flow. The Runge-Kutta procedure is then used to estimate the value of the dimensionless velocity at the pore wall $\alpha(1)$. If this estimate corresponds to the value of the boundary condition at the pore wall then the numerical estimates of $\alpha(\rho)$ are assumed to represent the shape of the velocity profile.

The number of iterations involved in obtaining the velocity profile can be greatly reduced by using prior knowledge of the relationship between $\alpha(1)$ and $\alpha(0)$. Tests indicated that the value of $\alpha(1)$ is a monotonous function of $\alpha(0)$ and that for reasonable variations in $\alpha(0)$; $\alpha(0) \propto \alpha(1)$. The best method to estimate the value of $\alpha(1)$ was by performing a first order fit through three data sets $(\alpha(1), \alpha(0))$; and estimating a new $\alpha(0)$ from the intercept of this correlation. This method was found to converge with a tolerance of $\alpha(1) \leq 10^{-8}$ on the first try for simple nearly parabolic profiles and after 3 to 5 tries for complex profiles. Once the the numerical values of $\alpha(\rho)$ are determined these values can then be substituted in one of the expressions for $C'_{A3}(R)/C_{A2}$.

Determining the exact shape of the velocity profile and using these results to predict solute separation is a computationally intensive procedure. This could be greatly reduced if conditions under which parabolic flow exists in the pore could be determined. Under such conditions, the existence of a parabolic velocity profile would no longer be a mathematical simplification but it would represent the true solution to Equation 2.22. The value of $C'_{A3}(R)/C_{A2}$ could then be evaluated without an iterative procedure. A set of parametric studies were performed using PEG 1000 and casein, two solutes commonly used in membrane characterization. The aim of this study was to use the SFPF model to determine the shape of the velocity profile within the pore, for conditions of solute adsorption and rejection, and at various concentrations and values of λ. The results of this study are presented in a later section.

2.2.6 Summary of transport equations

The equations describing solute separation for all four models, in convective and diffusive flow, have been summarized in Table 2.1 below.

Table 2.1: Ratio of the concentration at the pore outlet $C'_{A3}(R)$ to that of the pore inlet C_{A2}, for all restricted transport models under conditions of diffusive and convective flow.

Model	Convective Flow	Diffusive Flow
RAPM	$\frac{C'_{A3}(R)}{C_{A2}} = \int_0^{1-\lambda} 4G(1-\rho^2)\rho d\rho = \chi$	$\frac{C'_{A3}(R)}{C_{A2}} = \frac{\xi(1+Pe)}{\xi+Pe}$
SFPF	$\frac{C'_{A3}(R)}{C_{A2}} = \frac{\int_0^1 \frac{e^{-\phi}}{b(\lambda)}\alpha\rho d\rho}{\int_0^1 \alpha\rho d\rho}$	$\frac{C'_{A3}(R)}{C_{A2}} = \frac{\int_0^1 \left[\frac{1+\alpha}{1+\frac{b(\lambda)}{e^{-\phi}}\alpha}\right]\alpha\rho d\rho}{\int_0^1 \alpha\rho d\rho}$
MD – SFPF	$\frac{C'_{A3}(R)}{C_{A2}} = \frac{\int_0^1 \frac{e^{-\phi}}{b(\lambda)}\alpha\rho d\rho}{\int_0^1 \alpha\rho d\rho}$	$\frac{C'_{A3}(R)}{C_{A2}} = \frac{\int_0^1 \frac{e^{-\phi}}{b(\lambda)}(1+\alpha)\rho d\rho}{\int_0^1 \left[\alpha+\frac{e^{-\phi}}{b(\lambda)}\right]\rho d\rho}$
RDPM	$\frac{C'_{A3}(R)}{C_{A2}} = \frac{\int_0^1 Ge^{-\phi}\alpha'\rho d\rho}{\int_0^1 \alpha'\rho d\rho}$	$\frac{C'_{A3}(R)}{C_{A2}} = \frac{\int_0^1 Ge^{-\phi}(1+\alpha')\rho d\rho}{\int_0^1 \left[\alpha'+Ge^{-\phi}\right]\rho d\rho}$

2.3 Evaluation of the Interaction Parameters

2.3.1 Evaluation of the surface force function $\phi(\rho)$

The magnitude of solute-membrane interactions are represented by the surface force function $\phi'(\underline{d})$. These forces can originate from London-van der Waals (ϕ_{LvdW}) interactions, the presence of an electrostatic-double layer (ϕ_{DLVO}), or oriented dipoles (ϕ_{DP}) at the surface of the membrane.

For nonionized organic solutes this interaction can be represented by short range van der Waals forces and the even shorter range steric repulsive forces. These interactions are usually modeled by a Lennard-Jones potential function. The position of a solute molecule is represented by a "locator point" which is a body fixed origin at the center of a sphere representing the solute. In the case of interactions with a flat surface, the potential at a distance $\underline{d} > a_s$ away from the surface is given by

$$\phi'(\underline{d}) = -\frac{\underline{B}}{\underline{d}^3} + \frac{\underline{C}}{\underline{d}^{12}}. \tag{2.48}$$

Since $\underline{C}/\underline{d}^{12} \ll \underline{B}/\underline{d}^3$ when $\underline{d} > a_s$, then for nonionized solutes,

$$\phi'(\underline{d}) = \begin{cases} \text{very large} & \text{for } \underline{d} \leq a_s, \\ -\dfrac{\underline{B}}{\underline{d}^3} & \text{for } \underline{d} > a_s. \end{cases} \tag{2.49}$$

The value of $\underline{B}$ can be either positive or negative. In free space, the LvdW forces are always attractive [45], $\underline{B} > 0$. In a solution of high dielectric constant, such as water, the presence of the fluid can significantly modify the interaction between the two bodies and change it from attractive $\underline{B} > 0$ to repulsive $\underline{B} < 0$ [45,46].

The value of $\underline{B}$ can be determined experimentally from surface excess measurements performed on a solute-solvent-membrane system. For small solutes, these measurements can be performed using High Performance Liquid Chromatography (HPLC) [7]. Solute is assumed to be either concentrated or depleted in an interfacial water layer, of thickness t_i, at the surface of the membrane material. The quantity t_i can be obtained from Gas Chromatography measurements.

In this approach the partition coefficient K'_A is defined as,

$$K'_A = \frac{\text{concentration of solute A in the interfacial water phase}}{\text{concentration of solute A in the bulk water phase}}. \tag{2.50}$$

A serious problem arises in using point quantities to define large solutes ($a_s > t_i$) in this type of analysis. By definition, no solute exists at a distance $0 < \underline{d} < a_s$ away from a surface. For values of $a_s > t_i$, the ratio $K'_A = 0$ is undefined as seen in Figure 2.2.

This implies that the value of K'_A cannot be determined for solutes whose radius is greater than t_i, ($a_s > t_i$). In addition, due to the tailing of the concentration profile for $a_s \approx t_i$, an integration from $\underline{d} = 0$ to $\underline{d} = t_i$ cannot provide a good estimate of the surface excess [3]. In conclusion, HPLC measurements suggested in Reference [7] are only applicable to solutes having relatively small radii with respect to the boundary layer thickness.

The solutes used in this work, typically PEG200 - PEG6000 have values of a_s ranging from 0.34 nm to 2.0 nm respectively. These values are relatively high and in some cases exceed the value of $t_i = 1.17$ nm reported for cellulose [7]. This constraint made it impossible to use the analysis proposed in Reference [7] to determine values of the surface potential for individual solutes used in this work.

2.3.2 Evaluation of the surface force function based on van der Waals interactions

As seen in the previous section, for large solutes, the use of body fixed origins to represent solute molecules is insufficient to describe solute-membrane interactions. A solution to this problem is given by Hamaker (1937) [47] who assumed pairwise additivity of interatomic dispersion energies between a spherical body and a plane wall to obtain an expression for the London-van der Waals (LvdW) surface force.

The value of $\phi'_{\text{LvdW}}(\underline{d})$ for the interaction of a solute with a flat surface is given by [48],

$$\phi'(\underline{d}) = \frac{-A_{AM}}{6}\left[\frac{1}{x'} + \frac{1}{2+x'} + \ln\frac{x'}{2+x'}\right], \tag{2.51}$$

[3] Surface excess measurements are based on the following limits of integration $\underline{d} = 0$ to $\underline{d} = \infty$, Reference [7].

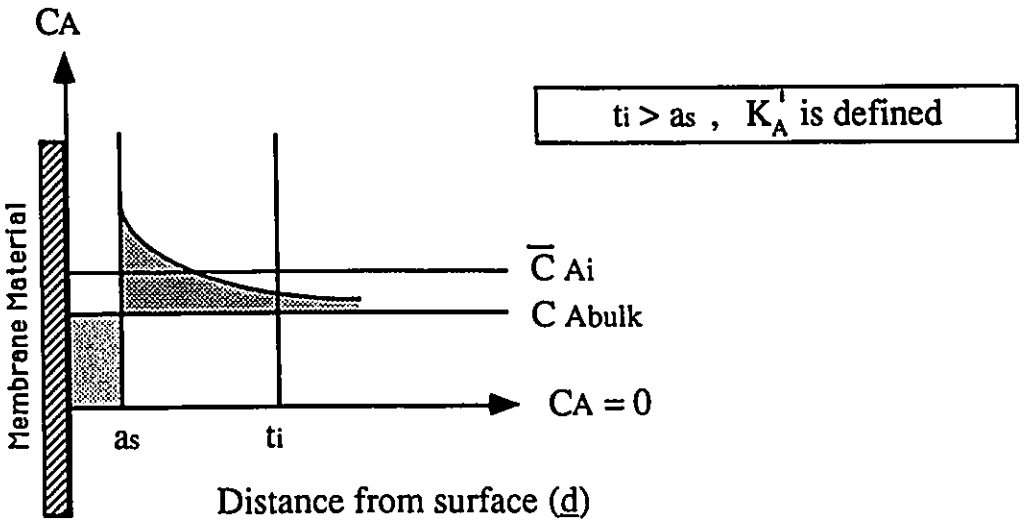

a)

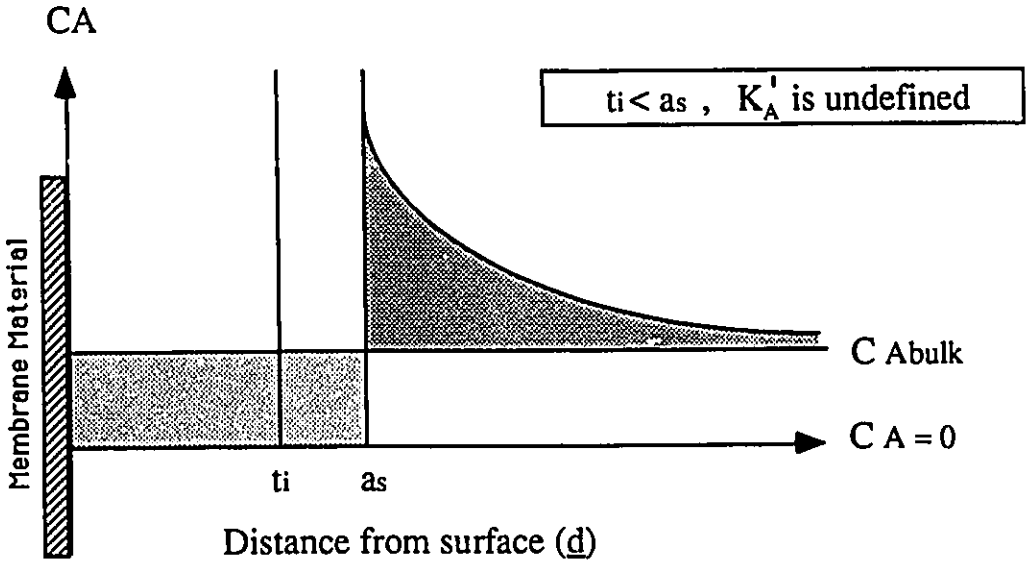

b)

Figure 2.2: Definition of K'_A.

where x' is the dimensionless distance away from the membrane given by,

$$x' = \frac{(\underline{d} - a_s)}{a_s}. \tag{2.52}$$

The concept of pairwise additivity is very useful in membrane characterization since an individual constant can be used to describe solute-membrane interactions for a polydisperse solute. If the constant A_{AM} is included as a variable in the analysis, a two parameter model is obtained in R and A_{AM} which can possibly be solved from a fit to the experimental data. The goodness of fit for the model can also be used to determine the importance of LvdW interactions on separation.

2.3.3 Evaluation of double layer interactions

There is a growing body of evidence to suggest that surface charges exist at nearly all solid-liquid interfaces, "especially when the liquid is water" [49]. The Double Layer theory of ionic dissociation at interfaces is well accepted and documented in the colloid [45,50,51] literature. The equations derived in the DLVO (Derjaguin-Landau-Verwey-Overbeek) theory are all based on electrostatic theory of charged surfaces taking into account the dielectric properties of the solvent. Levine *et al.* [52] derived the value of ϕ'_{DLVO} for the interaction of a non ionized sphere dissolved in a solvent containing ionic species. The value of ϕ'_{DLVO} can be expressed as,

$$\phi'_{DLVO}(\underline{d}) = -16\epsilon\left(\frac{kT}{e}\right)^2 a_s \Phi_M \Phi_A e^{-\kappa(\underline{d}-a_s)}. \tag{2.53}$$

Where ϵ is the dielectric constant of the fluid ($\epsilon = 78.54$ for water at 25°C), k is Boltzmann's constant, e is the protonic charge, Φ_M is the electrostatic potential of the membrane and Φ_A the potential of the surface of the solute.

For a given solute-membrane system several terms in Equation 2.53 can be combined to give an overall potential constant $\Psi_{\mathrm{DLVO}} = (16\epsilon\left(\frac{kT}{e}\right)^2 \Phi_{\mathrm{M}} \Phi_A)$. Equation 2.53 becomes,

$$\phi'_{DLVO}(\underline{d}) = -\Psi_{\mathrm{DLVO}} a_s e^{-\kappa(\underline{d}-a_s)}. \tag{2.54}$$

For a symmetrical electrolyte in water at 25°C [49],

$$\kappa = 3.288 \cdot z_i \cdot c^{1/2} \mathrm{nm}^{-1}. \tag{2.55}$$

Where z_i is the valence of the ion forming the double layer and c is the electrolyte concentration (moles/m^3) in water. The value of $1/\kappa$ is known as the "double layer thickness" or the Debye length and represents an estimate of the thickness of the charged layer.

In this study, the solvent used in all solution preparations was RO treated tap water. The resulting ionic concentration was approximately 1.1 ppm (based on conductivity measurements with NaCl). From Equation 2.55, $\kappa = 0.0142\,\mathrm{nm}^{-1}$ which gives a double layer thickness of 70.10 nm. Since most pores of the cellulose membranes produced in this work are not expected to exceed a value of 5.0 nm, it is highly doubtful that double layer effects are relevant in this study, however calculations based on this possible effect were performed on the experimental data obtained in this work.

2.3.4 Evaluation of structural repulsive forces

Many solvents contain dipoles which can be oriented to form ordered layers at solid interfaces. The presence of these "hydrated" layers of solvent molecules gives rise to short range repulsive forces at the interface which leads to the exclusion of solute molecules trying to occupy positions in the vicinity of the surface. These forces, usually termed "structural" or "hydration" forces, have been measured experimentally and are found to decrease monotonically with distance up to separations of ~6.0 nm [53]. For molecularly smooth surfaces, the force decays as an oscillatory function of distance, with a period which is roughly equal to the diameter of the solute molecules. In the case of a micro-rough or fluid (soft) surfaces the oscillations are smeared out resulting in the monotonic decay of the force with distance away from the surface.

For a surface of uniform polarity, the dipoles next to the surface are all oriented in the same direction as seen in Figure 2.3. This type of arrangement does not favour the structuring of solvent molecules and results in weaker, short range, interactions at the interface. In the case of a surface having Positive (P-type) and Negative (N-type) site, the dipoles are arranged opposite each other which gives rise to the

long range structuring of the solvent molecules. The stability of these structured layers of molecules increases if two NP surfaces are placed opposite each other [54], as seen in Figure 2.3.

The exclusion of solute molecules from hydrated layers present in gels and other porous materials has been studied by many workers [25]. The only problem in using bulk measurements to characterize such layers is the absence of positional information with respect to the solid surface. Recent work with molecularly smooth mica has increased the understanding of structural forces at interfaces. Israelachvili *et al.* [53] measured the force between two crossed cylindrical mica surfaces as a function of the distance from each other. Mica is a typical NP surface, and when placed in contact with water does produce long range structuring of water molecules. The result of this work indicates that structural forces can exist at distances of up to 6.0 nm from these surfaces. At distances < 1.5 nm the magnitude of the force oscillates with a periodicity of $\sim 0.25 \pm 0.03$ nm which is nearly the diameter of a water molecule (~ 0.3 nm [55,56]).

Although this hydrated network of molecules is induced by the presence of the surface, the intermolecular dipole interactions should give it a structural integrity of its own. The layer can then be considered to be a fluid substance whose penetrability can be quantified by the force required to destroy the network. The decay of this force, with increasing distances away from the surface, depends on the size of the solvent molecules and the ability of the interacting surface to structure the solvent molecules. It can be assumed that unless solute molecules destabilize or penetrate the dipole network, they will always be rejected by the hydrated layer. Molecules trying to occupy a site, next to the surface, must compete for positions with the oriented dipoles.

The peak values for each oscillation of the Repulsive Force/surface radius vs. distance curve generated in [53] were digitized and are presented in Table 2.2. A very standard exponential decay model, see Equation 2.56, was used to represent this data,

$$\phi'_{DP}(\underline{d}) = A_0 \exp^{-A_1 d}. \tag{2.56}$$

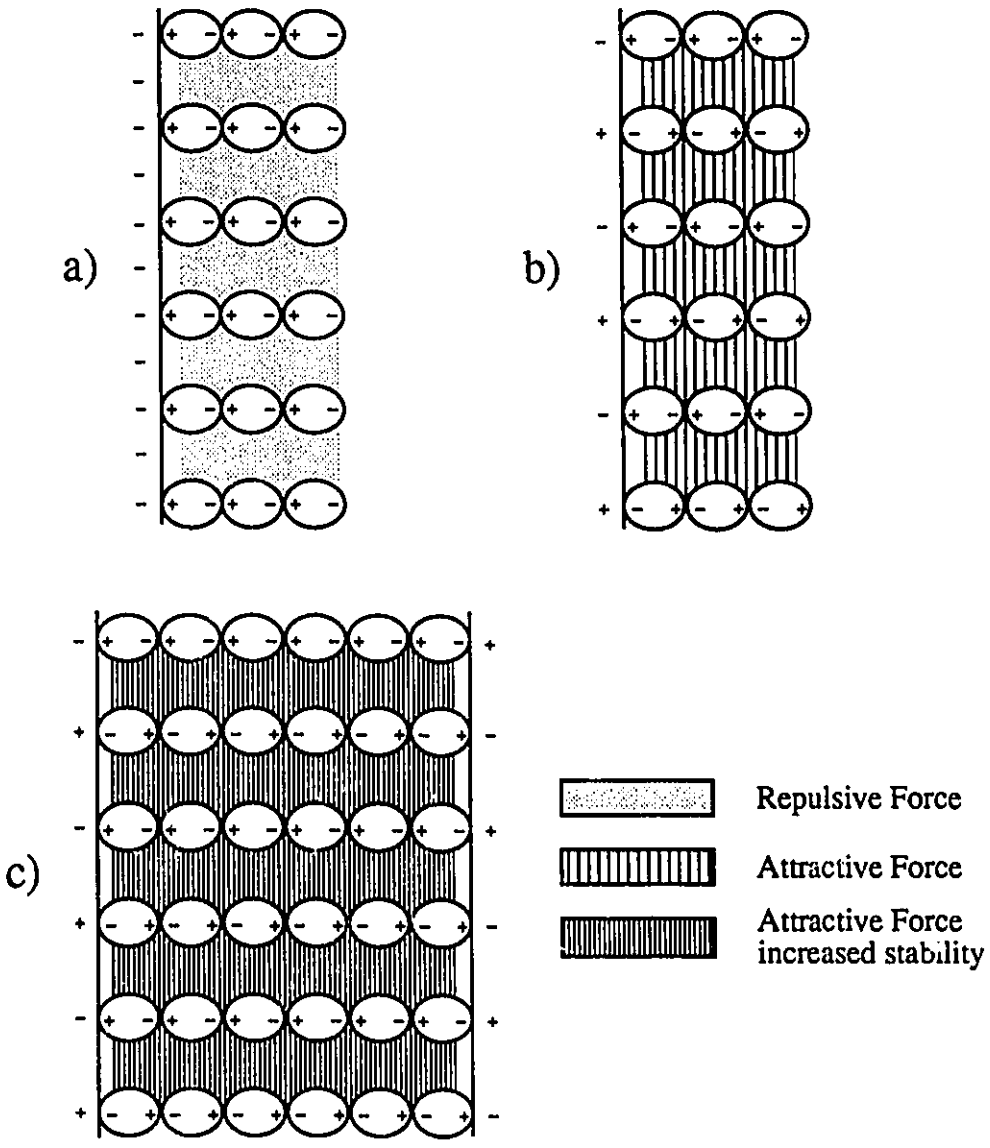

Figure 2.3: Oriented dipoles at a) negatively charged surface, b) NP type surface and c) two opposing NP type surfaces.

Equation 2.56 can be split into potential and distance related terms as in the DLVO case, see Equation 2.53. The first term A_0 represents the affinity of water for the surface and the extent of structuring at the surface. The actual force exerted on a solute will depend on its size. As in the DLVO case for the interaction of a sphere with a plane, the first term must be multiplied by the radius of the solute. The magnitude of this term will depend on the type of surface and is expected to be large in the case of hydrophilic surfaces and small in the case of hydrophobic surfaces.

The exponential term A_1 is correlated with distance and due to the periodicity of this type of interaction force, *i.e.*, this force originates from the presence of water and it is normal that it decays as a function of the number of of layers of water molecules away from the surface. Since this term is strictly related to the diameter of a solute molecule, it can be applied to interactions with any surface.

Equation 2.56 is a two parameter model and provides an **estimate** of the force at the surface. A better fit was obtained with a three parameter growth model, described in Reference [57], but its use in membrane characterization is limited since a term related specifically to distance is difficult to isolate in this case.

Due to the scarcity of the data near the wall, a weighted fit was used which gave a favorable bias to smaller distances from the surface. The parameter estimates for Equation 2.56 were evaluated from the data contained in Table 2.2. Their values are; $A_0 = 2114.3$ mN/m (standard error = 147.2) and $A_1 = 2.969$ nm^{-1} (standard error = 0.193). The data contained in Table 2.2 and Equation 2.56 are plotted in Figure 2.4. An expression has been derived, relating the hydration forces Ψ_{DP} for a specific solvent-membrane material combination, $\kappa' = A_1 \approx 2.969$ nm^{-1} and solute radius, a_s,

$$\phi'_{DP}(\underline{d}) = -\Psi_{DP} a_s e^{-\kappa'(\underline{d}-a_s)}. \tag{2.57}$$

Based on this approach, evaluating the pore size of a membrane would involve the solution of a two parameter model in R and Ψ_{DP}. The value of Ψ_{DP} for the PEG-water-cellulose system will be determined from a fit to the experimental data produced in this work. A unique solution for Ψ_{DP} would permit the quantification of the interaction force for a given polymer based on the permeation experiments.

Table 2.2: Data from peak values of the Repulsive Force/surface radius vs. separation distance, for two curved mica surfaces of initial radius $R \approx 10$ mm. from [53]. † - actual measurement, ‡ - interpolation performed by Israelachvili [53].

Distance $\underline{d}$ (nm)	Repulsive Force /surface radius (mN/m)
.3	841.4 †
.5	555.9 †
.7	234.4 †
.9	113.5 †
1.2	12.4 †
1.4	6.7 ‡
1.6	4.9 ‡
1.8	4.3 ‡
2.0	3.8 ‡
2.5	3.2 ‡
3.0	2.9 ‡
3.5	2.6 †
3.7	2.5 †

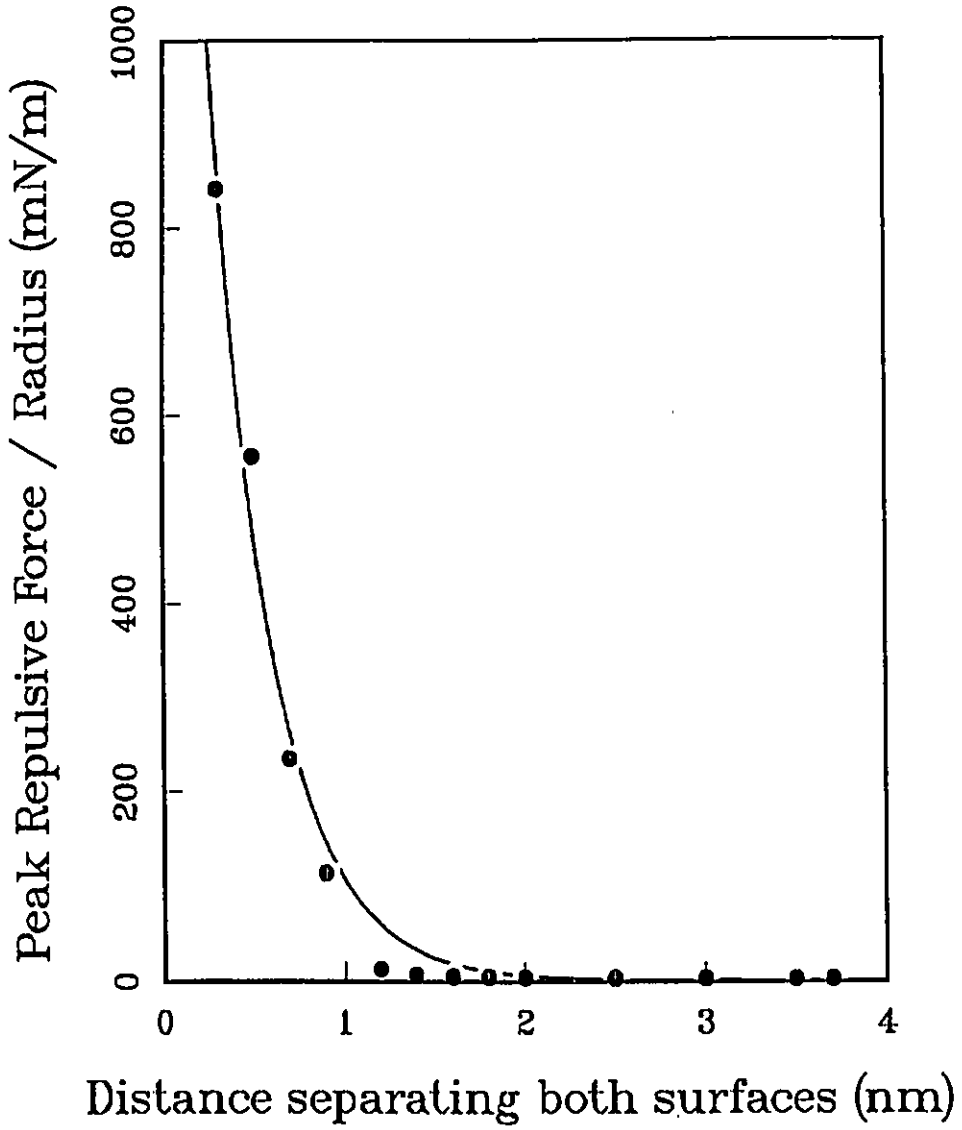

Figure 2.4: Direct measurement of the force between two crossed cylinders of molecularly smooth mica submerged in water.

Once the pore size of the membrane is obtained from this fit, it can be used to determine interaction parameters for other solutes. These quantities, determined for Transition membranes can then be used in predicting solute separations for RO membranes.

2.3.5 The case of strong hydration

For modeling purposes, conditions where the hydration forces were so strong that they rejected solute totally were examined. It was assumed that such an effect could be modeled as a layer of pure solvent, of thickness t_{ads}, at the surface of the membrane having the same properties as the bulk fluid. The significance of the hydration of surfaces for RO, Transition, and UF membrane transport is illustrated in Figure 1.1. It is easily seen from this figure that solvent preferential sorption would have a considerable effect on solute separation for RO membranes, little effect for UF membranes and a somewhat intermediate effect for Transition membranes.

This model was considered for purely steric solute transport. It is assumed that solute molecules cannot penetrate the adsorbed layer and are confined to a cylindrical region defined by $r = 0$ and $r = R - a_s - t_{\text{ads}}$, the concentration inside the pore is then assumed to be given by,

$$c(r,z) = \begin{cases} C_{A2} & \text{for} \quad r \leq R - a_s - t_{ads}, \\ \\ 0 & \text{for} \quad r > R - a_s - t_{ads}. \end{cases} \tag{2.58}$$

This effect of absolute hydration was studied for all membranes produced in this work.

2.4 Other Factors Affecting Solute Transport

2.4.1 Increased solution viscosity within the pore

A structuring effect on the solute molecules at hydrophilic interfaces has been observed by X-Ray diffraction studies of the water-mica interface [55] and by direct measurements [53]. Some contradiction exists as to the viscosity of water in the preferentially sorbed layer, Reference [37] reports that the viscosity of water in this layer is identical to that of the bulk solution while Reference [55] reports that this

ordering of solvent molecules causes a 39 to 100 fold increase in solution viscosity within the pore [25]. In order to verify if this had an effect on solute separation, calculations were performed using the the RDPM model with the viscosity term multiplyed by a factor of 39 and 100 for all membranes characterized in this work.

2.4.2 The effect of chain permeability

The hydrodynamic coefficients used in all four restricted transport models were calculated from the assumption that solute molecules behave as impermeable rigid spheres. Theory predicts that the coefficients K^{-1} and G be different for flexible and permeable molecules such as PEG and Dextran . Davidson *et al.* [58] have derived values of K^{-1} and G from theoretical considerations for values of the reciprocal coil permeability $\alpha'' = 10$, 34 and 60. Sedimentation experiments indicate that for most polymer-solvent systems the range of possible α'' values is $10 \leq \alpha'' \leq 60$ [58]. The values of K^{-1} and G obtained from the numerical solution of the Brinkman equation for flow through porous media reported in Reference [58] were digitized for the three values of α'' and the data fitted with fifth order polynomials. The results are shown in Table 2.3; all parameters found in this table fitted the digitized data with a regression factor of 1.000. The effect of chain permeability on solute separation was evaluated for all membranes characterized in this work for these three values of α''.

2.4.3 Determining the shape of the interacting surface

The "probe" solutes used in this study were expected to be rejected by the cellulose membrane material [4]. Some workers suggest that the function $\phi'(r)$ be defined for a solute interacting with a cylindrical geometry and not a flat surface as is the case in this analysis. In the case of interactions with a cylinder, under conditions of solute rejection, the pore can be viewed as a potential well with a minimum at the center of the pore, $r = 0$. Under conditions of solute rejection, the potential at any distance $\underline{d}$ from the membrane material is greater just inside the membrane pore than it is at the surface of the membrane material. This is obvious due to the presence of the adjacent pore wall in the cylindrical configuration. As solute molecules enter the pore they must migrate away from the membrane material to

[4] This was verified experimentally see Chapter 5.

Table 2.3: Coefficients used in the determination of K^{-1} and G for permeable solutes, equation is of the form,
K^{-1} or $G = B0 + B1 * \lambda + B2 * \lambda^2 + B3 * \lambda^3 + B4 * \lambda^4 + B5 * \lambda^5$.

Coefficients for K^{-1}

α''	range	B0	B1	B2	B3	B4	B5
10	$0 \leq \lambda \leq 1$	1.0	-2.5951	2.2626	0.39769	-1.6356	0.65256
34	$0 \leq \lambda \leq 1$	1.0	-2.8484	2.4966	1.4744	- 3.5299	1.4760
60	$0 \leq \lambda \leq 1$	1.0	-3.3346	4.5067	- 2.0185	- 0.72400	0.62599

Coefficients for G

α''	range	B0	B1	B2	B3	B4	B5
10	$0 \leq \lambda \leq 0.22$	1.0	- 0.068416	3.6029	- 73.473	363.85	- 579.52
10	$0.22 < \lambda \leq 1$	1.1471	- 1.4829	3.0553	- 3.9160	2.5747	- 0.66304
34	$0 \leq \lambda \leq 0.22$	1.0	- 0.039971	1.2655	- 6.0945	- 78.214	284.86
34	$0.22 < \lambda \leq 1$	1.0705	- 0.52530	- 0.38834	1.5322	- 1.4355	0.45528
60	$0 \leq \lambda \leq 0.22$	1.0	0.059195	- 2.0571	12.918	- 90.264	207.77
60	$0.22 < \lambda \leq 1$	1.0572	- 0.30478	- 1.5280	3.6598	- 3.1340	0.94545

reach a new equilibrium away from the pore wall. Eventually a molecule would tend to migrate away from the cylindrical surface and occupy a more central position in the pore.

The Reynolds number in the pore and the time required to reach the new radial equilibrium, versus, the time a molecule actually spends inside the pore, must be considered. Goldsmith and Masson [59] observed no radial displacement for rigid spheres translating through capillaries at Reynolds numbers less than 10^{-6}. The Reynolds number inside UF membrane pores was estimated to be approximately 10^{-6} [26]. The average permeation velocity in a 3.3 nm membrane pore is estimated to range from 0.1 to 0.35 mm/sec [26]. Electron micrographs of UF membranes indicate that the thickness of their selective layer ranges from 1 to 3 μm. From these numbers, permeation times through the selective layer of the membrane can be estimated at 0.03 and 0.003 secs respectively.

The time required for a molecule to reach new radial positions in the pore can be estimated by using diffusion as an example of molecular motion. The velocity of a molecule traveling a distance dx under a concentration gradient dc/dx is given by,

$$c\frac{dx}{dt} = -D_{\mathrm{AB}}\frac{dc}{dx}, \tag{2.59}$$

which can be rearranged to give,

$$dt = -(dx)^2\frac{1}{D_{\mathrm{AB}}}\frac{c}{dc}. \tag{2.60}$$

The time required for a molecule to travel 2.0 nm was taken as a representative example. Substituting the values for sucrose into Equation 2.60, dx = 2.0 nm, D_{AB}=0.56 x 10^{-9} m^2/sec (Table 4.5), assuming the lower concentration across the 2.0 nm distance is equal to zero and a linear concentration profile, then c/dc= 0.5. Solving for dt in Equation 2.60, dt=3.0 x 10^{-9} sec.

This short calculation indicates that molecular motion can occur on a time basis which is 6 orders of magnitude faster than the permeation time through the membrane. This also opens the possibility that radial displacements of molecules could be occuring at these low Reynolds numbers. Given these considerations it is not unreasonable to assume that under a sufficiently strong repulsive force from the

membrane material, the central confinement of solute molecules could occur during the transport of solute molecules through the selective layer of the membrane.

SEM micrographs of the surface of RO membranes indicate that the edge of the pores are smooth and that no abrupt discontinuities exist between the plane of the membrane and the start of the pore wall [25]. Since the velocity profile inside the pore is assumed to be independent of position along the pore axis, a radially averaged solute flux can be determined at for any z position along this axis. At these low Reynolds numbers existing in the pore [26], it can be assumed that the velocity profile is fully developed near the entrance of the pore. It is proposed that the most representative concentration profile is one based on the shape of the membrane material at the entrance of the pore. Given the smooth edges at the entrance of these pores, concentration profiles based on interactions with flat surfaces should provide realistic estimates of surface interactions.

An attempt was made to estimate if the data reflected a radial migration of solute towards the center of the pore. In this scheme, solute molecules are confined to a region close to the central axis of the pore defined by $r = R_{\text{well}}$. Solute concentration inside the pore is then given by,

$$c(r,z) = \begin{cases} C_{A2} & \text{for} \quad r \leq R_{\text{well}}, \\ 0 & \text{for} \quad r > R_{\text{well}}. \end{cases} \tag{2.61}$$

The predictions of such a model are expected to approach those of a steric model for large values in of R_{well}. Values of $R_{\text{well}} = a_s, 2a_s$, and $3.0a_s$ are evaluated with the data generated in this study.

2.5 New Fundamental Parametric Studies

It is often impossible to understand the implications of transport models by observing their constitutive equations. Parametric studies can provide insight on the behavior and the limits of applicability of such models. Knowing this information is important if these models are to be used as quantitative tools in order to reveal any fundamental inadequacies present in the original model and to detect numerical noise or subtle programming errors which might go unnoticed if the models are applied in a "black box" approach. Parametric studies also serve to identify possible asymptotic behavior and computational short cuts which reduce computation time by providing analytical solutions where numerical ones were thought necessary. In many cases this permits the production versions of these models to be run on much slower, less expensive computers without any loss in numerical accuracy.

Ideally this type of study should always be performed before the model is used in a predictive manner. Unfortunately this is not always the case and too often one is forced to accept mathematical equations without an in-depth knowledge of their limitations.

Several parametric studies were performed on the four models presented in the previous section.

The objectives of this study were to ;

- compare the four transport models by studying the effect of pressure on solute separation as a function of solute radius,
- determine the exact shape of the velocity profile in the pore, under conditions of solute attraction and repulsion for various feed concentrations and for different values of λ,
- study the effects of pore radius, pore size distribution, London-van der Waals interactions, electrical double layer and structural forces on solute separation, and,
- study some difficulties encountered in using the log-normal distribution to describe the distribution of pore sizes at the surface of the membrane.

The results of these parametric tests are presented and discussed in the following sections.

2.5.1 The shape of the velocity profile

The SFPF model can be used to determine the shape of the velocity profile within a membrane pore. In obtaining this profile, Equation 2.22 must be solved numerically, a difficult procedure since an abrupt change in solution properties occurs at a distance of one solute radius away from the pore wall [5]. Physico-chemical solution properties vary radially within the pore and must be re-calculated at every step in the numerical procedure. These considerations make the evaluation of the velocity profile within a membrane pore a computationally intensive procedure.

Typical runs to determine solute separation using the explicit solution of the SFPF model can take up to one hour on a VAX780 (based on a characterization run performed using 15 solutes) . It would be an asset to perform pore size calculations in less time and on a slower machine. Even with the considerable decrease in the cost/performance ratio of newer machines, performing a numerical calculation, when an analytical solution is available and provides an equally accurate result, is not a very useful exercise.

The shape of the velocity profile in a membrane pore was determined under the usual conditions of solute attraction ($A_{AM} > 0$) and repulsion ($A_{AM} < 0$) in which case the potential function for solute concentration is given by Equation 2.51. The simulations were performed for polyethylene glycol (PEG1000) and casein which are representative of solutes used in membrane characterization. For casein, the viscosity and osmotic pressure increase as a function of concentration is typical of many proteins.

The exact velocity profile was calculated for these solutes as a function of A_{AM} for an operating pressure of 2762 kPa (400 psig.) at 200 ppm (mg/L), 1, 5 and 10 wt.% feed concentrations, see Figures 2.5, and 2.6. These profiles were also calculated for λ = 0.1, 0.2, 0.3 and 0.4, at a concentration of 200 ppm, under the same operating pressure, see Figures 2.7, and 2.8. A limit of 20 wt.% was arbitrarily set on the radially dependent concentration of solute as predicted by Equation 2.27. This concentration was considered to represent a reasonable limit encountered in most membrane applications and served as an indication that predicted profiles reflected real operating conditions [6].

[5] By definition solute does not exist at a distance less than a_s from the pore wall.

[6] This concentration limit was only reached at high feed concentrations and for the larger positive

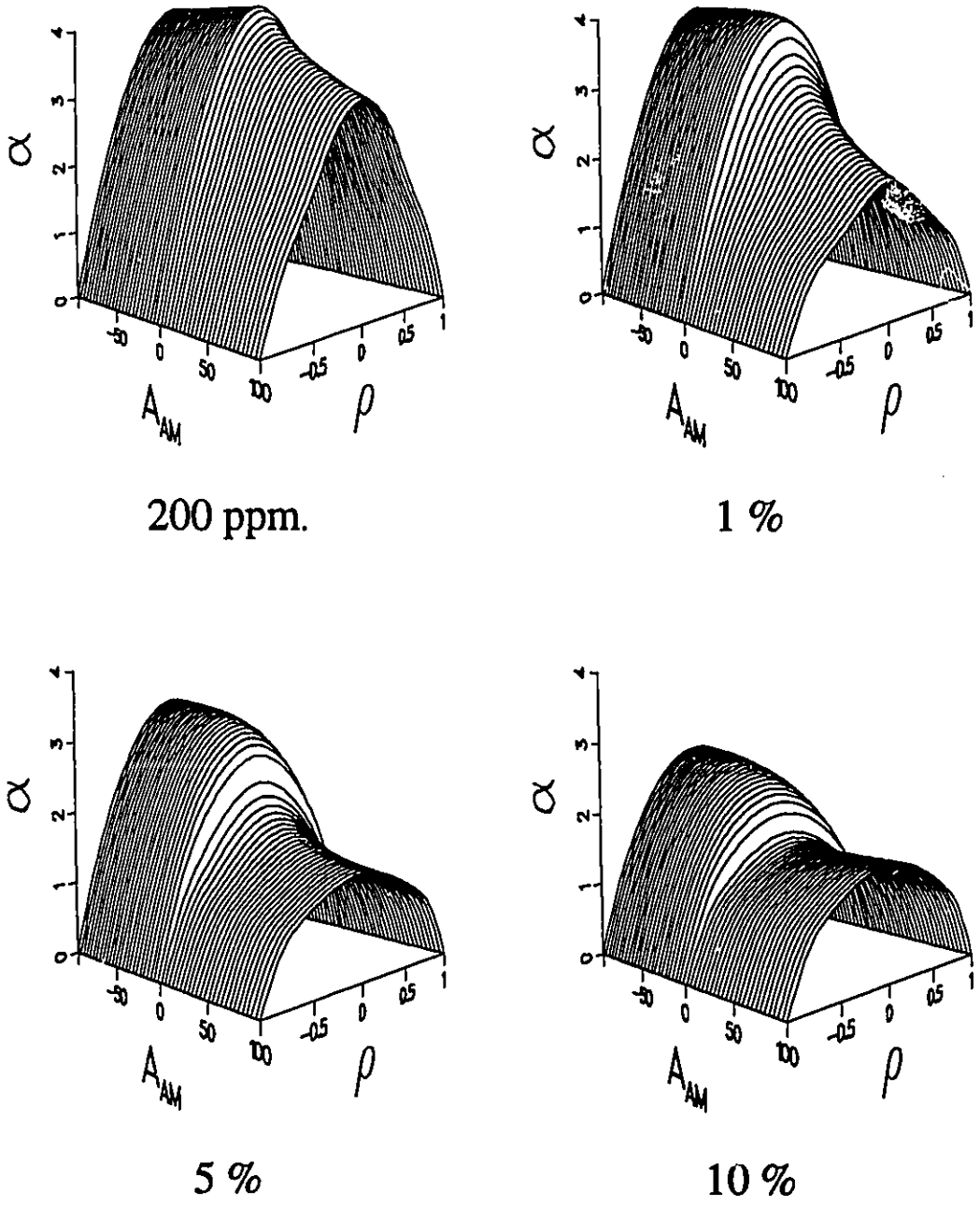

Figure 2.5: Velocity profiles obtained using PEG1000, parameterized for values of the Hamaker constant A_{AM} for solute adsorption $A_{AM} > 0$ and rejection $A_{AM} < 0$ at various pore inlet concentrations C_{A2} (R=3.0 nm, a_s=0.79 nm, concentrations in weight %).

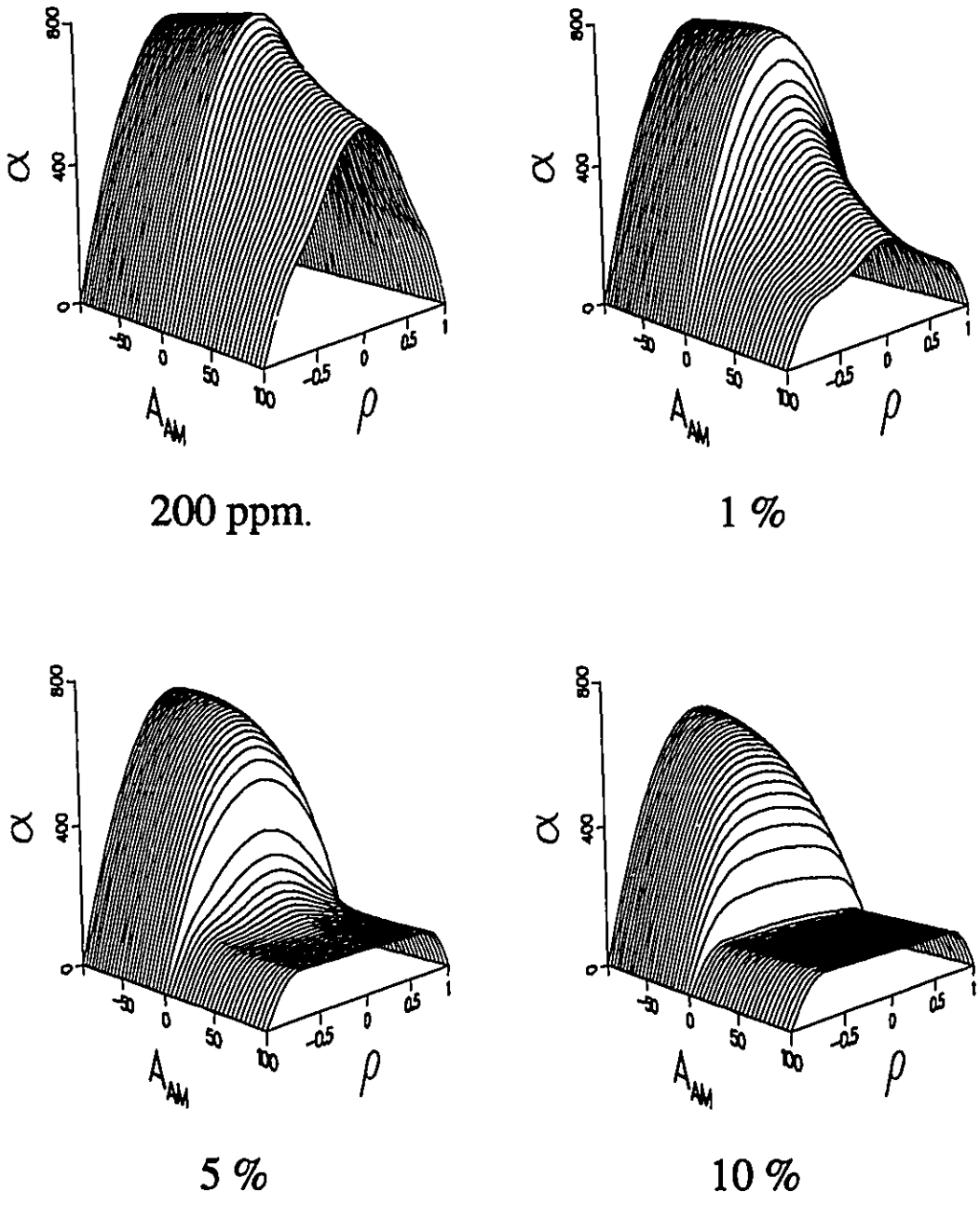

Figure 2.6: Velocity profiles obtained using casein, parameterized for values of the Hamaker constant A_{AM} for solute adsorption $A_{AM} > 0$ and rejection $A_{AM} < 0$ at various pore inlet concentrations C_{A2} (R =10.0 nm, a_s = 3.67 nm, concentrations in weight %).

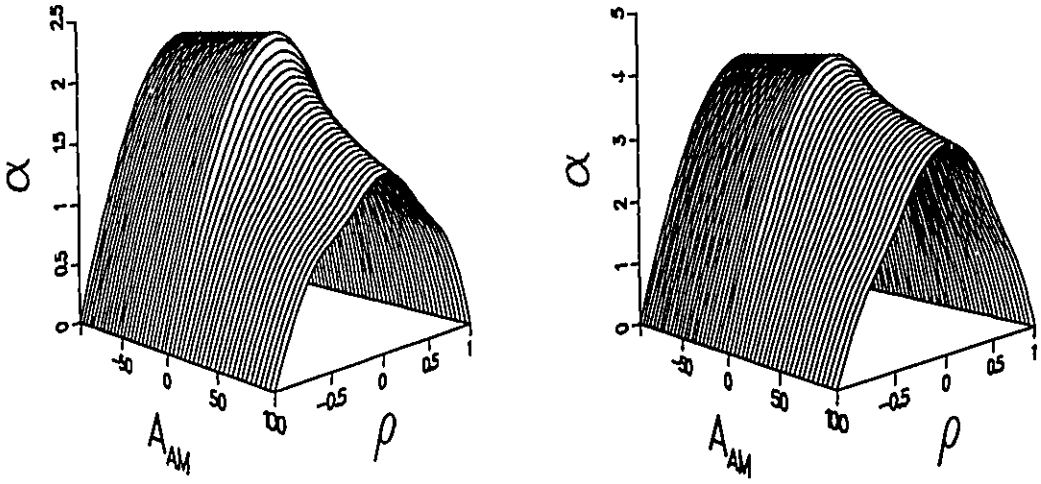

$\lambda = 0.4,\ R = 2.0$ nm

$\lambda = 0.3,\ R = 2.6$ nm

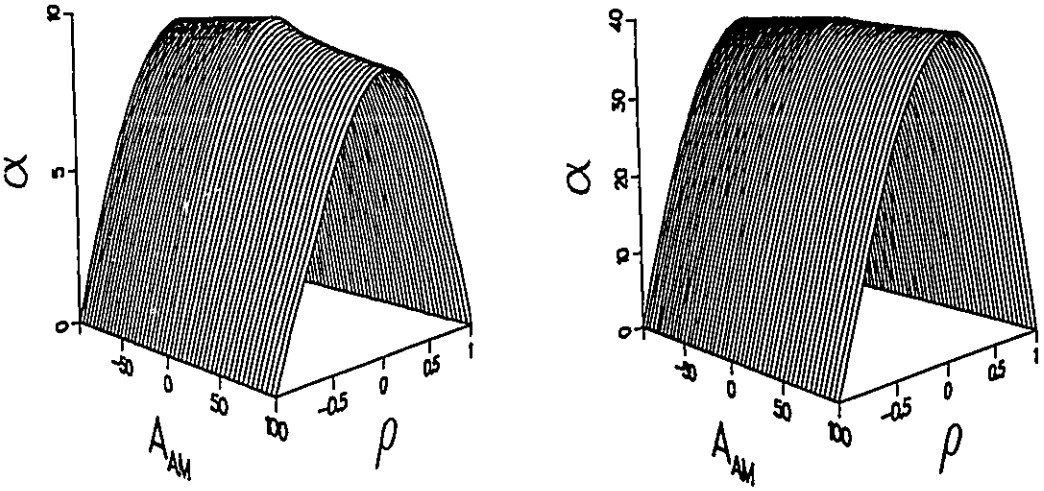

$\lambda = 0.2,\ R = 4.0$ nm

$\lambda = 0.1,\ R = 7.9$ nm

Figure 2.7: Velocity profiles obtained using PEG1000, parameterized for values of the Hamaker constant A_{AM} for solute adsorption $A_{AM} > 0$ and rejection $A_{AM} < 0$ for various values of λ based on a 200 ppm pore inlet concentrations C_{A2}, a_s=0.79 nm.

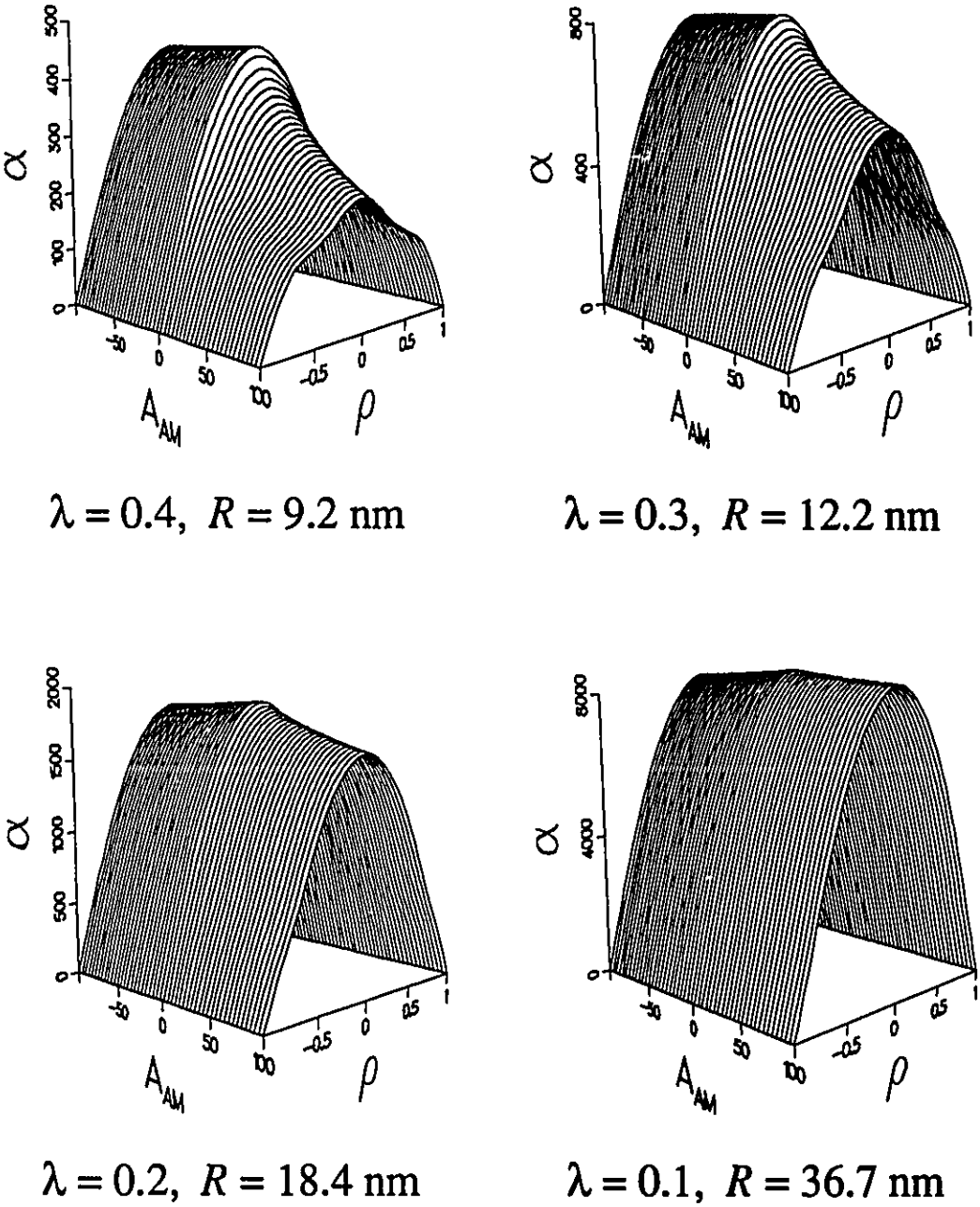

Figure 2.8: Velocity profiles obtained using casein, parameterized for values of the Hamaker constant A_{AM} for solute adsorption $A_{AM} > 0$ and rejection $A_{AM} < 0$ for various values of λ based on a 200 ppm pore inlet concentrations C_{A2}, a_s = 3.67 nm.

These results can be interpreted as follows;

- For conditions of strong solute rejection in the pore $A_{AM} << 0$, the velocity profile is always parabolic.
- For purely steric interactions $A_{AM} = 0$ and intermediate rejection $A_{AM} < 0$, the velocity profile for PEG1000 is always parabolic while that of casein is parabolic at concentrations below 5% but is distorted at higher concentrations.
- For intermediate adsorption $A_{AM} > 0$, the velocity profile for PEG1000 is parabolic up to 1% and distorted at and above 5%. The same occurs for casein but the distortion is more serious at higher concentrations.
- For severe adsorption $A_{AM} >> 0$, the velocity profile for both solutes is slightly distorted at low concentrations and becomes severely distorted at higher concentrations.
- At high concentrations of casein, the velocity profile is flat at the center and parabolic at its edges for $\rho > 1 - \lambda$. The presence of a slip near the wall is due to the absence of solute at a distance smaller than a_s from the pore wall.
- For conditions of adsorption, even at very low pore inlet concentrations of $C_{A2} = 200$ ppm, the value of λ plays an important role in the shape of the velocity profile. This is undoubtably due to the presence of $b(\lambda)$ in Equation 2.22, since this deformation is greatest at lower values of λ where $b(\lambda)$ becomes very large.
- For dilute feed solutions irrespective of λ, under purely steric interactions $A_{AM} = 0$ and in rejection $A_{AM} < 0$ the shape of the velocity profile is always parabolic.

This parametric study indicates that, if membranes are characterized using dilute solutions of "probe" solutes in the absence of strong adsorption, it is not necessary to solve Equation 2.22 explicitly and a parabolic velocity profile will represent the exact shape of the velocity profile.

---

values of A_{AM}. Its removal did not change the shape of the velocity profiles.

For the test conditions used in this experiment, *i.e.* dilute solutions of medium to low molecular weight polyethylene glycols, the existence of a parabolic velocity profile is no longer an assumption but represents the explicit solution of Equation 2.22. This simplifies and speeds calculations without sacrificing accuracy. A parabolic velocity profile will be used in all membrane characterization experiments performed in this work.

2.5.2 Comparing the four restricted transport models

The four restricted transport models RAPM, SFPF, MD-SFPF, and the RDPM were compared for dilute solutions of polyethylene glycol under purely steric interaction with the membrane pore. A simulation was performed for a 1.5 and 3.0 nm pore radius, at six operating pressures. Solute separation was predicted as a function of solute radius. The PEG solutes were assumed to behave as rigid spheres. The results are shown in Figures 2.9 – 2.12.

The results of this study indicate that;

- All models predict that above 500 kPa ($\approx$5 *atm*), solute separation is independent of pressure. Above this pressure, convection dominates solute transport as predicted by the Equations found in Table 2.1. Below this pressure, separation is pressure dependent and diffusion plays a part in solute transport. Note that these results do not account for concentration polarization at the surface of the membrane and only apply to low trans-membrane permeation velocities and cases of excellent mixing in the boundary layer. For steric interactions and convective dominated transport, the only difference existing between the models is in the use of a different hydrodynamic lag coefficient, G, and the solute friction, b.

- Both the SFPF and MD-SFPF predict the same separation at high pressures. While they are quite different in their predictions at lower pressures. From the point of view of membrane characterization using dilute solutes at pressures above 500 kPa (convection dominated flow), the choice of a boundary condition is mathematically irrelevant.

- The shape of the separation vs. solute radius plots for both the SFPF and MD-SFPF models has a marked irregularity (sharp peak) for the 3.0 nm pore which disappears in the predictions for the 1.5 nm pore. This irregularity is due to the shape of the b^{-1} vs. λ curve shown in Figure 2.1. The values of $b(\lambda)$ were derived from a fit to RO data, using them to fit larger pore sizes is an extrapolation. This function is not monotonous and produces numerical noise in fitting separation data when a solute has a value of $\lambda \approx 0.22$. This should be corrected in future uses of the correlation.

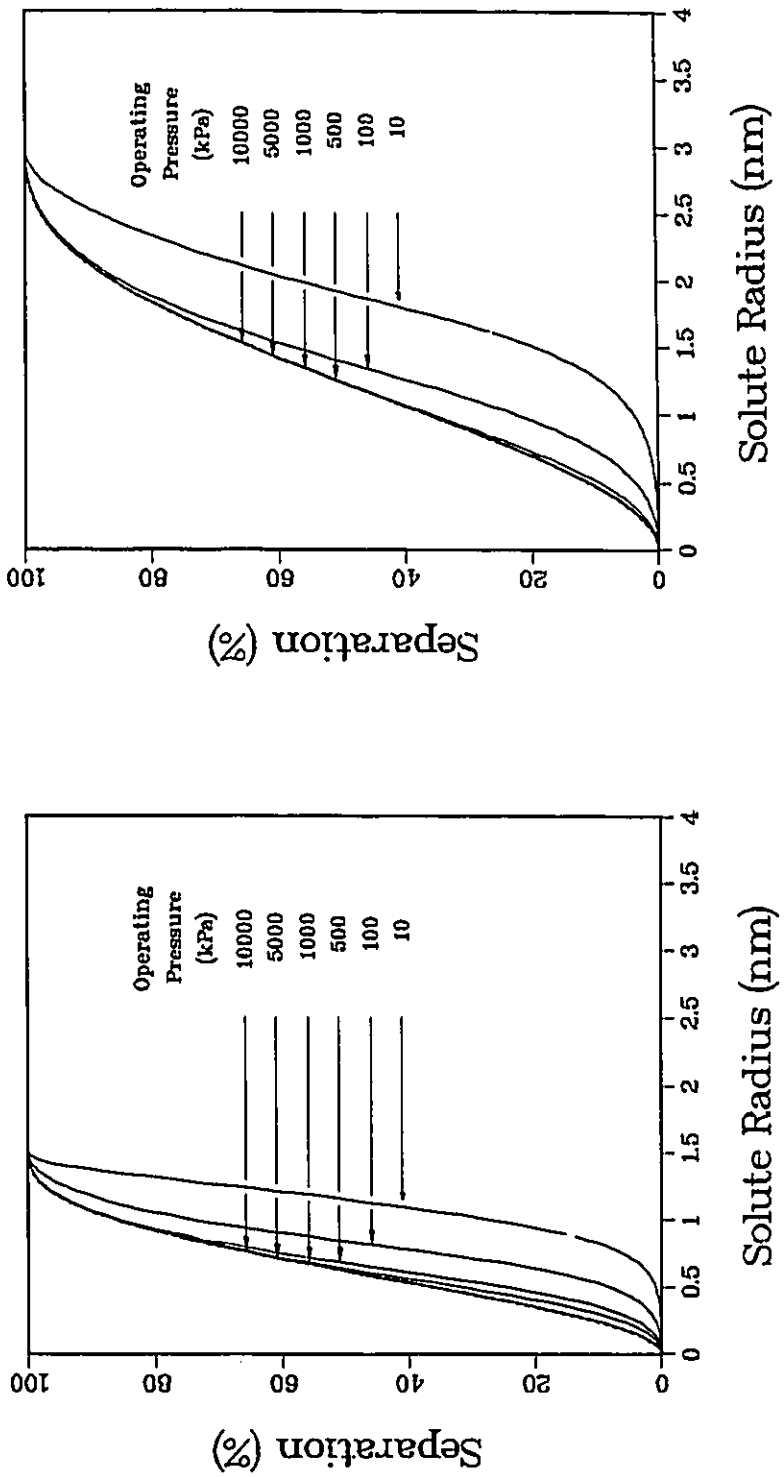

Figure 2.9 : Separation vs. solute radius as predicted by the RAPM for a 1.5 nm a) and a 3.0 nm b) pore radius.

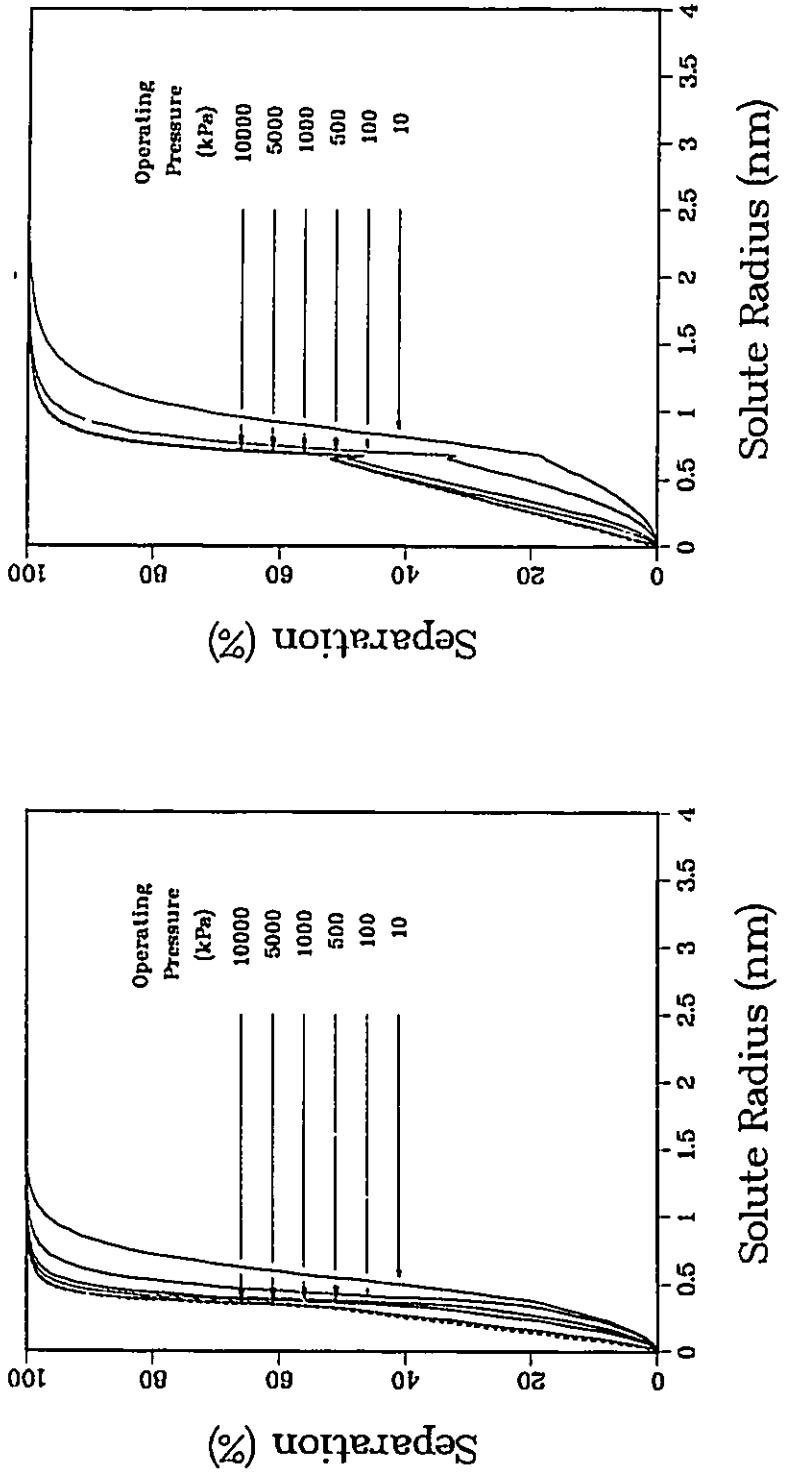

Figure 2.10: Separation vs. solute radius as predicted by the SFPF model, based on a parabolic velocity profile, for a 1.5 nm a) and a 3.0 nm b) pore radius.

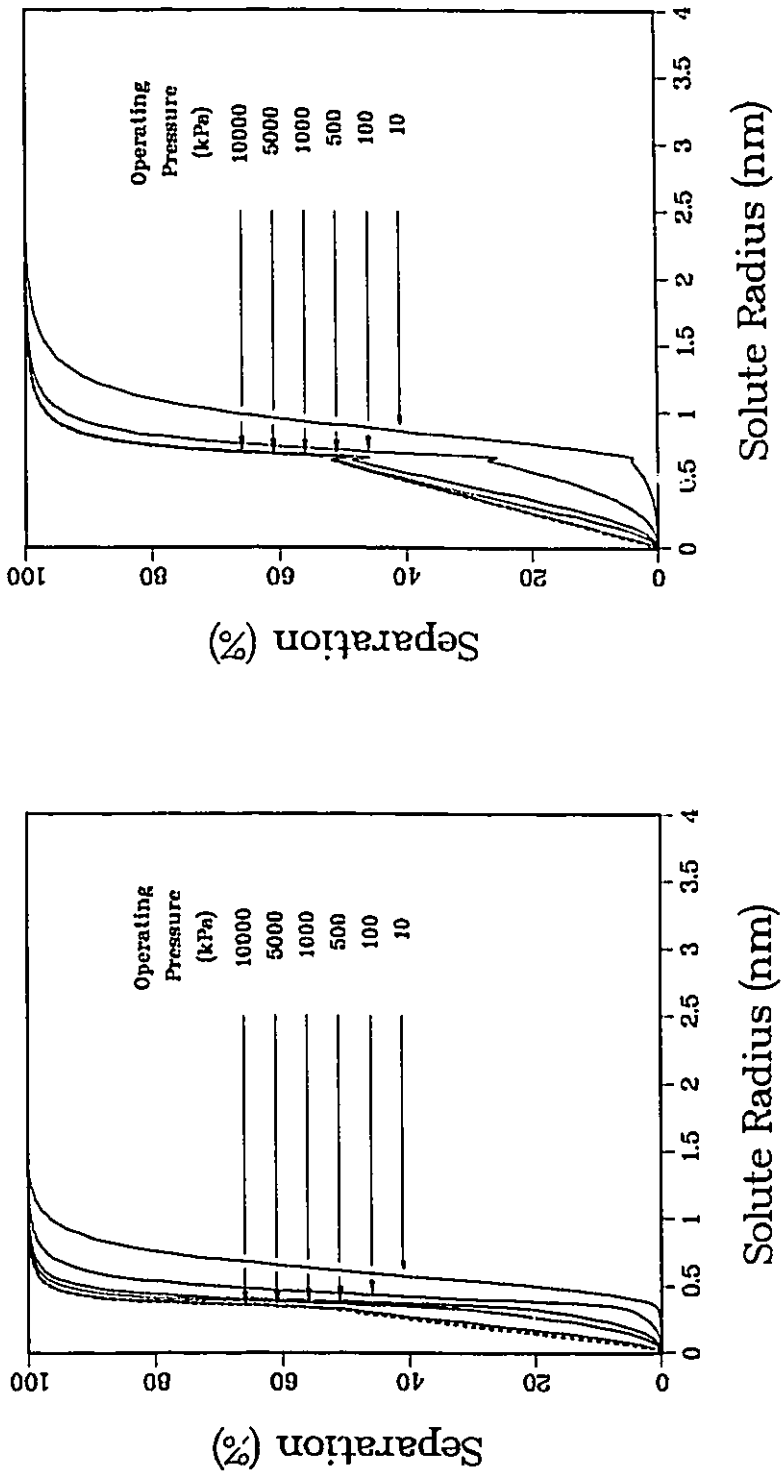

Figure 2.11: Separation vs. solute radius as predicted by the MD-SFPF model, based on a parabolic velocity profile, for a 1.5 nm a) and a 3.0 nm b) pore radius.

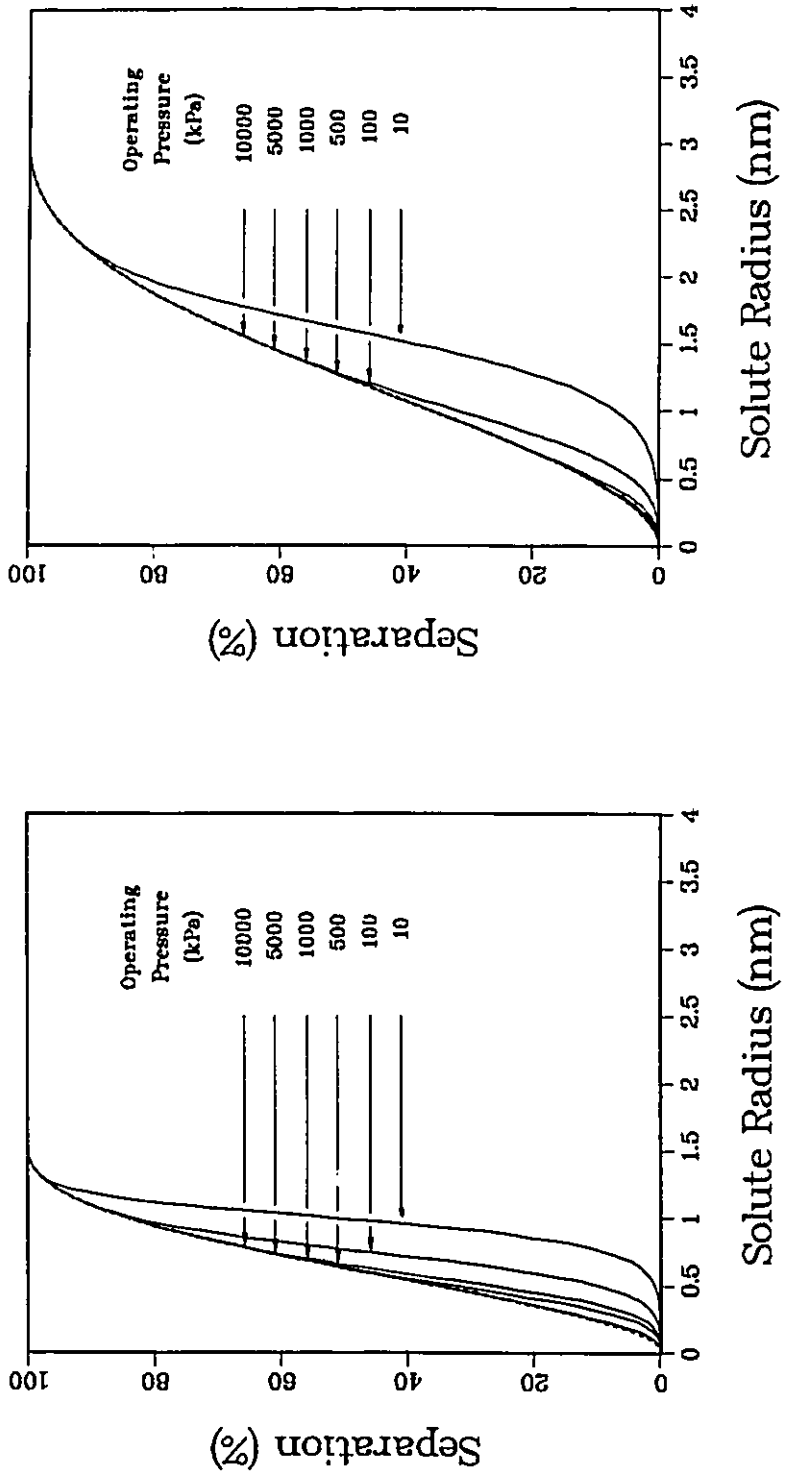

Figure 2.12: Separation vs. solute radius as predicted by the RDPM, based on a parabolic velocity profile, for a 1.5 nm a) and a 3.0 nm b) pore radius.

- The predicted separations based on the RAPM and the RDPM are slightly different due to the use of Anderson and Quinn's, K^{-1} and G, values in the derivation of the RAPM model and the values of K^{-1} and G from Bungay and Brenner in the derivation of the RDPM. Predictions were performed using Bungay and Brenner's correlation with the RAPM, this gave identical results to those obtained in RDPM (these results are not shown).
- The predicted separation for the SFPF and MD-SFPF models is always greater than that of the RAPM and the RDPM. The correlation of b originates from the modification of Faxen's Equation A.11 [31], by a fit to a large number of reverse osmosis permeation data. It is highly possible that solute-membrane interactions were confounded in this fit and that such effects are included in the estimate of b. This could have easily occurred since in convective flow, b and $e^{-\phi}$ are coupled in the calculation of solute separation. In qualitative terms, the shape of the curve above 50% separation is quite similar to that obtained from the parametric studies performed on polyethyene glycols based on van der Waals interactions, see Figure 2.14(b).
- It can easily be appreciated that the slope of the separation vs. solute radius plot at its point of inflection is a measure of the selectivity of the membrane. This slope is proportional to a certain fractionating power of the membrane. Ideally the membrane should permit the complete passage of solutes for $\lambda < 1$ and retain those where $\lambda \geq 1$. All models predict an increase in membrane selectivity as the operating pressure decreases. The main drawback in this observation, is that the greatest benefits occur at very low operating pressures. The porosity and asymmetry of present membranes would have to be increased in order to take full advantage of this concept on a commercial basis.

2.5.3 Factors affecting solute separation

Several other effects were studied, parametrically, using the RDPM model and polyethylene glycol as a solute. The results of these studies are summarized in this section. All tests in this section are based on a feed concentration of 200 ppm and a pressure of 2756 kPa (400 psi.).

The effect of pore radius on solute separation for steric interactions, was studied for a membrane having a fixed pore size (iso-porous membrane) and one having a log-normal distribution of pores. These results are plotted in Figure 2.13(a), and indicate that under steric interactions, pore sizes equal to or less than that of sodium chloride (0.152 nm) are needed to perform RO separations. Such membranes would not have any permeate flow. This clearly demonstrates that purely steric interactions cannot account for membrane transport in the RO and the Transition RO-UF range.

The presence of a distribution of pores at the surface of the membrane was also examined using the log-normal distribution (Figure 2.13(b)). A simple loss of separation efficiency with increasing σ, was observed as indicated by the decrease in the slope of the curves at their point of inflection.

The preferential sorption of solvent on the surface of the membrane was modelled by including the effect of a layer of sorbed water of thickness t_{ads} into the model. This was modeled for a membrane having a 3.0 nm pore radius (Figure 2.14(a)). This indicates that the preferential sorption of solvent at the surface of a membrane can explain the high separations obtained for small solutes having the same relative size as that of water, as in RO separations.

Solute interactions were modeled using Hamaker's approach and these results plotted in Figure 2.14(b). These curves are somewhat similar in shape to those found in 2.10 and 2.11. This illustrates the point about the possible confounding of the surface interactions in the fit to obtain $b(\lambda)$. These results indicate that repulsive London-van der Waals interactions can also explain RO separations.

A similar study was performed to study the effect of attractive London-van der Waals forces. For PEG's at low concentrations (200 mg/L) the velocity profile within the pore remains parabolic and this type of profile was used in all calculations. The results shown in Figure 2.15 indicate that negative separations are possible with this type of interaction and that for a given value of A_{AM} the tendency towards lower

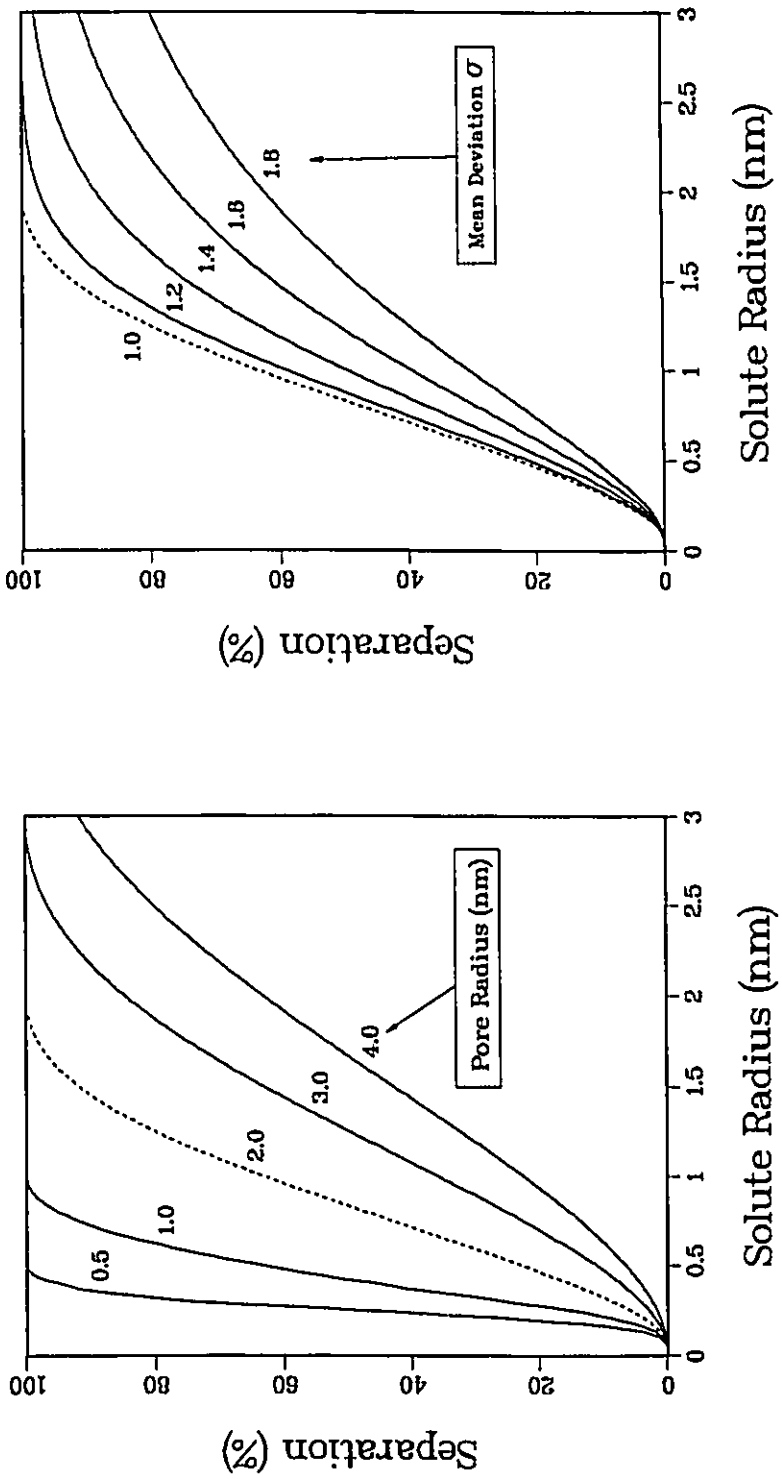

Figure 2.13: Separation vs. solute radius for various membrane pore sizes (iso-porous membrane) a) and the effect of a log-normal distribution of pores b).

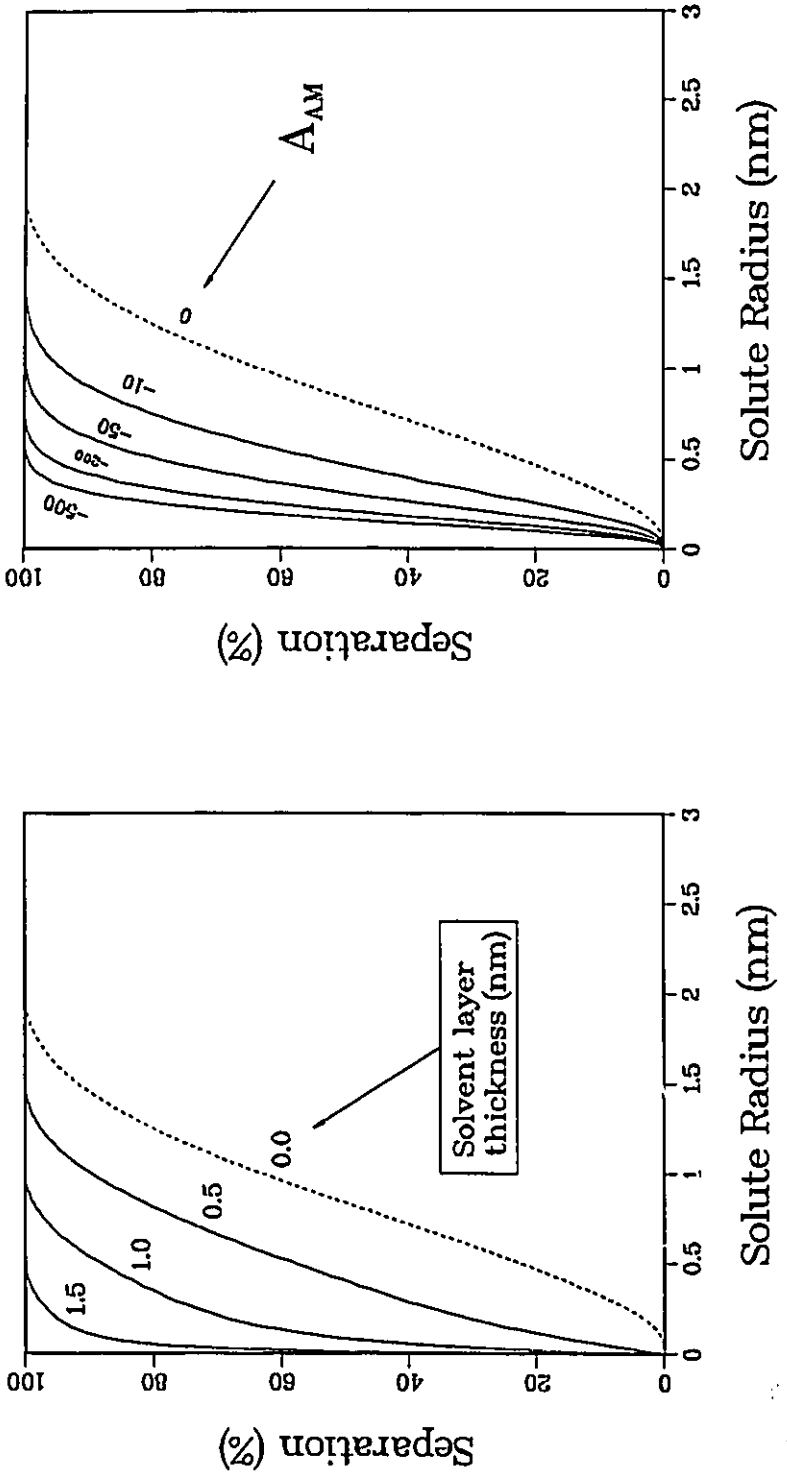

Figure 2.14: Separation vs. solute radius for the preferential sorption of solvent for parameterized values of t_{ads} a), and effects due to the presence of repulsive van der Waals interactions b) (R=2.0 nm).

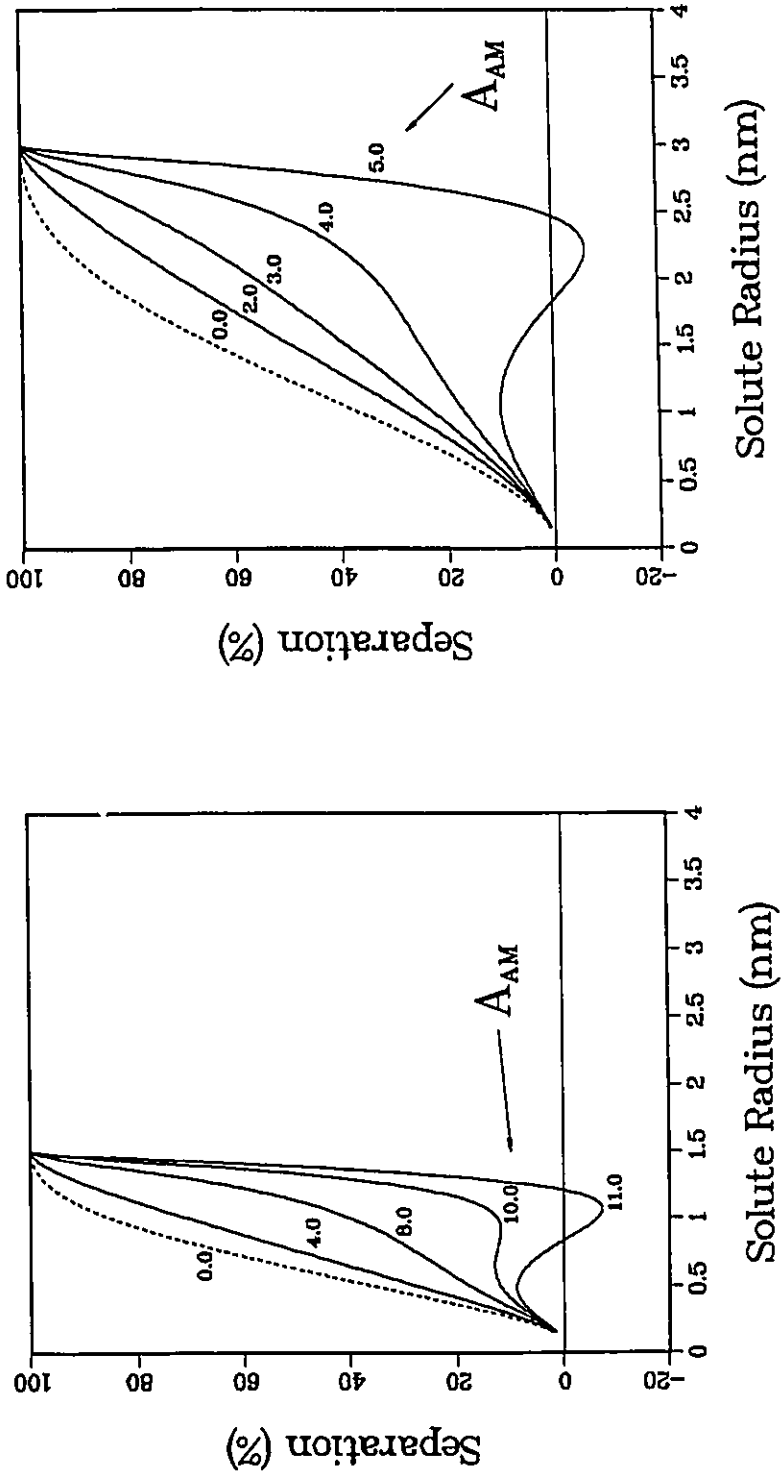

Figure 2.15: Separation vs. solute radius for attractive van der Waals interactions, for a 1.5 nm a) and 3.0 nm b) pore radius.

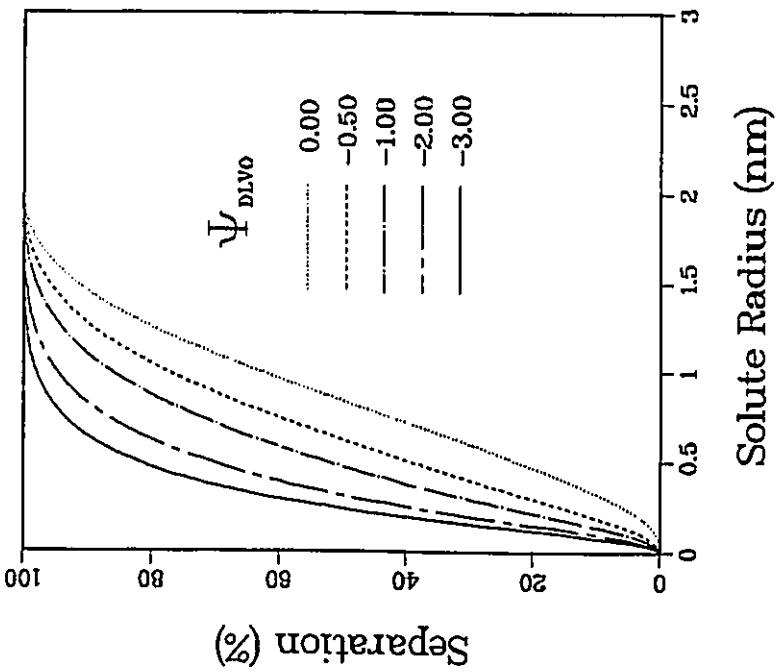

Figure 2.16: Separation vs. solute radius with the presence of an electrical double layer at the membrane surface, for values of Ψ_{DLVO} (nm^{-1}) and $\kappa = 0.0143\ nm^{-1}$ (R=2.0 nm).

separation is greater for large solutes.

Solute interactions due to the presence of an electrical double layer at the surface of the membrane were modeled and the results plotted in Figure 2.16. A similar study was performed based on the the presence of oriented dipoles at the surface of the membrane. These results are contained in Figure 2.17(a) for variable Ψ and $\kappa' = 2.5\ \text{nm}^{-1}$ and Figure 2.17(b) for variable κ' and $\Psi_{DP} = 7.0\ \text{nm}^{-1}$.

These results indicate that in going from the shorter range London-van der Waals interaction to the longer range electrostatic forces, the shape of the separation vs. radius curve changes. The separation curve is no longer straight linear up to 80% separation but can have a more convex shape as seen by comparing Figures 2.14(b) and 2.16. This difference in behavior can be used to determine the origin of the interaction force by examining a goodness of fit to experimental data.

2.5.4 Moments of the log-normal distribution

The most plausible shape of a pore size distribution for these membranes is that of the log-normal distribution. In this case, the normal distribution would predict negative values of the pore radius R which is obviously impossible. The log-normal distribution is most often found in nature and is often used to describe particle sizes [60].

The log-normal distribution has the unfortunate characteristic of having several moments. Fits to actual separation data obtained in this work indicated that a valley existed in a response surface of σ vs. R.

The bottom of this valley was easily fitted by an equation of the form,

$$\ln(\overline{R}_a) = \ln(R_{\text{avg}}) + 4 \cdot \ln^2(\sigma). \tag{2.62}$$

Parametric studies were performed for $\overline{R}_a$ values of 1.6 and 2.1 nm. Several values of $\ln^2(\sigma)$ and $\ln(R)_{\text{avg}}$ were chosen along the line defined by Equation 2.62. Separation curves were predicted for these points as indicated by Roman numerals in Figures 2.18 for $\overline{R}_a = 1.6$ nm and 2.19 for $\overline{R}_a = 2.1$ nm.

These results indicate that it is extremely difficult to determine the value of σ from permeation experiments and that accurate experimental data above 70% and around 40% separation are essential in determining this value.

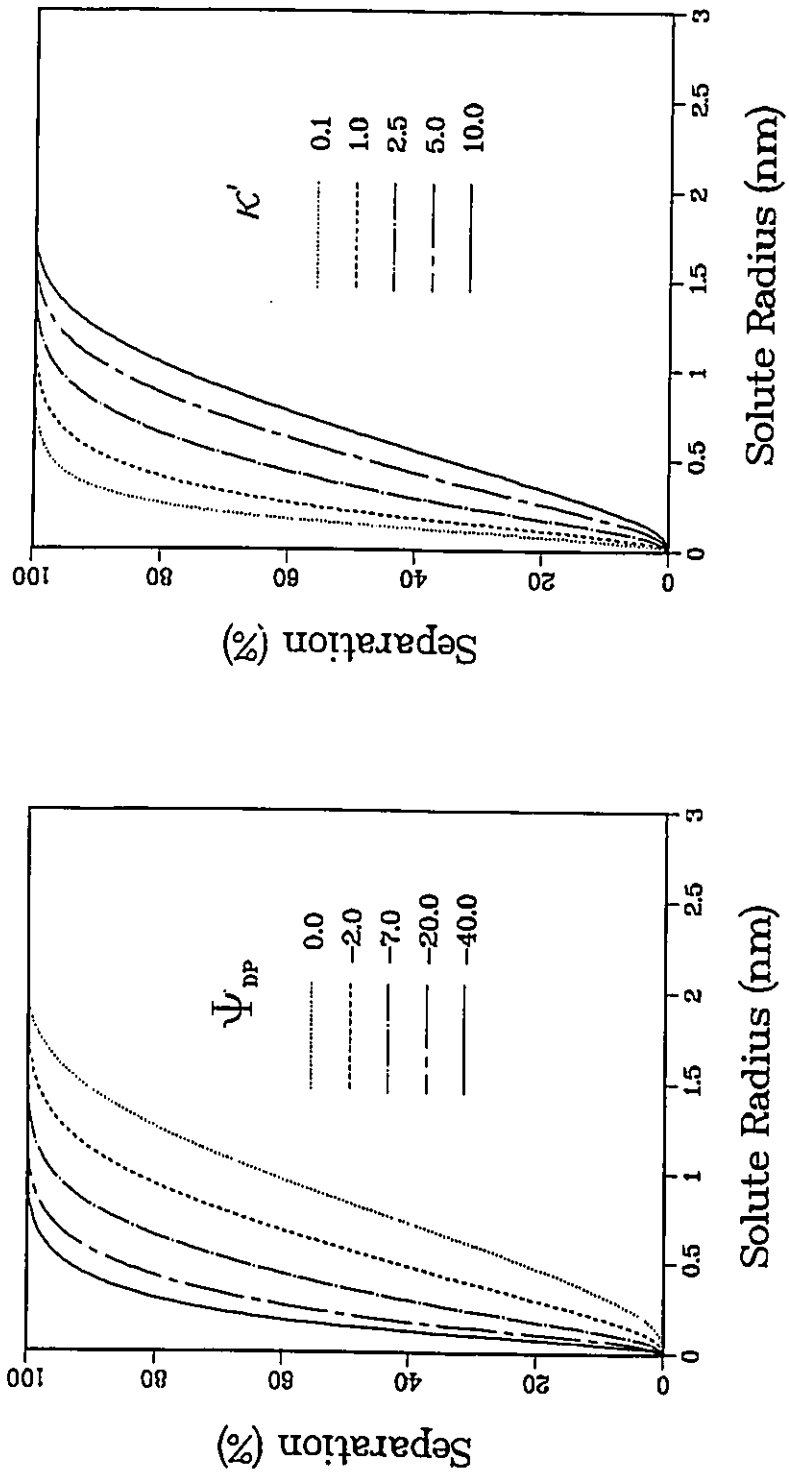

Figure 2.17: Separation vs. solute radius for structured solvent at the membrane surface, separation for Ψ_{DP} (nm^{-1}) variable and $\kappa' = 2.5\ nm^{-1}$ a) separation for κ' (nm^{-1}) variable and $\Psi_{DP} = -7.0\ (nm^{-1})$ b).

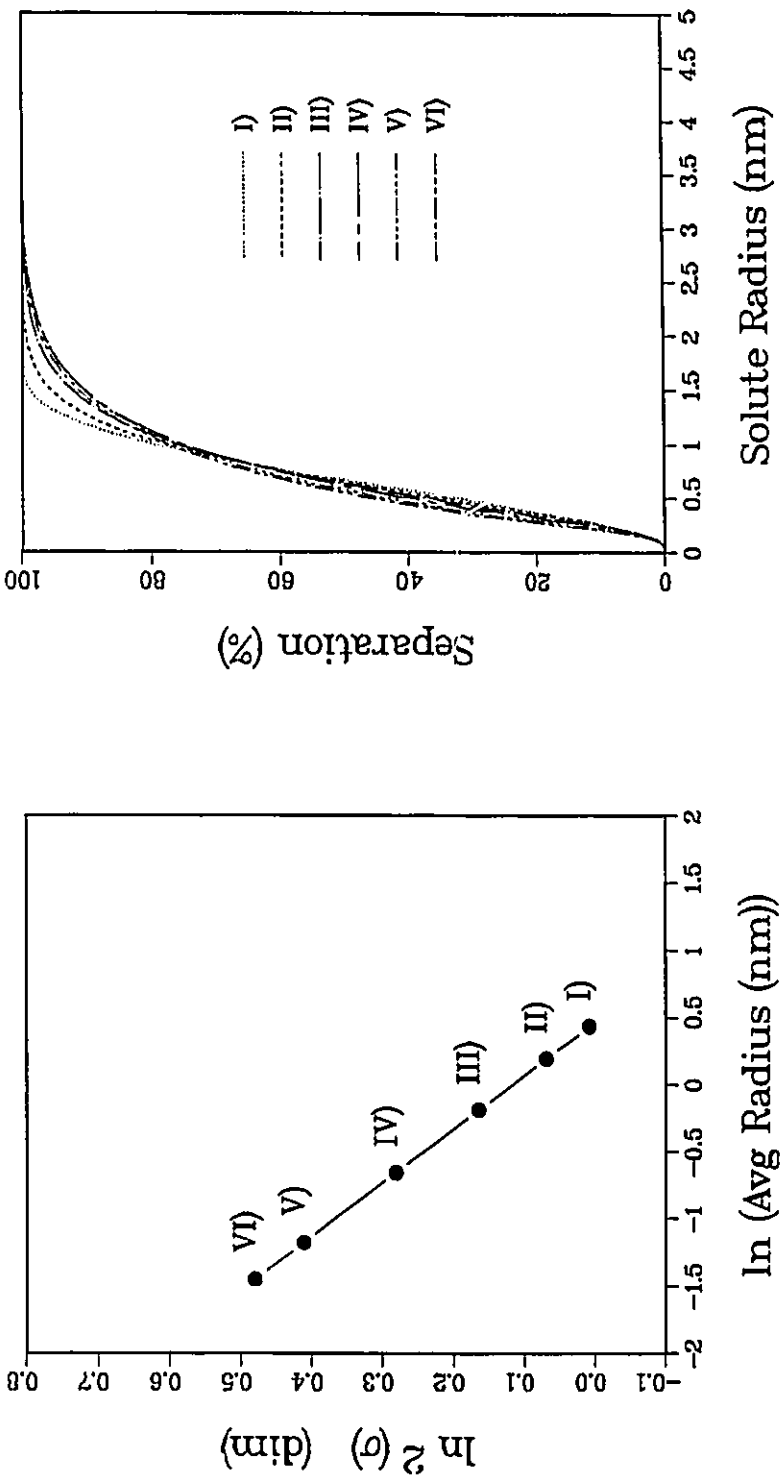

Figure 2.18: Effect of σ and the average pore radius on separation, $\overline{R_a}$ = 1.6 nm.

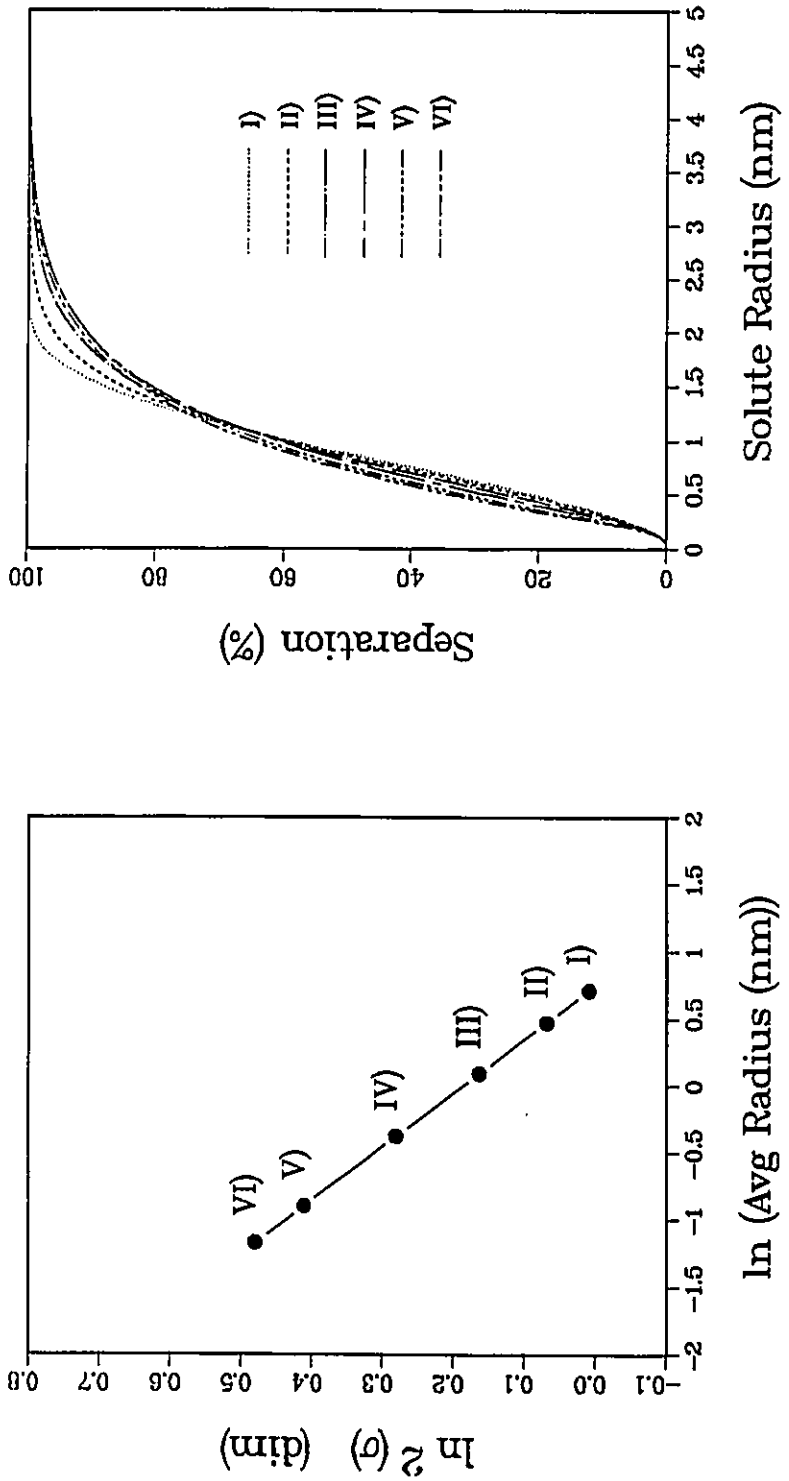

Figure 2.19: Effect of σ and the average pore radius on separation, $\overline{R}_a = 2.1$ nm.

Chapter 3

Cellulose Membranes

3.1 Literature Review

The most widespread use of cellulose as a barrier material is in the food industry where the high moisture permeability of cellophane film is desirable to prevent rotting and mildewing of fresh products. The use of extruded Cellophane film as a semipermeable membrane is severely limited due to its homogeneous morphology which results from the manufacturing method. Cellulose film was not considered in this work since the manufacturing procedure (extrusion) produces a homogeneous film of low permeability. This material is a bulk commodity item which has limited microstructural requirements and is often coated with lacquers to control its moisture permeability [61], a process which alters the nature of the membrane surface.

The most important use of cellulose as a material in synthetic membrane manufacture is in the biomedical area, specifically in dialysis and hemodialysis. Dialysis is a diffusion controlled process where the concentration difference across the membrane is the only driving force for separation. Cuprophane membranes make up 80% of the world market for hemodialyser units. Dialysis cartridges are produced by regenerating a cupriethylene solution into flat sheets or hollow fibres. The hollow fibre configuration resembles that of a shell and tube heat exchanger. As blood is circulated in the hollow fibres, water, creatine, urea, and chloride ion are transferred to a dialysis fluid at the exterior of the fiber. This fluid is usually a solution of lactate, acetate or bicarbonate.

The resistance of cellulose to solvent degradation has made it the preferred membrane material for use in membrane osmometry [62]. Cellophane membranes are prepared by regenerating cellulose xanthate (Viscose) solutions into thin films. They are gelled in water and must be preconditioned before use in an organic solvent. This is achieved by soaking in ethanol or acetone and subsequently in the solvent used in the osmometry experiment. The use of cellulose as a membrane material in this type of application is a definite proof of its morphological stability in organic media.

Regenerated cellulose has also been used as a hydrophilic support, to immobilize aqueous electrolytic solutions, in the manufacture of liquid membranes [27]. It is also used as an inert barrier material in membrane probes.

Cellulosics remain the work horse of the membrane industry. To this day, RO cellulose membranes do not exist. The highest sodium chloride separation reported to date is ~55% [63,64]. One of the objects of this work is to attempt to reduce the pore size of cellulose membranes and if this proves impossible, try to explain why these limitations exist.

3.2 Solutions of Cellulose

Most solutions described in the literature are not true "solutions" of cellulose since they involve the formation of a soluble intermediate which is usually regenerated to obtain the original cellulose. Cellulose xanthate is the most common solution intermediate and is obtained by treating cellulose with carbon disulfide followed by an aqueous solution of sodium hydroxide. The xanthate solution known as Viscose is then regenerated in a bath with sulfuric acid. A different type of intermediate can be obtained by reacting a solution of ammonial copper (cuprammonium) with cellulose. The compound can be regenerated by contact with an acid or an alkaline bath.

Over 60 solvent systems exist for dissolving cellulose and are listed in several excellent reviews [65,66,67]. The quality of these solutions are rather poor and the term dispersion used by some authors, is a more accurate description of the action of solvents on cellulose. Solution implies that normal fibre structure and fibril organization are destroyed. The criteria for dissolution are the optical, rheological and

filtration properties of the solution along with the amount and nature of undissolved particles. Herrick [68] reported that quality factors are not detailed in the literature and that the appearance of the cellulose solution is often deceptive.

Microscopic examination is often given as an additional test for dissolution [69, 70,71]. Such a criteria is suitable for the textile industry, where the main restriction imposed on solution heterogeneity is the ability to pass a casting solution through a spinneret to form fibres. This test is insufficient for the manufacture of RO and UF membranes. Solution imperfections such as microfibrils and mats up to 1 μm in length as observed in Reference [72] can create variations in the average pore size of the membrane, imparting several undesirable large pores or defects to the membrane, which reduces its selectivity towards one or several solution components.

3.3 Selecting a Solvent System for Cellulose

A potential solvent system for cellulose must meet certain stringent requirements for membrane making. From the literature on the formation of small pore cellulose acetate (CA), polyamide (PA), and polysulfone membranes [73,74,75], the guidelines for the choice of a suitable solvent system are as follows;

- The solution must form a tractable dope and dissolve over 10 wt.% polymer.
- The casting solution should be at a point of incipient precipitation.
- The removal of a volatile component should render the polymer insoluble.
- The major component of the solvent system should be miscible in the gelation bath.

The greatest problem in choosing a solvent system for this polymer, is that few good solvents capable of dissolving cellulose, in amounts greater than 10 wt.% are available. When such solvents are found in the literature, claims to form solutions of the quality required in membrane work remain questionable. On the basis of solvating power, the systems contained in Table 3.1 show promise. In this table, solvent systems 1 to 3 are true solvents, involving the formation of an electron donor

Table 3.1: Solution systems having the highest solvating power with respect to cellulose.

Solution System for cellulose	Formation of a chemical intermediate	Maximum cellulose concentration wt. %	D.P. of cellulose	Reference
1) LiCl/DMAc	NO [27]	3-15	570	[77,71,78]
		4	1700	[78]
2) LiCl/NMP	NO [27]	3-12	570	[69]
3) N-methylmorpholine N-oxide/water	NO [79]	10-25	N.A.	[80]
4) PF/DMSO	YES [78]	6-15	200-400	[81]

Where:

DMAc - N-N-Dimethylacetamide

NMP - 1-Methyl-2-Pyrrolidinone

DMSO - Dimethyl Sulfoxide

PF - Paraformaldehyde

D.P. - The degree of polymerization or the number of repeat units per molecule

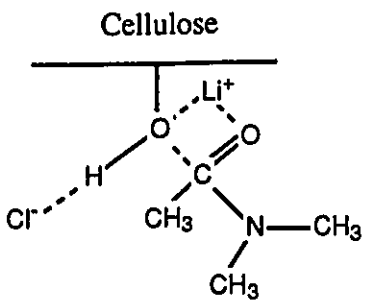

LiCl / DMA

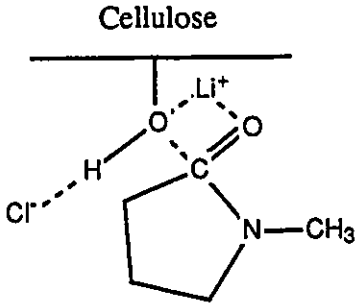

LiCl / NMP

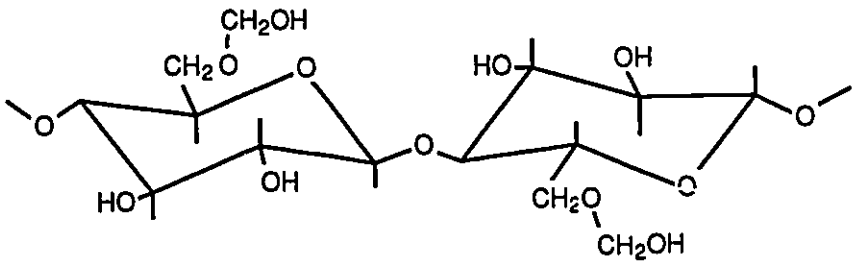

Methylol Cellulose (PF / DMSO solvent system).

Figure 3.1: Solubilized intermediates found in cellulose solutions.

acceptor (EDA) complex. The intermediate complexes proposed for systems 1 and 2 are shown in Figure 3.1 [76].

The high solubility of cellulose in the amine oxide system (item 3, Table 3.1) remains questionable, and might be due to a substantial degradation of cellulose [82]. System 4, Paraformaldehyde (PF)/Dimethyl Sulphoxide (DMSO), involves the formation of methylol cellulose which is soluble in DMSO. Cellulose can be regenerated by precipitation in methanol, water [81] or acetone [63]. There is evidence that fibres regenerated from the PF/DMSO system occlude PF [81].

Lafrenière [63] studied this solvent system as applied to the manufacture of RO membranes. Several membranes were cast using a 10.2 wt.% methylol cellulose solution in DMSO, these membranes had NaCl separations of 47.2% (NaCl 300 ppm. at 6892 kPag (1000 psig.)). Post treatments such as shrinking in hot acetic acid, ethylene glycol, toluene, glycerol, chlorobenzene, and dipentene, baths and crosslinking with formaldehyde were attempted without any substantial increase in NaCl separation.

The previous results obtained with the PF/DMSO system [63], the degradation of cellulose in the amine oxide solvent [81], and the lower solubility of cellulose in the LiCl/NMP system as compared to the LiCl/DMAc system [83] were considered in the selection of a solvent system. The LiCl/DMAc solution system was finally selected as a solvent, since it was a relatively new solvent which did not involve the formation of a chemically different intermediate in the dissolution procedure and showed most promise in producing RO cellulose membranes.

3.4 The Morphology of Cellulose Solutions

3.4.1 The fibrillar nature of cellulose solutions

The morphology of casting solutions, especially the nature of molecular aggregates in concentrated solutions, is of great interest in membrane making. The molecular aggregate of cellulose dissolved in organic solvents, such as the dimethylsulfoxide/paraformaldehyde (DMSO/PF) and hydrazine (N_2H_4/H_2) has been shown to exist in the form of chain-folded crystalytes with a fold period of ~25 nm [72]. This concept is similar to the folded ribbon model proposed by Manley [84], see Figure 3.2, for natural and regenerated celluloses. In this model single cellulose chains are folded in an antiparallel manner to form a micellar ribbon which is pleated on itself giving a planar zigzag structure. For most celluloses the protofibril has a fixed rectangular cross-section of ~ 3.5 x 2.0 nm and its length increases with molecular weight. For a viscosity average molecular weight of 65,000 the length of the protofibril is reported to be 38 nm [84].

The presence of intramolecular hydrogen bonds causes the cellulose molecule to fold onto itself. Manley states that protofibrils can be reconstituted from solution which implies that the chain can unfold and regain this conformation. Which leads to the conclusion that such a configuration represents the state of lowest free energy or highest stability of the cellulose chain. However no clear evidence of totally extended chains in solution are given and it is possible that the protofibril structure are not destroyed on solubilizing cellulose. Cellulose is a natural product and the ability of its chain to form protofibrils of constant rectangular section could be restricted to the synthesis process.

The shape and rigidity of the supermolecular aggregate present in the casting solutions can be determined from the slope of a plot of the viscosity at zero shear rate (η_0) vs. solution concentration. These measurements will be performed on a Haake M500 viscometer fitted with an SV II profiled cup and bob to minimize wall slip. Solutions containing 8, 10 and 12 wt.% cellulose (3:1 LiCl to cellulose ratio) will be tested.

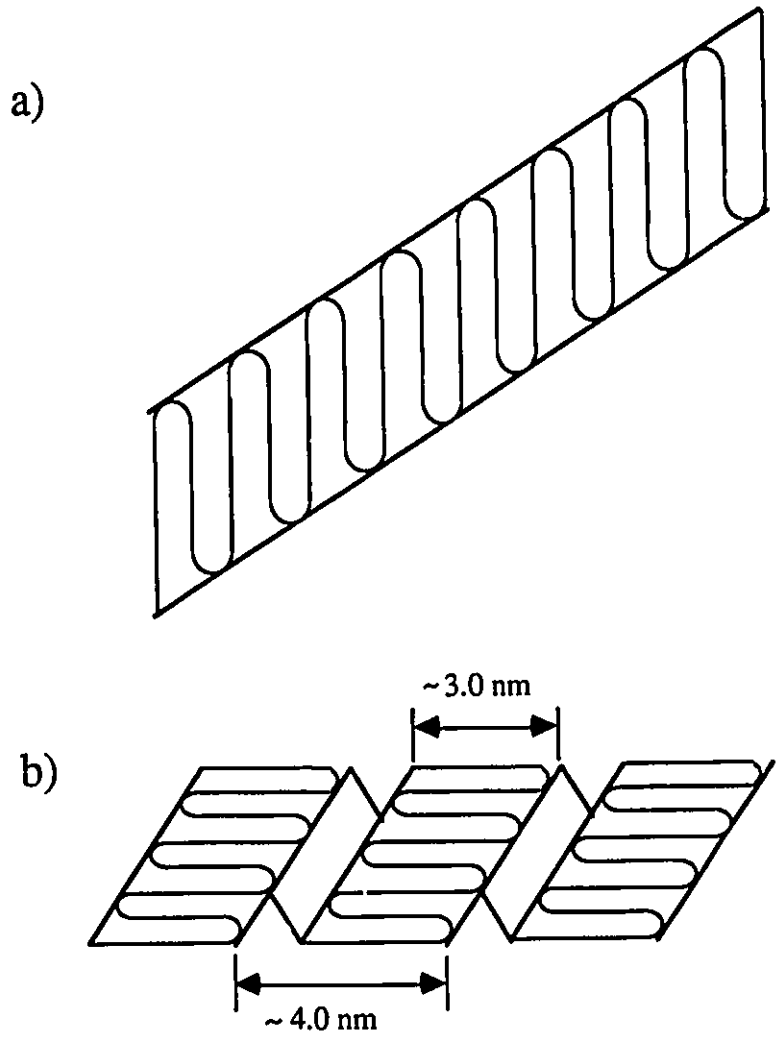

Figure 3.2: Model of a cellulose protofibril in the extended ribbon a) and the more stable, folded ribbon b) conformations. The structure in b) has a rectangular section of ~ 3.5 X 2.0 nm and a length of 38 nm, based on a molecular weight of 65,000 [84].

3.4.2 The effect of milling cellulose

Kouris *et al.* [88] found that milling reduced the degree of crystallinity of cellulose. Any crystallinity of cellulose was destroyed after pulverizing cellulose for 153 hrs. In order to determine if this had an effect on porosity, membranes were cast from two fractions 38-53 μm and <38 μm resulting from the dry milling operation.

3.4.3 Energy input on solubilization

From electron microscope examinations, Kolpak *et al.* [72] found that Fortisan rayon, a form of regenerated cellulose obtained from saponified cellulose acetate, consisted of microfibrils 4.0-5.0 nm in width aggregated into large fibres. They also observed that cellulose regenerated from PF/DMSO was fibrous but contained occasional mats measuring 0.7x0.7x1.0 μm. On ultrasonication some mats could be broken and were found to be composed of short rodlets 12.0 nm wide. On the other hand cellulose regenerated from hydrazine N_2H_2 consisted primarily of unoriented mats and some fibres. Two important observations can be made from Kolpak's work, no mats were observed when Fortisan was regenerated and to some extent sonication of PF/DMSO and Hydrazine/H_2O destroyed mats of undissolved cellulose.

These results indicate that the nature and amount of mechanical energy input on solubilizing cellulose, with a given solvent, affects the resulting solution morphology. In their study Kolpak *et al.* [72] claim that the ultrasonication of PF/DMSO solutions disrupts the undissolved fibrous mats, however, close observation of the electron micrographs (see Reference [72]) reveals that a substantial fibrous network remains after sonication.

A more localized and higher level of energy input must be used to destroy the mats and fibres. Homogenizing or the explosive decompression of particles passing through an orifice appeared very promising in this regard. Herrick [89] and Turbak [90], produced a 2% slurry of homogenized cellulose in water by passing an aqueous suspension of cellulose particles through a homogenizer at 55 MPa (8000 psig.). After 20 passes through the homogenizer, cellulose fibres had their diameters reduced from 2.3 to 0.1 μm , and a substantial increase in cellulose accessibility, reactivity and solubility was observed. The slurry was too thick to be homogenized above a concentration of 2% [89,90].

3.5 Preliminary Work on Casting Solution Homogenization

Homogenizing was attempted as a means to reduce the undissolved fibres and mats contained in the solutions. In a first test, a high pressure cylinder and piston assembly fitted with a homogenizing valve was used to evaluate the effect of homogenization on membrane performance. Mechanical problems occurred in the cylinder and piston unit after two passes at 6000 psig. Membranes produced from these solutions showed a slight increase in NaCl separation, it was also observed that any air pockets present in the casting solution were dispersed as fine bubbles which eventually created pinholes.

In view of these serious problems, a totally enclosed cyclic homogenizer was designed and constructed. Two high pressure cylinders were joined by a valve. Initially one cylinder contained a cellulose solution and the other was empty. The contents of these cylinders could be exchanged hydraulically by increasing the oil pressure on one side of the piston. The valve created a sudden expansion, which homogenized the casting solution by explosive decompression. This cycling procedure could be repeated as many times as desired.

Serious problems occurred at the O ring piston seals. N-dimethyl acetamide (DMAc) under high pressure (15,000-20,000 psi) would easily penetrate Kalrez and Viton O rings and destroy their binder material leading to the erosion of the O rings and an accumulation of O ring material in the treatment chamber. This destruction also occurred when nylon backup rings were used on the piston. Unfortunately, since these high pressures are needed to homogenize such viscous casting solutions, the equipment failed due to problems associated with the O rings. O rings were completely destroyed, even when they were manufactured from the most resistant perfluorinated elastomer available (Kalrez). Such a problem could have been amplified by the internal surface roughness of the cylinders. The erosion effects were not due to surface roughness alone since trials using distilled water showed no O ring wear. Confronted with these serious equipment problems, this promising method of solution pretreatment was dropped after a year of work and cellulose casting solutions were prepared by a more conventional dissolution method.

3.6 Membrane Making

Membranes used in this work were all prepared by the phase inversion technique. In this method, a single continuous phase is formed by dissolving a polymer in a suitable solvent which is then inverted by a process of drying or gelling to form a three-dimensional macromolecular network or gel. After removal of the solvent, the precipitated polymer forms the continuous phase of a porous structure which can be used as a barrier material.

The polymer solution used in producing membranes by the phase inversion method is termed "casting solution". Phase inversion can occur via the wet, dry or thermal processes as described in References [91] and [7].

In the dry process a volatile component is removed by evaporation creating a turbid two-phase polymer solution which can be gelled on further removal of the volatile component. This technique is mainly used to produce microporous membranes having pores above 0.1 μm. In the thermal process, a polymer is dissolved by a substance which is a solvent at high temperatures ($\sim 220^{\circ}$C) and a non-solvent at room temperatures. Phase inversion occurs when the temperature of the casting solution is reduced. The high temperature solvent is then removed by leaching with a volatile liquid such as an alcohol, a ketone, tetrahydrofuran or heptane. Porosity ranging from a totally nonporous to a microfiltration barrier, can be obtained with this technique.

On immersion in the gelation bath the polymer solution present at the gelation bath - solvent interface is immediately precipitated and solvent is leached out of the polymer solution. The solvent is then exchanged for the gelling agent by a process of diffusion. The exchange continues until virtually all of the solvent leaves the cast layer and a porous polymer matrix is formed.

The resulting membrane will have different morphological characteristics, depending on the rate of influx of precipitant and the rate of removal of solvent from the skin layer. Such relative exchange rates are influenced by the difference in chemical potential of the solvent and precipitant across the skin layer. If the solvent is not completely removed during the evaporation step, the precipitation of polymer in the skin layer is faster than that of the polymer under the skin layer. This leads to a difference in morphology or porosity in these two regions and gives rise to an

asymmetric membrane structure. This feature is highly desirable since very dense, thin selective layers can be supported by a thicker porous sublayer. This type of arrangement yields a membrane with increased flux for a given permselectivity. If the solvent is entirely removed during the evaporation step, this reorganization cannot occur and an undesirable dense film having a lower permeability is obtained.

Several variables such as the casting solution composition, evaporation time and temperature, and the nature and temperature of the gelation bath, affect the resulting membrane. The effect of these factors on the formation of cellulose membranes will be determined in this work.

Chapter 4

Experimental

4.1 Characterization and Pretreatment of Cellulose

The polymer used in this study was a Baker Co. reagent grade, acid washed, ash-less powder of cellulose suitable for chromatographic use. This "raw" cellulose was unsuitable for membrane preparation since it contained several large chunks of material which could not be readily dissolved in the LiCl/DMAc solvent system. Since solvent accessibility to pure cellulose is greatly influenced by its particle size [89], it was decided to mill the "raw" cellulose into two individual fractions of 38 to 53 μm (38-53 μm) and another containing particles of less than 38 μm (< 38μm).

The "raw" cellulose was milled in a high impact vibratory mill. Such a device was produced by loading a ceramic ball mill, with 0.01 m Corundum (Aluminium Oxide) balls, placed into a standard 1 imperial gallon paint container lined on the inside with 2.5 cm of high density neoprene. The entire assembly was then placed in a paint shaker. The high impact collision of the ceramic balls was very efficient in grinding cellulose to a finer particle size. The mill was cleaned by processing several 100 cm^3 volumes of dilute hydrochloric acid for a period of several hours in order to remove any loose Corundum chips and particulates. The cleaning procedure was repeated several times using distilled water over a period of a week after which a clear rinse water, having the same pH as that of distilled water, was obtained. Small batches containing 50 g of raw cellulose were milled in this fashion until 400 g of the 38-53 μm fraction and 300 g of the <38 μm fraction were obtained. The resulting

particle size distribution for the "raw", or as "received cellulose" and the milled cellulose are given in Table 4.1.

Table 4.1: Cellulose particle size distribution before and after milling.

Particle Size μm	Cellulose "as received" wt.%	Cellulose Dry Ground in Vibratory Mill wt.%
> 53	32.97	33.65
38-53	55.00	16.53
< 38	12.03	49.85

The molecular weight of cellulose was determined by intrinsic viscosity measurements in a cupriethylene-diamine solution, obtained from GFS Chemicals, Columbus Ohio, as per ASTM D1795-62 [92]. The intrinsic viscosities of both the original and milled celluloses were found to be 2.208 and 1.934 respectively. These values represent molecular weights of 68,000 and 60,000 for the original and milled celluloses.

All solutions were prepared as described in Turbak *et al.* [71]. This dissolution procedure is a three step procedure where the "raw" cellulose is first contacted with a swelling agent to open its pores, the swelling agent is then exchanged with DMAc and finally this "pretreated" cellulose is dissolved in a solution of LiCl/DMAc. Both fractions of cellulose were individually contacted with 4 kg of water, allowed to stand overnight and decanted. This water contacting procedure was repeated four times. Small batches of the cellulose were dam squeezed under house vacuum, in a 12 cm diameter Buchner funnel for a period of 15 min. The water swollen 38-53 μm and <38 μm fractions weighed 1.6 kg and 1.2 kg respectively.

The water swollen cellulose fractions were then individually contacted in a 4 L Wharing blender with equal weights of filtered reagent grade DMAc. The mixture was then blended at high speed for two 5 min periods, transferred into a beaker and allowed to sit overnight. The mixture was then decanted and four equal portions were dam squeezed for a period of 45 min, recombined and contacted with fresh DMAc. This procedure was repeated three times and a fluffy cellulose which could be dissolved readily in the LiCl-DMAc solvent was obtained. These final dam squeezed

portions were combined and stored at −10°C for future use. Two "pretreated" fractions were obtained, and labeled as 38-53 μm and <38 μm.

Care was taken not to remove all the DMAc in the "pretreatment" step. In an attempt to remove most of the water from the treated cellulose before dissolution, the treated cellulose was squeezed in a hydraulic press until a solid cake was obtained having the composition shown in Table 4.2. Cellulose prepared in this fashion would not dissolve in the LiCl-DMAc solvent. This indicates that both small amounts of water and a more open pore structure are necessary in the initial steps leading to the dissolution of cellulose with this solvent system. Dam squeezing provided just the right amount of DMAc and water removal. The composition of the "pretreated" cellulose polymer is given in Table 4.3.

Table 4.2: Composition of the milled and "pretreated" celluloses.

Component	Baker Reagent Grade without treatment		Cellulose "Pretreated" Cellulose Hydraulicaly pressed	
	wt.%	Standard deviation n=9	wt.%	Standard deviation n=6
cellulose	95.69	-	54.15	0.34
water	4.31 ‡	0.29	11.83 ‡	0.10
DMAc	-	-	34.02	-

‡ Karl-Fisher analysis

Several swelling agents less polar than water are proposed in Reference [71]. Preliminary dissolution studies were carried out on several of these agents. The results of these tests are summarized in Table 4.4.

Slight dissolution was obtained when acetone, methanol, acetonitrile and tetrahydrofuran were used as swelling agents while no dissolution occurred when ethanol and 2-propanol were used. Swelling with water gave the best results and it was decided to use this agent in the preparations of all casting solutions.

Table 4.3: Composition of pretreated celluloses prepared by dam squeezing.

Component	"Pretreated" Cellulose no milling Dam squeezed		"Pretreated" Cellulose milled, < 38 μm Dam squeezed		"Pretreated" Cellulose milled, 38-53 μm Dam squeezed	
	wt.%	Std. Dev. (wt.%)	wt.%	Std. Dev. (wt.%)	wt.%	Std. Dev. (wt.%)
cellulose	36.31 †	0.14 (6)	42.58 †	0.38 (4)	39.85 †	0.23 (4)
water	16.68 ‡	0.14 (15)				
			57.42 *	–	60.15 *	–
DMAc	47.01	–				

( ) Number of repeats

† Gravimetric analysis

‡ Karl-Fisher analysis

* Combined water and DMAc

Table 4.4: Solution preparation using various swelling agents for a solution containing, 13.6 wt.%, LiCl 9.7 wt.% and DMAc 76.6 wt.%.

Swelling media	Observations
H_2O	Good dissolution
acetone	Slight dissolution
methanol	Slight dissolution
ethanol	No dissolution
2-propanol	No dissolution
acetonitrile	Slight dissolution
tetrahydrofuran	No dissolution

In order to prepare casting solutions, it was necessary to know how much cellulose was present in the pretreated material. The total solids content for both milled fractions was determined by weighing approximately 4.5 g of pretreated cellulose and heating it in an oven at 105°C for two days. These results are summarized in Table 4.3. The amount of water present in the initial and pretreated celluloses was determined using a Karl-Fisher titration. Water was first extracted from ~4.0 g of the powders by contacting them with 50.0 cm^3 of dry methanol. The results of this analysis are listed in Table 4.2 with relevant standard deviations.

A large amount of condensation appeared on the walls of the reactor vessel at the start of the dissolution procedure and eventually dissapeared after one or two hours of stirring. It was assumed that most of the water contained in the pretreated cellulose would be released during the overnight dissolution period and that this factor would not appear as a variable in the analysis. In view of this, the amount of water contained in the pretreated fractions of the milled celluloses was not measured and the amount of solids contained in the casting solution was determined gravimetrically.

4.2 Casting Solution Preparation

A standard 0.5 L reactor vessel (Corning) was used to prepare all the casting solutions. The temperature of the solution inside the vessel was held constant by using a proportional integral derivative (PID) controller with a thermocouple probe directly immersed in the casting solution (see Figure 4.1). A stream of dry nitrogen provided a blanket over the solution preventing water contamination from the surrounding air and entrained any water vapor released from the solution.

Impurities such as small particles and fibres were found in the reagent grade DMAc and LiCl. Attempts to filter the casting solutions at temperatures of 90°C and pressures of 1500 psi were unsuccessful due to high solution viscosities.

Saturated solutions of LiCl contained a visible rust colored colloidal suspension which could be remove by filtration. This color was present in LiCl originating from three independent sources. A saturated solution of Lithium Chloride (Anachemia) was prepared by dissolving 0.5 kg of LiCl in 0.6 kg of boiling distilled water, filtered using a steam jacketed Buchner funnel and then recrystallized. This filtration-recrystallization procedure was repeated seven times.

The presence of small amounts of water in the hygroscopic LiCl was found to noticeably reduce the solvating power of the resulting LiCl/DMAc solvent. For these reasons, extensive efforts were deployed in order to keep water out of the extremely hygroscopic LiCl prior to its dissolution. The saturated LiCl solution, decribed above, was dried in a muffle furnace at 400°C for one day. The dry LiCl cake was then ground in a vibratory mill and the resulting pure white powder stored in a desiccator for future use.

Reagent grade DMAc (Fisher Scientific Co.) was contacted with molecular sieves in order to remove trace amounts of water. The solvent was then filtered using a 0.1 μm teflon filter.

Depending on the desired solution composition, given amounts of the DMAc and LiCl were added to a reaction kettle, see Figure 4.1, and stirred at 90°C for a period of one hour. This assured the complete dissolution of LiCl and the formation of a LiCl-DMAc complex. The "pretreated" cellulose was then added to this solution and the temperature held at 90°C for a period of 10 minutes after which the temperature was lowered to 70°C for a period of 4 hours. After this period, the vessel and stirring

rod were weighed and the amount of DMAc lost due to evaporation was replaced with fresh DMAc. The casting solution was stirred overnight under a nitrogen atmosphere at a temperature of 30°C after which the assembly was weighed and a suitable amount of DMAc added. After stirring for an extra hour the solution was transferred to a jar and hermetically sealed with Parafilm and stored in a refrigerator at 10°C for future use.

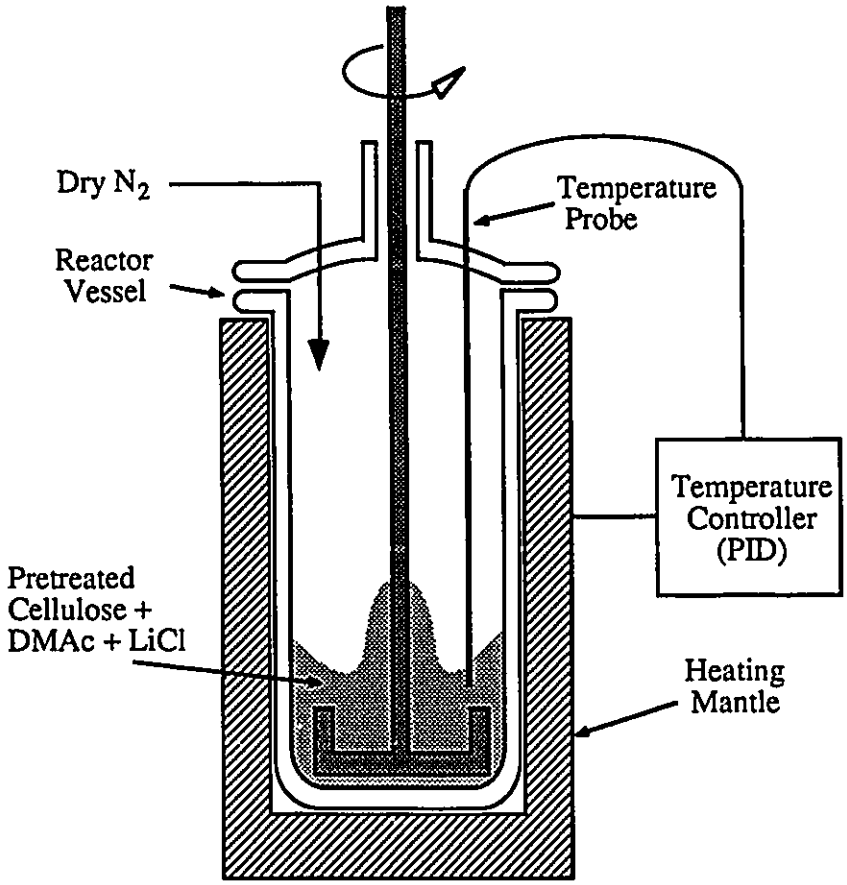

Figure 4.1: Schematic diagram of the mixing vessel.

4.3 Membrane Making

Casting solutions containing low concentrations of cellulose were clear viscous liquids while those containing higher solution concentrations were translucent, pasty gels. These solutions were too thick to be transferred directly from a storage container to the casting plate without a substantial amount of air being entrapped in the solution. Casting under such conditions was impossible since the presence of small air bubbles created pinholes in the final membrane.

A method for transferring viscous casting solutions onto a casting surface was developed where a hypodermic syringe was filled with casting solution, placed inside a standard 30 mm centrifuge holder and spun in an IEC Clinical Centrifuge centrifuge at moderate speed for a period of 15 min. The tip of the syringe was then severed leaving an 8 to 10 mm opening at the head of the syringe. The content of the syringe was extruded as a bead, one cm from the edge of a rectangular pyrex casting plate measuring 0.18 x 0.28 m. The bead of casting solution was then spread across the plate using a 0.15 m wide casting bar having a recessed 0.254 mm gap (0.01 in). This left a thin layer of casting solution on the surface of the pyrex plate. The plate was then placed in a forced air convection oven (Blue M Electric Co.) and held at a set temperature for a given amount of time. Dry air was fed to this oven at a rate of 0.29 m^3/min @STP which limited the accumulation of solvent in the oven and permitted a constant supply of fresh air to the surface of the cast film during the evaporation step.

The plate was then quickly immersed in a gelation bath of water or acetone held at 3-4°C and allowed to soak overnight. The polymer film was then transferred to a water bath held at 25°C and cut into 6.5 cm diameter coupons for testing. Membranes made using this casting procedure were found to be free of pinholes caused by air entrapment.

4.4 Membrane Testing and Automation

4.4.1 Conventional membrane testing

Conventionally membranes are tested according to the scheme shown in Figure 4.2. Several test cells connected in series or in parallel linked to a pump, a back-pressure valve and feed solution reservoir form the test system. The test cells have two separate chambers which are separated by the semipermeable membrane. The feed compartment is designed to produce a maximum fluid velocity parallel to the surface of the membrane in order to reduce concentration polarization at the surface of the membrane. Permeate from the low pressure side of the membrane is discharged to the atmosphere and can be collected in a sample bottle.

In the conventional scheme, membranes are cut into coupons, placed in test cells and pressurized for two hours using pure water at 20% above the desired operating pressure. The membranes are then allowed to rest for 1 hour before testing.

Pure water is circulated under pressure throughout the test system, ~10 cm^3 of permeate are then collected and the mass flowrate of permeate or "pure water permeability" (PWP) is then determined by weight difference. A dilute solution of the probe solute termed "feed solution" is then circulated under pressure through the test system. Approximately 10 cm^3 of permeate are collected and the mass flowrate of permeate or "product rate" (PR) determined by weight difference. The concentration of the permeate and feed solutions are determined by total organic carbon (TOC) analysis for solutes containing carbon and by conductivity measurements for electrolytes.

The entire testing procedure is repeated for eight to ten solutes having a range of molecular weights. Solute sizes are selected to span the entire range from 0 to 100% separation. The PWP, PR and separation data for all solutes are entered manually on a VAX microcomputer. This data is then combined with physico-chemical data of the respective "probe" solutes. The pore size of the membrane can then be determined by fitting a suitable restricted transport model to the data.

The main bottle necks in obtaining the pore size of a membrane is in performing the permeation experiments for all the solutes, in analyzing the permeate solutions, in entering the data into a computer and merging physico-chemical information to the permeation data. For a bank of twelve test cells, a single complete permeation

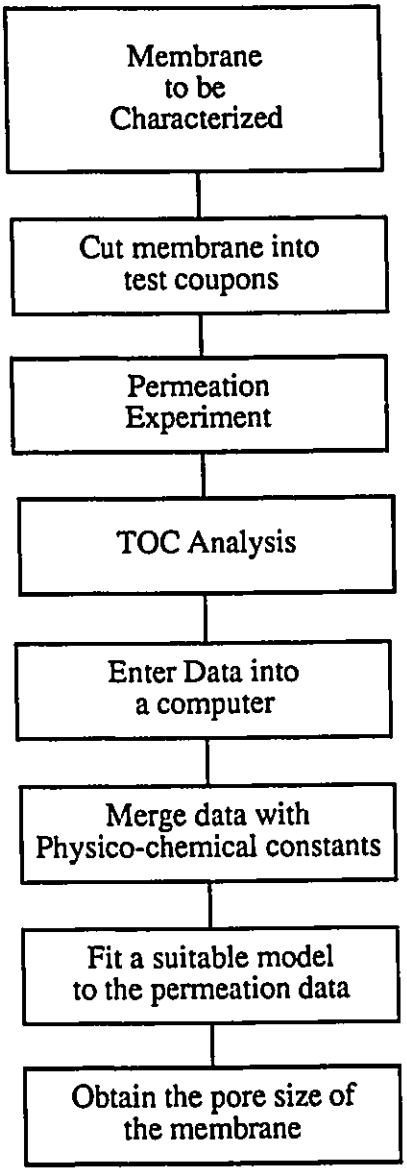

Figure 4.2: Membrane testing procedure.

run, including analysis, can be performed per day. In order to obtain a statistically significant evaluation of the pore size, at least ten to fifteen runs must be performed on each set of membranes which implies a testing rate of 4 membranes per week. This is not a very practical means of characterization.

In order to render this method more useful in determining the pore size of a membrane the points mentioned above were accelerated by the use of robotics, and the data input and manipulation were handled by a custom designed software both described in the following section.

4.4.2 Automation

The amount of time required to obtain membrane permeation data can be greatly reduced by the use of automation and robotics in the testing procedure. In the manual testing scheme, a set of tests which would provide a series of statistically meaningful results can take up to three working weeks to perform. While an automated test system capable of performing 3-5 permeation runs per day can do the same work in less than one working week.

An automated membrane testing unit was specifically designed, as part of this work, to perform the permeation runs. Special attention was given to conserve and if possible improve the accuracy of the original testing procedure. The system was designed to reproduce the mechanistic actions of a human being performing the permeation tests. The microprocessor controlled robot can perform a sequence of permeation runs 24 hours a day, 7 days a week with a high degree of reproducibility.

In the conventional testing scheme the operator's undivided attention was required for the duration of the tests which usually last one working day. The operator of an automated system must tend to the unit for one hour a day after which he/she is free to pursue other work.

Details of this particular system have been published elsewhere [93], and only a general discussion of the unit is included in this work. The automated testing system shown in Figure 4.3 consists of a loop containing a distilled water rinse tank, a set of three feed tanks, a pump, a pressure regulator, two banks of six test cells and a rotameter. A total of eight solenoid valves are used to selectively circulate the rinse and feed solutions through the set of twelve test cells linked in series.

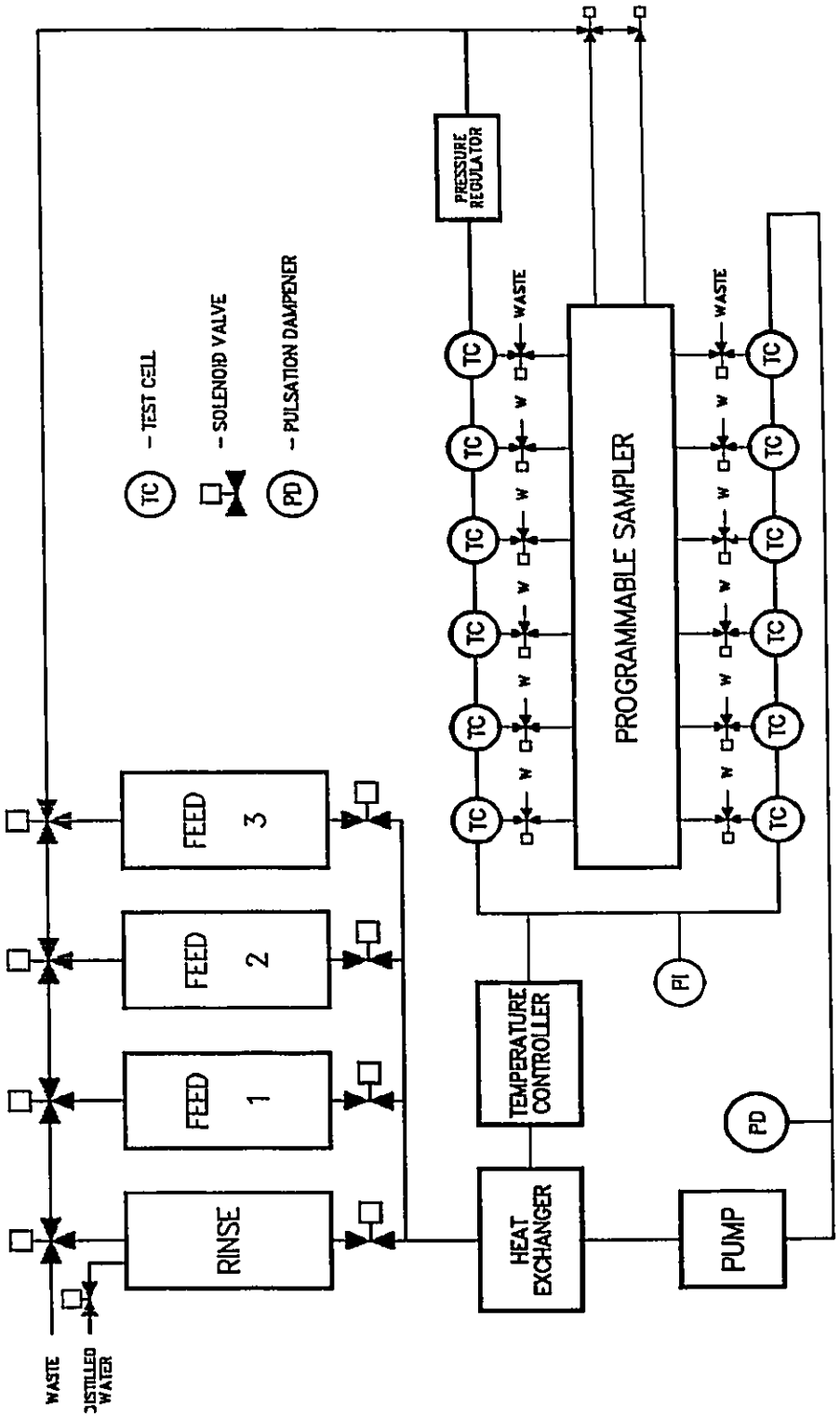

Figure 4.3: Flow diagram of the automated membrane testing apparatus designed and used in this study.

The system is designed to accommodate different types of test cells be they hollow fibre, plate and frame or tubular. The cells used in this work are standard RO/UF test cells described in Reference [7] which have an effective test area of 10.75 cm^2.

The temperature of the feed solution is controlled at 25.0 $\pm$0.1°C by a PID controller and a thermistor probe incorporated into the flow loop. The pressure is regulated to $\pm$1% of the set operating pressure. Permeate from a test cell can be directed, via a three way solenoid valve, to the programmable sampler or to waste. The permeate stream sent to the sampler can in turn be directed to a sample bottle or to waste. This arrangement provides for the purging of all lines before any samples are taken. The sampler can sample all test cells at once and stop sampling once a sufficient amount of permeate is collected. Separate lines are provided to sample the feed solutions before and after the permeation run. The twenty two solenoid valves and pump shown in Figure 4.3 are all controlled by a IBM-XT microcomputer which coordinates their actions. A specially designed computer program, written in Assembly and Q-Basic languages permits an operator to collect a sufficient amount of sample to determine the PWP, PR and separation for the permeation of three feed solutions.

A data management software was designed to keep track of all data produced by the automated systems including the TOC analyzer discussed bellow. This piece of software automatically transforms the information generated on a run basis into information for each test cell. It then combines the permeation data with a physico-chemical data bank on the properties of solutions containing the probe solutes. The final product is a file containing all the necessary data for a specific test coupon which can then be processed by a mainframe computer to determine the pore size of the membrane. The scource code listings for these programs have not been included in this work due to the "equipment specific" nature and size (180 pages) of the programs.

4.5 Determining Solute Concentration using TOC Analysis

The rapid and routine analysis of a solution containing ppm quantities of a probe solute poses a rather difficult problem. The use of a method involving a specific chemical reaction is out of the question since the probe solutes are quite different in composition. However, by limiting the choice to solutes containing carbon, solution concentration can be determined by reacting the solute with oxygen over a catalyst to give CO_2. This method known as Total Organic Carbon (TOC) analysis is well developed and has been in use for several years. In this method, a known amount of solution ranging from 1 to 4000 μL is drawn into a syringe and injected over a bed of catalyst held at 950°C. Substances containing carbon are transformed into CO_2 and the reaction gases are removed from the bed enclosure by a stream of CO_2 free air and analyzed for carbon dioxide content using infrared absorption.

The reproducibility of this method is greatly affected by the ability of the operator to physically transfer the solution onto the catalyst bed. This procedure is rather difficult since, in many cases, the solution does not land directly onto the bed and goes unreacted. The solution injected onto the catalyst reduces its temperature, which decreases its activity. This has a direct effect on the rate of transformation of carbonacious molecules to CO_2 and influences the TOC measurement if injections are not done at regular time intervals. The repetitive injection of solution at ~3 minute intervals cycles the temperature of the catalyst which in turn affects its activity. Finally in many cases only peak heights are measured from the IR analyzer where an integration of the signal from the IR analyzer would provide greater reproducibility. This manual injection procedure gives a reproducibility of ±2-3 %. According to Equation 2.3 this method would give separation measurements having a variation of ±4-6 % which is unacceptable for membrane characterization.

An added difficulty with this method is that it can take 10 to 15 min to obtain a TOC measurement. Since the collected permeate must be analyzed, a serious bottleneck in the automation procedure occurs when the permeation equipment is used.

This reproducibility in TOC measurement can be improved to ±0.5% by automating the injection procedure and by integrating the peak obtained from the

IR analyzer. This gives errors of ±1% in separation measurements which are quite acceptable for membrane characterization.

An automated TOC analyzer was produced by combining four pieces of equipment, the oven of a Beckman 915-B analyzer, a Beckman 865 Non-Dispersive infrared analyzer, a Hewlett Packard 7673A autoinjector and a Hewlett Packard 3393A integrator. This equipment was arranged as shown in Figure 4.4. A throughput of 100 samples a day could be obtained which was sufficient to handle the supply of samples from the automated membrane tester. The catalyst was changed only twice since the assembly of the system for a total of ~300,000 injections. This automated TOC analyzer was used to determine the concentration of the test solutions used in this study.

4.6 Flushing the Permeate Compartment

In this test, the volume of permeate required to flush the permeate compartment of the test cell was determined. This was achieved by monitoring the conductivity of the permeate as a function of eluted volume. A UF membrane having no NaCl separation was placed in the test cell, solute concentration was measured by a miniature conductivity cell while the eluted permeate volume was determined by counting the number of drops flowing out of the permeate compartment (droplet counts were calibrated in cm^3).

A 200 ppm NaCl solution was circulated in the feed compartment until the concentration of the permeate stabilized at 200 ppm. The feed solution was then changed to distilled water and the concentration and eluted volume measurements recorded. The same procedure was repeated in reverse by changing the feed to a 200 ppm NaCl solution. The results of this study are shown in Figure 4.5(a) and (b).

The results of this study indicate that after a change in the feed solution, once 10 cm^3 of permeate have eluted through the test compartment, less than 0.5% of the original solution remains in the permeate.

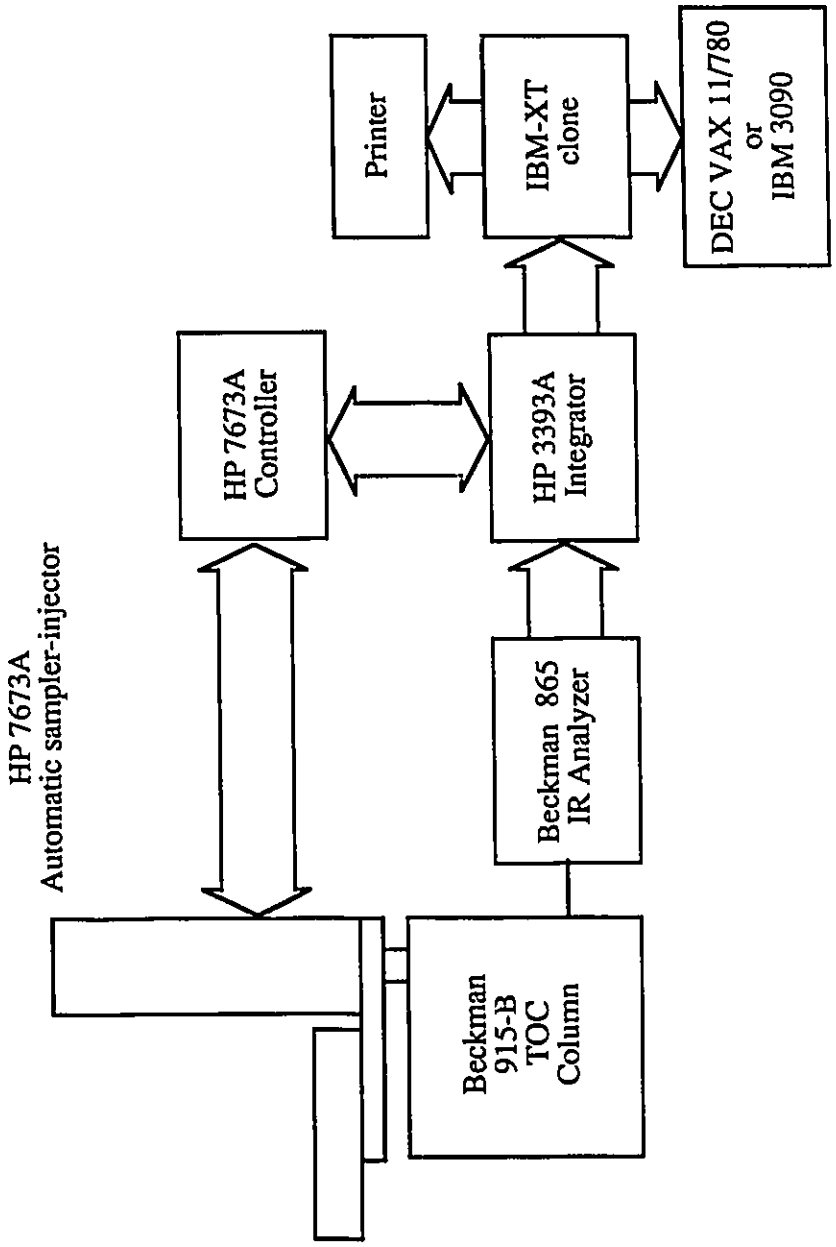

Figure 4.4: Schematic diagram of the automated total organic carbon analyzer designed and used in this study. Arrows indicate the direction of data transfer.

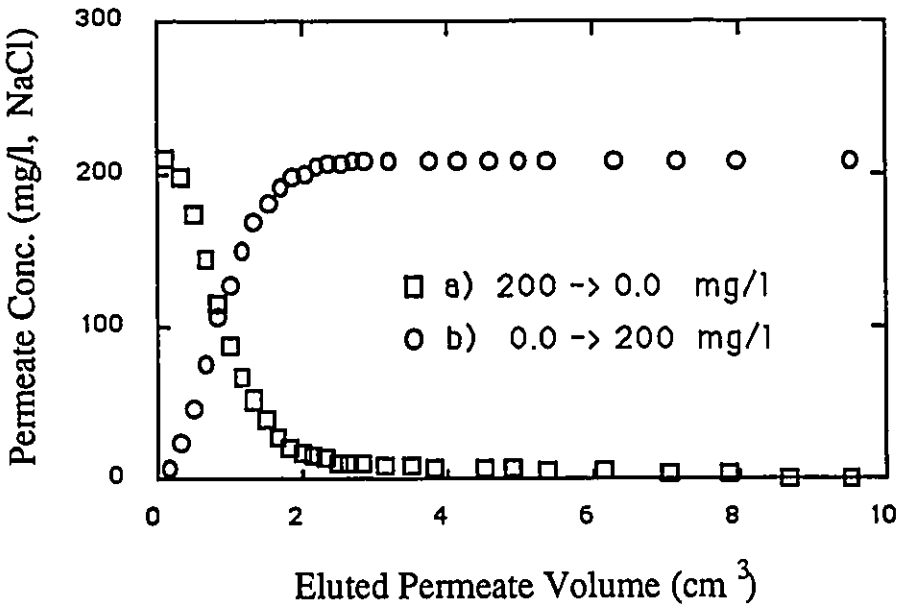

Figure 4.5: Concentration of the permeate as a function of the eluted volume.

4.7 Data on the "Probe" Solutes

The probe solutes used in this study are PEG200, PEG400, PEG1000, PEG6000 (BDH Chem. Co.), PEG300, PEG600, PEG1540 (J.T. Baker Chem. Co.), ethylene glycol, NaCl (Anachemia), d-sorbitol, sucrose, meso-erythritol, xylitol, glycerol (Aldrich Chem. Co.), raffinose (Calbiochem SanDiego), and ethanol 95% (Commercial Alcohols Ltd.).

A predictive equation for the radius of PEG, a_s, as a function of molecular weight was obtained by combining the data from References [94] and [95]. The solute radius, a_s, from [94] and the unperturbed radius of gyration from [95] vs. the square root of the molecular weight of PEG at 25°C were found to be linearly correlated as seen in Figure 4.6 [1]. This relation was expressed as follows,

$$a_s \text{ (nm)} = 0.02620 \cdot (\text{PEG Mol.Wt.})^{\frac{1}{2}} - 0.03 \qquad \text{for } r^2 = 0.9995 \qquad (4.1)$$

The molecular size of other solutes used in this work were taken from [27] and [7] and are listed in Table 4.5 along with the other PEG solutes.

The diffusivity of PEG was correlated with the inverse of the solute radius, using the data from [96] taken at 25°C, the following correlation was obtained,

$$D_{AB} \text{ (m}^2\text{/s)} = \frac{0.24424 \cdot 10^{-9}}{a_s \text{ (nm)}} \qquad \text{for } r^2 = 1.000 \qquad (4.2)$$

These physico-chemical data were used in all calculations to determine the pore size of the membranes.

[1] The value for PEG6000 from Reference [94] was excluded from this estimate since it is considered an outlier.

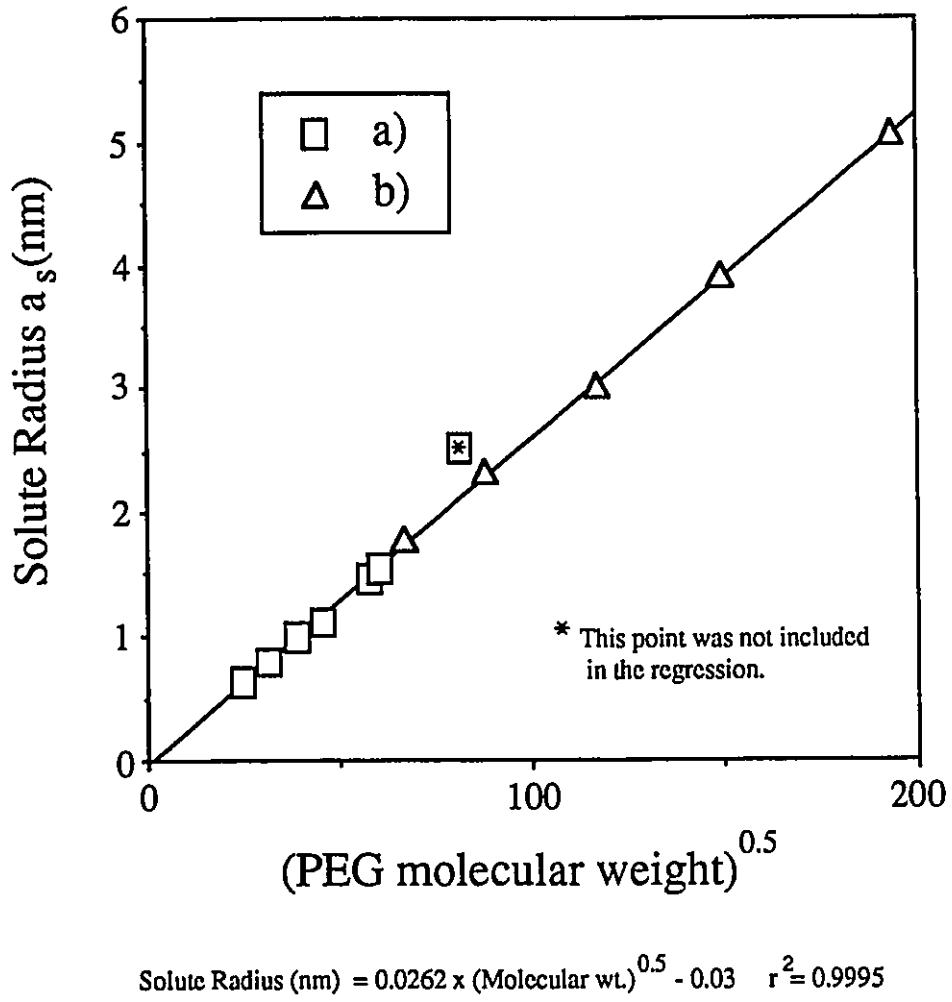

Figure 4.6: Solute radius a_s vs. the square root of the molecular weight, data obtained from References [94] a) and [95] b).

Table 4.5: Solute radius a_s, diffusivity D_{AB} and overall solubility parameters δ_{SP} of the probe solutes used in this work.

"Probe" Solute	Molecular wt.	a_s nm	D_{AB} $\times 10^9 m^2 s^{-1}$	$\delta_{SP} \times 10^{-3}$ † $(J\ m^{-3})^{1/2}$
PEG200	200	0.39 [94]	0.633[96]	19.25
PEG300	300	0.47 [94]	0.524[96]	19.22
PEG400	400	0.53 [94]	0.463[96]	19.21
PEG600	600	0.63 [94]	0.389[96]	19.19
PEG1000	1000	0.79 [94]	0.309[96]	19.18
PEG2000	2050	1.10 [94]	— [96]	19.17
PEG3000	3350	1.46 [94]	— [96]	19.16
PEG4000	3650	1.54 [94]	0.159[96]	19.16
PEG4000	4500	1.74 [95]	—	19.16
PEG6000	6750	2.12 [Eqn.4.1]	0.0976[96]	19.16
PEG9000	7746	2.29 [95]	—	19.16
PEG20000	13470	3.02 [95]	—	19.16
PEG37000	22445	3.90 [95]	—	19.16
PEG100000	37640	5.05 [95]	—	19.16
sucrose	342.3	0.51 [27]	0.56[94]	44.48
raffinose	594.5	0.65 [27]	0.41[94]	43.25
ethylene glycol	62.07	0.21[94]	1.12[94]	30.33
ethanol	46.07	0.21 [7]	1.28[94]	25.73
glycerol	92.09	0.23[7]	0.940[94]	33.50
erythritol	122.12	0.28 [7]	0.819[94]	35.58
xylitol	152.15	0.30 [7]	0.741[94]	37.03
sorbitol	182.2	0.33 [7]	0.68[94]	38.14
NaCl	58.44	0.152[56]	1.61 [56]	—
casein	23000	3.67 [7]	0.0343 [7]	—

†- Calculated from group contributions reported in Reference [7].

4.8 Experimental Plan

In order to prepare small pore cellulose membranes, it is important to gain some knowledge about cellulose casting solutions and the membranes they produce. An experimental program was designed to study two important features of the membrane making process, namely, effects related to the casting solution proper and those associated with the membrane making procedure.

The initial cellulose powder received from Baker Chemicals was characterized with respect to moisture content and particle size. The effects of the initial cellulose particle size, cellulose concentration and the LiCl:cellulose mole ratio were studied with respect to the pore size of the membranes they produce. Swelling agents and pretreatments for dissolving cellulose in the LiCl/DMAc solvent system were also evaluated. Effects related to the casting procedure, such as the evaporation time and temperature and the type of gelation agent producing the smallest pores were also studied. Shrinking the membrane in liquid ammonia was also examined.

In order to characterize the membranes with respect to pore size, the applicability of the transport models must be verified. These models were tested parametrically in a previous section. These various modelling approaches were applied to all the membranes produced in this work.

Many parameters of the membrane making procedure affect membrane performance. The phase inversion step in this procedure imparts some variability to membrane performance. Such variations can occur even when most known features of the membrane making procedure are tightly controlled. Obtaining a global outlook on the effects of all parameters would be very time consuming and the present experimental design is planned at gaining the most information about this solution system by exploring factors which will cover the expected limits of membrane performance.

This experimental design is based on the premise that for a given solute-solvent-membrane system, higher separations are due to smaller pore sizes in the selective layer of the membrane. Optimizing solvent flux was not attempted in this work, the only persuit was to obtain a cellulose membrane which had sufficiently small pores in order to separate sodium chloride. The result being that the cellulose membranes produced in this work should have very low permeabilities. In order to complete

the permeation tests within a reasonable time frame, it was decided to test the membranes at a pressure of 6892 kPag (1000 psig.).

The basic guiding factors in this experimental design were that higher casting polymer concentrations generally lead to smaller pores, that the solvated nature of the polymer in the casting solution affects membrane performance, that higher evaporation temperatures [2] and longer evaporation times produce tighter membranes. The type of solvent used in the dissolution procedure affects membrane porosity, for previously mentioned reasons, the LiCl/DMAc solvent system was selected for this work. The effects of the starting material, the gelation medium and shrinking in liquid ammonia will be evaluated in this work.

All membranes will be tested in the automated membrane testing device which was specially designed for this work. The details of the planned experimental procedure are given in the following sections.

4.9 Effects Related to the Casting Solution

4.9.1 Effect of cellulose concentration

In this study the entire solubility range reported by References [69,70,71] (see Figure 4.7) was investigated. The limits of highest cellulose solubility could not be reached and a second region bound by the criteria of highest polymer solubility and a reasonable solution concentration to cast a membrane was defined. This new region, bound by 6-14 wt.% cellulose, and 4.71-18.82 wt.% LiCl is shown in Figure 4.7.

The pore size of membranes cast from solutions containing 6,8,10,11,12, and 14 wt.% cellulose (3:1 LiCl:cellulose mole ratio) were determined. All membranes were treated at 95°C for 10 min and gelled in acetone at 4°C. Detailed casting solution compositions are included in Table 4.6.

4.9.2 Initial cellulose particle size

The effect of particle size and solution concentration on membrane porosity was determined by casting two sets of membranes, containing 6,8,10,11,12, and 14 wt.% cellulose using the <38 μm and 38-53 μm milled celluloses. A mole ratio of 3:1

[2] Below the polymer's temperature of decomposition.

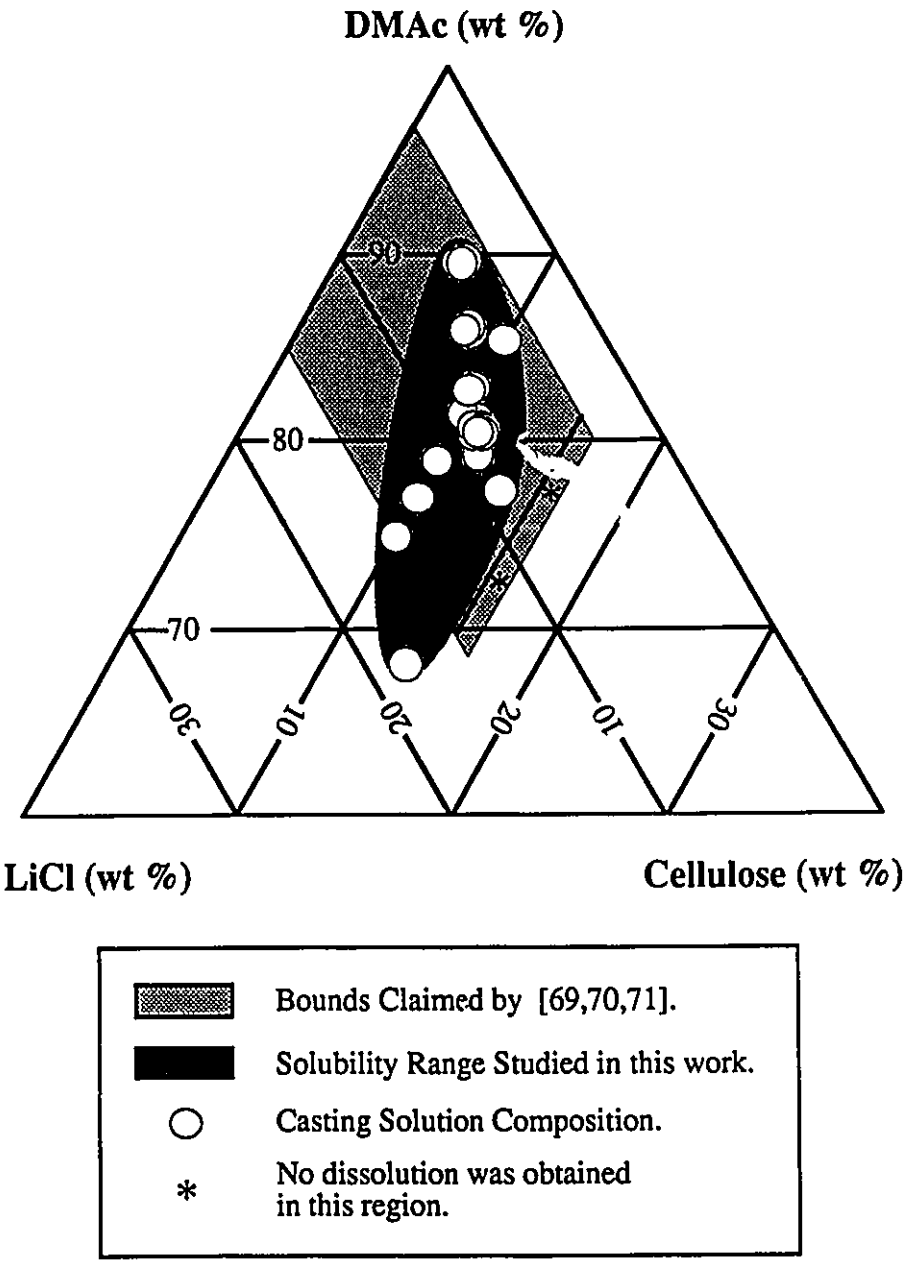

Figure 4.7: Solubility diagram for cellulose in LiCl/DMAc.

LiCl:cellulose was used in all these tests. All membranes were treated at 95°C for 10 min and gelled in acetone at 4°C.

The compositions of these membranes and their respective number are shown in Table 4.6. The pore sizes of these membranes were determined using PEG solutes and the effect of the initial particle size evaluated from these results.

4.9.3 LiCl to cellulose mole ratio

In a review of several non-aqueous solvent systems for cellulose, Philipp *et al.* [76] reported that at least 3 moles of "active agent" per mole of cellulose are needed for the complete dissolution of cellulose in these solvent systems. This number refers to the solvation of the three hydroxyl groups on the cellulose repeat unit. A study aimed at evaluating the importance of this parameter in membrane making was designed and several membranes containing 2:1, 3:1, 3.5:1, 4:1, and 5:1 mole ratio LiCl:cellulose were cast using the 38-53 μm cellulose. The standard procedure of an evaporation at 95°C for 10 min and gelling in acetone at 4°C was followed to produce the membranes. The composition and identification of these membranes are included in Table 4.7.

4.10 Effects Related to the Membrane Making Procedure

4.10.1 Evaporation time and temperature.

One of the main effects related to the membrane making procedure, is that of the evaporation time and temperature. These were extensively studied using a set of 26 membranes. These membranes were produced using an 11% solution of the <38 μm cellulose in a mole ratio of 3:1 (LiCl:cellulose). The evaporation times and temperatures for these membranes are listed in Table 4.8.

In general the resulting membranes cast under different evaporation times and evaporation temperatures have smaller pore sizes at higher evaporation temperatures and longer evaporation times. This provides a method to produce "graded" membranes which have a known direction of change with respect to pore size.

Table 4.6: Composition of the membranes used to determine the effect of the initial cellulose particle size and concentration(mole ratio of 3:1 LiCl:Cellulose). All membranes were treated at 95°C for 10 min and gelled in acetone at 4°C.

Membrane Number	Part. Size μm	Cellulose wt. %	LiCl wt. %	DMAc wt. %
Cell5	<38	6.0	4.71	89.29
Cell6	<38	6.0	4.71	89.29
Cell1	<38	8.0	6.28	85.72
Cell2	<38	8.0	6.28	85.72
Cell3	<38	10.0	7.84	82.16
Cell4	<38	10.0	7.84	82.16
Cell55	<38	11.0	8.62	80.38
Cell56	<38	11.0	8.62	80.38
Cell51	<38	12.0	9.41	78.59
Cell48	<38	12.0	9.41	78.59
Cell71	<38	14.0	11.0	75.00
Cell72	<38	14.0	11.0	75.00
Cell13	38-53	6.0	4.71	89.29
Cell11	38-53	8.0	6.28	85.72
Cell12	38-53	8.0	6.28	85.72
Cell7	38-53	10.0	7.84	82.16
Cell8	38-53	10.0	7.84	82.16
Cell49	38-53	11.0	8.62	80.38
Cell52	38-53	11.0	8.62	80.38
Cell54	38-53	12.0	9.41	78.59
Cell57	38-53	12.0	9.41	78.59
Cell53	38-53	14.0	11.0	75.00
Cell50	38-53	14.0	11.0	75.00

Table 4.7: Composition of the casting solutions used in evaluating the effect of the mole ratio of LiCl:cellulose. The initial particle size of cellulose was 38-53 μm. All membranes were treated at 95°C for 10 min and gelled in acetone at 4°C.

Membrane Number	Mole Ratio LiCl:Cell	Cellulose wt. %	LiCl wt. %	DMAc wt. %
Cell45	2:1	10.0	5.23	84.77
Cell46	2:1	10.0	5.23	84.77
Cell9	3:1	10.0	7.85	82.15
Cell10	3:1	10.0	7.85	82.15
Cell40	3.5:1	10.0	9.15	80.85
Cell41	3.5:1	10.0	9.15	80.15
Cell42	4:1	10.0	11.51	78.49
Cell43	4:1	10.0	11.51	78.49
Cell44	4:1	10.0	11.51	78.49
Cell73	5:1	10.0	13.07	76.93
Cell47	5:1	10.0	13.07	76.93

The permeation results obtained with these membranes will be used in future model discrimination.

4.10.2 Effect of the gelation bath

Preliminary work indicated that when water at 3-4°C was used as a gelling agent, precipitation occurs without the formation of a film at the surface of the membrane. Microscopic observations indicate that a symmetric gel was obtained when this precipitant was used as a gelation medium. This suggests that the diffusion of water into the film is faster than the diffusion of DMAc out of the film, and little DMAc was found to leave the gelled membrane as evidenced by the plasticized, hydrophobic nature of these membranes. Water droplets tended to bead on the surface of the membrane which had been allowed to soak in water for a period of a week. It seems that this gelation medium was incapable of removing the LiCl/DMAc solvent from the gelled film even after extended periods of soaking.

Table 4.8: Evaporation time and temperature for the series of graded membranes. Initial particle size of <38 μm, casting solution composition 11.0 : 8.62 : 80.38 (Cell:LiCl:DMAc), gelled in acetone at 4°C.

Membrane Number	Evaporation Time (min)	Evaporation Temperature °C
Cell15	10.0	55.0
Cell21	20.0	55.0
Cell26	15.0	55.0
Cell29	15.0	55.0
Cell31	7.5	55.0
Cell34	5.0	55.0
Cell38	5.0	55.0
Cell16	10.0	75.0
Cell24	5.0	75.0
Cell22	5.0	75.0
Cell27	7.5	75.0
Cell32	2.5	75.0
Cell37	15.0	75.0
Cell39	15.0	75.0
Cell17	10.0	95.0
Cell19	10.0	95.0
Cell23	15.0	95.0
Cell28	5.0	95.0
Cell33	2.5	95.0
Cell35	7.5	95.0
Cell14	10.0	115.0
Cell18	10.0	115.0
Cell20	5.0	115.0
Cell25	2.5	115.0
Cell30	7.5	115.0
Cell36	1.0	115.0

When acetone was used as a gelation medium, a clearly defined skin was formed at the surface of the membrane while the sublayers remained quite fluid after immersion into the gelation bath. The resulting membranes did not have a plasticized nature and were hydrophilic as evidenced by the absence of water beading at the surface of the membrane. This suggests that acetone can displace DMAc in the cast film.

Preliminary tests indicated that acetone gelation increased NaCl separations by 50 to 62% over water gelation (based on 12 wt.% cellulose) [97]. In view of this increased performance, all membranes used in this work were cast using acetone as a gelation medium.

4.10.3 Effects of shrinking in liquid ammonia

Based on the experience gained by Lafrenière [63], on the post-treatment of membranes cast from the PF/DMSO solvent system, post-treatment efforts will be confined to the shrinking of membranes in liquid ammonia [68]. The shrinking properties of liquid ammonia towards cellulose were reported in 1935, by Mahn [98]. Regenerated cellulose was reported to shrink up to 24% in liquid ammonia at $-33°C$ [99]. Its accessibility to dying increases after this treatment. This is a most interesting behavior since all materials made from pure cellulose have an inherent porosity, the overall shrinking of the polymer material should be accompanied by a reduction in the porosity of the material.

This behavior was investigated by performing several post-treatments on cellulose membranes. Standard, water impregnated, cellulose membranes were dipped in liquid ammonia at $-33°C$ for given amounts of time and quenched in water. The effect of repeating this operation was also studied. Membranes were also solvent exchanged with 2-propanol and acetone prior to quenching in water or acetone.

Chapter 5

Results and Discussion

5.1 Selecting the Best Model to Describe Solute Transport

The purpose of this section is to determine what type of interaction or effect can best describe the transport of solute through cellulose membranes. In doing so, material dependent and morphology dependent contributions to solute transport must be evaluated. Material dependent contributions such as surface interactions and viscosity increases in the pore are specific to a solute-solvent-membrane system. While morphology dependent contributions such as pore size, skin thickness and tortuosity are related to a specific membrane film.

Since both types of contributions are included in all models, model selection must be performed with a large data set containing information for a variety of pore sizes. Efforts in the automation of membrane testing procedures and analysis, facilitate the generation of the large amounts of data required in this type of study. A total of 965 individual observations on 70 cellulose membranes having a large distribution of molecular weight cutoffs (based on polyethylene glycol measurements) were used for this study. These membranes were tested with aqueous solutions containing 200 ppm of probe solute at 25°C and 6892 kPag (1000 psig.) operating pressure.

Residuals for the separation of each probe solute were calculated according to Equation 5.1 as follows,

$$e_i = f_{\text{exptl}} - f_{\text{calc}}, \tag{5.1}$$

and plotted against the predicted or calculated separation f_{calc}. The values of f_{calc} were chosen for model discrimination since they are not correlated with the residuals, while the values of f_{exptl} usually are [57].

In an attempt to obtain representative values for the interaction parameters an optimization scheme consisting of a fit within a fit was used to determine the overall interaction parameter and the membrane pore size. This was done by using the simplex method to search for the interaction parameters and Brent's one-dimensional minimization routine to obtain the pore radius [40]. The results obtained for individual membranes were optimized using the permeation of solutes as in Equation 2.5 and the sum of squares obtained in this fit was then used in the simplex method to calculate an overall optimum. This procedure required up to 1.5 hours of CPU time on an IBM 3090 to converge for a set of 70 membranes characterized with a total of 965 solutes[1].

In view of the low NaCl separations obtained in this work and based on pore size measurements of RO polyamide and cellulose acetate membranes, the pore size of the cellulose membranes should not be less than 1.1 nm (the adsorbed water thickness as determined by GC measurements [7]). The predicted pore sizes for a series of "graded" membranes produced in the time and temperature study were modeled by a third order polynomial surface and the results are presented with the residual plots for a given model or calculation approach. These values were used along with the residuals to determine model adequacy.

The residuals of these 965 observations were fitted to a fifth order polynomial which gave ample flexibility in representing abrupt changes in the residual plot. The entire range of the predicted separation (0-100 %) was divided into 20 segments. The number of points and the variance of these points about a segment mean was determined and superimposed onto the polynomial fit. The contours for one and two standard deviations (σ, 2σ) about the polynomial fit are indicated in the residual plots. These results are presented in the following sections.

[1]Computation times varied with the proximity of the initial guess to the optimum solution.

5.1.1 Steric interactions

As seen in the summary of equations, Table 2.1, for all four transport models under convective flow and for the specific case of purely steric interactions, the only difference between the models is that the SFPF and MD-SFPF use $b(\lambda)$ as an interaction parameter and the RAPM and RDPM use G. The residuals and predicted pore sizes for a fit to the 70 membranes are illustrated in Figure 5.1 for the RAPM and RDPM models, and in Figure 5.2 for the SFPF models.

The fit is very poor and in both cases the residuals are highly correlated . This indicates that in all models, steric interactions alone cannot explain the permeation data and that some other unaccounted factor must be present. The value for the minimum pore radius of the "graded' membranes (Figure 5.1) is ~0.9 nm. which is the pore radius observed in RO membranes with NaCl separations >95%. This value is far from the ~50% NaCl separation obtained for these membranes.

The predicted values determined by the correlation of $b(\lambda)$ are very reasonable and in agreement with dye penetration experiments performed on commercially available regenerated cellulose membranes where pore sizes of 2.1 to 2.3 nm were reported [100]. Since the values of $b(\lambda)$ were determined by an experimental fit to a large amount of RO data, interaction effects might be confounded in the $b(\lambda)$ correlation. This would explain the unusual and rapid decrease of the $b(\lambda)$ correlation with respect to Faxen's equation at values of $\lambda > 0.22$, see Figure 2.1. In view of this possible confounding of effects, the correlation for G was used in the rest of this work.

5.1.2 Fit for solute adsorption based on van der Waals interactions

The possibility of solute adsorption was determined by confining A_{AM} to positive values ($A_{AM} \geq 0$) and using Equation 2.51 as an expression for the potential. The residuals and predicted pore sizes for a fit to the 70 membranes are illustrated in Figure 5.3 using the RDPM model. Even when the optimization routine was started at large positive values of A_{AM} the fitting algorithm returned to $A_{AM} = 0$ and was blocked at this limit. This explains why the result obtained for adsorption, Figure 5.3, is identical to that of the steric case, see Figure 5.1.

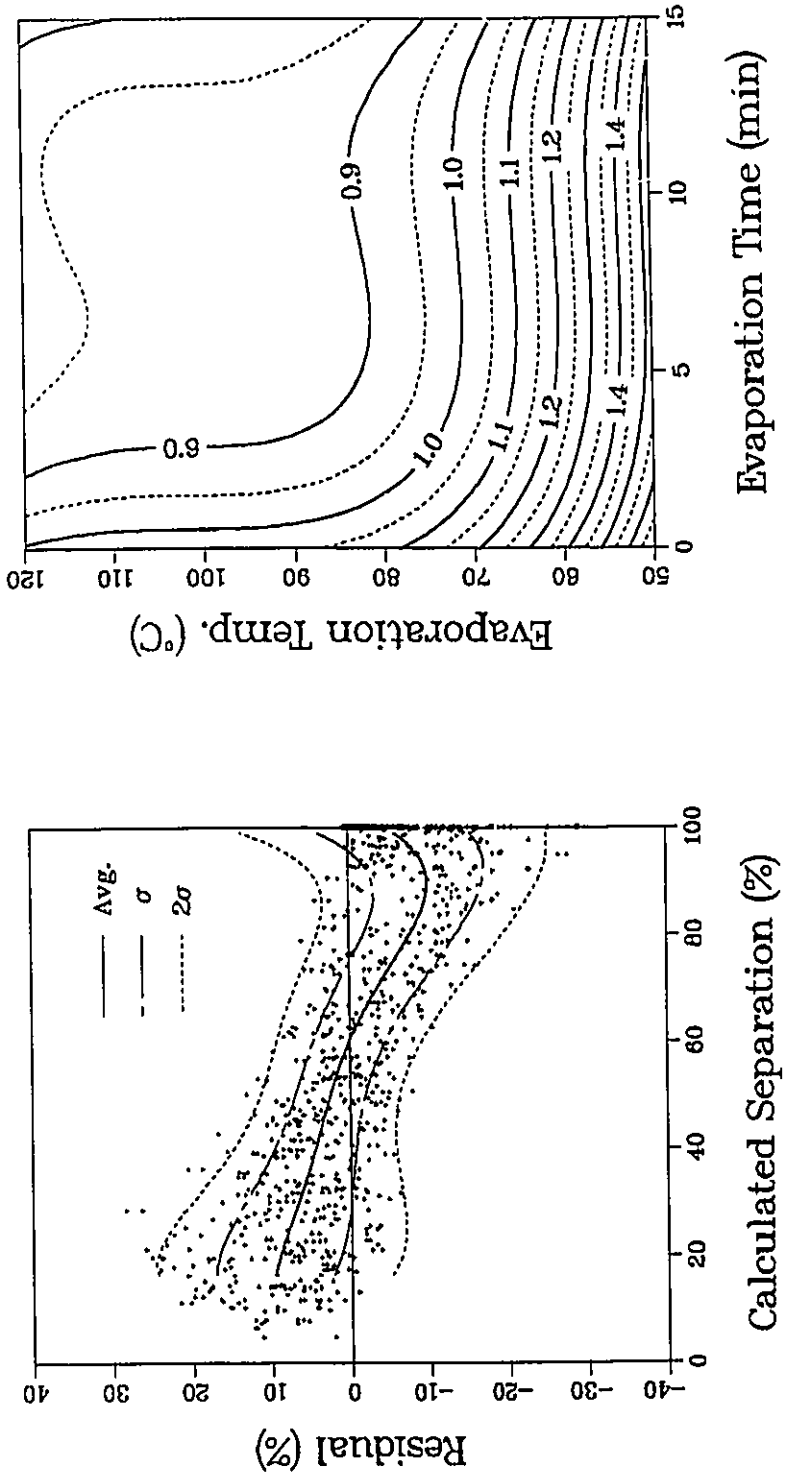

a) Residual Plot. b) Contour Plot.

Figure 5.1: Fit for steric interactions using the RDPM and RAPM models, residual plot a) and contour plot for the "graded" membranes b), predicted membrane pore size in elevation (nm).

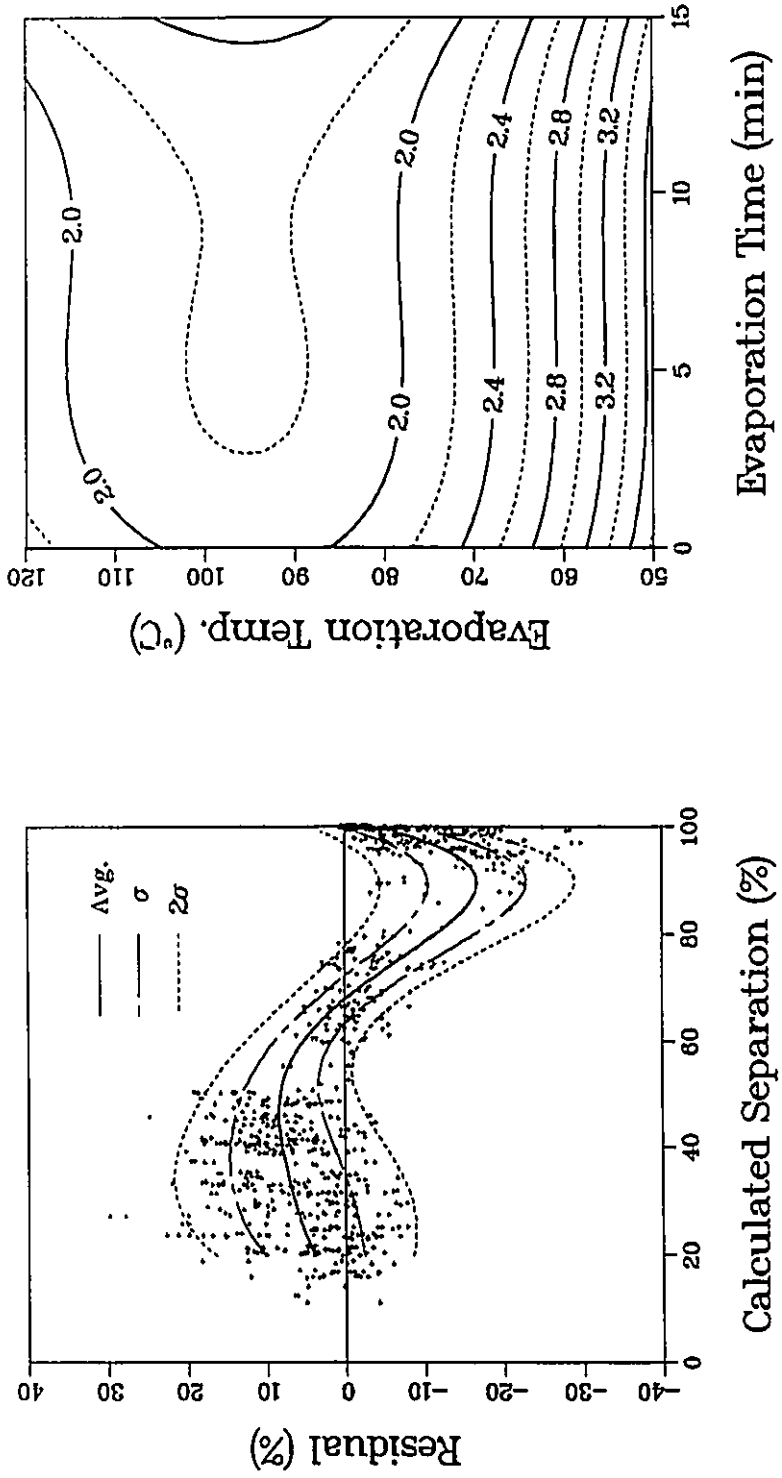

Figure 5.2: Fit using the value of b^{-1} instead of G, (SFPF and MD-SFPF models) residual plot a) and contour plot b), predicted membrane pore size in elevation (nm).

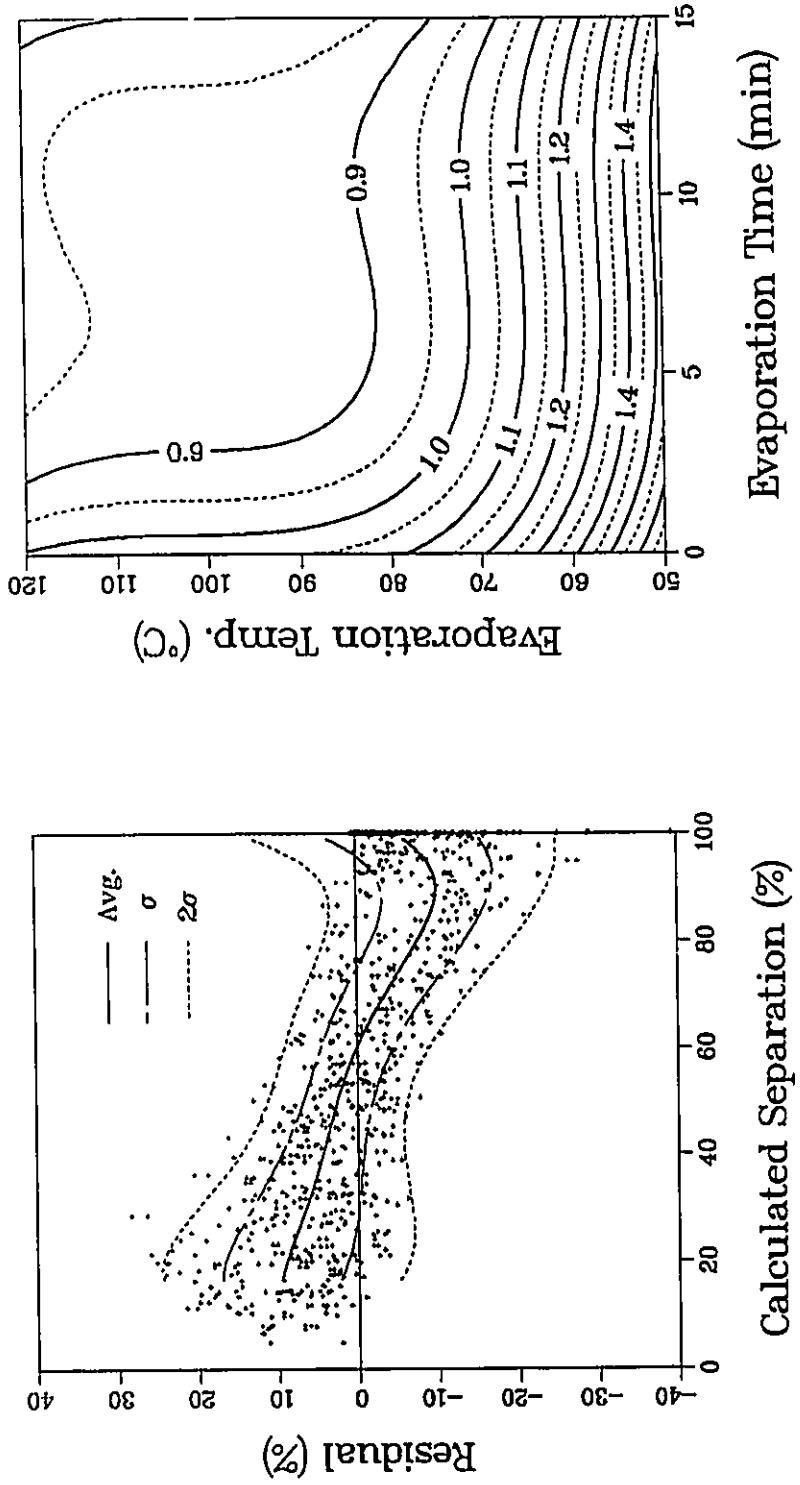

a) Residual Plot. b) Contour Plot.

Figure 5.3: Fit for conditions of adsorption based on van der Waals interactions, residual plot a) and contour plot b) predicted membrane pore size in elevation (nm).

This test indicates that molecules are not attracted to the membrane surface and if surface forces do exist, they must be repulsive. However, this result does not prove that surface forces are causing the lack of fit to the permeation data and the contributions of several other possible effects must also be considered.

5.1.3 Increased viscosity within the Pore

The possibility of an increase in viscosity within the pores of the membrane was evaluated by simply mutiplying the viscosity term in the RDPM model by a factor of 39 (Figure 5.4), and 100 (Figure 5.5). It is clear from both the residual plots and the predicted pore sizes of the "graded" series of membranes that a viscosity increase inside the membrane pore cannot explain a the lack of fit observed in Figure 5.1.

This also indicates that diffusion controlled transport, *i.e.* small Peclet numbers, cannot account for this lack of fit. In fact these results indicate that a model based on diffusion controlled transport gives a poorer fit than a combined diffusive and convective flow model. They also indicate that the actual solution viscosity in these "hydrodynamic" pores is within an order of magnitude of that measured in the bulk solution, which is in agreement with the direct measurements of the solution viscosity of water between two mica surfaces separated by 1.85 nm [37].

5.1.4 Chain permeability

The effect of chain permeability (α''), calculated from theoretical considerations, has also been tested as a possible explanation for the lack of fit observed in Figure 5.1. These results have been included in Figures 5.6 – 5.8. They indicate that chain permeability cannot explain this discrepancy and that in all cases, very little change from the steric case was observed in using this concept.

5.1.5 Central Confinement of solute molecules

The effect of the central confinement of solute molecules was also examined. The graphic results have been included in Figures 5.9 – 5.11. These results indicate that the transport of solute molecules through membrane pores cannot be represented by central confinement within the pore. These plots are experimental evidence that

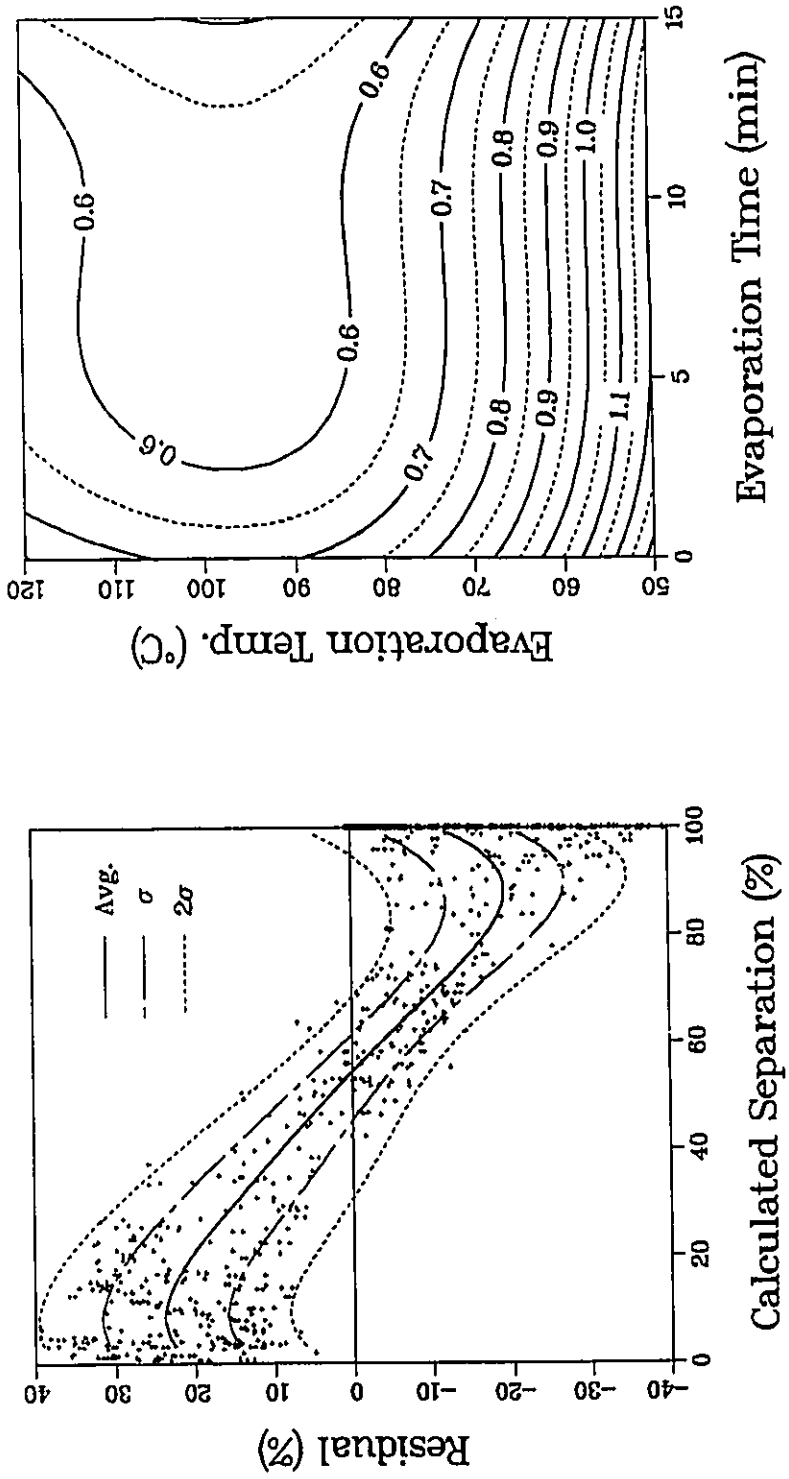

Figure 5.4: Fit based on a 39 X increase in viscosity, residual plot a) and contour plot b), predicted membrane pore size in elevation (nm).

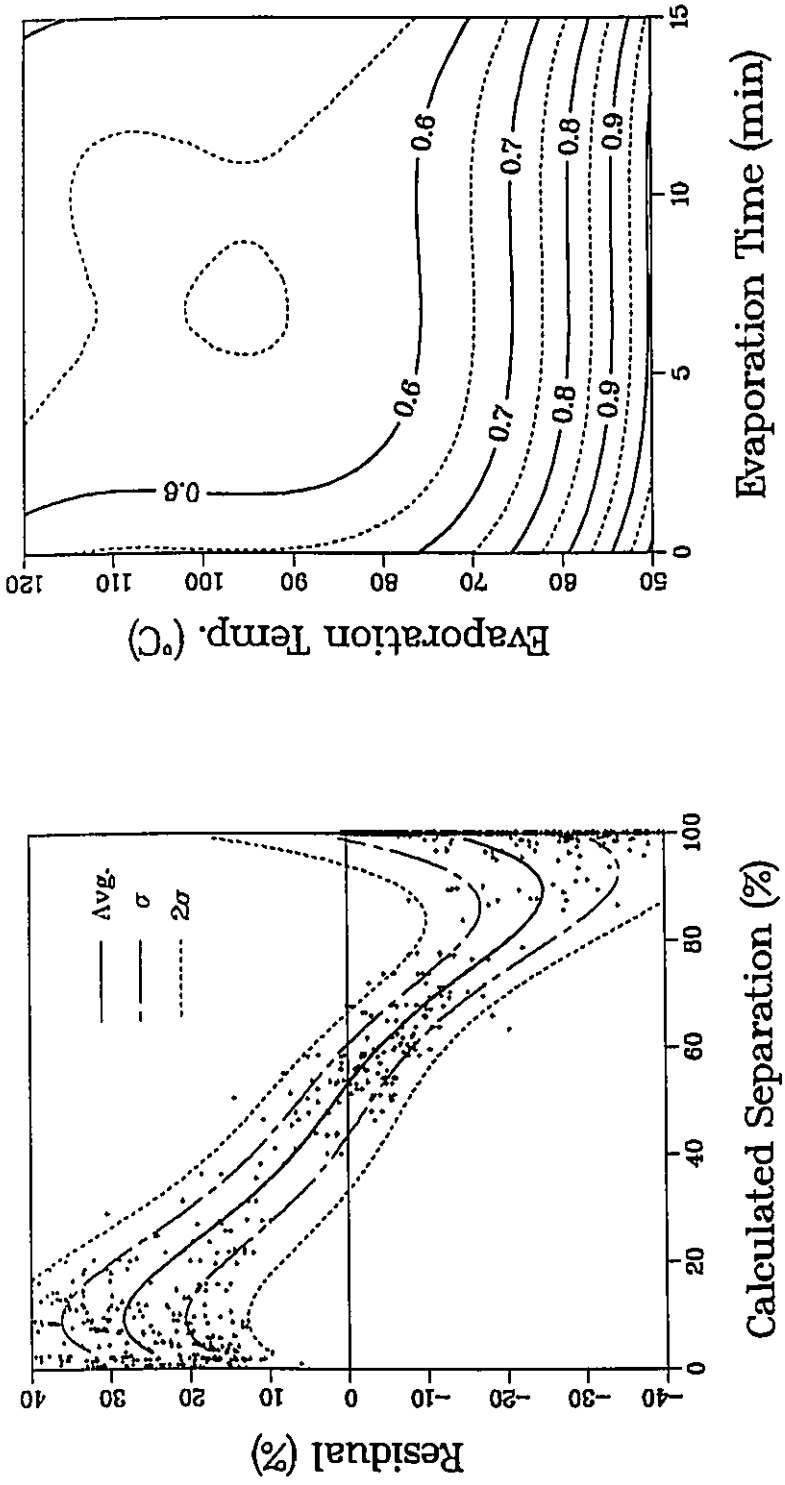

a) Residual Plot. b) Contour Plot.

Figure 5.5: Fit based on a 100 X increase in viscosity, residual plot a) and contour plot b), predicted membrane pore size in elevation (nm).

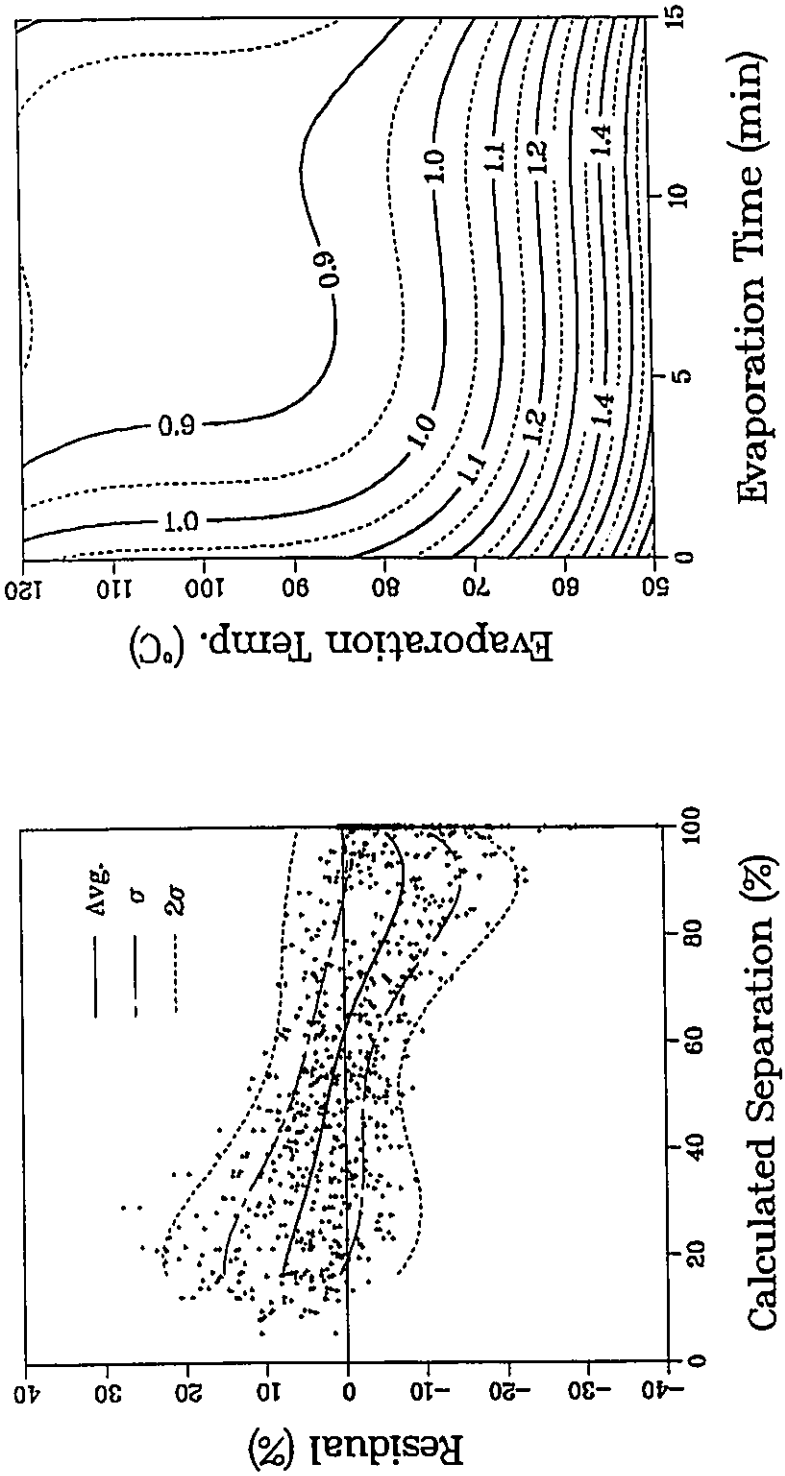

Figure 5.6: Fit based on a chain permeability of α"= 10, residual plot a) and contour plot b), predicted membrane pore size in elevation (nm).

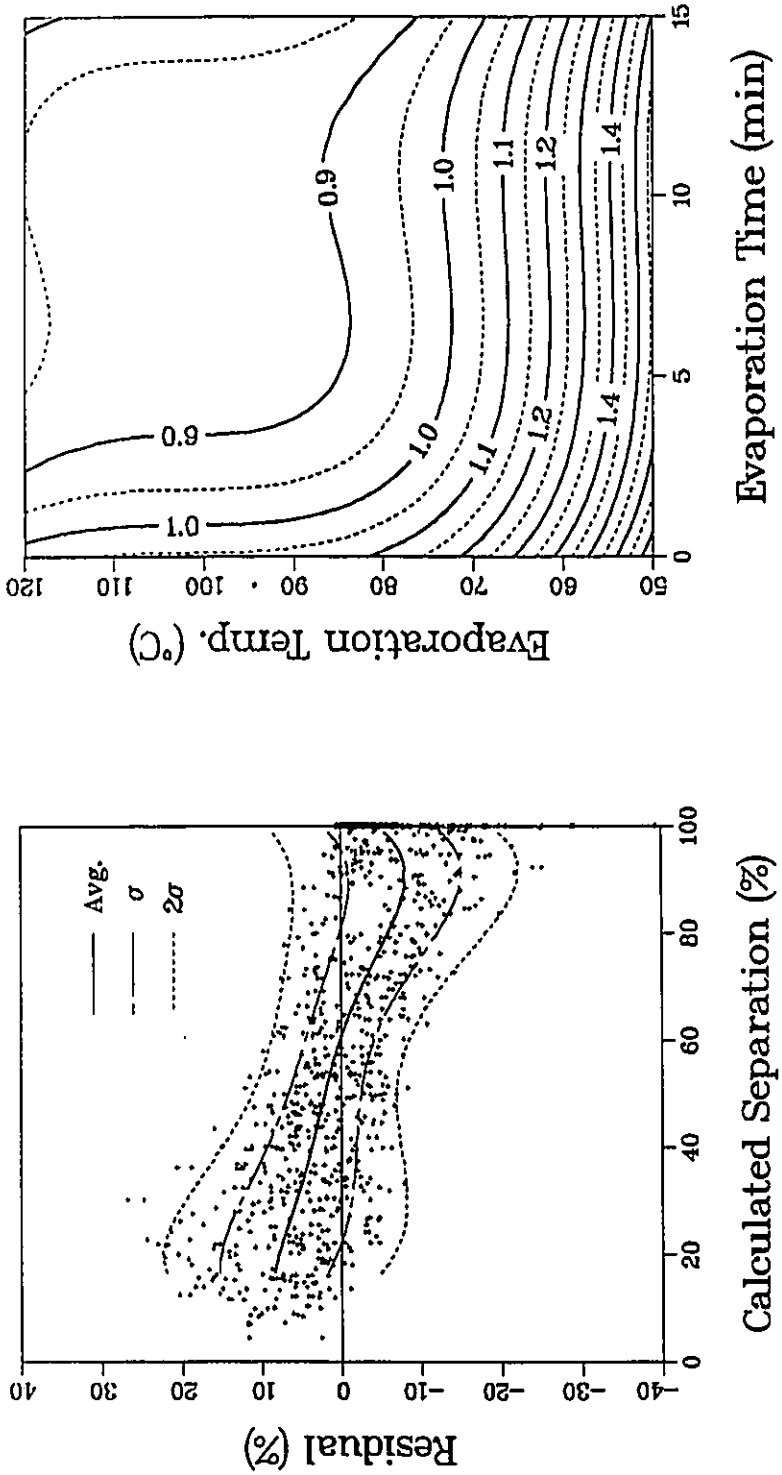

Figure 5.7: Fit based on a chain permeability of α"= 34, residual plot a) and contour plot b), predicted membrane pore size in elevation (nm).

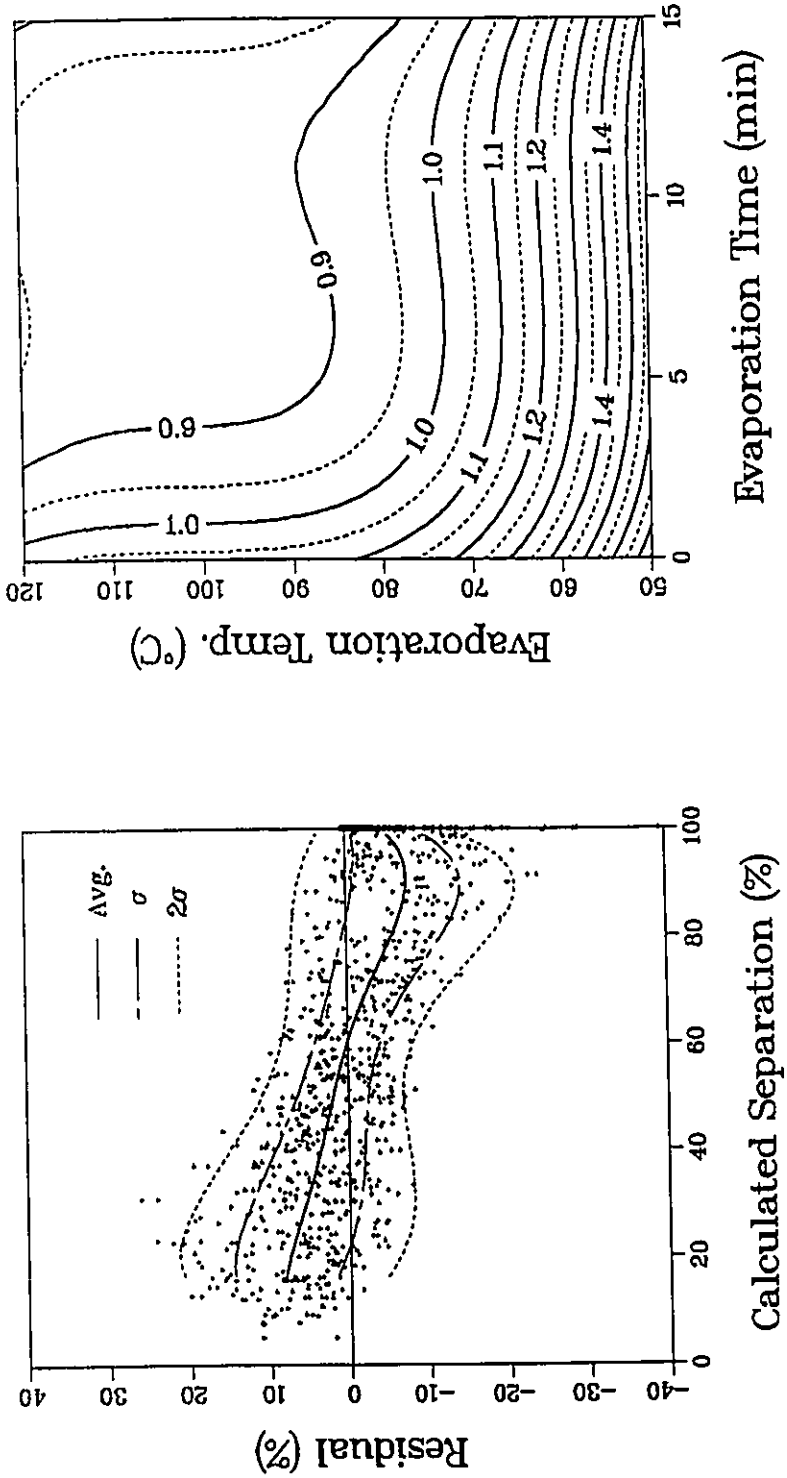

a) Residual Plot. b) Contour Plot.

Figure 5.8: Fit based on a chain permeability of α "= 60, residual plot a) and contour plot b), predicted membrane pore size in elevation (nm).

solute molecules do not prefer central positions while translating through membrane pores.

Since molecules do not migrate towards the center of the pore, the concentration profile within the pore must be similar to that found at the pore entrance.
As seen in SEM micrographs, the shape of the surface at this point is fairly smooth [25]. Solute and solvent interactions with a flat geometry were used in all surface interaction calculations.

5.1.6 Fit using the log-normal distribution

A fit to the experimental data using the log-normal distribution was performed under conditions of steric interaction with the pore wall. The residual and contour plots can be found in Figures 5.12 and 5.13. These results would seem to indicate that a distribution of pore sizes provides a better fit than a single pore size. Unfortunately this calculation is somewhat of an artifact since the predicted average pore sizes are of the order of the diameter of water molecules . The situation is somewhat improved when the value of $\overline{R}_a$ is plotted (see Equation 2.62) instead of R see Figure 5.12(b). These pore sizes are still too low for this type of membrane. Since pores of 0.2 nm or less must be capable of permeating solution, this result is impossible, and implies that such a fit is a mathematical artifact.

From the parametric studies shown in Figures 2.18, and 2.19, it is easily seen why the log-normal distribution is difficult to fit to the permeation data. It is for these reasons that only one morphology dependent parameter, the average pore radius, was evaluated in this work.

5.1.7 DLVO interactions

In a previous section the value of the double layer thickness κ was calculated to be 70.1 nm. This is quite large compared to the expected pore radius of cellulose membranes. Given this dimension, it is not very likely that double layer interactions have any effect on the transport of solute molecules through these cellulose membranes but the possibility of this contribution has been evaluated for $\kappa = 0.0142$ nm^{-1} and the results plotted in Figure 5.14.

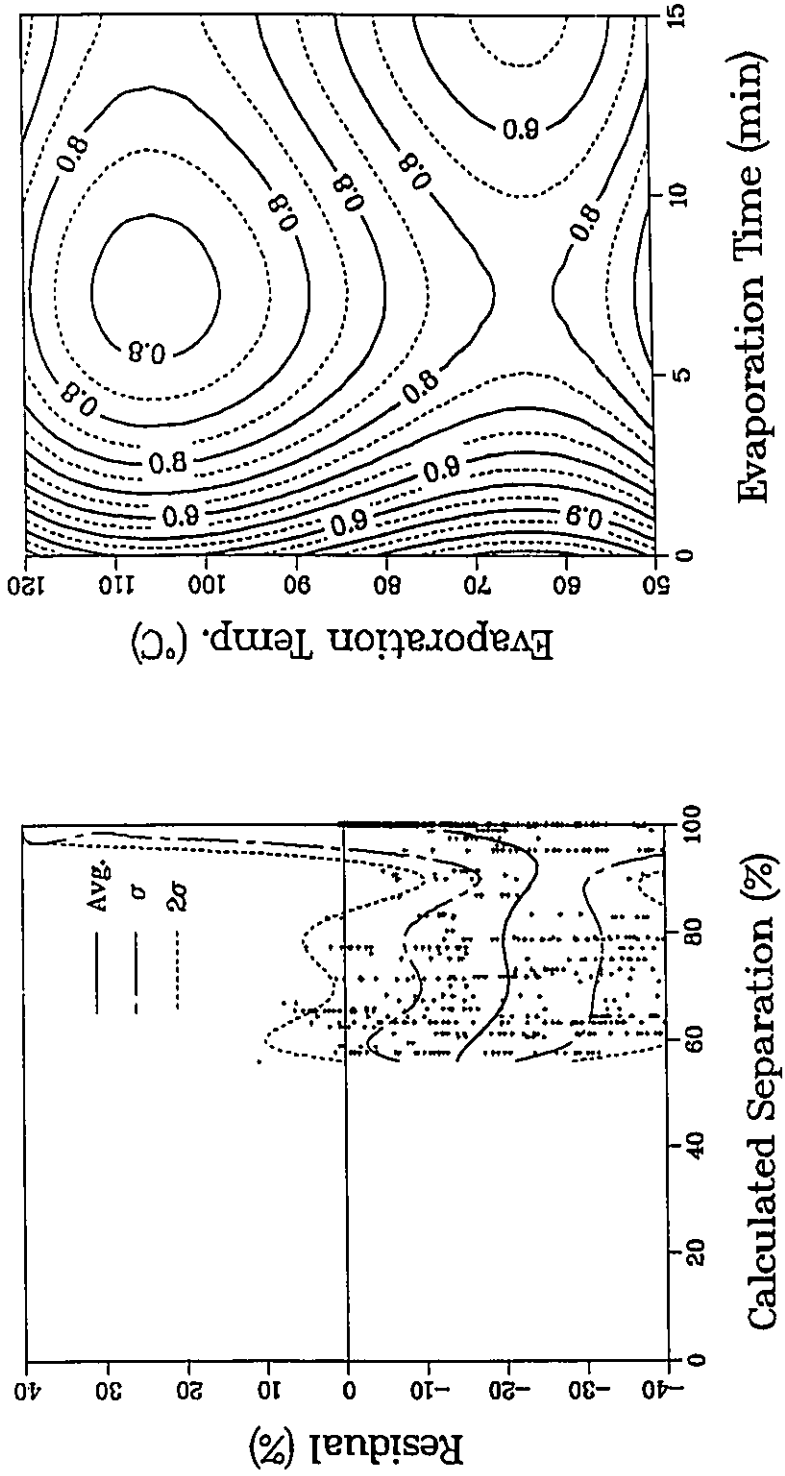

a) Residual Plot. b) Contour Plot.

Figure 5.9: Fit based on a molecule confined to a radius of $1.0 \times a_s$, residual plot a) and contour plot b), predicted membrane pore size in elevation (nm).

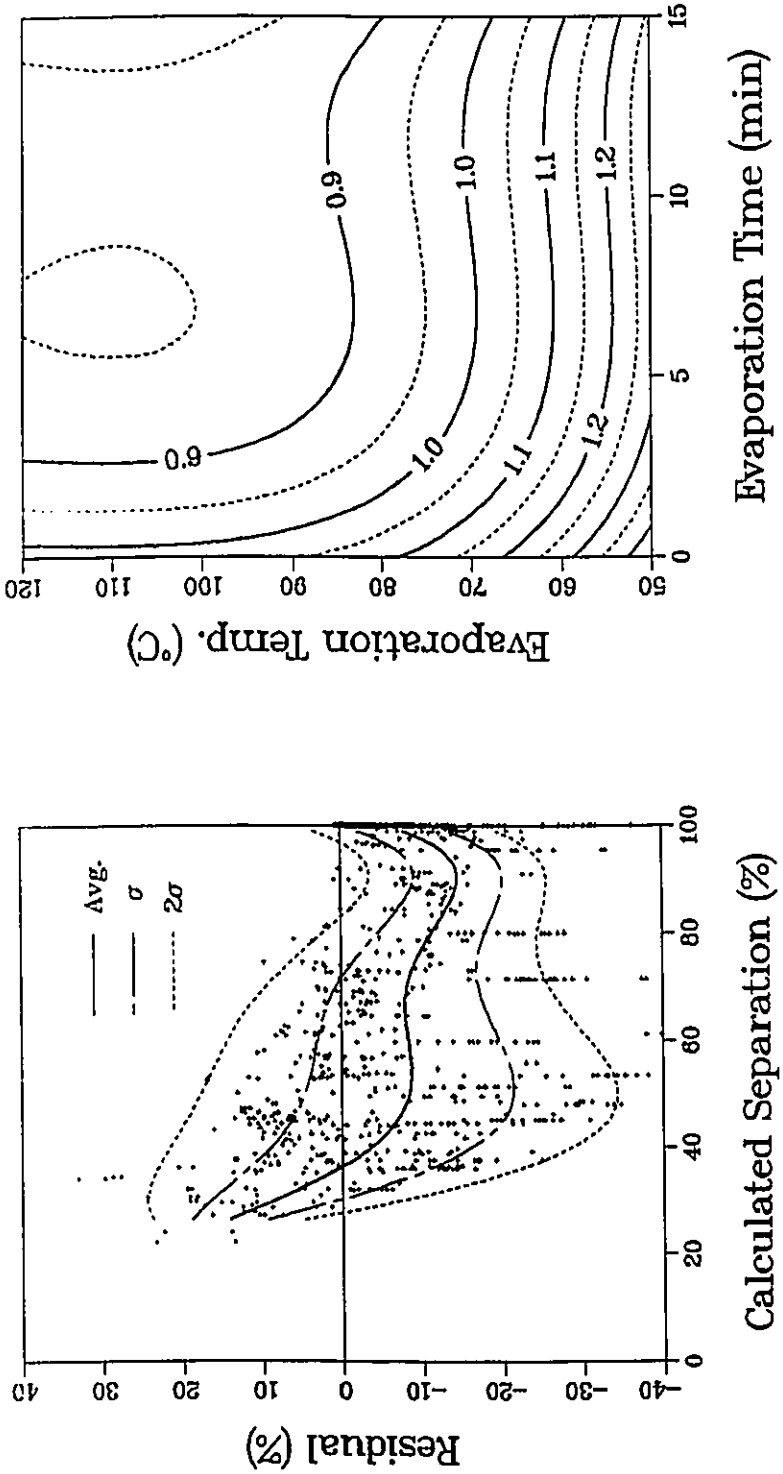

Figure 5.10: Fit based on a molecule confined to a radius of 2.0 x a_s, residual plot a) and contour plot b), predicted membrane pore size in elevation (nm).

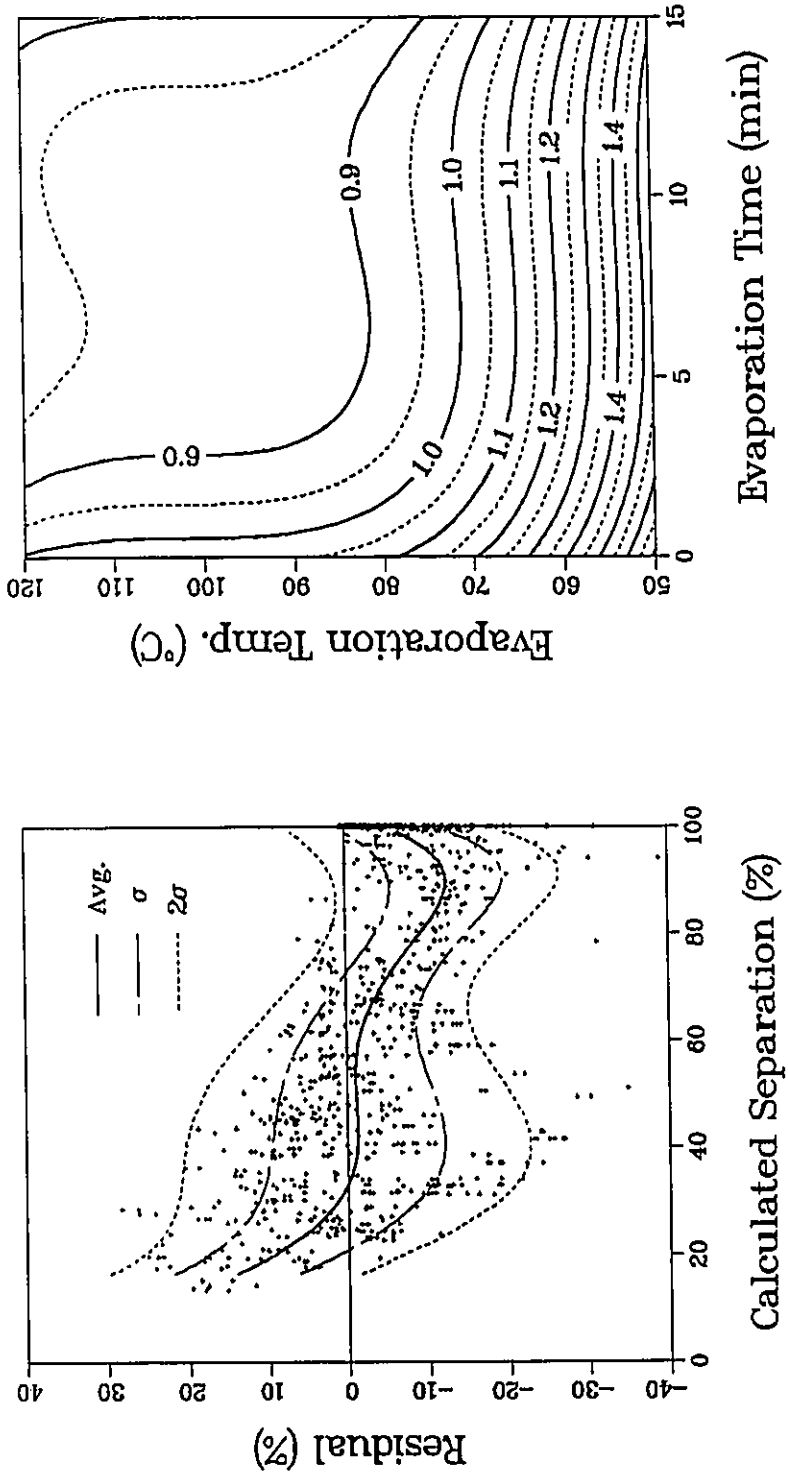

a) Residual Plot. b) Contour Plot.

Figure 5.11: Fit based on a molecule confined to a radius of 3.0 x a_s, residual plot a) and contour plot b), predicted membrane pore size in elevation (nm).

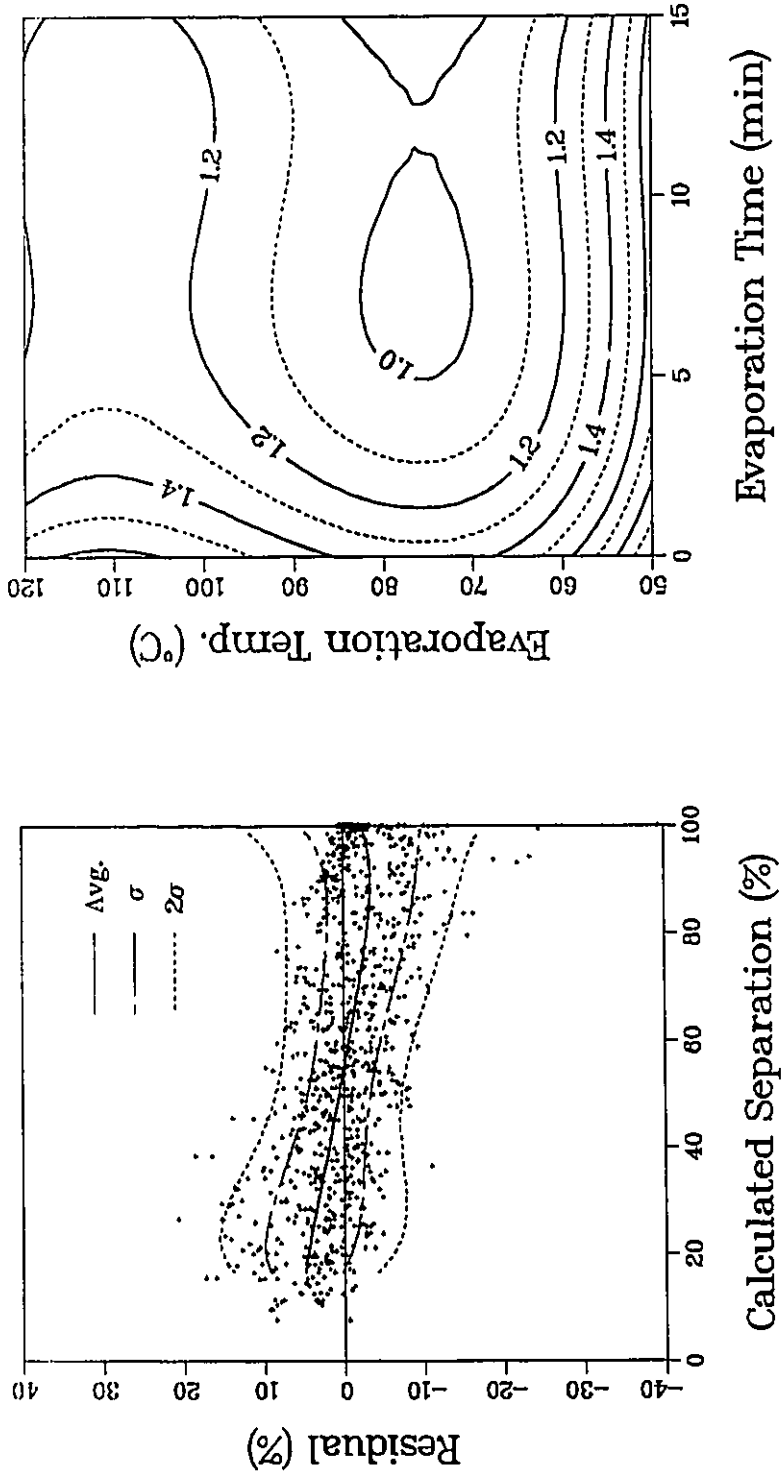

a) Residual Plot. b) Contour Plot for $\overline{R}_s$.

Figure 5.12: Fit for the log-normal distribution, residual plot a), and contour plot b), predicted moment of the pore size distribution $\overline{R}_s$ in elevation (nm).

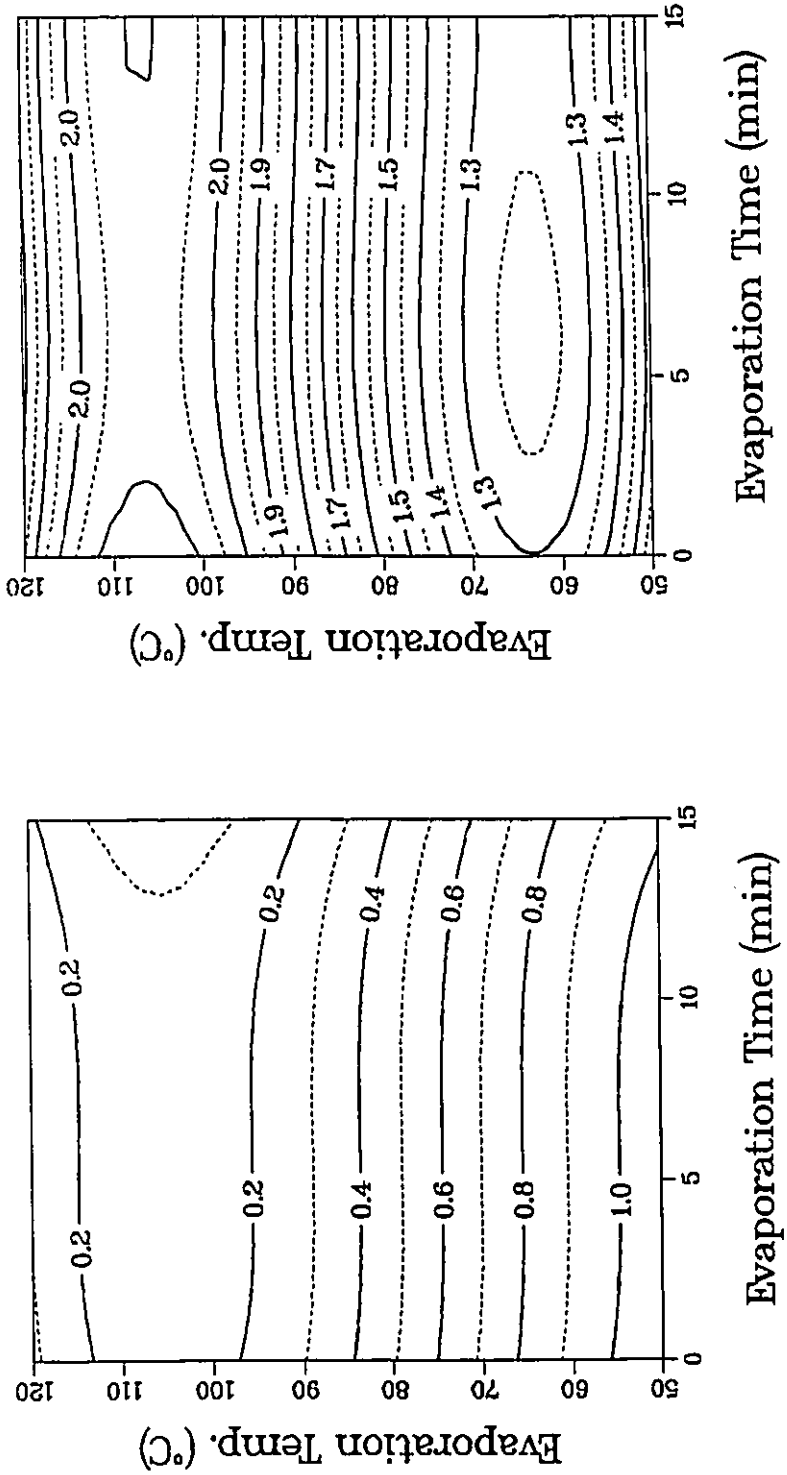

Figure 5.13: Fit for the log-normal distribution R and σ, residual plot a) and contour plot b), predicted membrane pore size in elevation (nm).

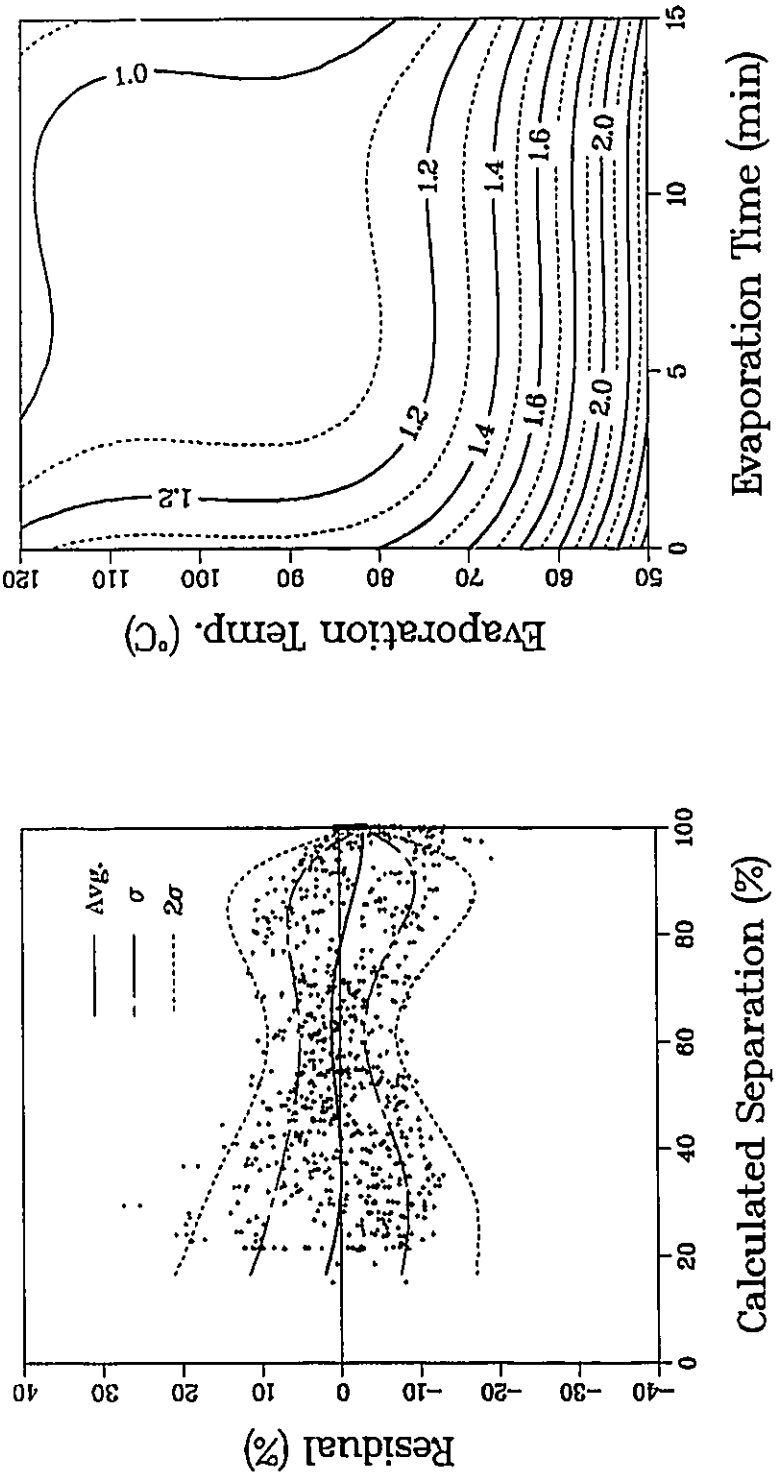

a) Residual Plot. b) Contour Plot.

Figure 5.14: Fit based on the DLVO theory, residual plot a) and contour plot b), predicted membrane pore size in elevation (nm).

The pore radii predicted by this interaction are too low and the increase in variance at each end of the "cloud" of residuals indicates a rather poor fit to this data.

5.1.8 The case of strong hydration

The possibility of strong solvent adsorbtion onto the pore wall was studied. It is assumed in this type of interaction that solute molecules are totally rejected from a layer of thickness t_{adsor} near the wall. The results obtained from this fit have been plotted in Figure 5.15.

The residuals are randomly distributed and the predicted pore sizes are very reasonable. The calculated thickness of this layer is 0.44 nm which is nearly 1.5 layers of water molecules. Water cannot flow as in the bulk solution at such small distances from the pore wall. Hence, an adsorbed layer, if present, is diffuse rather than composed strictly of solvent.

5.1.9 Fit for solute rejection based on van der Waals interactions

The effect of solute rejection based on Hamaker's approach was evaluated for values of $A_{AM} < 0$ by using Equation 2.51. This interaction parameter could not be obtained directly from the permeation data since the model did not converge for values of $A_{AM} < 0$ see Figure 5.16. The value of A_{AM} was found to be positively correlated with that of R. Values of A_{AM} at a low sum of squares predicted ridiculous values of R, these results are shown for $A_{AM} = -1000$ (Figure 5.18).

The value of $A_{AM} = -214$ giving the same SS_{Resid} as that obtained for the fit based on dipole interactions described below was also used in the model and the results plotted in Figure 5.17. The predicted pore radii are slightly better but they are still quite high.

The fit based on this type of interaction is ill-defined and an external scource of information is needed to evaluate this interaction force. The concentration profile, expressed as $e^{-\phi(\underline{d})}$ was plotted versus the distance away from the membrane surface see in (Figure 5.19(a)). The distance at which total rejection of solute from the membrane surface occurs was found to be approximately twice the radius of the solute molecule (based on $e^{-\phi(\underline{d})} = 0.01$). This would suggest that UF and MF

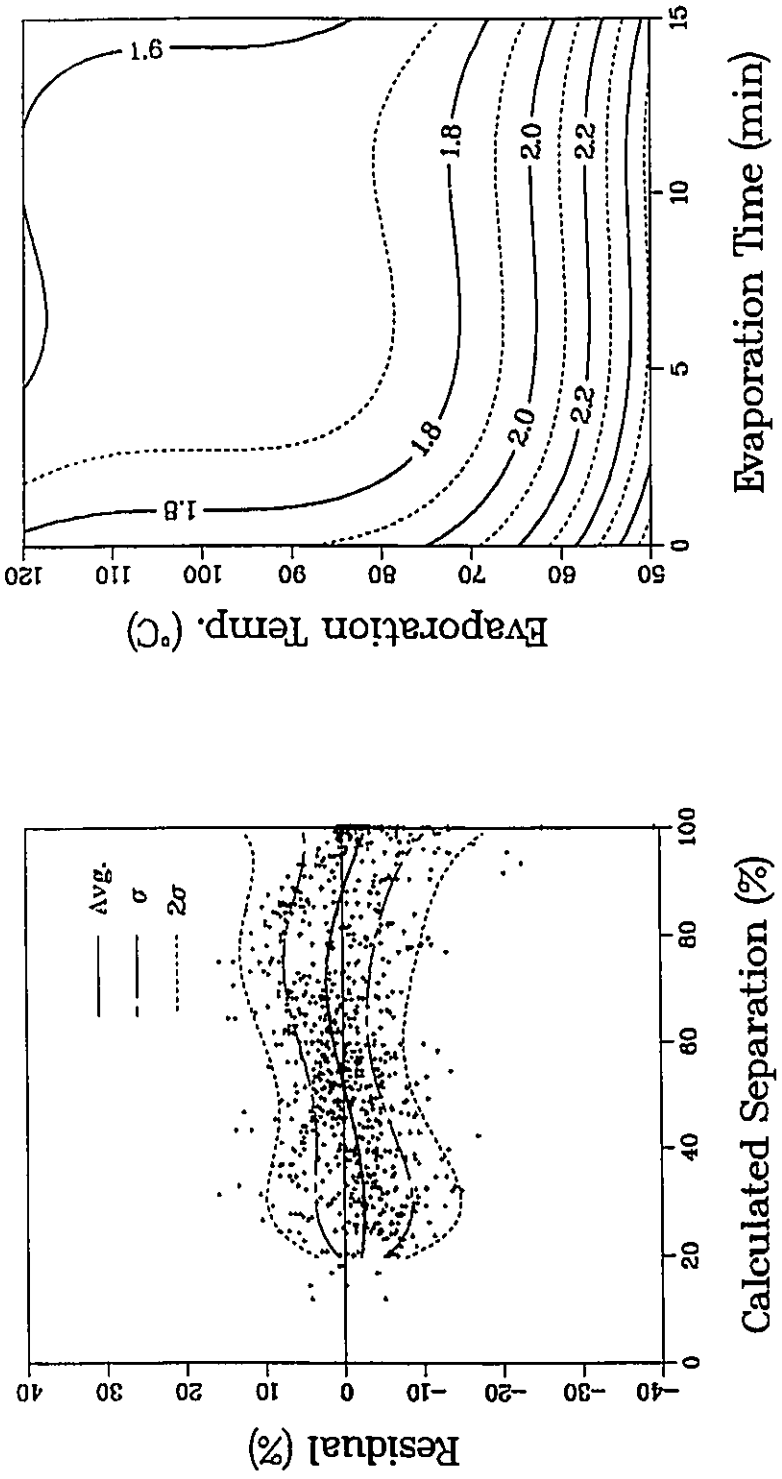

a) Residual Plot. b) Contour Plot.

Figure 5.15: Fit based on an adsorbed solute layer t_{adsor} = 0.44 nm , residual plot a) and contour plot b), predicted membrane pore size in elevation (nm).

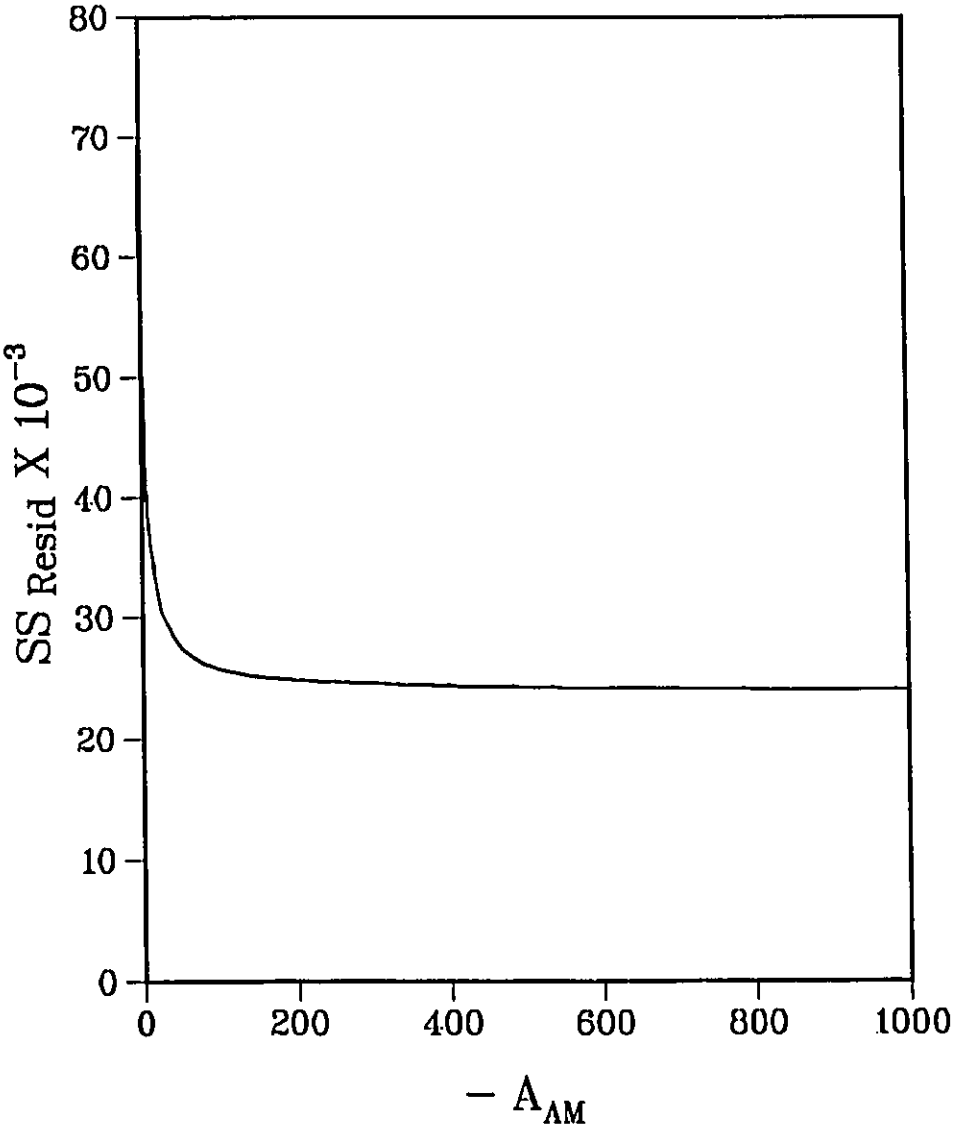

Figure 5.16: Plot of the residual sum of squares SS_{Resid} vs. A_{AM} for all 70 membranes.

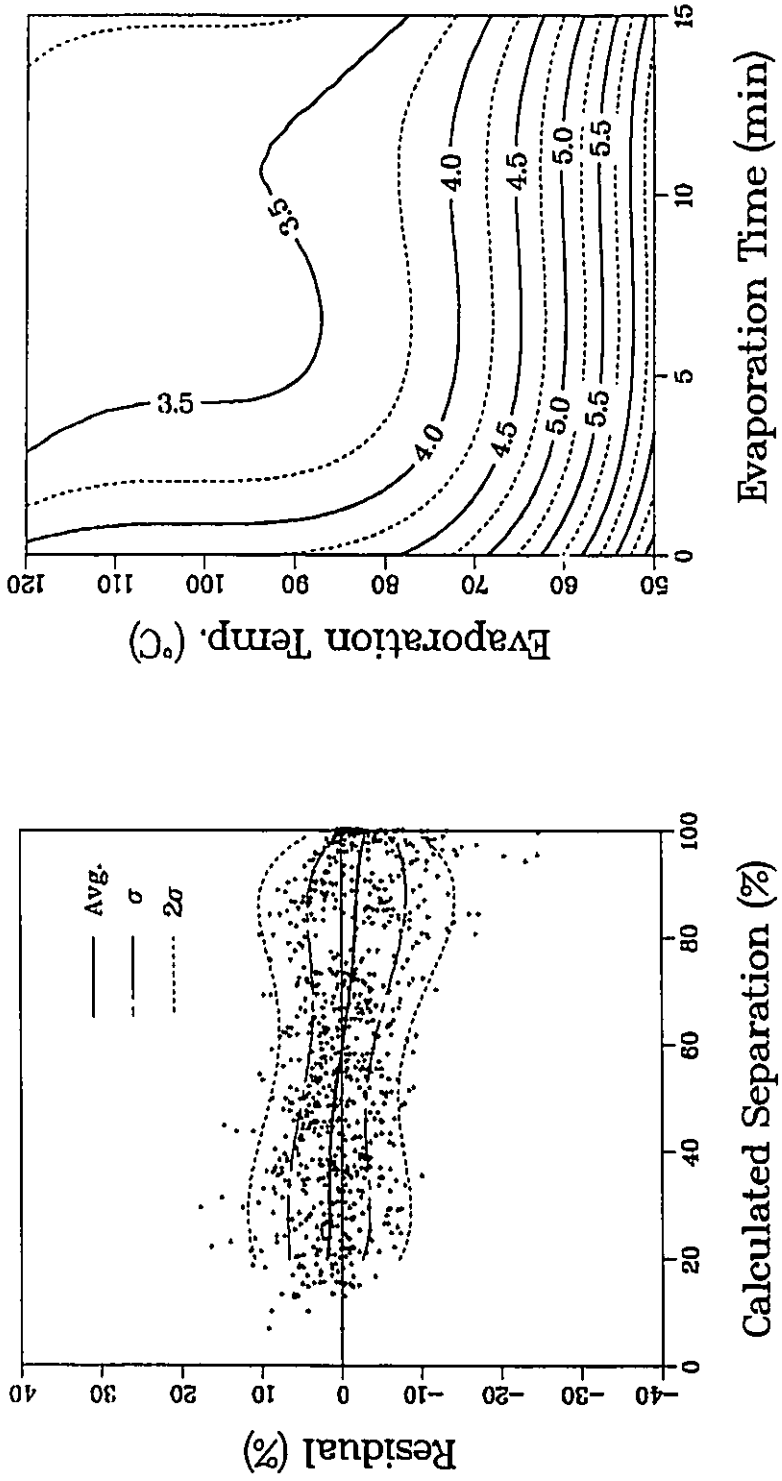

a) Residual Plot. b) Contour Plot.

Figure 5.17: Fit for pairwise additivity A_{AM} = - 214 nm^{-1}, residual plot a) and contour plot b), predicted membrane pore size in elevation (nm).

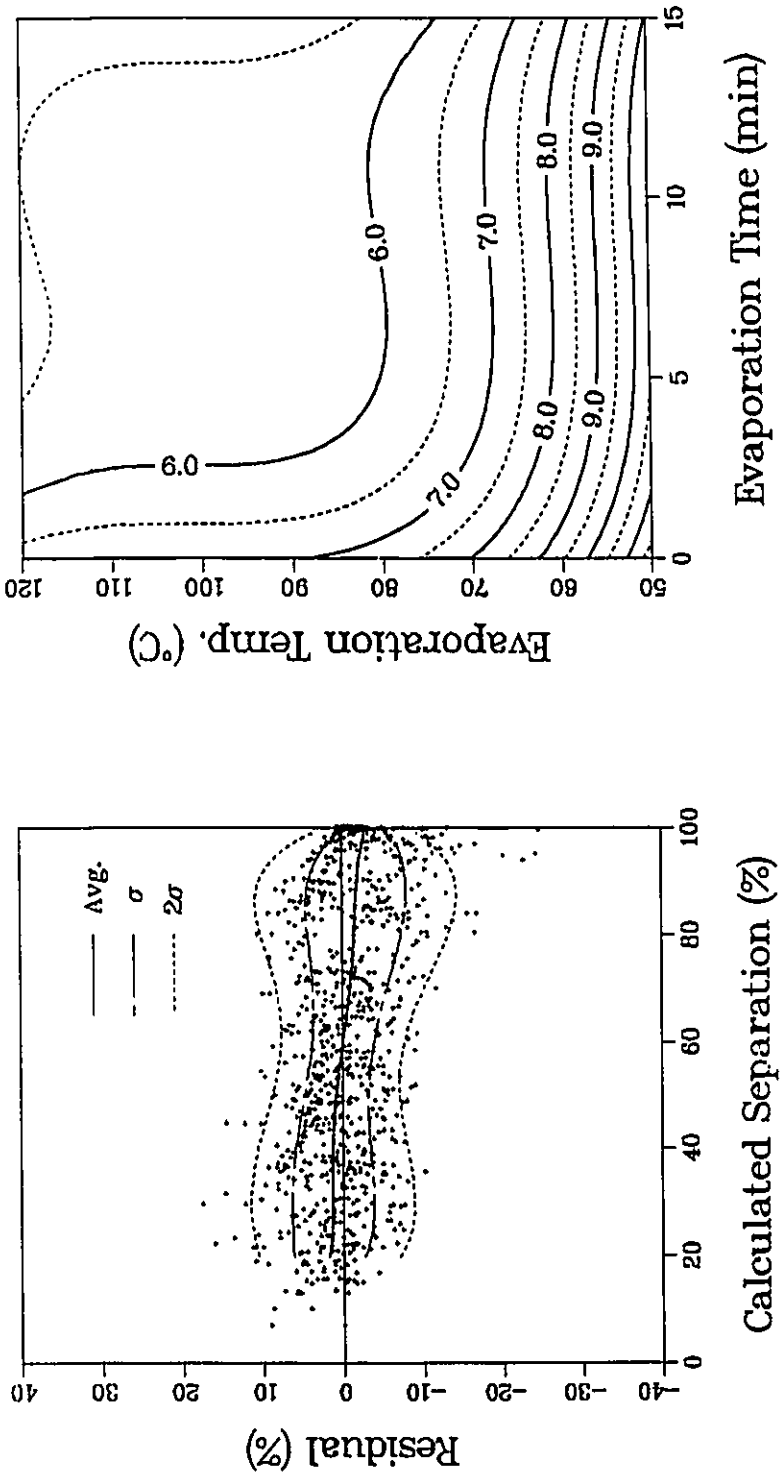

a) Residual Plot. b) Contour Plot.

Figure 5.18: Fit for pairwise additivity $A_{A,M}$= -1000 nm^{-1}, residual plot a) and contour plot b), predicted membrane pore size in elevation (nm).

separations would be greatly affected by surface interactions of the van der Waals type. This is not the case however since these separations are mainly influenced by sieving.

5.1.10 Forces of hydration or structural forces

The effect of solvent mediated transport due to the structuring of oriented dipoles at the surface of the membrane material has been quantified and the residual plots for $\kappa' = 2.969\ \text{nm}^{-1}$ are shown in Figure 5.20.

The low value of SS_{Resid} and the reasonable pore radii obtained for the graded series of membranes indicate that structural forces are by far the most likely type of interaction occurring at the surface of the cellulose membrane. Cellulose with its abundance of hydroxyl groups is a perfect NP-type surface which can give rise to dipole interactions as shown in Figure 2.3. The values of the pore radius are very reasonable and coincide with the data obtained from dying measurements [100].

The concentration profile, expressed as $e^{-\phi(\underline{d})}$ was plotted versus the distance away from the membranes surface (see Figure 5.19(b)). For large solutes, rejection begins at a distance of one solute radius away from the surface (based on $e^{-\phi(\underline{d})} = 0.01$). For smaller molecules, the dipoles are not capable of totally rejecting the solute molecules and a finite concentration exists at a distance of one solute radius from the membrane surface (see prediction for PEG200 in Figure 5.19(b)). This condition is more reasonable than that predicted for repulsive van der Walls interactions where the potential at $\underline{d} = a_s$ is infinite (see Equation 2.51) and always predicts zero concentration at the pore wall for any value of A_{AM}.

5.2 Summary of the Residual Analysis

The sum of squares of residuals obtained for various fits are summarized in Table 5.1. By process of elimination, the presence of structural or hydration forces at the membrane surface seems to be the best interaction mechanism to explain solute transport through cellulose membranes. It is for the above reasons that the RDPM with solvent mediated interactions was selected to calculate the pore size of the cellulose membranes produced in this work.

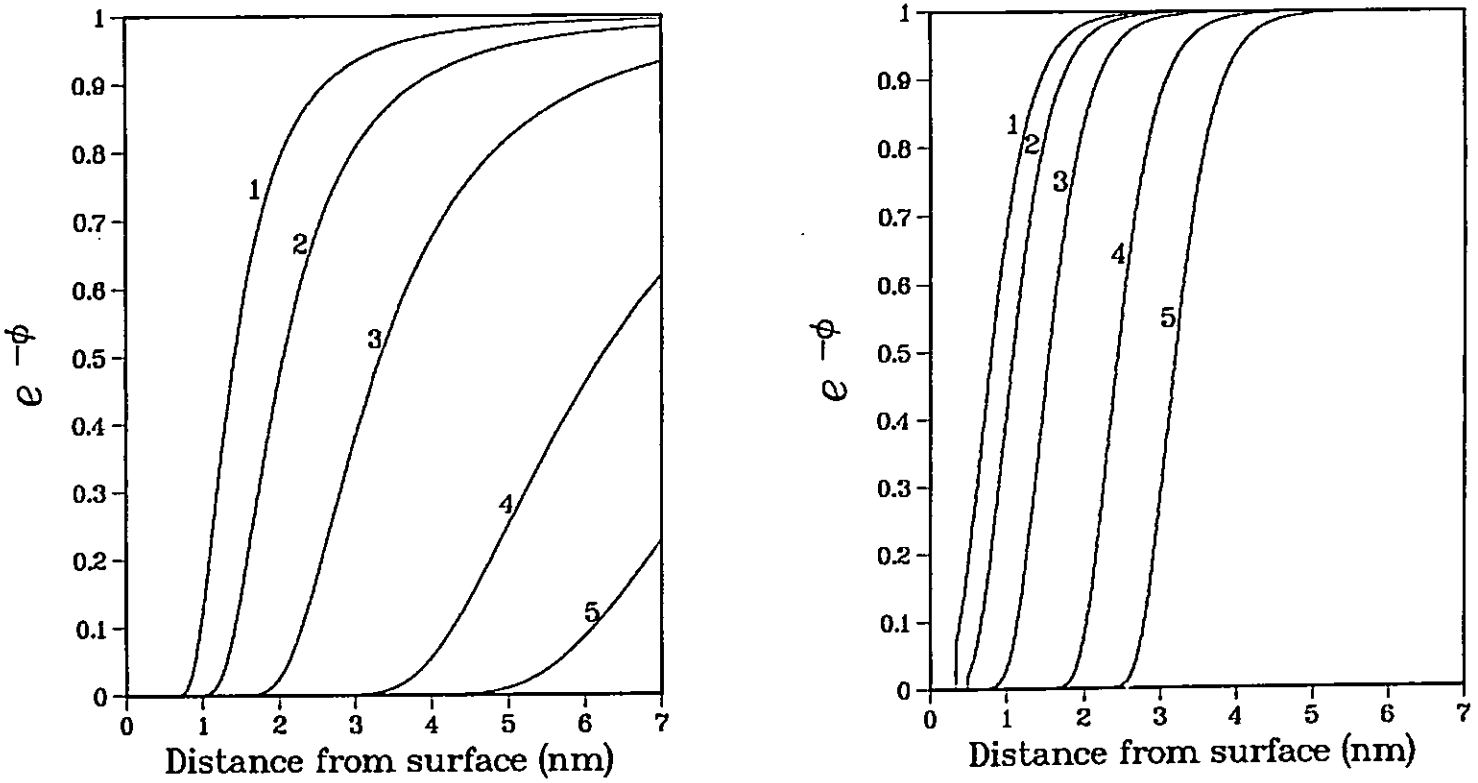

Figure 5.19 : Exponential of the potential force for van der Waals (Hamaker) interactions a) (A_{AM}= - 214), and solvent mediated or dipole interactions b) (κ'=2.969 nm^{-1}, Ψ_{DP} = - 8.901 nm^{-1}) vs. distance from the center of the molecule to the membrane surface. Numbered curves represent profiles for PEG200 (1), PEG600 (2), PEG 1000 (3), PEG3000 (4), and PEG6000 (5).

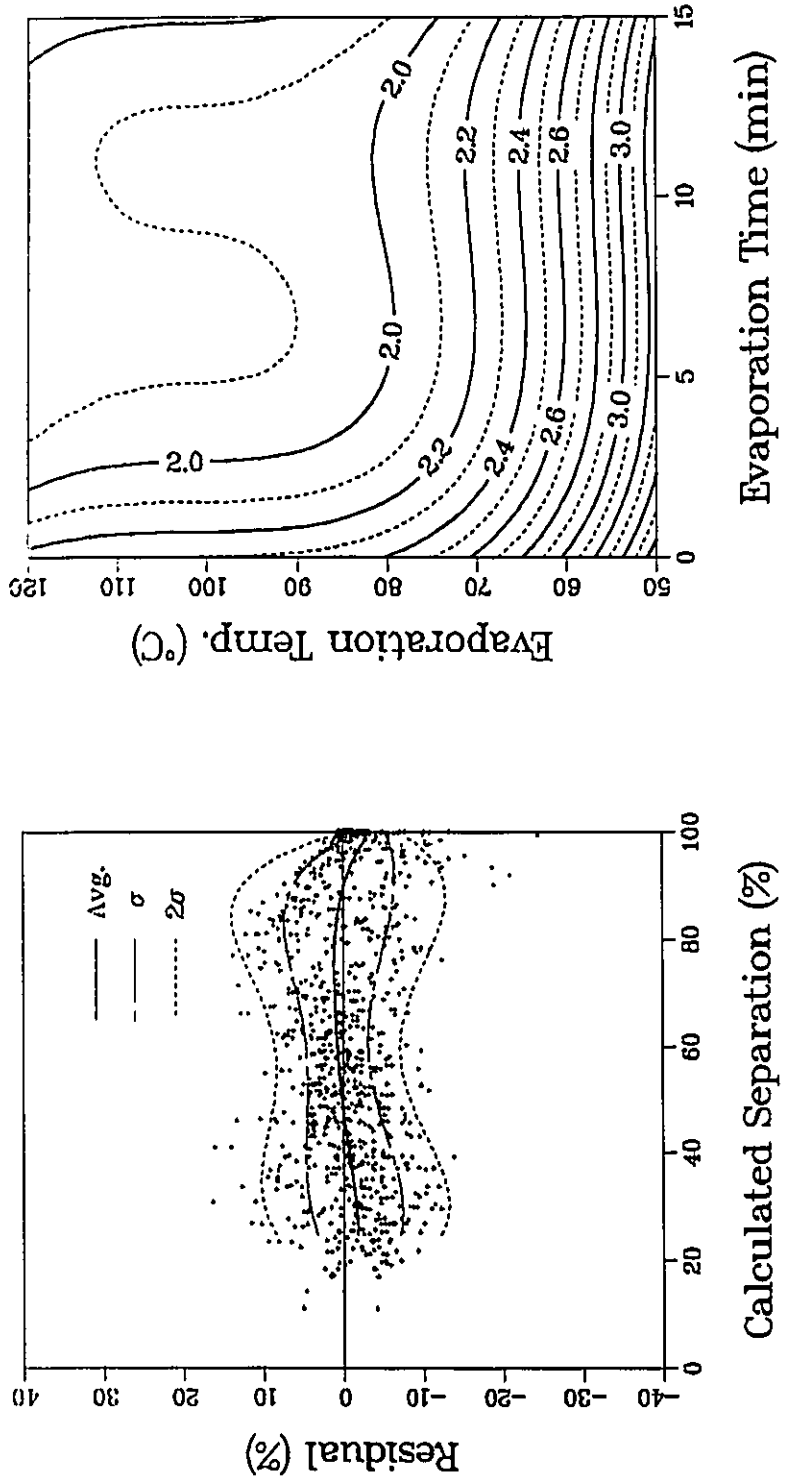

Figure 5.20 : Fit for structural forces due to structured solvent at the membrane surface, residual plot a) and contour plot b), predicted membrane pore size in elevation (nm).

Table 5.1: Sum of Squares of Residuals (SS_{Resid}) based on all 70 membranes, for all fits investigated in this work. Comments for calculated values of R are based on reported values from dye measurements [100].

Type of Solute Interaction used in the RDPM Model	Figure Number	SS_{Resid} $(\%)^2$	Comments: fit to the residuals	Comments: calculated R for the graded membranes
Steric Interaction, G value	5.1	70026.56	Poor	Very low
Steric Interaction, b^{-1} value	5.2	84967.99	Poor	Good
Solute Adsorption	5.3	71290.75	Poor	Very Low
Increased Viscosity, x 39	5.4	305102.80	Very Poor	Very Low
Increased Viscosity, x 100	5.5	367651.10	Very Poor	Very Low
Chain Permeability, $\alpha'' = 10$	5.6	59845.50	Poor	Very Low
Chain Permeability, $\alpha'' = 34$	5.7	60753.18	Poor	Very Low
Chain Permeability, $\alpha'' = 60$	5.8	57147.52	Poor	Very Low
Central Confinement, 1.0x a_s	5.9	288342.30	Very Poor	Very Low
Central Confinement, 1.5x a_s		226692.00	Very Poor	Very Low
Central Confinement, 2.0x a_s	5.10	159138.80	Very Poor	Very Low
Central Confinement, 2.5x a_s		122882.80	Very Poor	Very Low
Central Confinement, 3.0x a_s	5.11	92381.63	Very Poor	Very Low
Central Confinement, 3.5x a_s		78993.70	Very Poor	Very Low
Central Confinement, 4.0x a_s		74386.30	Poor	Very Low
Log-normal Distribution	5.12	15710.43	Excellent	Low
Double Layer, $\kappa = 0.0142\,\mathrm{nm}^{-1}$	5.14	40105.75	Good	Very Low
Fit for strong Hydration	5.15	28742.90	Very Good	Good
Repulsive vdW, $A_{AM} = -214$	5.17	24770.75	Very Good	High
Repulsive vdW, $A_{AM} = -1000$	5.18	24064.41	Very Good	Very High
Structural forces, $\Psi_{DP} = -2.969(\mathrm{nm}^{-1})$	5.20	24767.33	Very Good	Good

5.3 Parameter Estimates of the Structural forces

The best interpretation for solute-membrane interactions affecting the entire set of permeation experiments is that due to the presence of oriented dipoles at the surface of the membrane. The analytical use of this type of interaction requires that Ψ_{DP} and κ' be determined for the solute-water-cellulose system.

The value of κ' is assumed to be related to the nature of the solvent and can be determined from direct force measurements [53]. A test was performed to verify if the value of κ' predicted by Equation 2.56 agreed with the value obtained from the permeation data. A response surface was generated, using the RDPM, for various values of Ψ_{DP} and κ', and is plotted in Figure 5.21. The general response surface is shown in Figure 5.21(a) and the 90% contour region in Figure 5.21(b). It can be seen from Figure 5.21(b) that both values of Ψ_{DP} or κ' cannot simultaneously be determined from a fit to the permeation data. The overall optimum, although not confined by a 90% interval, was found to be at $\kappa' = 2.502$ nm^{-1} and $\Psi_{DP} = -7.094$ nm^{-1}. It is interesting to note that the inverse of κ' calculated from direct measurements $1/\kappa' = 0.34$ nm (standard error =0.02 nm), is in reasonable agreement with the overall optimum of $1/\kappa' = 0.40$ nm.

This agreement between two values obtained from very different experimental observations adds support to the claim that solvent molecules play a major role in membrane transport. This also indicates that the period of decay of the structural force is a property of the solvent molecules and that the two contributions of strength of the dipole network Ψ_{DP} and the period of decay of the structural forces κ' can be separated into distinct parameters. Since water was used as a solvent in all permeation tests, the value of κ'=2.969 nm^{-1}, determined from a fit to the direct force measurements performed in Reference [53], was used in all parameter estimations. The value of Ψ_{DP} and the average pore radius R for each membrane were determined by the two level optimization procedure described in this chapter.

The two level optimization procedure was performed for a set of 70 test coupons and for 68 coupons which contained the original set of 70 excluding two coupons suspected of having pinholes[2]. A total of 965 individual observations were used to

[2]Pinholes are micron sized holes through the selective layer of the membrane. Their presence is easy to discern since the separation of large solutes tends towards asymptotic values other than 100% for such membranes.

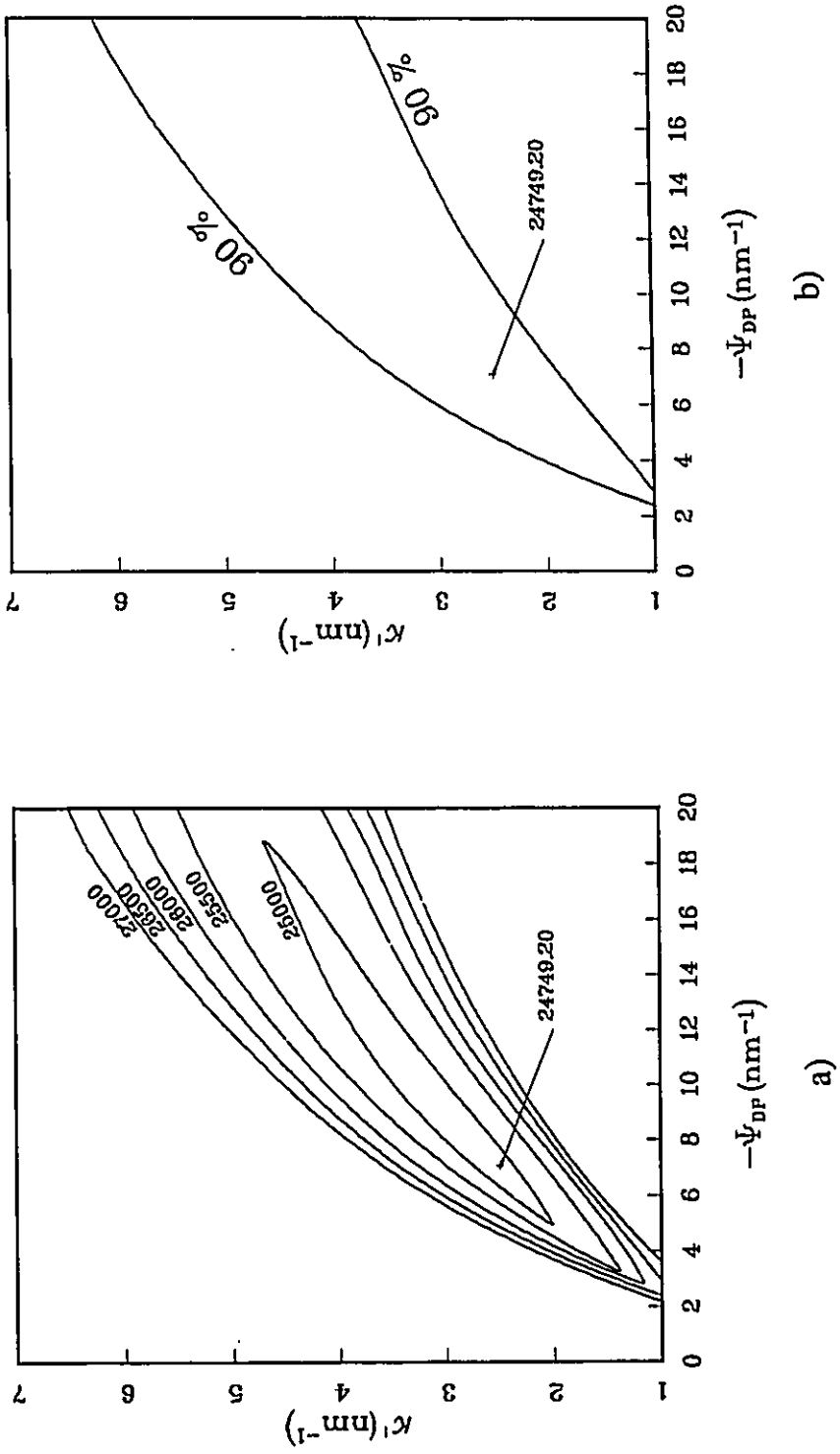

Figure 5.21: Contour plot of the SS_{Reid} based on dipole interactions, for specific contour values a) and the 90 % confidence region. The value of SS_{Reid} = 24,749.20 at Ψ_{DP} = - 7.088 nm^{-1} and κ' = 2.503 nm^{-1} is the overall minimum for 70 membranes.

characterize these membranes. The residuals for the set of 70 coupons are shown in Figure 5.20 and the predicted pore sizes are given in Tables C.1 and C.2. The convergence of the SS_{Resid} to a single minimum for the fit using both 70 and 68 membranes is shown in Figure 5.22. The value of $\Psi_{DP} = -8.902 nm^{-1}$ is reduced to $\Psi_{DP} = -8.045 nm^{-1}$ when the two membranes suspected of containing pinholes are removed from the fit, however the magnitude of the confidence region for Ψ_{DP} is slightly reduced from 8.070 to 6.923 nm^{-1}.

The error involved in predicting the membrane pore radius was determined by summing the respective errors obtained from variations in the estimate of κ' based on the actual force measurements, the error in estimating Ψ_{DP} from the overall fit, and the error in estimating R at the optimum values of κ' and Ψ_{DP} a complete estimate of these errors has been performed and is described in Appendix C.

The estimate of the pores sizes resulting from the data set containing 68 membranes were chosen as the effective pore radius of the membrane and the values listed in Table C.2 were used in the following sections.

5.4 Evaluation of Ψ_{DP} for Various Solutes

Values of Ψ_{DP} were determined for solutes contained in Table 4.5. The pore radius obtained in the PEG characterization (see Table C.2) was used to calculate the value of Ψ_{DP} for each individual solute. These results are listed in Table 5.2 below. Recall that solute interactions with the solvent at the membrane surface and a solute molecule, were split into two contributions. One related to the size of the solute and the other related to the ability of a material to penetrate the dipole layer.

Solute size taken as the Stokes-Einstein radius of the solute is easily obtained from diffusivity measurements. It would be useful to have a predictive relation of Ψ_{DP} for various solutes. Since the sign and magnitude of Ψ_{DP} is assumed to be related to the compatibility of the solute molecule with that of the dipole layer, then Ψ_{DP} must be related to the affinity of the solvent molecules for the solute. This interaction should be related to the enthalpy of mixing of solute molecules in the solvent which can be calculated from the heat of vaporization (ΔE) of the solute and solvent molecules as shown in Equation 5.2, below,

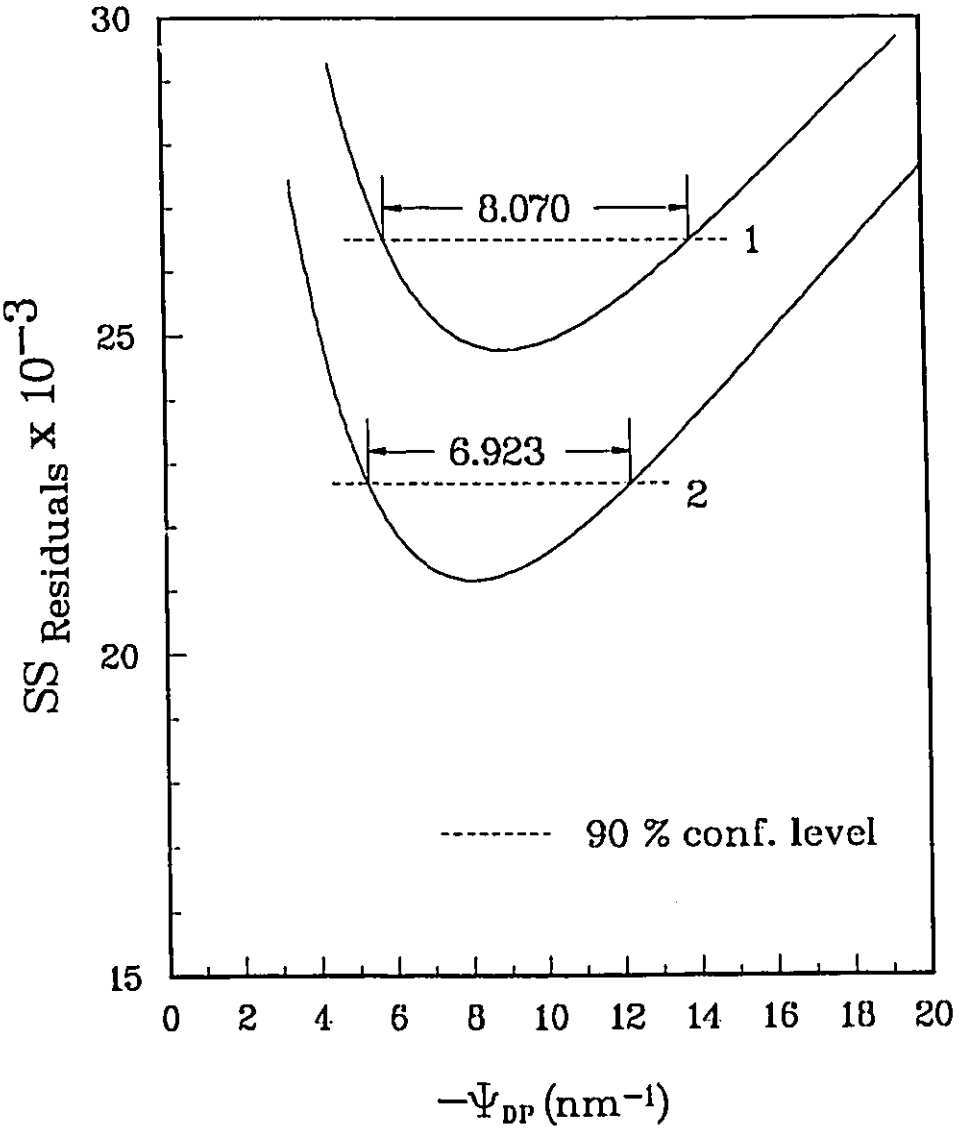

Figure 5.22: Plot of the residual sum of squares SS_{Resid} vs. Ψ_{DP} for all 70 membranes curve 1) and 68 membranes curve 2), dashed lines represent the 90% confidence levels.

$$\frac{\Delta H_{MIX}}{V_{MIX}\phi_A\phi_B} = \left[\left(\frac{\Delta E_A}{V_A'}\right)^{\frac{1}{2}} - \left(\frac{\Delta E_B}{V_B'}\right)^{\frac{1}{2}}\right]^2 . \quad (5.2)$$

Where ΔH_{MIX} is the enthalpy of mixing, ΔE the heat of vaporization, V_i' is the molar volume and ϕ_i the molar fraction of a component in solution. The quantity $(\Delta E/V)$ is known as the "internal pressure" or the "cohesive energy density" of the solute molecules. The quantity $\delta_{SP} = (\Delta E/V)^{1/2}$ is the solubility parameter of a particular component and can be obtained from group contributions (see Reference [7]). The heat of mixing ΔH_{MIX} is related to the affinity of a solvent molecules for a particular solute, in such a case a correlation should exist between ΔH_{MIX} and Ψ_{DP} . Then a plot of $\sqrt{\Psi_{DP}}$ vs. the solubility parameter δ_{SP} should be linear as suggested by Equation 5.2.

The square root of $-\Psi_{DP}$ for the solutes listed in Table 5.2 [3] were plotted vs. the solubility parameter for the particular solute and the results shown in Figure 5.23. Solutes having an experimental separation in the range of 10% to 90% were retained for this study since it was impossible to obtain reproducible results for Ψ_{DP} above and below these limits. This limitation is simply due to the non linear aspect of the separation vs. solute radius curve, where, for example, any value of Ψ_{DP} can be calculated at 100% separation.

Given the number of steps involved in generating values of Ψ_{DP}, this correlation is excellent and has a squared regression factor of 0.919. The following equation can be used to predict Ψ_{DP} for the transport of the polyethylene glycols, sugars and alcohols used in this study,

$$\Psi_{DP(\mathrm{nm}^{-1})} = \left[1.4612_{(\mathrm{nm}^{-1})} - 3.0016 \cdot 10^{-5}\left(\frac{\mathrm{nm}^{-1}}{(\mathrm{J\ m}^{-3})^{1/2}}\right) \cdot \delta_{SP(\mathrm{J\ m}^{-3})^{1/2}}\right]^2 . \quad (5.3)$$

The ordinate's intercept for this regression predicts a value of 48.69 $\cdot 10^3$ (J $m^{-3})^{1/2}$ which is in the range of 47.85 and 49.28 $\cdot 10^3$ $(Jm^{-3})^{1/2}$ reported for water in References [66] and [7] respectively.

[3] Errors in the estimates of $\sqrt{-\Psi_{DP}}$ were obtained by a standard differential method and plotted in Figure 5.23.

Table 5.2: Calculated values of Ψ_{DP} for various probe solutes based on the pore sizes listed in Table C.2.

"Probe" Solute	Ψ_{DP} (nm^{-1})	Confidence Region, 90 %	$\delta_{SP} \times 10^{-3}$ $(J\ m^{-3})^{1/2}$ †	Number of runs
PEG200	− 7.076	± 0.729	19.25	140
PEG300	− 9.439	± 3.752	19.22	149
PEG400	− 9.562	± 2.395	19.21	117
PEG600 ‡	− 9.006	± 5.627	19.19	117
PEG1000 ‡	− 7.477	± 8.030	19.18	112
PEG2000	− 7.073	± 1.714	19.17	46
ethylene glycol	− 1.931	± 0.077	30.33	29
ethanol	− 3.414	± 0.095	25.73	73
glycerol	− 1.624	± 0.613	33.50	36
erythritol	− 1.293	± 0.452	35.58	68
xylitol	− 0.956	± 0.156	37.03	63
sorbitol	− 1.018	± 0.048	38.14	57
sucrose	− 0.876	± 0.323	44.48	78
raffinose	− 0.436	± 0.265	43.25	80

†- Calculated from group contributions reported in Reference [7].

‡- These solutes had an excessive number outliers and were not included in Figure 5.23.

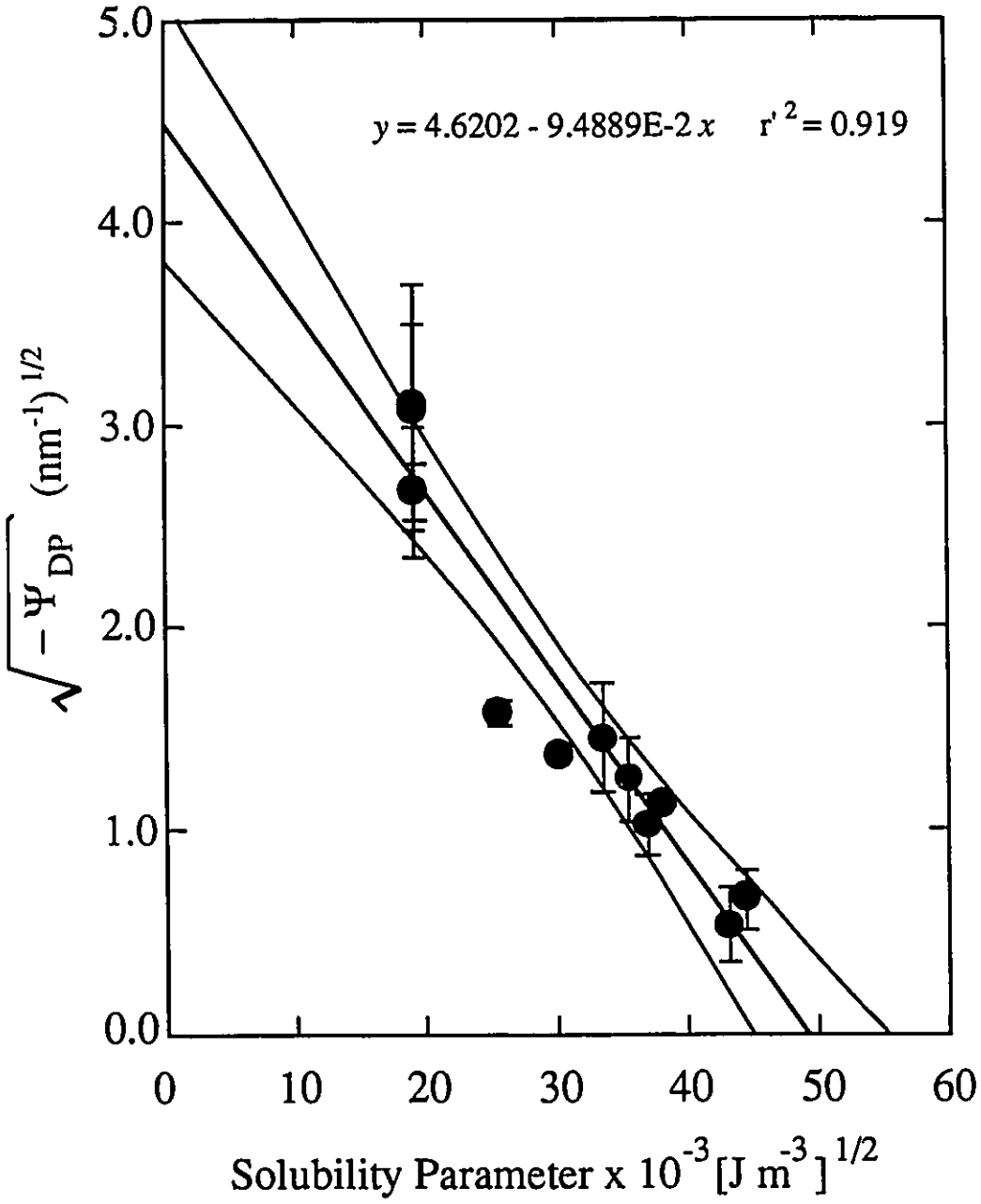

Figure 5.23: Plot of Ψ_{DP} vs. δ_{SP} for PEG's, sugars and alcohols.

It is easily seen from these results that solute molecules which are dissimilar to the solvent are rejected to a greater extent from the hydrated solvent layer than other molecules with values of δ_{SP} nearly equal to that of the solvent. In Figure 5.23, the magnitude of Ψ_{DP} decreases to zero as the value of δ_{SP} tends towards that of the solvent. This behavior indicates that solute molecules which are similar to the solvent are only subjected to steric interactions ($\Psi_{DP} = 0$) when transported through the membrane. This result implies that solutes whose values of $\delta_{SP}(solute) \rightarrow \delta_{SP}(solvent)$ tend to penetrate and integrate the solvent layer at the surface of the membrane. The result is in agreement with the intuitive result that water should be transported sterically in the membrane pore, recall that the slip plane lies within one molecular layer of water from the surface [37].

These observations also suggest that molecules having δ_{SP}(solute) $\rightarrow$ δ_{SP}(solvent) do not travel with fixed hydrated shells through the membrane and most likely share the solvent molecules in their hydrated shells with those of the membrane material. These results are very significant in membrane characterization since they provide means to select solutes which have a minimal interaction with the membrane material.

5.5 Effects Related to the Casting Solution

5.5.1 The initial cellulose particle size

The effect of the initial particle size was determined for several solution concentrations. The calculated pore size of the membranes produced from the <38 μm and 38-53 μm celluloses vs. the casting solution concentration were plotted in Figure 5.24. Details of the casting solutions used to produce these membranes are listed in Table 4.6.

These membranes ranged from thin, clear films at low concentrations to opaque white films at high concentrations. Some difficulties were encountered in producing membranes from the 14% solution using the < 38 μm cellulose. These membranes were opaque, very fragile and tended to split along striated imperfections caused, during the casting procedure, by dragging small mats of undissolved cellulose with the casting blade. All coupons produced from these 14% casting solutions had

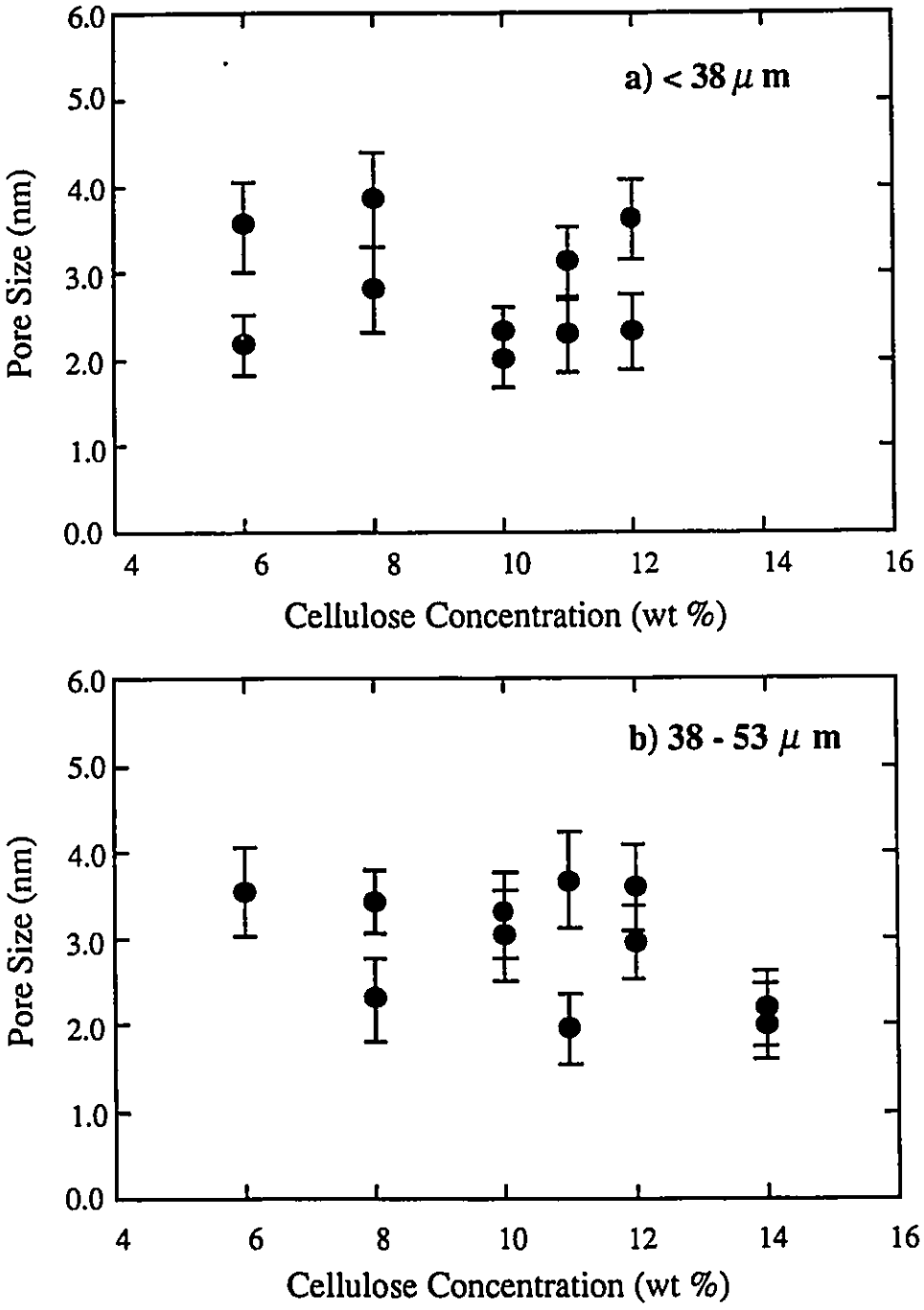

Figure 5.24: Plot of the estimated pore radius as a function of concentration for the <38 μm cellulose a) and 38-53 μm cellulose b). Data for this plot can be found in Table C.2.

evidence of structural failure and extremely high permeation rates which prohibited testing.

These results demonstrate that the limit of dissolution for high cellulose concentrations shown in Figure 4.7 depends on solvent accessibility to the cellulose polymer. The <38 μm cellulose powder either due to a greater crystallinity or lower free volume has less accessibility to the LiCl/DMAc solvent than the 38-53 μm cellulose. This also indicates that, within the limits of dissolution, the initial particle size of the cellulose polymer does not affect the pore size of the membrane.

5.5.2 Cellulose concentration in the casting solution

The effect of the casting solution concentration, on the pore size of cellulose membranes was determined and the results plotted in Figure 5.24. As seen in Figure 5.24 these values fall between 2.0 and 4.0 nm for all concentrations. This demonstrates that within these limits, the pore size of a cellulose membrane is independent of the amount of polymer in the casting solution. This result suggests that a limiting distance must exist between the structural units, be they supermolecular aggregates or crystallites during the phase inversion process.

Scatter plots for the cellulose concentration, pore radius R, pure water permeability PWP, and the ratio of R^4 to the cellulose concentration were generated for both celluloses. These results are shown in Figures 5.25 for the <38 μm cellulose and 5.26 for the 38-53 μm cellulose.

In both cases no correlation exists between the cellulose concentration and R as previously discussed. The PWP is inversely correlated with the cellulose concentration and directly correlated with R. A good correlation was obtained between the PWP and the ratio of R^4/cellulose concentration. The ratio of R^4/cellulose concentration was plotted against the PWP based on a $10.75 \cdot 10^{-4} m^2$ area (see Figure 5.27). Linear correlations were obtained for this data with a fitting parameter of r'^2=0.743 for the <38 μm and r'^2=0.849 for the 38-53 μm. Reasonable correlations were found for this data which indicates that an increase in concentration simply increases the thickness of the selective layer while keeping the pore size of the membrane within the range of 2.0 and 4.0 nm.

5.5.3 LiCl to cellulose mole ratio

The effect of the LiCl:cellulose ratio was investigated for a 10 wt.% solution of 38-53 μm cellulose. The exact casting solution compositions for these membranes are described in Table 4.7 and the calculated pore size of the resulting membranes plotted vs. the mole ratio of LiCl:cellulose in Figure 5.28 (data in Table C.1).

The large amount of scatter in these results and those of Figure 5.24 can be attributed to the inhomogenous nature of the casting solution which contained microgels of swolen or nearly dissolved polymer. All attempts to filter the casting solutions failed since micron sized filters were rapidly clogged by the presence of microgels or undissolved cellulose in the casting solutions. These microgels produced membranes with thin patches typically one half the thickness of the actual membrane. These irregularities caused large variations in pore size between repeats.

However, the best[4] membranes obtained in this study indicate that an optimum mole ratio of 3 to 4 produces the smallest pore sizes. High and low LiCl:cellulose ratios give rise to larger pore sizes, see Figure 5.28.

5.6 Effects Related to the Membrane Making Procedure

5.6.1 Effect of the casting time and temperature

These two variables were selected to produce the series of graded membranes since their effect on solute separation is well known[5]. The results obtained with the set of graded membranes are evident, where high temperatures and high evaporation times give smaller pores than low temperatures and low evaporation times as seen throughout Figures 5.1 to 5.20.

The pore size of the membrane could not be reduced beyond an average of 2.0 nm by increasing temperature or time. This indicates that the aggregate structure of the membrane cannot be shrunk by heat input during the evaporation procedure.

[4] Lowest pore size for a repeated cellulose concentration.

[5] This only applies for operating temperatures which are well below the decomposition point of the polymer.

5.6.2 Effect of liquid ammonia

The effect of liquid ammonia on membrane porosity was investigated by three basic treatments. In a first treatment (method 1) a membrane was soaked in liquid ammonia at $-33°C$ for a given time and quenched in water at room temperature. In a second treatment (method 2) a cast cellulose solution was treated with liquid ammonia prior to evaporation and the film gelled in acetone in the conventional manner. In a third treatment (method 3) water present in the membrane was exchanged by 2-propanol or acetone prior to its immersion in liquid ammonia and then quenched in liquid ammonia or acetone, the film was then contacted with water prior to testing.

Membranes used in this study were cast from an 14% cellulose solution (38-53 μm), 3:1 LiCl:cellulose mole ratio, treated at 95°C for 5 min and gelled in acetone at 4°C. The pore sizes obtained for the three preparation methods are described in Table 5.3.

These results indicate that treating wet membranes (method 1) and treating the cast solution prior to evaporation (method 2) caused a slight increase in the pore size of the resulting membrane. The last method of treatment (method 3) did actually shrink the pore size of the cellulose membranes from 2.28 to 1.61 nm for the 2-propanol solvent exchange.

The results from method 1 and 2 tend to indicate that the presence of sorbed water increases the pore size of the membrane, which is to be expected since solutions of ammonia in water can act as solvents for cellulose. The pore size of membranes Cell66 and Cell65 in Table 5.3 (method 3) were reduced from 2.58 nm to 1.86 nm by solvent exchange with acetone before dipping in liquid ammonia.

Finally, when most of the sorbed water is removed by solvent exchange, pore shrinkage occurs but does not proceed below 1.6 nm. This can be attributed to a slight amount of adsorbed water left in the original cellulose membrane which could act to limit the distance at which two supermolecular aggregates can approach each other.

Table 5.3: The effect of various liquid ammonia treatments on the pore size of cellulose membranes. Except stated otherwise, membranes were cast from an 14% cellulose solution (38-53 μm), 3:1 LiCl:cellulose mole ratio, treated at 95°C for 5 min and gelled in acetone at 4°C.

Method 1

Membrane Number	Comments	Pore Size (nm)
Cell55	No Treatment	2.28
Cell56	No Treatment	3.12
Cell58	5 seconds in NH_3, quench in H_2O	2.13
Cell63	15 seconds in NH_3, quench in H_2O	2.18
Cell67	0.5 hour in NH_3, quench in H_2O	2.64
Cell68	0.5 hour in NH_3, quench in H_2O	2.69
Cell62	1.5 hour in NH_3, quench in H_2O	3.07
Cell69	1.5 hour in NH_3, quench in H_2O	2.82
Cell70	24 hours in NH_3, quench in H_2O	2.60
Cell60	6% solution , 5 sec in NH_3, quench in H_2O	>4.0
Cell64	11% solution, 5 sec in NH_3, quench in acetone	>3.22

Method 2

Membrane Number	Comments	Pore Size (nm)
Cell59	1 min in NH_3 before evaporation and gelation	2.88

Method 3

Membrane Number	Comments	Pore Size (nm)
Cell61	2-propanol exch., 2 min in NH_3, quench in H_2O	1.61
Cell66	No exchange, 2 min in NH_3, quench in acetone	2.58
Cell65	Acetone exch., 2 min in NH_3, quench in acetone	1.86

5.7 Casting Solution Morphology

A considerable Weisenberg effect (rod climbing) [101] was noticed on the stirrer rod used in solution preparation (see Figure 4.1) which indicated that the cellulose solutions were non-newtonian. Preliminary tests were performed using a Rheometrics Mechanical Spectrometer, in the cone and plate configuration, which revealed that such concentrated solutions of cellulose had very long relaxation times (~1.5 hours). This indicates the presence of well defined rigid structural elements in the solution. The characteristics for both linear (flexible) molecules and rod like polymers in concentrated solutions are listed in Table 5.4.

Table 5.4: Comparing solutions of flexible chains and rod like molecules.

Linear (flexible) molecules	Rod-like molecules
• Moderate shear thinning	• Highly shear thinning
• Any flexible high molecular weight polymer	• Many bio-polymers and polyelectrolytes
• Critical molecular weight for the onset of molecular entanglement is ~100,000	• Critical molecular weight for the onset of molecular interaction is ~2300
• Short relaxation times	• Very long relaxation times
• Linear viscoelastic properties on a wide range of deformations	• Linear viscoelastic behavior at extremely small deformations
• η_0 concentration dependence is $\eta_0 \propto \text{Conc}^{4-5}$[86]	• η_0 concentration dependence is $\eta_0 \propto \text{Conc}^{11-12}$ [85,86]

The viscosity of casting solutions at zero deformation (η_0) were determined from the slope of the shear stress vs. shear rate curve at vanishing shear rates. Three cellulose concentrations 8, 10 and 12 % (3:1 mole ratio of LiCl:cellulose) were tested

and the results listed in Table 5.5.

This plot of the log(viscosity) vs. concentration, see Figure 5.29, was found to be linear with a slope of ~12. This value compares fairly well with a slope of ~11.3 obtained for a rigid helical polypeptide, poly-γ-benzyl-L-glutamate (PBLG) in *m*-cresol (data adapted from Reference [85]). A slope of ~12.0 was obtained for poly(1,4-benzamide) (PBA), a rigid synthetic condensation polymer, in DMAc/LiCl (data adapted from Reference [86]). Slopes of ~8 are reported for branched poly(vinyl acetate) (PVAc) in ethyl *n*-bultyl ketone [87], and 4-5 for the flexible chains of linear PVAc [86,87].

Table 5.5: Viscosity of the casting solution at vanishing shear rates (η_0).

Cellulose Concentration 3:1 LiCl:cellulose ratio (wt.%)	Viscosity η_0 (kg $m^{-1}sec^{-1}$)
8.0	0.72
10.0	10.59
10.0	11.61
12.0	92.01

The casting solutions used in this study were highly shear thinning, had very long relaxation times, were made from a bio-polymer, and had an exponent of 12 for the concentration dependence of η_0, all of which indicate that rigid, rod-like structures were present in the casting solutions. These observations suggest that cellulose molecules do not exist as random coils or spherical supermolecular aggregates in solution but as the original single protofibrils or rod-like aggregates of the protofibrils found in natural cellulose. Unfortunately such experiments do not verify the existance of large supermolecular aggregates in solution. However, if such structures are present, they must be rigid and rod-like or filamentous.

The ribbon-like structure of a protofibril proposed by Manly [84] of dimension 3.5 x 2.0 x 38 nm (based on a viscosity average molecular weight of 65000) could explain the lower limit of 1.5 nm for the pore size of cellulose membranes. A cellulose molecule, in the ribbon configuration, shown in Figure 3.2, has alternating gaps on both sides of the protofibril structure which have been estimated to be 1.0 nm wide for dry cellulose [84].

In this work, the protofibril is swollen with water, which tends to increase the gap size[6] by at least two molecular diameters of water, giving a value of 1.6 nm. Since the folded ribbon is the conformation with lowest energy, protofibrils would tend to be stacked in order to favor the largest amount of hydrogen-bonding. The optimum or ideal intramolecular stacking is one where the ribbons forming the protofibrils are in perfect sequence and face each other. In the best case, adjacent stacking of protofibrils imposes, a minimum pore radius of one gap size or 1.6 nm. This implies that even in the best possible molecular packing, cellulose, as a material, has inherent porosity.

In practice, these fibrils are swollen with water, their stacking is not perfect and they are oriented in a random three dimensional structure. All these considerations cannot justify a lower limit on the pore size of cellulose membranes since cellulose acetate has these limitations but remains one of the most widely used RO membrane materials. The best justification for this lower limit, is that protofibrils are not destroyed in the dissolution process. These rigid, notched structures combined with stacking limitations due to the corregated surfaces and the presence of non-volatile solvating agents in the casting solutions (precipitated during the evaporation process) create natural barriers to the formation of small pore cellulose membranes. These morphological limitations would explain why, to this day, a small pore cellulose membrane has not been produced.

[6]The macroscopic evidence of an increase in the size of a protofibril, is the swelling of cellulose on contact with water.

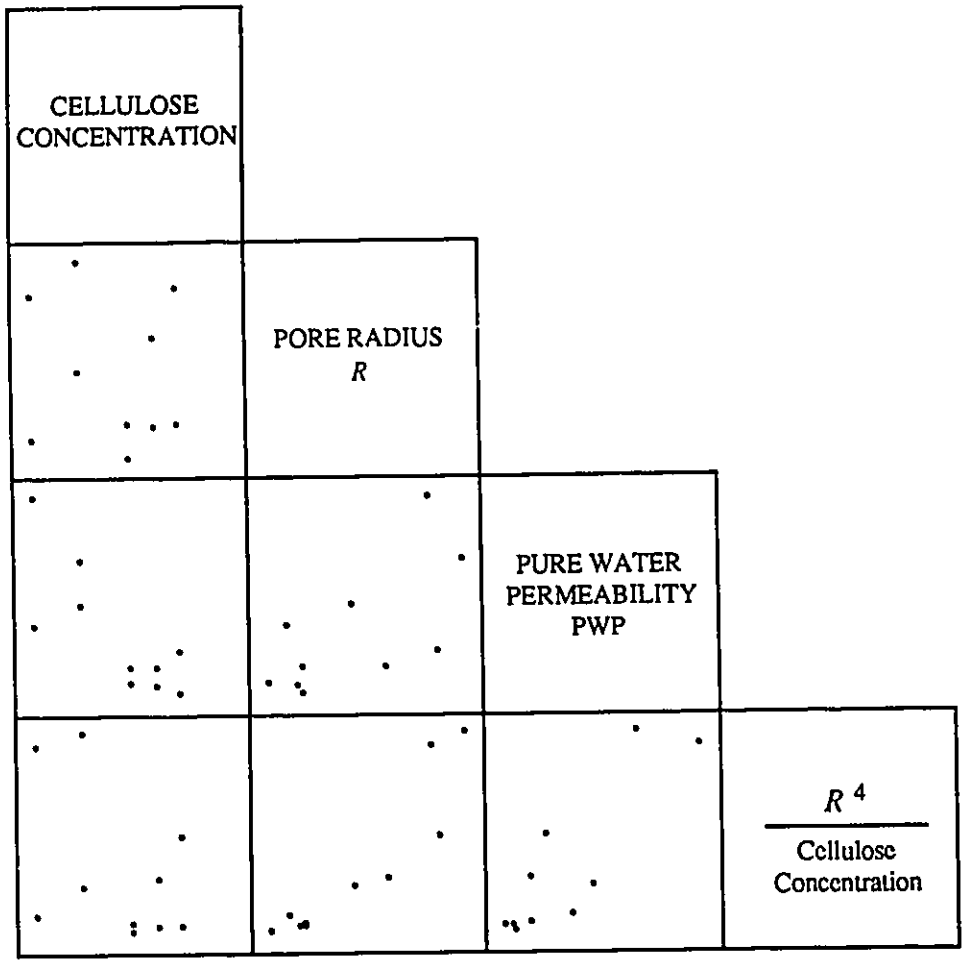

Figure 5.25: Scatter Plot Matrix for the <38 μm cellulose. Indicates possible correlation between the cellulose concentration (wt.%), pore radius R (nm), PWP (g/hr, 10.75 cm^2 basis), and the ratio R^4/cellulose concentration.

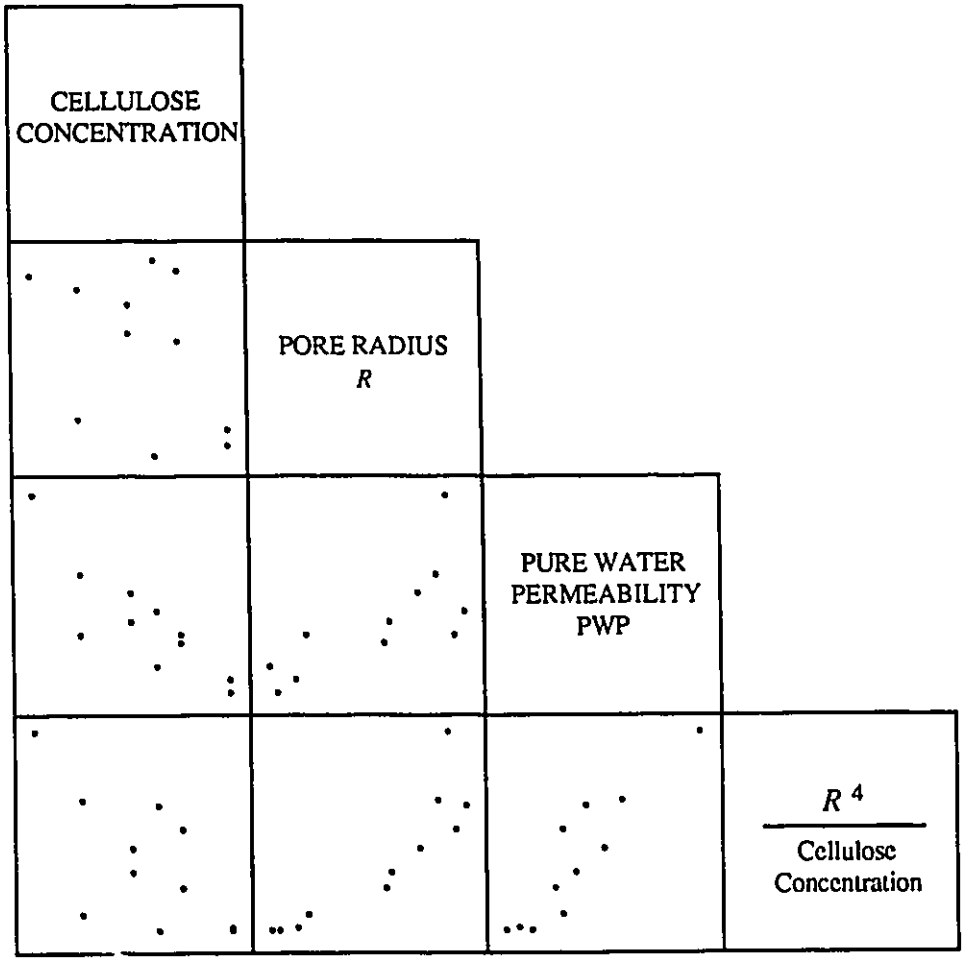

Figure 5.26: Scatter Plot Matrix for the 38-53 μm cellulose. Indicates possible correlation between the cellulose concentration (wt.%), pore radius R (nm), PWP (g/hr, 10.75 cm^2 basis), and the ratio R^4/cellulose concentration.

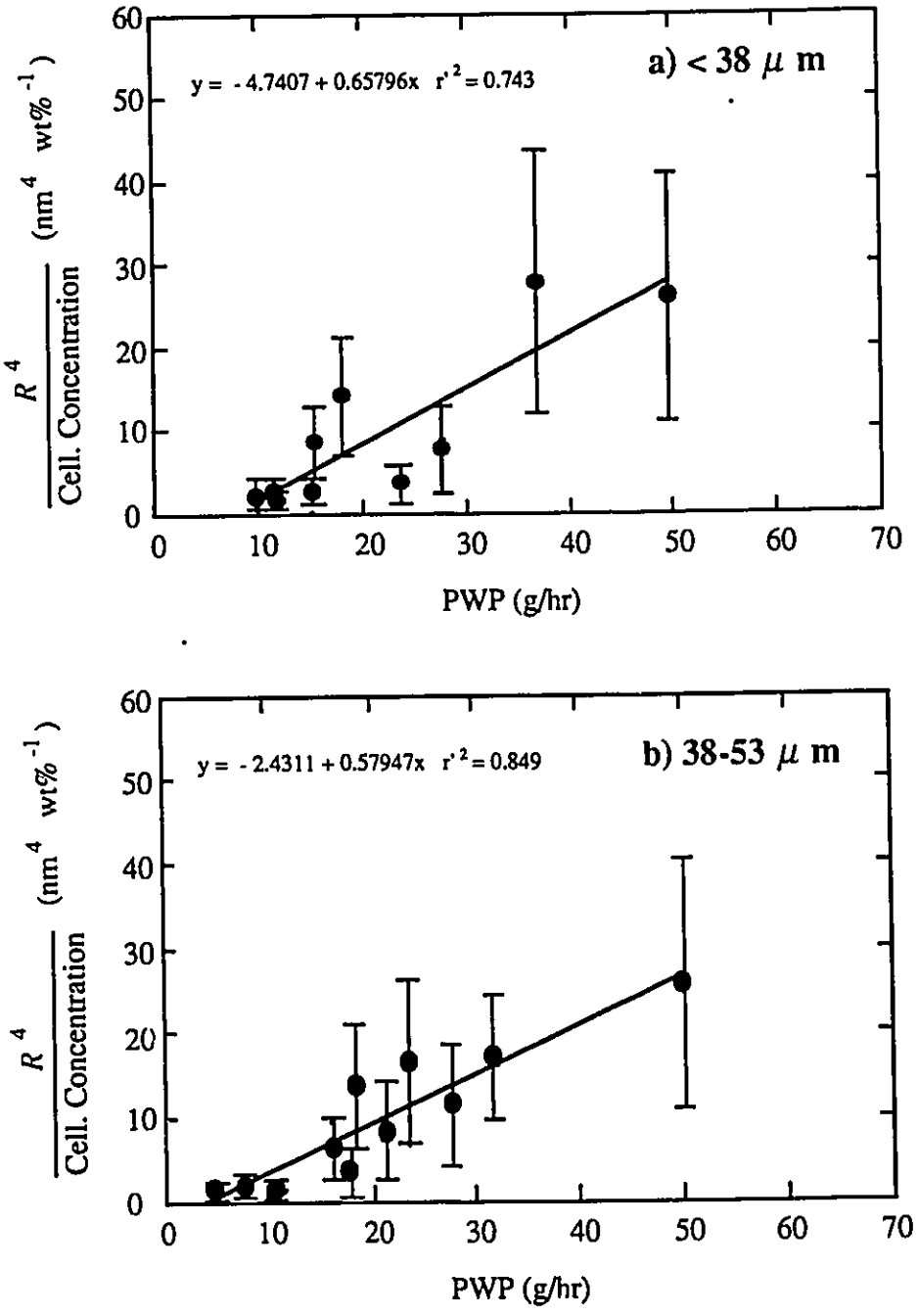

Figure 5.27: Plot of the ratio R^4/cellulose concentration vs. the PWP based on a 10.75 X $10^{-4}m^2$ area for the <38 μm and 38-53 μm particle sizes.

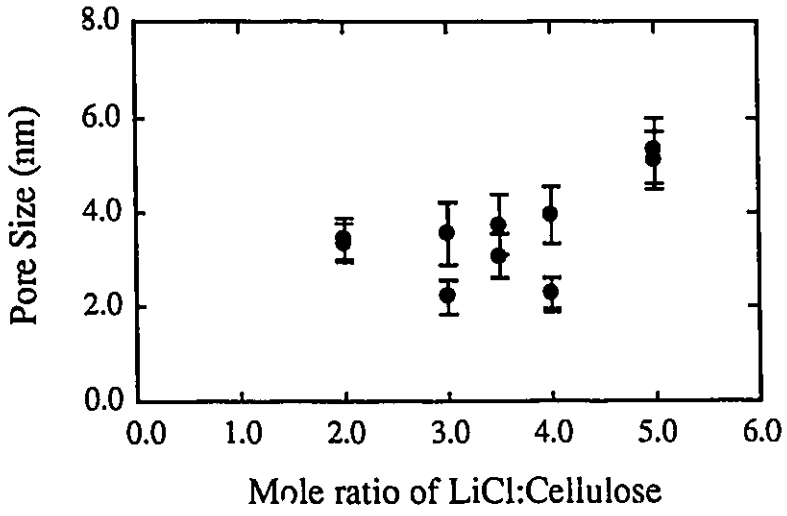

Figure 5.28: Plot of the estimated pore radius as a function of the mole ratio of LiCl to cellulose, for a 10 wt.% solution of 38-53 μm cellulose. Data for this plot can be found in Table C.2.

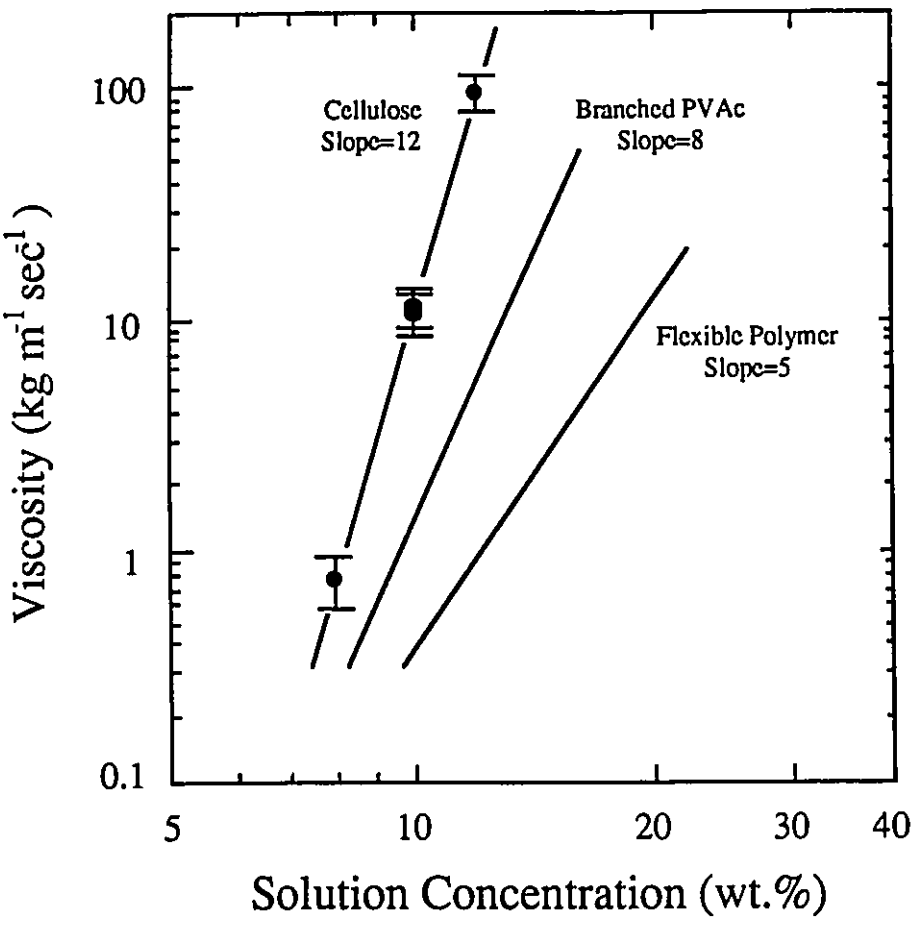

Figure 5.29: Plot of the casting solution viscosity at vanishing shear rates (η_0) vs. cellulose concentration for 8, 10 and 12 wt.% cellulose solutions based on a LiCl:cellulose ratio of 3:1. Fictitious lines represent slopes for branched PVAc and a flexible polymer.

Chapter 6

Conclusions and Recommendations

6.1 Conclusions

The following conclusions for modelling membrane transport and the production of small pore cellulose membranes can be drawn from this work;

- Several possible transport mechanisms such as the increase in the viscosity inside the pore, the shape of the interacting surface, electrostatic double layer, van der Waals and structural solvent interactions were quantified for a polydisperse solute and their relevance determined from the goodness of fit to the residuals and from the predictions for a set of graded membranes. The model which best suited both criteria was a radially dependent pore model (RDPM) with solute interactions based on the presence of oriented dipoles at the surface of the membrane.
- Interactions between the material forming the solute and membrane play a minor role in solute-membrane interactions. It is rather the interaction of the solute with structured dipoles at the surface of the membrane which controls solute-membrane interactions. In such a case solute transport through a membrane is "solvent mediated".

- Two new interaction parameters Ψ_{DP} and κ' describing the interaction of solute molecules with structured solvent molecules present at a submerged surface have been defined. A method to evaluate these parameters is also given. Their values can be determined from simple permeation experiments for Ψ_{DP} and direct force measurements for κ'.

- The pore size of 70 membranes have been evaluated from polyethylene glycol (PEG) permeation experiments. These pore radii along with permeation experiments for various sugars and alcohols were used to determine values of Ψ_{DP} for these solutes. A linear correlation was found to exist between the square root of Ψ_{DP} and the solubility parameter of the solute. The slope of this line is considered to be characteristic of the ability of the membrane material to structure solvent at a solid-liquid interface. Solutes having solubility parameters close to those of water were found to have small values of Ψ_{DP} which indicated a tendency towards steric interaction ($\Psi_{DP} = 0$). This suggests that solvent molecules can become an integral part of the hydration layers present at the surface of the membrane and have finite concentrations at distances of one solute radius, a_s, away from the membrane surface, a concept which is impossible based on van der Waals interactions.

- The value of $b^{-1}(\lambda)$ predicted by Equation 2.21 seems to combine the effects of restricted transport and solvent interactions into one parameter.

- This work rejects the possibility of steep viscosity increases within the membrane pores. This conclusion agrees with the direct measurements performed in Reference [37] which indicate that the viscosity of water is the same as that of the bulk solution down to surface separations of 1.85 nm. This suggests that the restricted transport parameters defined for, K^{-1}, and, G, are applicable down to the RO range of porosities.

- For dilute solutions under both repulsive and steric solute-membrane interactions, a parabolic velocity profile represents the explicit solution of Equation 2.22 and can be used to describe the permeation of most "probe" solutes through membrane pores. This is not the case however for characterizations based on proteins such as casein which are often attracted to the membrane

material. Such solutes would have flat velocity profiles (see Figures 2.6 and 2.8) which must be accounted for in a complete analysis.

- The unusually high dependence of solution viscosity on concentration indicates that the natural structure of cellulose is that of rigid, ribbon-like protofibrils which are not destroyed by the LiCl:DMAc solvent. The cellulose protofibrils have the shape of folded ribbons which explains the 1.5 nm, minimum pore size attainable for cellulose.

- The use of solvent exchange followed by liquid ammonia treatment was successful in reducing the pore size of cellulose membranes. The lower limit of 1.5 nm could not be broken via this method of treatment.

- In view of the morphological constraints imposed by cellulose, any amount of mechanical energy will not destroy the protofibril structure which is held by hydrogen bonding. This implies that mechanical energy input or ultrasonication cannot be used to obtain small pore cellulose membranes.

- Since membrane permeation results seem to display some amount of randomness, model discrimination based on permeation data can only be done with large amounts of data. This emphasizes a need for further development in automating the time consuming membrane permeation experiments.

6.2 Recommendations

The following improvements are recommended;

- The regeneration of cellulose from solutions where the protofibril structure is destroyed[1], is probably a better route to obtain small pore cellulose membranes, and should be thoroughly investigated.
- The polydisperse and single solute methods of membrane characterization should be rigorously compared with a large amount of permeation runs to determine if the use of single solutes provides such a definite advantage.
- The universality of the Ψ_{DP} vs. δ_{SP} correlation should be determined for other solutes, solvents and membrane materials. In the case of the separation of phenolic compounds correlations based on the contributing elements of δ_{SP} such as the dispersion, polar and hydrogen bonding components [7] of the total solubility parameter might be better correlated than the overall parameter itself.
- On-line concentration measurement with a high degree of accuracy should be added to the automated testing device. The selection of a reproducible method of analysis is not evident in ppm detection ranges.

[1] Cellulose tributyrate for example exists as flexible chains in several solvents [102].

Bibliography

[1] E.K.L. Lee, W.C. Babcock, and P.A. Bresnahan, *Countercurrent Reverse Osmosis for Ethanol-Water Separation*, U.S. Dept. of Energy, Final Report, 1983, DE83 009725.

[2] G.D. Mehta, *J. Membrane Sci.*, **12**, 1-26 (1982).

[3] T. Matsuura, Y. Taketani, and S. Sourirajan, *Proceedings of the Fourth Bioenergy R & D Seminar*, Winnipeg, Canada, March 1982, 529.

[4] M. Soltanieh and W.N. Gill, *Chem. Eng. Commun*, **12**, 269-363 (1981).

[5] T.K. Sherwood, P.L.T. Brian, and R.E. Fisher, *I. & E. C. Fund.*, **6**, 2-12(1967).

[6] S. Sourirajan, *Reverse Osmosis*, Academic Press (1970).

[7] S. Sourirajan and T. Matsuura, *Reverse Osmosis/Ultrafiltration Process Principles*, National Research Council Canada, Ottawa, NRCC No. 24188, (1985).

[8] J.R. Pappenheimer, E.M. Renkin, and L.M. Borrero, *Am. J. Physiol.*, **167**, 13 (1951).

[9] E.M. Renkin, *J. Gen. Physiol.*, **38**, 225 (1954).

[10] A. Verniory, R. Du Bois, P. Decoodt, J.P. Gassée, and P.P. Lambert, *J. Gen. Physiol.*, **62**, 489-507 (1973).

[11] R. Du Bois and E. Stoupel, *Biophys. J.*, **16**, 1427-1445 (1976).

[12] J.L. Anderson and J.A. Quinn, *Biophys. J.*, **14**, 130-149 (1974).

[13] H. Mehdizadeh and J.M. Dickson, *J. Mem. Sci.* , **42**, 119-145(1989).

[14] A. Fick, *Pogg. Ann.*, **94**, 59-86 (1855).

[15] H. Dutrochet, *Mémoires pour servir* , **1**, Bailliere, Paris, (1837), in [44].

[16] E. Brück, *Pogg. Ann. d. Physik.*, **58**, 77-94 (1843).

[17] M. A. Guérout, *Compt. Rend.*, **75**, 1809 (1872).

[18] C. Barus, *Am. J. Sci.*, **48**, 451-454 (1894).

[19] H. Bechhold, *Z. Physik. Chem.*, **60**, 257 (1907).

[20] H. Bechhold, *Biochem. Z.*, **6**, 379-408 (1907).

[21] H. Bechhold, *Z. Physik. Chem.*, **64**, 328-342 (1908).

[22] J.D. Ferry, *Chemical Reviews*, **18**(3), 373-455 (1936).

[23] V.E. Manegold, *Kolloid-Z.*, **50**, 22-39 (1930).

[24] J.D. Ferry, *J. Gen. Physiol.*, **20**, 95-104 (1936).

[25] R.D. Schultz and S.K. Asunmaa, in *Recent Progress in Surface Science*, J.F. Danielli, A.C. Riddiford and M. Rosenberg, Eds., Academic Press, New York, **3**, 291-332 (1970).

[26] O. Velicangil and J.A. Howell, *J. Phys. Chem.*, **84**(23), 2991-2992 (1980).

[27] M.N. Sarbolouki, *J. Appl. Poly. Sci.*, **29**, 743-753 (1984).

[28] R. Ladenburg, *Annalen der Physik*, **23**, 447-458 (1907).

[29] R. Ladenburg, *Annalen der Physik*, **22**(4), 287-309 (1907).

[30] A. Westgren, *Annalen der Physik*, **52**, 308-322 (1917).

[31] H. Faxen, *Annalen der Physik*, **68**, 89-119 (1922).

[32] J. R. Pappenheimer, E. M. Renkin and L.M. Borrero, *Am. J. Physiol.*, **167**, 13-46 (1951).

[33] J.A. Quinn, J.L. Anderson, W.S. Ho, and W.J. Petzny, *Biophys. J.*, **12**, 990-982 (1972).

[34] A. K. Solomon, *J. Gen. Physiol.*, **51**, 335 (1968).

[35] C. P. Bean, in *Membranes*, G. Eisenman, ed., Dekker, New York, **1**, 1 (1972).

[36] W. M. Deen, *A. I. Ch. E.*, **33**, No. 9, 1409-1425 (1987).

[37] J. N. Israelachvili, *J. Colloid Interface Sci.*, **110**, 263-271 (1986).

[38] W. Spendley, G.R. Hext and F.R. Himsworth, *Technometrics*, 4, 441-461 (1962).

[39] J.A. Nedler and R. Mead, *Computer J.*, 7, 308-313 (1965).

[40] W.H. Press, B.P. Flannery, S.A. Teukolsky, and W.T. Vetterling, *Numerical Recipes, The Art of Scientific Computing*, Cambridge University Press, Cambridge, 1986.

[41] U. Merten, in *Desalination by Reverse Osmosis*, U.Merten, Ed., M.I.T. Press, Cambridge, Mass., 15-54(1966).

[42] H. Brenner and L.J. Gaydos, *J. Colloid and Interface Sci.*, 58(2), 312-356 (1977).

[43] P.M. Bungay and H. Brenner, *Int. J. Multiph. Flow*, 1, 25 (1973).

[44] W. Pfeffer, *Osmotische Untersuchungen* (1887), translated as *Osmotic Investigations, Studies on Cell Mechanics*, Van Nostrand Reinhold Company Inc., (1985).

[45] P.C. Hiemenz, *Principles of Colloid and Surface Chemistry*, Marcel Deckker, Inc., New York, (1986).

[46] M. Rigby, E.B. Smith, W.A. Wakeham, and G.C. Maitland, *The Forces Between Molecules*, Clarendon Press, Oxford, (1986).

[47] H.C. Hamaker, *Physica*, 4, 1058 (1937).

[48] J. Mahanty, *Dispersion Forces*, Academic Press, New York, (1976).

[49] S. Ross and I.D. Morrison, *Colloidal Systems and Interfaces*, John Wiley & Sons. Inc., New York, 1988.

[50] E.J.W. Verwey and J.T.G. Overbeek, *Theory of the Stability of Lyophobic Colloids*, Elsevier, New York, 1948.

[51] *Electrical Phenomena at Interfaces; Fundamentals, Measurement, and Applications*, A. Kitahara and A. Watanabe, Eds., Surfactant Science Series, 15, Marcel Dekker Inc., New York, (1984).

[52] G.M. Bell, S. Levine, and L.N. McCartney, *J. Colloid and Interface Sci.*, **33**(3), 335-359 (1970).

[53] J. N. Israelachvili and R. Pashley, *Nature*, **306**, 249-250 (1982).

[54] G.N. Ling, in *Water and Aqueous Solutions: Structure, Thermodynamics, and Transport Processes*, R.A. Horne , Ed., Wiley-Interscience, John Wiley & Sons, Inc., New York, (1972).

[55] M.S. Metzik, V.D. Perevertaev, V.A. Liopo, G.T. Timoshtchenko, and A.B. Kiselev, *J. Colloid and Interface Sci.*, **43**(3), 662-669 (1973).

[56] D. Bhattacharyya, M. Jevtitch, and J.T. Schrodt, *Chem. Eng. Commun.*, **42**, 111-128 (1986).

[57] N.R. Draper and H. Smith, *Applied Linear Regression Analysis*, John Wiley & Sons, Inc., New York, (1981).

[58] M.G. Davidson and W.M. Deen, *J. Memb. Sci.*, **35**, 167-192 (1988).

[59] H.L. Goldsmith and S.G. Mason, *J. Colloid. Sci.*, **17**, 448 (1962).

[60] R.R Irani and C.F. Callis, *Particle Size: Measurement, Interpretation, and Application*, John Wiley & Sons. Inc., New York, 1963.

[61] W.D. Paist, *Cellulosics*, Reinhold Publishing Corp, New York, (1958).

[62] J.F. Rabek, *Experimental Methods in Polymer Chemistry*, John Whiley & Sons, New York, 1980.

[63] L. Lafrenière, *Development of the Cellulose Reverse Osmosis Membrane*, Workterm Report Univ. of Ottawa, Sept. 16, (1983).

[64] B. A. Farnand, *A Study of Reverse Osmosis Separations Involving Nonaqueous Solutions*, Ph.D. Thesis, Univ. of Ottawa, Ottawa, (1983).

[65] N.M. Bikales and L. Segal, in *Cellulose and Cellulose Derivatives, High Polymers Vol V*, John Whiley & Sons Inc., New York, Part IV, 381 (1971).

[66] J. Brandrup and E.H. Immergut, Eds., *Polymer Handbook*, John Whiley & Sons Inc., New York, V-87 (1975).

[67] A.F. Turback, R.B. Hammer, R.E. Davies, and H.L. Hergert, *Chemtech*, **Jan**, 51 (1980).

[68] F.W. Herrick, *J. Appl. Poly. Sci.***36**, 993 (1983).

[69] A. El-Kafrawy, A.B. Averbach, F.W. Snyder, and A.F. Turbak, Br. Patent 2,055,107B, Apr. 13, (1983).

[70] A.F. Turbak, El-Kafrawy, W. Snyder and A.B. Averbach, U.S. Patent 4,352,770, Oct. 5, (1982).

[71] A.F. Turbak, El-Kafrawy, W. Snyder and A.B. Averbach, U.S. Patent 4,302,252, Nov. 24, (1981).

[72] F.J. Kolpak and J. Blackwell, *Textile Res. J.*, **Aug**, 458 (1978).

[73] S. Sourirajan and B. Kunst, in *Reverse Osmosis and Synthetic Membranes*, S. Sourirajan, Ed., Chap. 7, National Research Council Canada, Ottawa, 1977.

[74] H.K. Lonsdale and H.E. Poldall, Eds., *Reverse Osmosis Membrane Research*, Plenum Press, New York, 1972.

[75] K.E. Kinzer, D.R. Lloyd, J.P. Wightman, and J.E. McGrath, *Desalination*, **46**, 327-334 (1983).

[76] B. Philipp, H. Schleicher, and W. Wagenknecht, *Chemtech*, **Nov**, 702 (1977).

[77] N.W. Taylor and S.H. Gordon, *J. Appl. Poly. Sci.*, **27**, 4377-4386 (1982).

[78] M.E. Cohen, B.M. Riggleman, and P.D. Drechsel, in *Membranes from Cellulose and Cellulose Derivatives; App. Poly. Symp.*, A.F. Turbak, Ed., **13**, 47 (1970).

[79] T. Matsuura and S. Sourirajan, *J. Colloid Interface Sci.*, **66**, 589 (1978).

[80] A.F. Turbak, *T.A.P.P.I. Proc., Int. Dissolving and Specialty Pulps*, 105-110 (1983).

[81] R.B. Hammer, M.E. O'Shaughnessy, E.R. Strauch, and A.F. Turbak, *J. Appl. Poly. Sci.*, **23**, 485-494 (1979).

[82] D. Gagnaire, D. Mancier, and M. Vincendon, *J. Poly. Sci.: Poly. Chem. Ed.*, **18**, 13-25 (1980).

[83] A. El-Kafrawy, *J. Appl. Poly. Sci.*, **27**, 2435-2443 (1982).

[84] R. St. J. Manley, *J. ,P. Sci., Part A-2*, **9**,1025-1059 (1971).

[85] J. Hermans, *J. Colloid Sci.*, **17**, 638, (1962).

[86] S.P. Papkov, V.G. Kulichikhin and V.D. Kalmykova, *J. of Poly. Sci.: Poly. Phys. Ed.*, **12**, 1753-1770, (1974).

[87] S. Onogi, T. Masuda, N. Miyanaga and Y. Kimura, *J. of Poly. Sci.: Part A-2*, **5**, 899-913, (1967).

[88] M. Kouris, H. Ruck and S.G. Mason, *Can. J. Chem.*, **36**, 931-948, (1958).

[89] F.W. Herrick, R.L. Casebier, J.K. Hamilton, and K.R. Sandberg, *J. Appl. Poly. Sci.: Appl. Poly. Symp.*, **37**, 797-813 (1983).

[90] A.F. Turbak, F.W. Snyder, and K.R. Sandberg, *J. Appl. Poly. Sci.: Appl. Poly. Symp.*, **37**, 815-827(1983).

[91] R.E. Kesting, *Synthetic Polymeric Membranes: a Structural Perspective*, Wiley, New York, (1985).

[92] A.S.T.M. D1795-62, *Standard Method for Intrinsic Viscosity of Cellulose*, Reapproved (1979).

[93] A.Y. Tremblay and F.D.F. Talbot, in *Proc. of the International Membrane Conference on the 25th Anniversary of Membrane Research in Canada*, M. Malaiyandi, O. Kutowy and F.D.F. Talbot, Eds., Sept. 24-26, (1986).

[94] S. Sourirajan, *Lectures on Reverse Osmosis*, National Research Council of Canada, (1983).

[95] T.C. Amu,*Polymer*, **23**, 1775-1779 (1982).

[96] F-H. Hsieh, T. Matsuura, and S. Sourirajan, *J. Appl. Poly. Sci.*, **23**, 561-573(1979).

[97] A.Y. Tremblay, *Formation and Characterization of Cellulose Reverse Osmosis Membranes*, Ph.D. Proposal, Univ. of Ottawa, Ottawa, (1984).

[98] H. Mahn, U.S. Patent 1,998,551, April 23, 1935.

[99] R. Woodell, U.S. Patent 2,509,549, May 30, 1950.

[100] K. Sakai, H. Chiba and A. Naitoh, *J. Memb. Sci.*, **37**, 101-112(1988).

[101] A.S. Lodge, *Elastic Liquids*, Academic Press, New York, (1964).

[102] R.F. Landel, J.W. Berge and J.D. Ferry, *J. Colloid Sci.*, **12**, 400-411(1957).

[103] R.N. Goldberg, J.L. Manley and R.L. Nuttall, *GAMPHI - A Database of Activity and Osmotic Coefficients for Aqueous Electrolyte Solutions*, NBS Technical note , 1206, U.S. Dept. of Commerce, Gaithersburg, MD.

[104] M.K. Karapetyants, *Chemical Thermodynamics*, Mir Publishers, Moscow, Eng. Translation (1978).

[105] P. Kruus, *Liquids and Solutions, Structure and Dynamics*, Marcel Dekker, Inc., New York, (1977).

[106] *Handbook of Chemistry and Physics, 69th Ed.*, R.C. Weast, Ed., The Chemical Rubber Co., Cleveland, Ohio, (1988).

[107] R.A. Horne, *Water and Aqueous Solutions*, Wiley-Interscience, New-York, 1972.

Appendix A

Detailed Model Derivations

A.1 A Simple Radially Averaged Pore Model (RAPM)

This derivation presents a very simple restricted transport model, and demonstrates the case of purely steric solute interactions with the pore wall. In this model a rejection coefficient between the concentration of solute in the pore to that of the solution at the pore entrance is determined as a function of the ratio of the solute radius, a_s, to the membrane pore radius R, where $\lambda = a_s/R$. Once this relation is established, the separation of a given solute as a function of pore size, can be determined. The model can be used in conjunction with permeation experiments to obtain the pore size of a membrane.

In this analysis, the effects of solute-membrane attraction or repulsion are neglected and two factors which limit solute flux through the pores are considered,

- a steric or geometric factor for the restricted entrance of a solute into the pore,
- a hydrodynamic factor characterizing the increase in viscous drag due to the presence of the pore wall once the solute has entered the pore.

The membrane is modeled as an array of capillary pores, of cylindrical or rectangular cross-section, whose axis is perpendicular to the surface of the membrane. Solvent inside the pore is assumed to form a continuous phase having the same properties as that of the bulk solution and the usual continuum equations for conservation of momentum are assumed to remain applicable inside the pore. The viscosity of

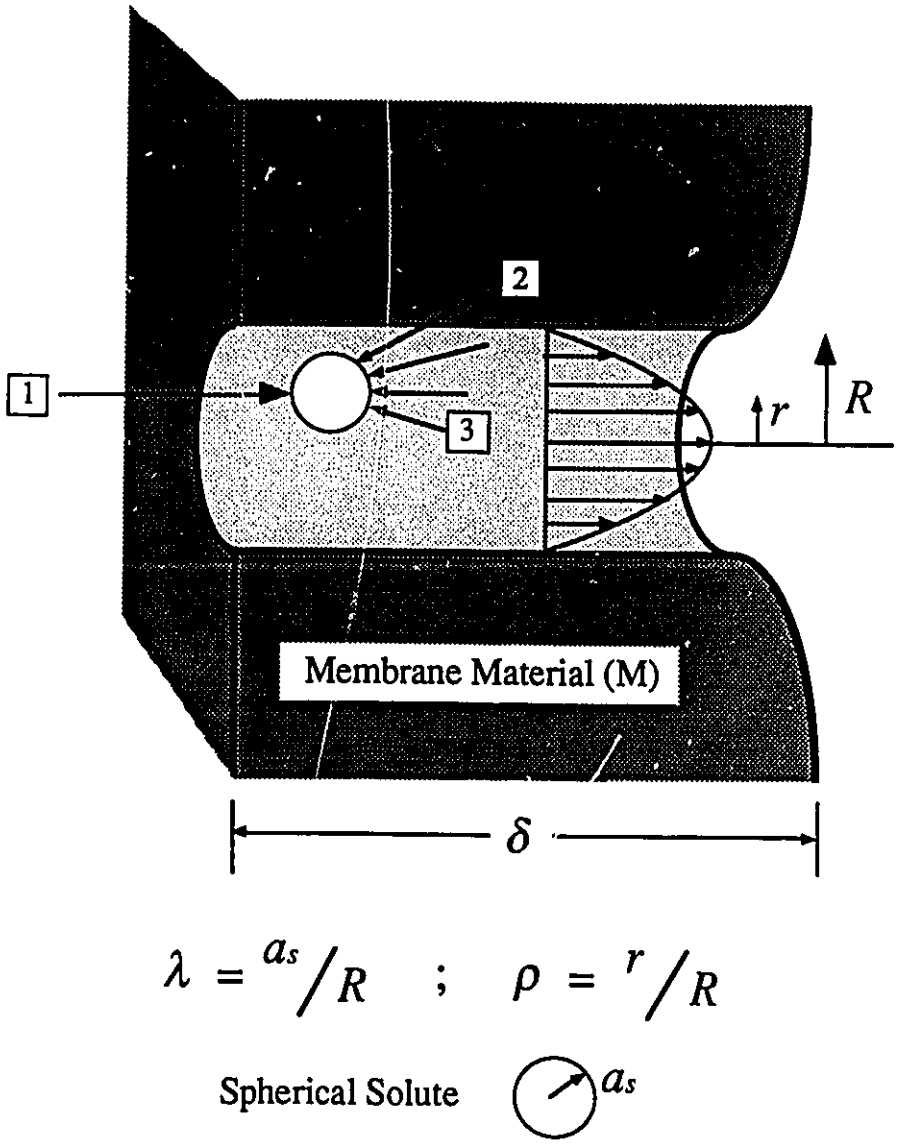

Figure A.1: Forces acting on a solute translating through a pore of radius R, 1) driving force for solute flux, 2) resistance due to the presence of the pore wall and 3) increased molecular friction due to the confined nature of the pore.

water has been measured between two molecularly smooth mica surfaces and found to be equal to that of bulk water down to separations of 1.85 nm [37]. Laminar flow is assumed to exist in the pores and the "plane of slip" is within one adsorbed layer of solvent molecules from the polymer surface [37].

Dissolved solute is considered to be in the form of rigid spheres having both hydrodynamic and Brownian characteristics. A solute molecule is represented by a "locator point" which is a body-fixed origin placed by convention at the center of a sphere of radius, a_s, see Figures 0.2 and A.1. The hydrodynamic resistance to Brownian motion of a solute (A) dissolved in a solvent (B) can be expressed in terms of Einstein's equation,

$$D_{AB} = \frac{kT}{f_\infty}. \tag{A.1}$$

When D_{AB} is the bulk solution diffusivity at infinite dilution, this term is equivalent to D_∞ in Reference [12] and f_∞ is the molecular friction coefficient between the solute and solvent.

If the radius of this solute is at least two to three times that of the solvent, the Wilke-Chang correlation for binary diffusivities is equivalent to that given by the Stokes-Einstein equation and the molecular friction coefficient is defined as follows,

$$f_\infty = 6\pi\eta a_s, \tag{A.2}$$

where, a_s, is the Stokes-Einstein radius of the solute.

Anderson and Quinn [12] used the following arguments to obtain an expression for the radial average of the solute flux within a pore. The velocity profile inside a pore of radius R is assumed to be parabolic and the fluid velocity V at any dimensionless radial position $\rho = r/R$ can be expressed as,

$$V = 2\langle V\rangle(1 - \rho^2). \tag{2.6}$$

In this single dimension model, a mass balance on solute transport in the axial direction (z) is obtained by equating the driving force for solute flux ($-\nabla\mu$) expressed in terms of concentration with the drag on a solute molecule F_A as follows,

$$F_A = -kT\frac{d\ln C}{dz}. \tag{A.3}$$

Solute drag within the pore can be expressed as

$$F_A = f_\infty K\left[U_A - GV\right]. \tag{A.4}$$

Where U_A is the net solute velocity with respect to the pore wall, $K(\lambda,\rho)$ is the "enhanced friction" which represents the ratio of the pore to bulk friction coefficients and $G(\lambda,\rho)$ is the "lag coefficient" which accounts for the retarding effect of the pore wall. The value of f_∞ is the molecular friction coefficient for the bulk solution as calculated in Equation A.1.

Combining Equations A.1, A.3, A.4 and substituting for the axial solute flux $N_A = CU_A$,

$$N_A = -K^{-1}D_{AB}\frac{dC}{dz} + GCV. \tag{A.5}$$

The concentration of solute being assumed to be radially independent, both Equations 2.6 and A.5 can be integrated over the pore cross-section to give an average solute flux

$$\langle N_A\rangle = -\xi D_{AB}\frac{dC}{dz} + \chi C\langle V\rangle, \tag{A.6}$$

where,

$$\xi \equiv \frac{D}{D_{AB}} = \int_0^{1-\lambda}\left[2\rho K^{-1}\right]d\rho, \tag{A.7}$$

$$\chi = \int_0^{1-\lambda}\left[4\rho(1-\rho^2)G\right]d\rho. \tag{A.8}$$

The average flux of solute through a pore can be separated into radially averaged diffusive (ξ) and a hydrodynamic (χ) components. These quantities can be expressed as a function of the steric hindrance factor Φ given by Equation 2.13. The radial averages of ξ and χ are obtained as follows,

$$\xi = \Phi \overline{K}^{-1}(\lambda), \tag{A.9}$$

$$\chi = \Phi\,[2 - \Phi]\,\overline{G}(\lambda), \tag{A.10}$$

where the steric factor Φ for a solute is given by the ratio of the true pore area to that available for solute transport,

$$\Phi = (1 - \lambda)^2. \tag{2.13}$$

The values of $\overline{K}^{-1}(\lambda)$ and $\overline{G}(\lambda)$ necessary for the evaluation of ξ and χ can be evaluated from theoretical calculations for the friction and lag of spheres in cylinders under Stokes flow conditions. Several workers have shown that the radially dependent quantities $K^{-1}(\lambda,\rho)$ and $G(\lambda,\rho)$ can be approximated by their values derived for spheres confined to the center-line of a pore [36]. The use of center-line values for radially dependent quantities is commonly referred to as the "center-line approximation'.

Brenner and Gaydos [42] introduce the concept that the translational Brownian movement of a sphere in a quiescent fluid is not a scalar as in unbounded fluids but a symmetric second rank tensor or dyadic. The evaluation of ξ and χ as proposed in Reference [12] is reported to be valid for the range $0< \lambda <0.4$ but provides reasonable estimates in the range $0.4< \lambda <1.0$ as predicted by Bungay and Brenner [43] for the entire range of λ as seen in Figure A.2.

In this simple model, the quantities $\overline{K}^{-1}$ and $\overline{G}$ proposed by Anderson and Quinn [12] were used as estimates of ξ and χ for the entire range of λ values and are given as follows,

$$\overline{K}^{-1}(\lambda) \approx K^{-1}(\lambda,0) \doteq 1 - 2.1044\lambda + 2.089\lambda^3 - 0.948\lambda^5, \tag{A.11}$$

$$\overline{G}(\lambda) \approx G(\lambda,0) = 1 - 2/3\lambda^2 - 0.163\lambda^3. \tag{A.12}$$

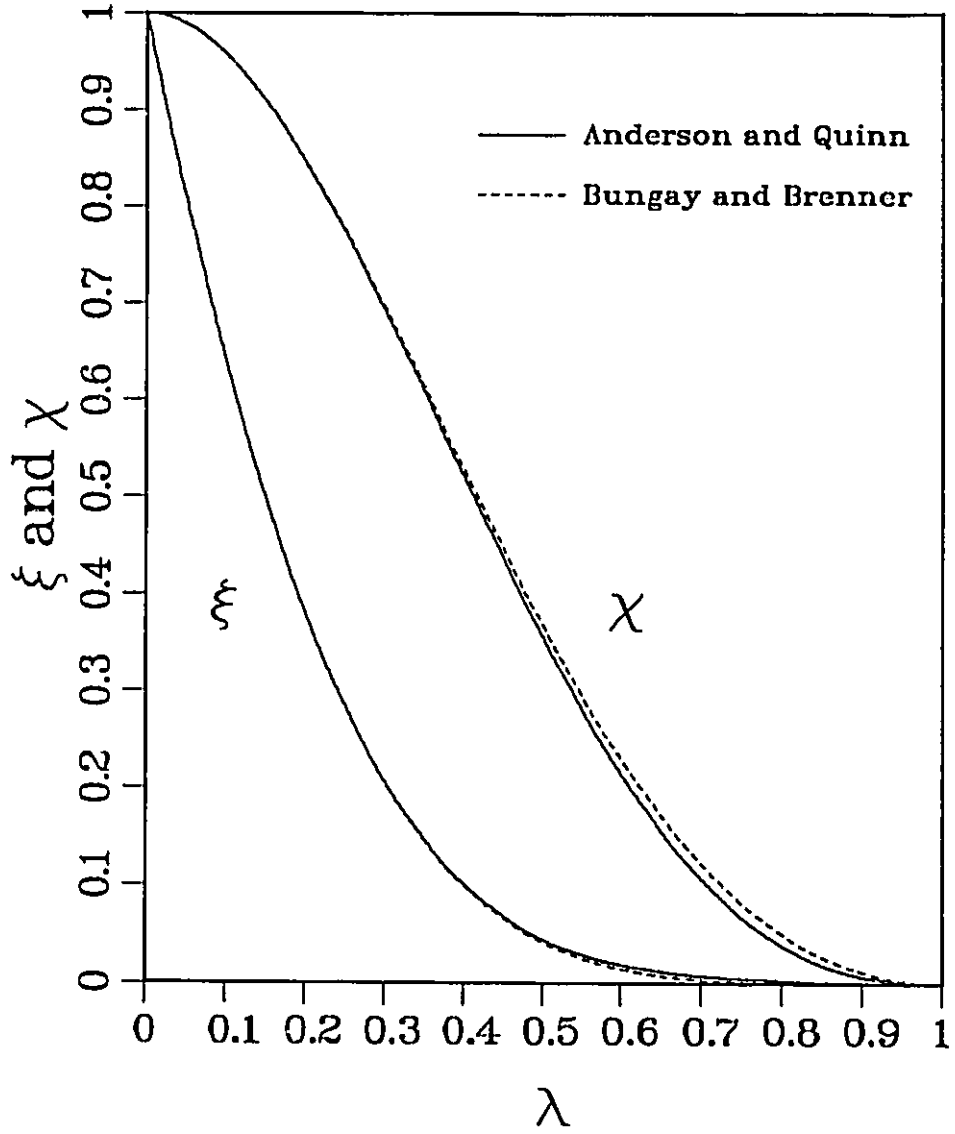

Figure A.2: Plot of the radially averaged quantities ξ and χ vs. λ.

The radially averaged values of ξ and χ based on a center-line approximation can be obtained as follows,

$$\xi = \Phi(1 - 2.1044\lambda + 2.089\lambda^3 - 0.948\lambda^5), \tag{2.11}$$

$$\chi = \Phi(2 - \Phi)(1 - 2/3\lambda^2 - 0.163\lambda^3). \tag{2.12}$$

Equation A.6 can be solved using the boundary conditions for the average concentrations at the inlet and outlet of the pore $z = 0$, $C = C_{A2}$ and $z = \delta$, $C = C'_{A3}(R)$ which gives the following,

$$\langle N_A \rangle = \chi \langle V \rangle C_{A2} \frac{\left[1 - (C'_{A3}(R)/C_{A2})e^{-Pe}\right]}{[1 - e^{-Pe}]}, \tag{A.13}$$

where Pe is the pore Peclet number,

$$Pe = \frac{\chi \langle V \rangle \delta}{\xi D_\infty}. \tag{A.14}$$

Solute flux at the pore exit is given by $\langle N_A \rangle = C'_{A3}(R)\langle N_B \rangle = C'_{A3}(R)\langle V \rangle$. Substituting into A.13, an expression for the rejection coefficient $\varphi(\lambda)$ of the pore, is obtained as follows,

$$\varphi(\lambda) = \frac{C'_{A3}(R)}{C_{A2}} = \frac{\chi}{1 - e^{-Pe}(1 - \chi)}. \tag{2.7}$$

Given slight differences in nomenclature, Equation 2.7 is identical to that of Verniory *et al.* [10] derived for purely steric interactions in parabolic flow.

Since the assumption of a parabolic velocity profile in the pore (Poiseuille flow) is at the basis of the rejection coefficient described by 2.7, then the product $\langle V \rangle \delta$ in the Peclet number can be evaluated as follows,

$$Q_B = \langle V \rangle \pi R^2 = \frac{\pi R^4 \, \Delta P}{8\eta\delta}, \tag{A.15}$$

$$\langle V \rangle \delta = \frac{R^2 \, \Delta P}{8\eta}. \tag{A.16}$$

Combining Equations A.14 and A.16,

$$Pe = \frac{\chi}{\xi D_\infty}\left[\frac{R^2\,\Delta P}{8\eta}\right]. \tag{2.8}$$

The quantity ΔP is the actual trans-membrane pressure including the effect of osmotic pressure. If dilute solutions are used in the characterization experiments, ($\Delta P \gg \Delta\pi$), and the operating pressure, P_g, becomes the driving force, $P_g = \Delta P$.

In the case where a membrane has pores of a fixed size, the true separation, f', would be given by $f' = 1 - \varphi(\lambda)$; then from Equation 2.7,

$$f'(\lambda) = 1 - \frac{\chi}{1 - e^{-Pe}(1-\chi)}. \tag{A.17}$$

Equation A.17 is of great significance in membrane characterization since it indicates that the rejection coefficient for a given pore size is independent of the pore length and depends on the size of solute being separated, the solution viscosity, and the trans-membrane pressure.

Having derived a unique relation between the rejection coefficient of a pore and its pore size, the analysis can be extended to a membrane having a distribution of pores sizes. Let the value $Y(R)dR$ represent the fraction of pores, the radii of which lie between R and $R + dR$, on the surface of the membrane, where,

$$\int_0^\infty Y(R)dR = 1. \tag{A.18}$$

The solute separation for a membrane with a distribution of pores is then obtained from,

$$f' = 1 - \frac{\int_0^\infty Y(R)\varphi(\lambda)R^4 dR}{\int_0^\infty Y(R)R^4 dR}. \tag{A.19}$$

This model represents the limiting case of restricted transport for rigid spheres flowing in a cylindrical pore, without solute-membrane interactions.

A.2 The Surface Force Pore Flow Model (SFPF)

Introduced in the late 1970's, the Surface Pore Flow Model (SFPF) provides an added degree of flexibility in describing restricted transport through porous media. The basic ideas of this model resemble those advanced in the finely porous model proposed by Merten [41]. But this model remains unique, since, the exact shape of the velocity profile can be determined as a function of radial varying solution properties and solute-membrane interactions are quantified using High Performance Liquid Chromatography (HPLC). The SFPF model differs from the RAPM model in its choice of a boundary condition at the pore exit and that the "enhanced friction" and "lag coefficient" are grouped into one quantity.

A complete description of the SFPF model can be found in Reference [7], it includes the effects of solute-membrane interaction and solute size on separation. The SFPF model performs a series of force, momentum, and mass balances, on a solute molecule flowing through a straight cylindrical pore whose axis is perpendicular to the surface of the membrane. This shape of pore is assumed for mathematical simplicity, no attempt is made to account for the tortuosity and varying cross-sectional geometry of the actual paths in the membrane. Steady state conditions are assumed to exist within the pore and the solution within the pore is considered to behave as a continuum. Radial concentration gradients exist due to the attraction or repulsion of the solute molecules with respect to the membrane material. Solute molecules are assumed to be distributed following a Maxwell-Boltzmann distribution law at the proximity of the pore wall. Long range coulombic forces, van der Waals or Lennard-Jones type interactions have been included as expressions in the surface potential functions of the Maxwell-Boltzmann distribution.

Radial variations in concentration, viscosity and osmotic pressure are taken into account in this model and the exact velocity profile inside the pore is obtained numerically. Basic assumptions of a parabolic velocity profile are unnecessary. The model is very general and can be extended to concentrated solutions and component mixtures. The price for the broader scope of this model compared to the radially averaged pore model is an increase in computational complexity.

The model performs a balance of the frictional forces and driving forces acting over the entire pore. This yields a solute concentration and a velocity profile for the solution inside the pore as a function of the cylindrical coordinates (r,z). A suitable pore size distribution is then assumed and solute separation calculated. The nomenclature used in the present analysis is similar to that found in Reference [7]. Since Reference [7] is very complete only the broad lines of the derivation are included in this work.

Consider a solute molecule flowing at steady state through a small cylindrical pore of radius R and length δ. In cylindrical coordinates, a differential element along the pore axis as an annular volume bounded by the radii r and $r+dr$, can be defined. The subscripts A, B, and C represent solute, solvent and the pore wall or membrane material respectively.

Under steady state conditions, a force balance on a solute molecule along the axis of the pore gives

$$F_A(r,z) = -[F_{AB}(r,z) + F_{AM}(r,z)] \tag{A.20}$$

where;

$F_{AB}(r,z)$ = friction force between solute A and solute B,
$F_{AM}(r,z)$ = friction force between solute A and the pore wall or membrane surface,
$F_A(r,z)$ = driving force for movement of solute A due to the chemical potential gradient (μ_A).

Assuming the friction force F_{AM} is proportional to the relative velocity of the solute in the pore to that of the solute at the pore wall, then $F_{AM}(r,z) \propto [u_A(r,z) - u_{Aw}(R)]$

where;

$u_A(r,z)$ = velocity of solute at position (r,z).
$u_{Aw}(R)$ = velocity of solute at pore wall R.

$$F_{AM}(r,z) = -\chi_{AM}(r)[u_A(r,z) - u_{Aw}(R)] \tag{A.21}$$

The quantity χ_{AM} is a proportionality constant which is a function of the radial component r.

If the flow through the pore is assumed to be a continuum then

$$u_{Aw}(R) = 0, \tag{A.22}$$

and,

$$\begin{aligned} u_A(r,z) &= \frac{\text{molar flux of solute at distance } r}{\text{molar concentration of solute at position } (r,z)}, \\ &= \frac{J_A(r)}{c_A(r,z)}. \end{aligned} \tag{A.23}$$

Combining Equations A.22, A.23 and A.21,

$$F_{AM}(r,z) = -\chi_{AM}(r)\frac{J_A(r)}{c_A(r,z)}. \tag{A.24}$$

Similarly for the case of the relative velocity of the solute and solvent,

$$F_{AB}(r,z) = -\chi_{AB}\left[u_A(r,z) - u_B(r)\right]. \tag{A.25}$$

Combining Equations A.23 and A.25,

$$J_A(r) = \frac{1}{\chi_{AB}}c_A(r,z)[-F_{AB}(r,z)] + c_A(r,z)u_B(r). \tag{A.26}$$

Since $F_A(r,z)$ is the gradient in chemical potential of the solute in the z direction,

$$F_A(r,z) = -\left.\frac{\partial \mu_A(r,z)}{\partial z}\right|_{r=r} = -\frac{d\mu_A(r,z)}{dc_A(r,z)} \cdot \left[\left.\frac{\partial c_A(r,z)}{\partial z}\right|_{r=r}\right]. \tag{A.27}$$

The chemical potential can be expressed as

$$\mu_i = \underline{R}T \ln a_i + \mu_i^\circ. \tag{A.28}$$

In the case of a dilute solution,

$$\mu_A(r,z) = \underline{R}T \ln c_A(r,z) + \mu_A^\circ. \tag{A.29}$$

Combining Equations A.27 and A.29,

$$F_A(r,z) = -\frac{\underline{R}T}{c_A(r,z)}\left[\frac{\partial c_A(r,z)}{\partial z}\bigg|_{r=r}\right]. \tag{A.30}$$

Combining Equations A.20, A.24 and A.30,

$$-F_{AB}(r,z) = F_A(r,z) + F_{AM}(r,z), \tag{A.31}$$

$$-F_{AB}(r,z) = -\frac{\underline{R}T}{c_A(r,z)}\left[\frac{\partial c_A(r,z)}{\partial z}\bigg|_{r=r}\right] - \chi_{AM}(r)\frac{J_A(r)}{c_A(r,z)}. \tag{A.32}$$

Inserting Equation A.32 into A.26 and rearranging,

$$J_A(r) = \left[\frac{-\underline{R}T}{\chi_{AB}}\left(\frac{\partial c_A(r,z)}{\partial z}\bigg|_{r=r}\right) + c_A(r,z)u_B(r)\right] \div \left[1 + \frac{\chi_{AM}(r)}{\chi_{AB}}\right]. \tag{A.33}$$

The values of $\chi_{AM}(r)$ and χ_{AB} are combined into an overall friction coefficient $b(r)$,

$$b(r) = \frac{[\chi_{AB} + \chi_{AM}(r)]}{\chi_{AB}}. \tag{A.34}$$

Substituting into Equation A.33 ,

$$J_A(r) = -\frac{\underline{R}T}{\chi_{AB} b(r)} \left[\frac{\partial c_A(r,z)}{\partial z}|_{r=r} \right] + \frac{c_A(r,z) u_B(r)}{b(r)}. \tag{A.35}$$

Since $\chi_{AB} = \underline{R}T/D_{AB}$ rewrite Equation A.35 as,

$$J_A(r) = -\frac{1}{b(r)} D_{AB} \left[\frac{\partial c_A(r,z)}{\partial z}\Big|_{r=r} \right] + \frac{1}{b(r)} c_A(r,z) u_B(r). \tag{A.36}$$

Assuming that the concentration of solute close to the pore wall follows a Maxwell-Boltzmann distribution law, solute concentration at a distance $\underline{d}$ from the pore wall $c_A(\underline{d})$ can be expressed in terms of the bulk solution concentration c_A^o,

$$c_A(\underline{d}) = c_A^o e^{-\phi'(\underline{d})/\underline{R}T}, \tag{A.37}$$

$$\underline{d} = R - r. \tag{A.38}$$

At the entrance and exit of the pore, radial concentrations are given by,

$$c_A(r,0) = C_{A2} e^{-\phi'(r)/\underline{R}T}, \tag{2.17}$$

$$c_A(r,\delta) = c_{A3}(r) e^{-\phi'(r)/\underline{R}T}. \tag{2.18}$$

Define the radial concentration $c_{A3}(r)$ as follows,

$$c_{A3}(r) = \frac{J_A(r)}{u_B(r)}. \tag{A.39}$$

As in Reference [7] notice that Equation 2.36 is a simple differential equation whose boundary conditions are given by Equations 2.17 and 2.18. Rearranging Equation A.36,

$$\frac{dc_A(r,z)}{c_A(r,z) - \frac{J_A(r) b(r)}{u_B(r)}}\Bigg|_{r=r} = \frac{u_B(r)}{D_{AB}} dz\Big|_{r=r}. \tag{A.40}$$

Integrating both sides of this equation gives,

$$\ln\left[c_A(r,z) - \frac{J_A(r)b(r)}{u_B(r)}\right] = \frac{u_B(r)}{D_{AB}}z + cst. \tag{A.41}$$

For $z = 0$, insertion of Equation 2.17 gives,

$$\ln\left[C_{A2}e^{-\phi'(r)/\underline{R}T} - \frac{J_A(r)b(r)}{u_B(r)}\right] = cst. \tag{A.42}$$

Substituting for *cst* in Equation A.41,

$$\ln\left[\frac{c_A(r) - \frac{J_A(r)b(r)}{u_B(r)}}{C_{A2}e^{-\phi'(r)/\underline{R}T} - \frac{J_A(r)b(r)}{u_B(r)}}\right] = \frac{u_B(r)}{D_{AB}}z. \tag{A.43}$$

At $z = \delta$, Equation A.41 becomes,

$$\ln\left[c_{A3}(r)e^{-\phi'(r)/\underline{R}T} - \frac{J_A(r)b(r)}{u_B(r)}\right] = \frac{u_B(r)}{D_{AB}}\delta + cst. \tag{A.44}$$

Substituting for *cst* in eqn A.44,

$$\ln\left[\frac{c_{A3}(r)e^{-\phi'(r)/\underline{R}T} - \frac{J_A(r)b(r)}{u_B(r)}}{C_{A2}e^{-\phi'(r)/\underline{R}T} - \frac{J_A(r)b(r)}{u_B(r)}}\right] = \frac{u_B(r)\delta}{D_{AB}}. \tag{A.45}$$

Substituting Equation A.39 into A.45 gives,

$$\left[c_{A3}(r)e^{-\phi'(r)/\underline{R}T} - c_{A3}(r)b(r)\right] = \left[C_{A2}e^{-\phi'(r)/\underline{R}T} - c_{A3}(r)b(r)\right] \cdot \exp\left[\frac{u_B(r)\delta}{D_{AB}}\right]. \quad \text{(A.46)}$$

Equation A.46 can be rearranged as follows,

$$\frac{c_{A3}(r)}{C_{A2}} = \frac{\exp\left[\frac{u_B(r)\delta}{D_{AB}}\right]}{1 + \frac{b(r)}{e^{-\phi'(r)/\underline{R}T}}\left(\exp\left[\frac{u_B(r)\delta}{D_{AB}}\right] - 1\right)}. \quad \text{(2.16)}$$

Equation 2.16 is the expression for the concentration at the exit of the pore. The concentration C_{A3} at the pore outlet can be determined by taking the radial average of $c_{A3}(r)$,

$$C'_{A3}(R) = \frac{\int_0^R c_{A3}(r)u_B(r)rdr}{\int_0^R u_B(r)rdr}. \quad \text{(2.19)}$$

The true separation f' can be calculated from the boundary layer concentration C_{A2}, as follows,

$$f' = \frac{C_{A2} - C'_{A3}(R)}{C_{A2}} = 1 - \frac{C'_{A3}(R)}{C_{A2}}. \quad \text{(2.2)}$$

Combining Equations 2.19 and 2.2,

$$f' = 1 - \left[\left(\int_0^R \frac{c_{A3}(r)}{C_{A2}} \cdot u_B(r)rdr\right) \div \left(\int_0^R u_B(r)rdr\right)\right]. \quad \text{(A.47)}$$

The value of $[u_B(r)\delta/D_{AB}]$ is a dimensionless quantity which is somewhat equivalent to a radially dependent Peclet number as in Equation A.14.

A.2.1 Dimensionless analysis

The transport equations derived in the SFPF model can be expressed in the following dimensionless variables:

Dimensionless radial distance	ρ	=	r/R
Dimensionless solute conc. at the pore outlet	$C_A(\rho)$	=	$\frac{c_{A3}(r)}{C_{A2}}$
Dimensionless solution velocity in the pore	$\alpha(\rho)$	=	$\frac{u_B \delta}{D_{AB}}$
Dimensionless solution viscosity	$\beta_1(\rho)$	=	$\frac{\eta}{\chi_{AB} R^2 C_{A2}}$
Dimensionless operating pressure	$\beta_2(\rho)$	=	$\frac{(P_i - P_o)}{\underline{R}TC_{A2}}$
Dimensionless potential function	$\phi(\rho)$	=	$\phi'(r)/\underline{R}T$

Substituting into Equation 2.16, the radial dependence of the dimensionless solute concentration is given by,

$$C_A(\rho) = \frac{\exp(\alpha(\rho))}{1 + \frac{b(\lambda)}{e^{-\phi(\rho)}}[\exp(\alpha(\rho)) - 1]}. \tag{A.48}$$

From Equation 2.47 the differential equation for the dimensionless fluid velocity becomes,

$$\frac{d^2\alpha(\rho)}{d\rho^2} + \frac{1}{\rho}\frac{d\alpha(\rho)}{d\rho} + \frac{\beta_2}{\beta_1} + \frac{1}{\beta_1}(1 - e^{-\phi(\rho)})(C_A(\rho) - 1) - \frac{(b(\rho) - 1)\alpha(\rho)C_A(\rho)}{\beta_1} = 0. \tag{2.22}$$

The boundary conditions for Equation 2.22 are now expressed as follows,

$$\text{at} \quad \rho = 0, \quad \frac{d\alpha(\rho)}{d\rho} = 0,$$

$$\text{at} \quad \rho = 1, \quad \alpha(\rho) = 0.$$

A.2.2 Calculation of solute separation for a distribution of pores

For a membrane having a single pore size, solute separation can be calculated from Equation A.47 as follows,

$$f' = 1 - \frac{\int_0^\infty Y(R)[\int_0^1 C_A(\rho)\cdot\alpha(\rho)\rho d\rho]_{R=R}R^2 dR}{\int_0^\infty Y(R)[\int_0^1 \alpha(\rho)\rho d\rho]_{R=R}R^2 dR}. \tag{A.49}$$

The normal distribution is an inadequate description of the distribution of pore sizes at the surface of the membrane. This distribution includes negative pore sizes which is impossible. The log-normal distribution is often found in nature and includes only positive values [60]. The value of $Y(R)$ for a log-normal distribution is given by,

$$\mathrm{Y(R)} = \frac{1}{\sqrt{2\pi}\ln\sigma}\exp\left[-\frac{\ln^2(\mathrm{R}/\mathrm{R_{avg}})}{2\ln^2\sigma}\right]. \tag{A.50}$$

The problem in using this distribution is that it is susceptible to have moments, and in the case of the present transport model the presence of a 4^{th} power dependency on solute separation would tend to indicate the following moment,

$$\ln\left(\overline{\mathrm{R_a}}\right) = \ell\mathrm{n}\left(\mathrm{R_{avg}}\right) + 4\ln\left(\sigma\right)^2. \tag{A.51}$$

A.3 Notes on the Derivation of the MD-SFPF Model

As mentioned in Chapter 2, the most significant difference between the SFPF and MD-SFPF models lies is in the choice of the boundary condition at the pore exit. This is not immediately evident by looking at the derivation found in Reference [13]. This section describes how to obtain Equation 2.31 from the equations given in Reference [13]. Equation numbers in bold face refer to those found in Reference [13].

The osmotic pressure of dilute solutions containing non-electrolytes can be evaluated using van't Hoff's equation,

$$\pi = \underline{R}T \cdot C_A. \tag{A.52}$$

For solvent flux Equation **38** (see Reference [13]),

$$\overline{J}_B = 2\left(\frac{C\underline{R}T}{\tau\chi_{AB}}\right)\int_0^1 \alpha(\rho)\rho d\rho, \tag{A.53}$$

where C is the molar density of the solution, and τ is the average pore lenght taking tortuosity into account.

Solute flux is given by Equation **39** (see Reference [13]),

$$\overline{J}_A = \frac{2}{\tau\chi_{AB}}\int_0^{1-\lambda}\frac{\alpha(\rho)}{b(\rho)}\left(\pi_{A2} + \frac{\pi_{A2} - \pi'_{A3}}{e^{\alpha(\rho)} - 1}\right)e^{-\phi(\rho)}\rho d\rho. \tag{A.54}$$

The permeate concentration is given by Equation **41** (see Reference [13]),

$$C'_{A3} = C\,\frac{\overline{J}_A}{\overline{J}_A + \overline{J}_B}. \tag{A.55}$$

For the transport of dilute solutions in pressure driven membrane processes, the solute flux $\overline{J}_A$ through a membrane pore is several orders of magnitude smaller than the solvent flux $\overline{J}_B$ (molar basis), $\overline{J}_A << \overline{J}_B$. Substituting Equations A.52, A.53 and A.54 into A.55 and dividing throughout by C_{A2},

$$\frac{C'_{A3}}{C_{A2}} = \frac{\int_0^{1-\lambda}\frac{\alpha(\rho)}{b(\rho)}\left[1 + \frac{1 - \frac{C'_{A3}}{C_{A2}}}{e^{\alpha(\rho)} - 1}\right]e^{-\phi(\rho)}\rho d\rho}{\int_0^1 \alpha(\rho)\rho d\rho}. \tag{A.56}$$

Equation A.56 is easily rearanged to give Equation A.57 below,

$$\frac{C'_{A3}}{C_{A2}} = \frac{\int_0^{1-\lambda} \left[\frac{e^{-\phi}e^{\alpha} - \frac{C'_{A3}}{C_{A2}}e^{-\phi}}{b(\rho)(e^{\alpha}-1)} \right] \alpha\rho d\rho}{\int_0^1 \alpha\rho d\rho}. \tag{A.57}$$

Given the fact that no solute exists for values of $1-\lambda < \rho < 1$, which implies that $e^{-\phi} = 0$ in this range, and that $b(\rho)$ is equivalent to $b(r)$, Equation A.57 is essentialy the same as 2.31. All further manipulations of Equation A.57 are identical to those described in Chapter 2. The similarity in these two results implies that, for dilute solutions of non-electrolytes, the MD-SFPF given in Reference [13] is identical to the SFPF model derived with a different boundary condition at the pore exit. It is also interesting to note that for dilute solutions this approach also predicts, (as in the case of the SFPF and RDPM models), that solute separation is independent of pore length and tortuosity.

Appendix B

Concentration Polarization

Conventional thinking assumes that semi-permeable membranes used in RO and UF applications reject dissolved solutes which tend to accumulate on the high pressure side or selective side of these membranes. It is thought that at the high pressure membrane-solution boundary, the relative rate of solute removal by convection and molecular diffusion towards the bulk solution is slower than the rate of buildup due to the exclusion of solute by the membrane. In order to estimate if this effect is reflected by the permeation data, values of C_{A2} were predicted for all PEG characterization runs to determine if they are reasonable.

Evaluation of C_{A2}

By definition, a semipermeable membrane will allow the permeation of solvent and retain a considerable amount of solute which tends to accumulate on the high pressure or selective side of the membrane. This causes an accumulation of solute or polarization in the concentration profile at this interface where the concentration of solute C_{A2} is greater than that of the bulk solution C_{A1}.

The selective side of the membrane is in direct contact with the enriched layer and will always perform a separation based on C_{A2}. As previously mentioned, this leads us to define two different separations, the apparent or observed separation, f, based on C_{A1} (see Equation 2.3) and the true separation, f', based on C_{A2} (see Equation 2.2). The apparent or observed separation, f, is easily obtained from standard permeation tests. In most cases the value of C_{A2} is unknown and, f',

is usually predicted from experiments performed using a reference solute such as sodium chloride. The discussion will be limited to the evaluation of C_{A2} to see if the predicted values are reasonable.

The thickness of the boundary layer for sodium chloride solutions is typically 20 to 200 μm [7]. Direct sampling methods cannot be used on such thin layers which imposes serious constraints on the type of analytical procedure available to evaluate C_{A2}.

The boundary layer concentration is usually evaluated by an indirect method involving knowledge of membrane transport and the osmotic pressure–concentration relationship of solutions. In this technique a solution is permeated through an RO membrane and the operating pressure, product rate (PR) and pure water permeability (PWP) are used to evaluate C_{A2} as described below.

The solvent flux N_B through a membrane subjected to a differential pressure ΔP can be expressed as

$$N_B = A \cdot (\Delta P - \Delta\pi), \tag{B.1}$$

where,

$$A = \frac{PWP}{3600 \cdot S \cdot M_B \cdot P_g}, \tag{B.2}$$

$$N_B = \frac{PR}{3600 \cdot S \cdot M_B}. \tag{B.3}$$

If the permeate is discharged at atmospheric pressure,

$$N_B = A \cdot (P_g - \pi(C_{A2}) + \pi(C_{A3})), \tag{B.4}$$

which leads to the following expression for $\pi(C_{A2})$,

$$\pi(C_{A2}) = \pi(C_{A3}) + P_g \cdot \left(1 - \left[\frac{PR}{PWP}\right]\right). \tag{B.5}$$

Variables on the RHS of equation B.5 can be determined from simple permeation experiments and $\pi(C_{A2})$ evaluated. The value of C_{A2} is then obtained from

a pressure–concentration relationship for the solute. Two methods to calculate the osmotic pressure of a solution are described, the freezing point depression method and van't Hoff's method. The first method is very accurate and takes into account non-idealities of a particular solution and is more accurate than van't Hoff's method which is based on the colligative nature of the osmotic pressure. The osmotic pressure for sodium chloride is used to compare both methods.

Assuming the feed solution is incompressible, then the osmotic pressure can be calculated as follows,

$$\pi = -\frac{RT}{\overline{v}_B} \ln a_B. \tag{B.6}$$

A comprehensive data base of activity and osmotic coefficients for aqueous electrolyte solutions can be found in Reference [103]. Exact integral methods to calculate activities for both dissociated and non-dissociated solutes are described in Reference [104]. The activity of the solvent can be determined from freezing point measurements performed on the solution using the following equation [41,105],

$$\ln(a_B) = \frac{\Delta H_{B,f}}{R} \left(\frac{1}{T_B} - \frac{1}{T_{sol}} \right). \tag{B.7}$$

An extensive amount of data on the freezing point depression of aqueous solutions is available in the literature [106]. Substituting into equation B.7, at 25°C the osmotic pressure of a solute dissolved in water can be expressed as

$$\pi(atm.) = 9.8286 \cdot 10^5 \left(\frac{1}{T_{sol}} - \frac{1}{T_B} \right). \tag{B.8}$$

In a similar fashion the osmotic pressure of a dilute solution containing an electrolyte can be approximated by van't Hoff's equation for non electrolytes (Equation A.52). The osmotic pressure of sodium chloride solutions were calculated based on freezing point measurements given in Reference [106] using equation B.8 and van't Hoff's equation A.52, selected values have been included in Table B.1. These values are in excellent agreement with published values of the osmotic pressure for sodium chloride solutions [107,6].

When the complete dissociation of NaCl is assumed, equation A.52 tends to overpredict π for solutions containing less than 10% NaCl and underpredict π for concentrations above 10% as seen in Table B.1. This discrepancy in the value of π

Table B.1: The osmotic pressure of sodium chloride solutions.

Weight % NaCl	*ppm* NaCl	Freezing pt. depression K	Mole fraction NaCl	$\pi(atm.)$ equn. B.8	$\pi(atm.)$ equn. A.52
.10	1,001	.062	$3.0846 \cdot 10^{-4}$	.82	.82
.20	2,003	.121	$6.1735 \cdot 10^{-4}$	1.59	1.65
.30	3,006	.181	$9.2667 \cdot 10^{-4}$	2.39	2.47
.40	4,011	.240	$1.2364 \cdot 10^{-3}$	3.16	3.30
.50	5,017	.299	$1.5466 \cdot 10^{-3}$	3.94	4.13
1	10,070	.593	$3.1040 \cdot 10^{-3}$	7.83	8.29
2	20,281	1.186	$6.2515 \cdot 10^{-3}$	15.69	16.70
3	30,636	1.790	$9.4434 \cdot 10^{-3}$	23.74	25.22
4	41,138	2.409	$1.2681 \cdot 10^{-2}$	32.02	33.87
5	51,791	3.046	$1.5965 \cdot 10^{-2}$	40.58	42.64
10	107,432	6.564	$3.3116 \cdot 10^{-2}$	88.60	88.44
20	232,113	16.458	$7.1549 \cdot 10^{-2}$	230.70	191.08

varies for different solutes and depends on the extent of dissociation or association in solution. The value of π obtained by the freezing point method equation B.8 is a preferred method since it is derived from an experimental observation which accounts for non idealities in solution behavior and should provide a better estimate of π.

However, the osmotic pressure predicted by van't Hoff's equation is reasonable and can be used to provide an estimate of C_{A2}. The value of C_{A2} was calculated for all characterization runs based on polyethylene glycol. A feed concentration of C_{A1}=200 ppm and the experimental separation were used in Equation 2.3 to determine C_{A3}. The operating pressure of 6892 kPag (1000 psi.) was used with the experimental PWP and PR to predict C_{A2}. These values were plotted as a histogram in Figure B.1, and fitted to a normal distribution. The distribution indicates that at least half of the membranes should have a boundary layer concentration above 6 wt.% which is 300 times the feed concentration. Some predicted values of C_{A2} (not shown in Figure B.1) would need to be 200 to 300 wt.% to satisfy Equation B.5 which is clearly unreasonable.

Fouling of the membrane must be ruled out as a possible explanation for this discrepancy since the PWP came back to its original value after each permeation run. This indicates that the cause of the flux reduction had disappeared from the boundary layer or the membrane pores during the pure water runs.

A possible reason for this flow reduction is that the effects of solute retardation due to the confined nature of the pore are affecting the flow of solvent molecules. The extreme case of this phenomenon is pore blockage when $\lambda = 1$. A considerable amount of collisions with the membrane material must occur in the tortuous network of pores traversed by a molecules in such a short period of time (0.03 to 0.003 sec as previously calculated). These collisions should lead to a reduction in permeate flow through the membrane.

One of the reasons given for the presence of concentration polarization is that solvent molecules are entraining solute molecules towards the entrance of the pore at a faster rate than solute can diffuse away from this area. Assuming that the flow of solvent into the pore affects a region roughly 20 pore diameters away from the pore entrance. Taking PEG6000 as an example and setting the ratio of c/dc in Equation 2.60 to c/dc=0.5. Given a 3.3 nm pore radius, for example, the time

required for a molecule to diffuse 132 nm is $8.92 \cdot 10^{-5}$ sec. As previously mentioned, the average permeation velocity in a 3.3 nm membrane pore is estimated to range from 0.1 to 0.35 mm/sec [26]. In the absence of diffusion, a solute molecule would travel these 132 nm in 1.32 to 0.38 secs.

These rough calculations indicate that molecular movement in the boundary layer due to diffusion is at least four orders of magnitude greater than that due to pore entrainment, which weakens the arguments in favor of concentration polarization.

Given these results, the effects of concentration polarization were neglected in this study and it was assumed that PR/PWP ratios <1 were mostly due to solute retardation occuring in membrane pores.

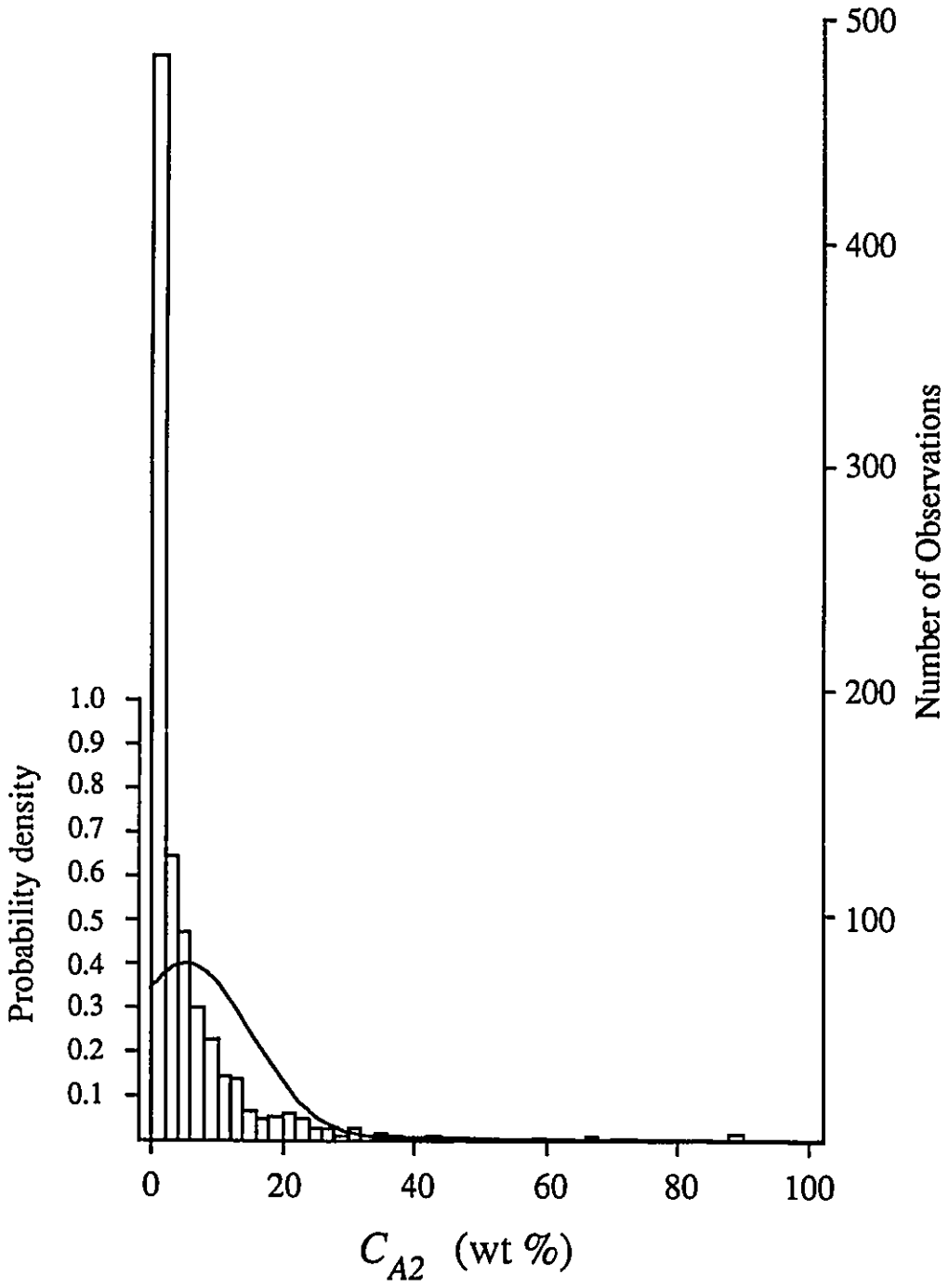

Figure B.1: Boundary layer concentration C_{A2} predicted from the PR/PWP ratio for all polyethylene glycol permeation runs.

Appendix C

Error Analysis

The residual analysis performed in Chapter 5 indicated that solute-solvent-membrane interactions were mediated by the presence of solvent at the surface of the membrane. This type of interaction was used to determine the hydrodynamic pore radius of the membranes produced in this work. The error involved in predicting the membrane pore radius was determined from variations in the estimate of κ' based on the actual force measurements, the error in estimating Ψ_{DP} from the overall fit, and the error in estimating R at the optimum values of κ' and Ψ_{DP}. The confidence intervals for these three contributions were generated for two sets of data, one based on 70 membranes and the other contained the original set less two membranes (numbers 60 and 64) suspected of having pinholes in their selective layer.

A first contribution to the overall error was associated with the original estimate of κ'. Pore sizes were calculated based on values of $\kappa' = 2.776$, 2.969, and 3.162 (nm^{-1}) obtained from a fit to the hydration forces measured in Reference [53] and values of Ψ_{DP} optimized at each value of κ'. These results have been plotted in Figure C.1, fitted residuals of the pore size at κ'=2.969 represent "0.0" values on the abscissa of this graph. These results indicate that the value of κ' as determined by the fit to the data contained in Reference [53] had very little effect on the predicted radius.

The second contribution to the overall error was that due to the estimate of Ψ_{DP} from the overall fit to both sets of membranes . The 90% confidence limits for Ψ_{DP} at $\kappa' = 2.969$ was determined to be $\Psi_{DP} = -5.082$ and -13.906 (nm^{-1}) with an

overall minimum of Ψ_{DP} =−8.901 (nm^{-1}). The predicted pore size for these values was determined at the high and low confidence limits. These values are plotted in Figure C.2 with respect to the predicted values at the overall minimum set at "0.0".

A third contribution to the overall error was due to Ψ_{DP} at a fixed κ'. The 90% confidence limits for the pore radius R were determined for both sets of membranes and are plotted in Figure C.3. The baseline of "0.0" for the residual of the pore radius were based on κ'=2.969 (nm^{-1}) and Ψ_{DP}= −8.901 (nm^{-1}).

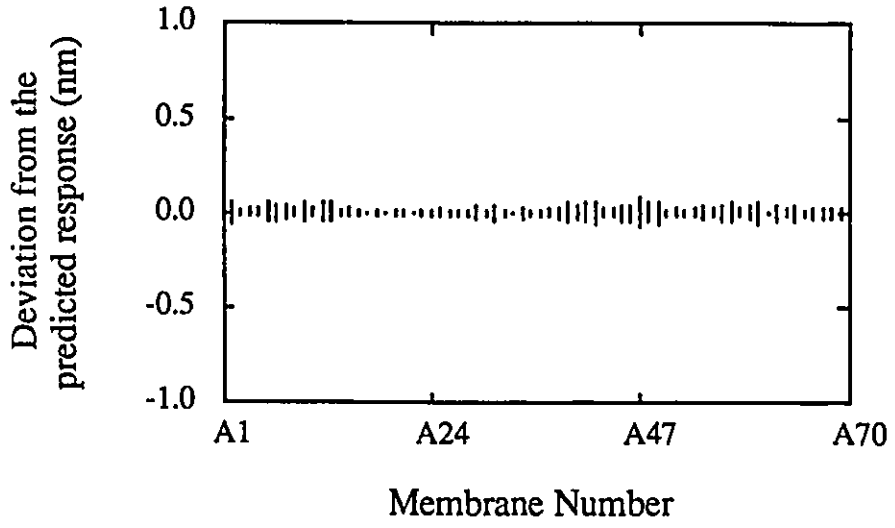

Figure C.1: Confidence regions for the calculated pore size due to errors in estimating κ' from the actual force measurements [53]. Upper and lower limits represent 90% contour levels obtained from a fit to the permeation data for all 70 membranes. Zero level represents the actual calculated pore radius for $\kappa' = 2.969$ nm^{-1}, high values are for $\kappa' = 2.776$ nm^{-1} and low values are for $\kappa' = 3.162$ nm^{-1}, at $\Psi_{DP} = -8.901$ (nm^{-1}).

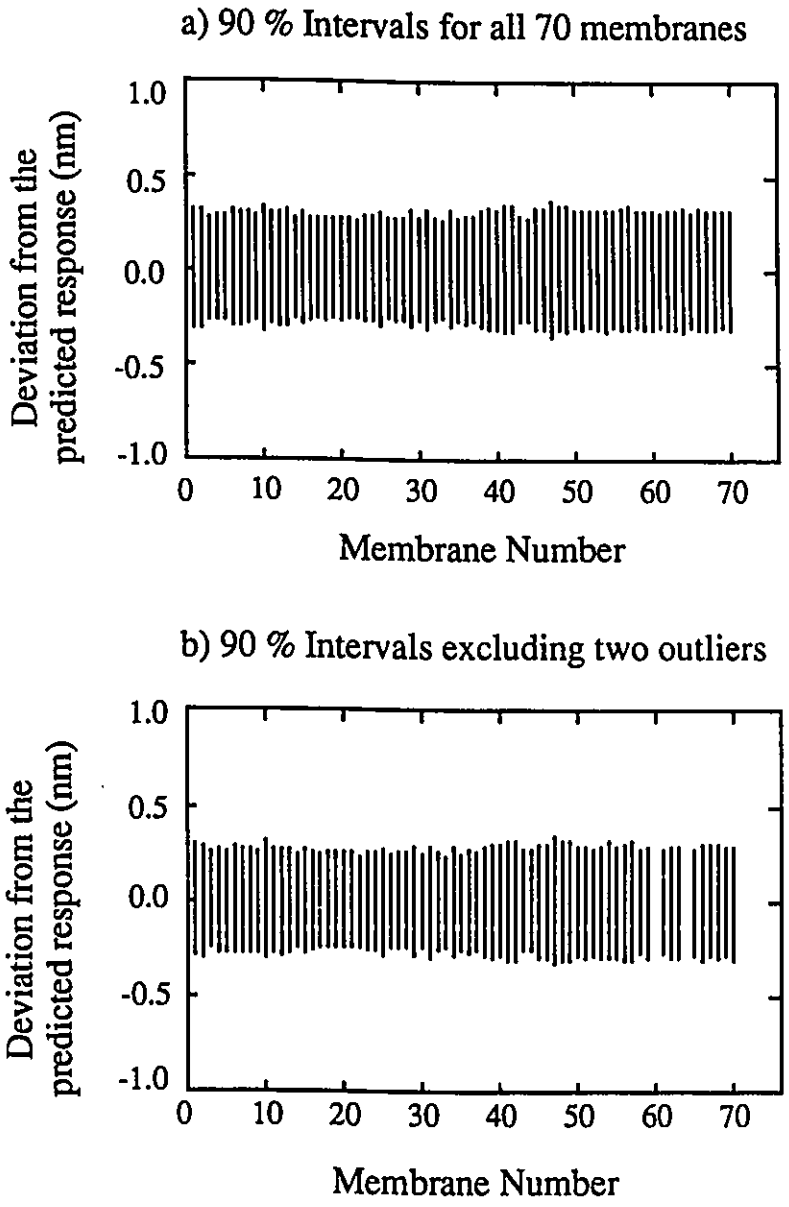

Figure C.2: Confidence regions for the calculated pore size due to errors in estimating Ψ_{DP}. Upper and lower limits represent 90% contour levels obtained from a fit to the permeation data for a) all 70 membranes, b) all excluding two outliers (membranes 60 and 64). Zero level represents the actual calculated pore radius for Ψ_{DP} =-8.901 nm^{-1}, high values are for $\Psi_{DP} = -13.906$ nm^{-1}, and low values are for $\Psi_{DP} = -5.802$ nm^{-1}, at $\kappa' = 2.969 nm^{-1}$. Data for these plots can be found in Tables C.1 and C.2.

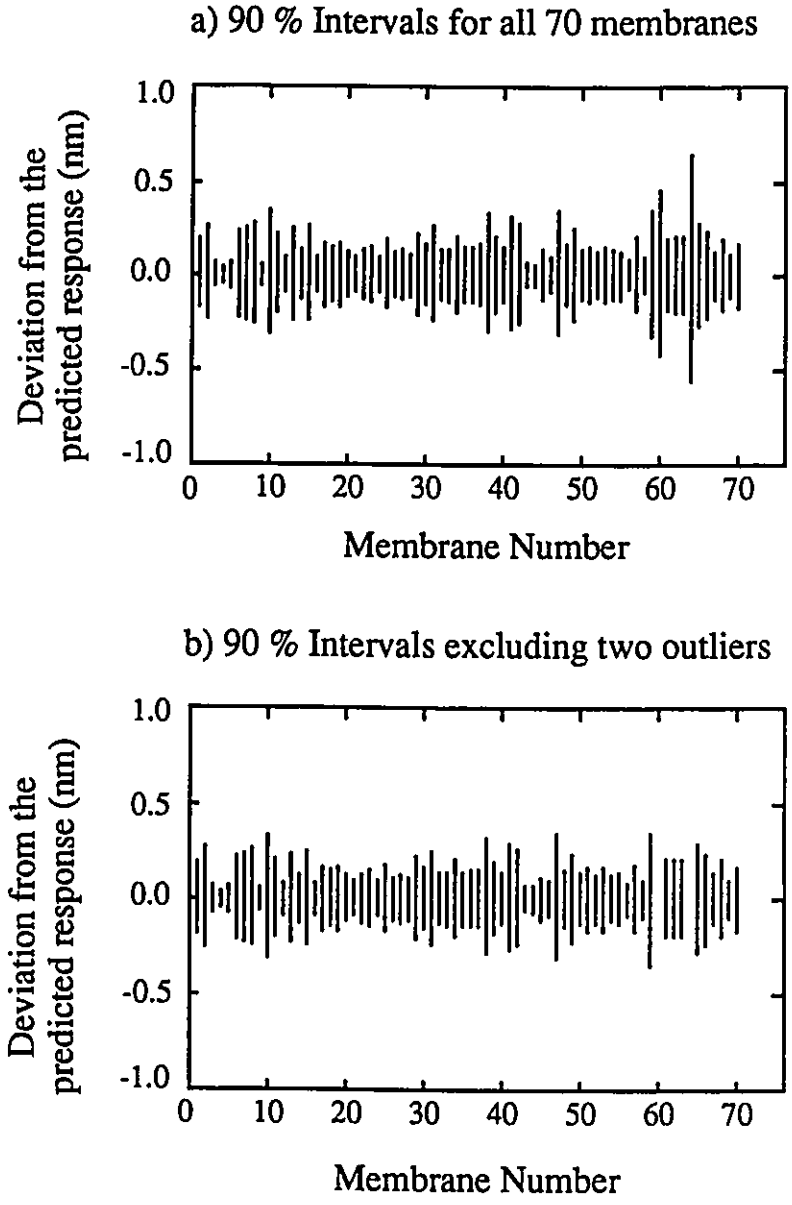

Figure C.3: Confidence regions for the calculated pore size due to errors in estimating R. Upper and lower limits represent 90% contour levels obtained from a fit to the permeation data for a) all 70 membranes, b) all excluding two outliers (membranes 60 and 64). Zero level represents the actual calculated pore radius for $\Psi_{DP} = -8.901$ nm^{-1} and $\kappa' = 2.969$nm^{-1}, high values are for the upper 90% limit in estimating R, and low values are for the lower 90% limit in estimating R. Data for these plots can be found in Tables C.1 and C.2.

From these three considerations, it can be seen that the contribution to the error in estimating pore radius from κ' is relatively small compared to that of Ψ_{DP} and R. In order to obtain a truly representative estimate of the error, the 90% confidence intervals for the predicted pore radius R were determined at the lower limit of $\Psi_{DP} = -5.802$ nm^{-1} and the higher limit $\Psi_{DP} = -13.906$ nm^{-1}. The extreme values of the predicted pore sizes (low R, low Ψ_{DP} and high R, high Ψ_{DP}) were used as approximate 90% confidence intervals for the estimate of the pore size. These values have been plotted in Figure C.4.

A comparison between the overall errors for both sets of data indicates a slight benefit exists when the two outliers (membranes 60 and 64) are excluded from the analysis. This is easily seen in Figure 5.22 where the magnitude of the confidence region decreases when both membranes suspected of containing pinholes are removed from the data set. It is for these reasons that the set containing 68 membranes was chosen to evaluate Ψ_{DP} for all "probe" solutes.

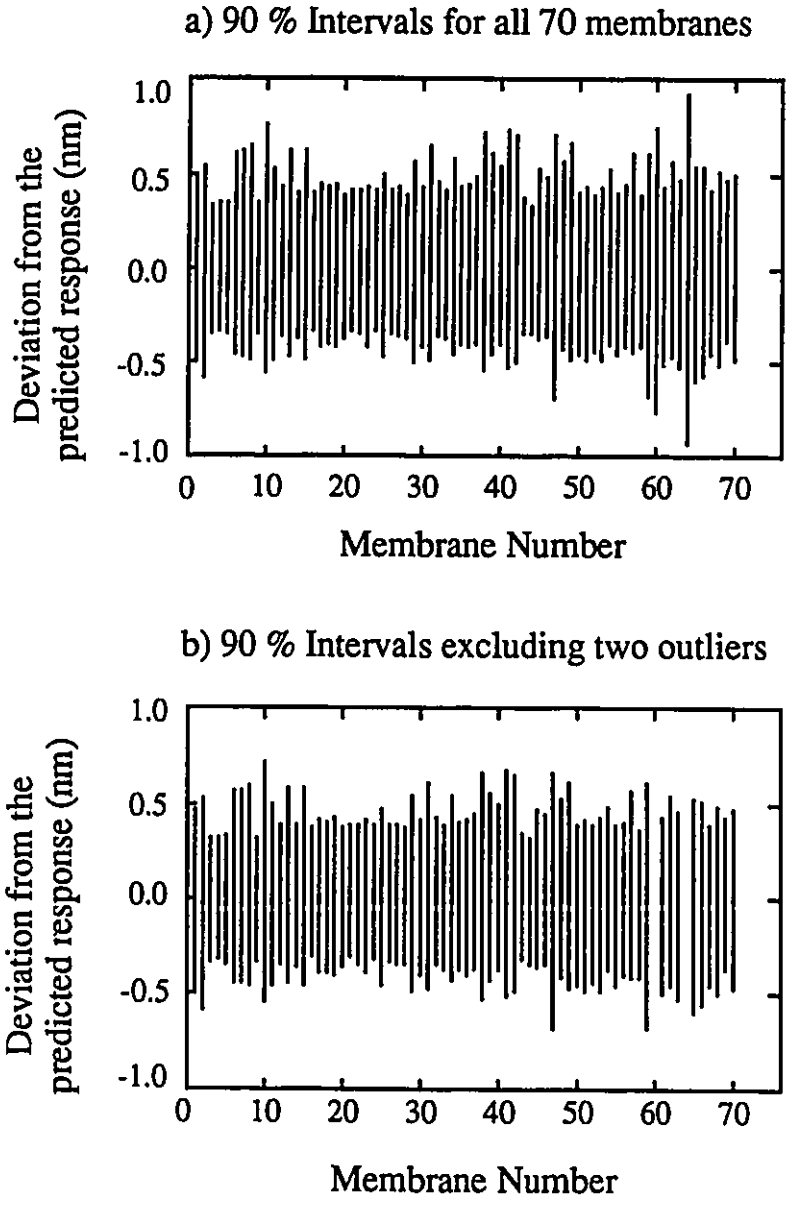

Figure C.4: Combined 90% confidence limits due to errors in estimating both Ψ_{DP} and R. Upper and lower limits represent 90% contour levels obtained from a fit to the permeation data for a) all 70 membranes, b) all excluding two outliers (membranes 60 and 64). Zero level represents the actual calculated pore radius for $\Psi_{DP} = -8.901$ nm^{-1} and $\kappa' = 2.969$nm^{-1}, high values are for $\Psi_{DP} = -13.906$ nm^{-1} and the upper 90% confidence limit obtained from the estimate of the pore radius, and low values are for $\Psi_{DP} = -5.802$ nm^{-1} and the lower 90% confidence limit obtained from the estimate of the pore radius. Data for these plots can be found in Tables C.1 and C.2.

Table C.1: Optimum pore sizes and related 90% confidence intervals based on a fit for all 70 membranes.

Membrane Number	Optimum Pore Size (nm)	SS_{Resid} (%²)	90% Conf. Int. Based on R		90% Conf. Int. Based on Ψ_{DP}		90% Conf. Int. Total	
			Low Diff. (nm)	High Diff. (nm)	Low Diff. (nm)	High Diff. (nm)	Low Diff. (nm)	High Diff. (nm)
Cell1	2.87	225.07	−0.17	0.19	−0.30	0.32	−0.50	0.49
Cell2	3.93	412.76	−0.24	0.26	−0.30	0.31	−0.58	0.54
Cell3	2.06	73.85	−0.06	0.07	−0.26	0.27	−0.34	0.33
Cell4	2.37	22.58	−0.04	0.04	−0.27	0.29	−0.33	0.34
Cell5	2.23	70.88	−0.07	0.07	−0.27	0.29	−0.35	0.35
Cell6	3.60	487.52	−0.22	0.24	−0.29	0.31	−0.46	0.61
Cell7	3.34	627.39	−0.23	0.25	−0.29	0.30	−0.47	0.62
Cell8	3.08	854.50	−0.25	0.28	−0.28	0.30	−0.49	0.64
Cell9	2.22	53.81	−0.06	0.06	−0.27	0.29	−0.34	0.35
Cell10	3.54	820.40	−0.31	0.35	−0.32	0.33	−0.56	0.76
Cell11	2.35	591.91	−0.20	0.22	−0.28	0.30	−0.48	0.52
Cell12	3.49	62.41	−0.08	0.09	−0.29	0.30	−0.36	0.43
Cell13	3.59	532.99	−0.23	0.25	−0.29	0.31	−0.47	0.62
Cell14	1.85	186.32	−0.12	0.13	−0.25	0.28	−0.38	0.40
Cell15	2.46	725.01	−0.24	0.26	−0.28	0.30	−0.48	0.62
Cell16	2.08	104.26	−0.08	0.09	−0.27	0.28	−0.33	0.40
Cell17	1.75	338.14	−0.16	0.17	−0.25	0.27	−0.41	0.44
Cell18	1.87	258.85	−0.14	0.15	−0.26	0.28	−0.40	0.43
Cell19	1.79	339.66	−0.16	0.17	−0.25	0.28	−0.42	0.44
Cell20	1.89	160.16	−0.11	0.12	−0.26	0.28	−0.38	0.39
Cell21	1.97	146.58	−0.09	0.10	−0.25	0.28	−0.33	0.41
Cell22	1.74	249.11	−0.12	0.13	−0.25	0.26	−0.35	0.41
Cell23	1.96	243.45	−0.14	0.15	−0.26	0.29	−0.41	0.43
Cell24	2.06	129.43	−0.09	0.10	−0.26	0.29	−0.33	0.41
Cell25	2.45	260.82	−0.17	0.19	−0.29	0.30	−0.47	0.49

Table C.1 : Continued.

Membrane Number	Optimum Pore Size (nm)	SS_{Resid} ($\%^2$)	90% Conf. Int. Based on R		90% Conf. Int. Based on Ψ_{DP}		90% Conf. Int. Total	
			Low Diff. (nm)	High Diff. (nm)	Low Diff. (nm)	High Diff. (nm)	Low Diff. (nm)	High Diff. (nm)
Cell26	1.86	206.25	−0.11	0.12	−0.25	0.28	−0.35	0.41
Cell27	1.97	224.71	−0.12	0.13	−0.26	0.27	−0.36	0.42
Cell28	1.89	150.68	−0.11	0.11	−0.26	0.28	−0.37	0.39
Cell29	3.08	340.77	−0.21	0.22	−0.29	0.32	−0.50	0.56
Cell30	1.85	302.66	−0.15	0.16	−0.26	0.28	−0.41	0.43
Cell31	3.21	458.57	−0.24	0.26	−0.30	0.32	−0.49	0.65
Cell32	2.05	266.11	−0.13	0.14	−0.26	0.28	−0.36	0.46
Cell33	1.68	256.27	−0.14	0.14	−0.25	0.26	−0.38	0.41
Cell34	2.83	363.55	−0.19	0.21	−0.29	0.32	−0.45	0.58
Cell35	1.88	245.71	−0.14	0.15	−0.26	0.28	−0.40	0.42
Cell36	2.11	219.69	−0.14	0.15	−0.28	0.29	−0.42	0.44
Cell37	2.18	320.99	−0.15	0.16	−0.26	0.29	−0.40	0.48
Cell38	2.88	1093.47	−0.29	0.33	−0.29	0.32	−0.54	0.71
Cell39	3.51	276.26	−0.19	0.20	−0.31	0.33	−0.45	0.60
Cell40	3.08	201.40	−0.14	0.15	−0.30	0.32	−0.40	0.53
Cell41	3.73	558.69	−0.28	0.31	−0.32	0.34	−0.53	0.73
Cell42	3.92	405.19	−0.25	0.28	−0.32	0.34	−0.50	0.70
Cell43	2.26	64.76	−0.06	0.07	−0.27	0.29	−0.34	0.37
Cell44	2.28	58.04	−0.06	0.06	−0.27	0.28	−0.35	0.33
Cell45	3.45	108.28	−0.12	0.13	−0.30	0.33	−0.38	0.52
Cell46	3.34	73.16	−0.09	0.10	−0.30	0.33	−0.36	0.48
Cell47	5.31	224.24	−0.30	0.34	−0.35	0.37	−0.69	0.70
Cell48	3.68	156.06	−0.15	0.16	−0.31	0.34	−0.43	0.56
Cell49	3.74	360.22	−0.23	0.25	−0.32	0.34	−0.49	0.66
Cell50	2.11	193.36	−0.12	0.13	−0.29	0.31	−0.46	0.40

Table C.1: Continued.

Membrane Number	Optimum Pore Size (nm)	SS_{Resid} (%²)	90% Conf. Int. Based on R		90% Conf. Int. Based on Ψ_{DP}		90% Conf. Int. Total	
			Low Diff. (nm)	High Diff. (nm)	Low Diff. (nm)	High Diff. (nm)	Low Diff. (nm)	High Diff. (nm)
Cell51	2.39	245.31	−0.14	0.15	−0.30	0.32	−0.49	0.43
Cell52	2.02	169.72	−0.11	0.12	−0.29	0.31	−0.44	0.39
Cell53	2.26	265.33	−0.14	0.15	−0.30	0.31	−0.49	0.43
Cell54	3.04	142.74	−0.12	0.13	−0.32	0.32	−0.40	0.52
Cell55	2.34	167.45	−0.12	0.12	−0.29	0.32	−0.46	0.40
Cell56	3.19	46.92	−0.07	0.08	−0.31	0.33	−0.41	0.44
Cell57	3.65	231.76	−0.18	0.20	−0.31	0.34	−0.44	0.61
Cell58	2.20	101.07	−0.09	0.09	−0.29	0.31	−0.41	0.38
Cell59	2.95	936.29	−0.32	0.34	−0.31	0.32	−0.68	0.61
Cell60	4.00	1091.15	−0.41	0.46	−0.30	0.32	−0.76	0.74
Cell61	1.68	398.22	−0.18	0.19	−0.29	0.30	−0.51	0.43
Cell62	3.14	415.90	−0.19	0.21	−0.30	0.31	−0.47	0.57
Cell63	2.25	495.42	−0.19	0.20	−0.30	0.31	−0.53	0.47
Cell64	3.22	2429.52	−0.56	0.65	−0.32	0.33	−0.93	0.92
Cell65	1.93	996.94	−0.26	0.28	−0.29	0.30	−0.60	0.53
Cell66	2.65	534.65	−0.22	0.23	−0.31	0.33	−0.57	0.53
Cell67	2.71	160.51	−0.12	0.12	−0.30	0.32	−0.46	0.41
Cell68	2.76	382.74	−0.18	0.19	−0.30	0.32	−0.51	0.51
Cell69	2.89	139.23	−0.11	0.11	−0.29	0.32	−0.39	0.47
Cell70	2.67	310.91	−0.16	0.17	−0.31	0.32	−0.48	0.50

Table C.2: Optimum pore sizes and related 90% confidence intervals based on a fit for 68 membranes. Films Cell60 and Cell64 have been excluded from the original fit.

Membrane Number	Optimum Pore Size (nm)	SS_{Resid} ($\%^2$)	90% Conf. Int. Based on R		90% Conf. Int. Based on Ψ_{DP}		90% Conf. Int. Total	
			Low Diff. (nm)	High Diff. (nm)	Low Diff. (nm)	High Diff. (nm)	Low Diff. (nm)	High Diff. (nm)
Cell1	2.80	242.27	−0.18	0.19	−0.28	0.30	−0.48	0.47
Cell2	3.86	451.24	−0.25	0.27	−0.29	0.29	−0.58	0.52
Cell3	1.99	84.28	−0.07	0.07	−0.24	0.26	−0.33	0.31
Cell4	2.31	25.90	−0.04	0.04	−0.26	0.27	−0.32	0.31
Cell5	2.17	78.54	−0.07	0.07	−0.26	0.26	−0.34	0.33
Cell6	3.53	438.99	−0.21	0.22	−0.27	0.29	−0.44	0.57
Cell7	3.27	570.21	−0.22	0.24	−0.27	0.28	−0.44	0.57
Cell8	3.02	787.05	−0.24	0.26	−0.27	0.27	−0.46	0.59
Cell9	2.16	60.15	−0.06	0.06	−0.26	0.26	−0.33	0.32
Cell10	3.46	756.89	−0.30	0.33	−0.29	0.31	−0.54	0.71
Cell11	2.28	598.85	−0.20	0.21	−0.27	0.28	−0.46	0.50
Cell12	3.42	55.57	−0.08	0.08	−0.28	0.28	−0.35	0.39
Cell13	3.52	482.03	−0.22	0.23	−0.27	0.28	−0.44	0.58
Cell14	1.79	194.44	−0.12	0.12	−0.24	0.25	−0.36	0.38
Cell15	2.40	680.54	−0.23	0.25	−0.27	0.27	−0.45	0.58
Cell16	2.02	93.64	−0.08	0.08	−0.25	0.26	−0.31	0.37
Cell17	1.69	349.85	−0.16	0.17	−0.23	0.25	−0.39	0.41
Cell18	1.81	269.53	−0.14	0.15	−0.24	0.26	−0.39	0.40
Cell19	1.73	355.29	−0.16	0.17	−0.23	0.26	−0.40	0.42
Cell20	1.83	169.03	−0.11	0.12	−0.24	0.26	−0.36	0.37
Cell21	1.91	132.45	−0.09	0.09	−0.24	0.26	−0.31	0.38
Cell22	1.68	242.18	−0.12	0.12	−0.23	0.24	−0.34	0.38
Cell23	1.90	254.38	−0.14	0.15	−0.25	0.26	−0.39	0.41
Cell24	2.00	117.78	−0.09	0.09	−0.25	0.26	−0.32	0.38
Cell25	2.38	270.66	−0.17	0.18	−0.28	0.28	−0.45	0.47

Table C.2: Continued.

Membrane Number	Optimum Pore Size (nm)	SS_{Resid} (%²)	90% Conf. Int. Based on R		90% Conf. Int. Based on Ψ_{DP}		90% Conf. Int. Total	
			Low Diff. (nm)	High Diff. (nm)	Low Diff. (nm)	High Diff. (nm)	Low Diff. (nm)	High Diff. (nm)
Cell26	1.81	195.89	−0.11	0.11	−0.24	0.25	−0.33	0.38
Cell27	1.90	216.12	−0.12	0.12	−0.24	0.26	−0.34	0.39
Cell28	1.83	156.34	−0.11	0.11	−0.24	0.26	−0.35	0.37
Cell29	3.01	339.69	−0.21	0.22	−0.28	0.29	−0.49	0.53
Cell30	1.79	315.41	−0.15	0.16	−0.24	0.25	−0.40	0.41
Cell31	3.14	418.66	−0.23	0.25	−0.29	0.29	−0.47	0.60
Cell32	1.99	244.42	−0.12	0.13	−0.25	0.26	−0.34	0.42
Cell33	1.62	266.73	−0.14	0.14	−0.23	0.24	−0.37	0.38
Cell34	2.76	332.19	−0.19	0.20	−0.28	0.29	−0.43	0.54
Cell35	1.82	255.12	−0.14	0.14	−0.25	0.25	−0.38	0.40
Cell36	2.04	229.59	−0.14	0.15	−0.26	0.27	−0.40	0.41
Cell37	2.12	306.23	−0.14	0.15	−0.25	0.26	−0.38	0.44
Cell38	2.81	1029.72	−0.28	0.31	−0.28	0.29	−0.52	0.66
Cell39	3.44	245.10	−0.18	0.19	−0.29	0.30	−0.43	0.55
Cell40	3.01	173.16	−0.13	0.14	−0.28	0.30	−0.37	0.49
Cell41	3.66	507.00	−0.26	0.29	−0.31	0.31	−0.51	0.68
Cell42	3.84	361.66	−0.24	0.26	−0.30	0.32	−0.48	0.65
Cell43	2.19	66.20	−0.06	0.07	−0.25	0.27	−0.32	0.34
Cell44	2.21	70.27	−0.07	0.07	−0.25	0.27	−0.34	0.31
Cell45	3.38	87.89	−0.11	0.11	−0.29	0.30	−0.36	0.47
Cell46	3.27	57.80	−0.08	0.09	−0.29	0.30	−0.35	0.44
Cell47	5.22	240.19	−0.31	0.35	−0.32	0.35	−0.68	0.66
Cell48	3.61	134.83	−0.14	0.15	−0.30	0.31	−0.41	0.52
Cell49	3.67	322.76	−0.22	0.23	−0.31	0.31	−0.47	0.61
Cell50	2.04	227.79	−0.13	0.13	−0.28	0.29	−0.45	0.39

Table C.2: Continued.

Membrane Number	Optimum Pore Size (nm)	SS_{Resid} ($\%^2$)	90% Conf. Int. Based on R		90% Conf. Int. Based on Ψ_{DP}		90% Conf. Int. Total	
			Low Diff. (nm)	High Diff. (nm)	Low Diff. (nm)	High Diff. (nm)	Low Diff. (nm)	High Diff. (nm)
Cell51	2.32	286.80	−0.16	0.16	−0.29	0.29	−0.48	0.41
Cell52	1.96	202.60	−0.12	0.12	−0.28	0.28	−0.44	0.38
Cell53	2.19	307.10	−0.16	0.16	−0.29	0.29	−0.48	0.42
Cell54	2.96	120.61	−0.11	0.12	−0.29	0.31	−0.38	0.48
Cell55	2.28	199.52	−0.13	0.13	−0.29	0.29	−0.45	0.39
Cell56	3.12	48.52	−0.08	0.08	−0.30	0.30	−0.40	0.40
Cell57	3.58	199.81	−0.17	0.18	−0.30	0.31	−0.42	0.56
Cell58	2.13	120.09	−0.10	0.10	−0.27	0.28	−0.41	0.36
Cell59	2.88	1004.81	−0.34	0.35	−0.29	0.29	−0.68	0.60
Cell61	1.61	457.71	−0.20	0.20	−0.27	0.28	−0.50	0.43
Cell62	3.07	390.45	−0.19	0.20	−0.29	0.29	−0.45	0.53
Cell63	2.18	553.52	−0.20	0.21	−0.29	0.29	−0.52	0.46
Cell65	1.86	1095.62	−0.28	0.29	−0.28	0.28	−0.59	0.52
Cell66	2.58	578.09	−0.23	0.24	−0.30	0.30	−0.56	0.51
Cell67	2.64	186.95	−0.13	0.13	−0.28	0.30	−0.45	0.39
Cell68	2.69	402.74	−0.19	0.20	−0.29	0.30	−0.50	0.48
Cell69	2.82	124.71	−0.10	0.10	−0.28	0.29	−0.38	0.43
Cell70	2.60	319.51	−0.16	0.17	−0.30	0.29	−0.47	0.47

Appendix D

Permeation Data

The following tables list the permeation data for the 70 membranes tested in this work. Note that the compositions defined by Cell71, Cell72 (Table 4.6) and Cell73 (Table 4.7) were not tested due to the mechanical failure of the test coupons.

These tables list the following information[1];

1. Type of solute used in the permeation experiment.
2. Date of the permeation experiment.
3. Pure water permeability (PWP) for an operating pressure of 6893 ± 69 kPag (1000 ± 10 psig) and an active test surface of 10.75 cm^2 at temperature of 25 ±0.02°C .
4. Product rate (PR) for a 200 ppm solution of the solute at an operating pressure of 6893 ± 69 kPag (1000 ± 10 psig) and an active test surface of 10.75 cm^2 at temperature of 25 ±0.02°C .
5. Rejection coefficient, calculated as the ratio of the permeate concentration to the average feed concentration. The average feed concentration is taken as the mean of the feed concentration at the beginning and end of the run. These rejection coefficients were used to evaluate membrane pore size.
6. Solute separation.

[1]Note: eth. glycol is ethylene glycol and ethanol* indicates that a 10 wt.% feed solution was used in the permeation run.

Experimental data for membrane, Cell1.

Solute	Date of Test	PWP (g/hr)	PR (g/hr)	$\left(\frac{C_{A3}}{C_{A1}}\right)_{expt}$ x 10^2	Solute Separation (%)
PEG 200	6 4 86	35.24	31.76	72.00	28
PEG 200	10 4 86	29.36	27.20	68.71	31
PEG 300	7 4 86	28.00	26.28	58.41	42
PEG 300	10 4 86	28.08	26.46	60.63	39
PEG 400	7 4 86	29.30	28.52	52.70	47
PEG 600	7 4 86	28.26	27.10	42.11	58
PEG 600	11 4 86	29.30	27.04	46.97	53
PEG 1000	8 4 86	48.86	30.70	41.70	58
PEG 1000	11 4 86	27.08	25.82	33.69	66
PEG 2000	11 4 86	26.08	24.98	14.63	85
PEG 3000	12 4 86	26.26	25.44	14.22	86
PEG 6000	9 4 86	30.66	31.92	1.50	99
eth. glycol	10 4 86	33.36	32.02	91.35	9
glycerol	5 4 86	35.42	36.18	87.10	13
erythritol	4 4 86	39.50	29.34	82.69	17
xylitol	4 4 86	33.30	30.48	83.91	16
sorbitol	9 4 86	35.40	31.56	79.87	20
sucrose	5 4 86	40.38	36.18	74.77	25
raffinose	5 4 86	38.68	33.94	68.34	32
ethanol	12 4 86	25.60	24.74	87.77	12
NaCl	4 4 86	33.58	28.80	60.90	39

Experimental data for membrane, Cell2.

Solute	Date of Test	PWP (g/hr)	PR (g/hr)	$\left(\frac{C_{A3}}{C_{A1}}\right)_{expt}$ x 10^2	Solute Separation (%)
PEG 200	6 4 86	40.09	38.62	79.12	21
PEG 200	10 4 86	39.15	39.15	80.73	19
PEG 300	7 4 86	35.33	31.99	69.94	30
PEG 300	10 4 86	42.23	35.25	75.88	24
PEG 400	7 4 86	34.73	33.56	65.32	35
PEG 600	7 4 86	38.59	34.39	59.42	41
PEG 600	11 4 86	38.92	33.52	63.29	37
PEG 1000	8 4 86	47.47	35.36	51.09	49
PEG 1000	11 4 86	32.89	31.43	50.77	49
PEG 2000	8 4 86	39.52	35.44	37.19	63
PEG 2000	11 4 86	31.65	30.11	37.14	63
PEG 3000	8 4 86	38.21	32.14	20.39	80
PEG 3000	12 4 86	36.68	37.16	31.65	68
PEG 4000	9 4 86	41.33	35.06	27.08	73
PEG 6000	9 4 86	38.03	33.11	15.97	84
eth. glycol	10 4 86	39.94	35.03	92.84	7
glycerol	5 4 86	52.39	44.18	88.74	11
erythritol	4 4 86	46.20	33.53	85.11	15
xylitol	4 4 86	41.89	34.69	83.67	16
sorbitol	9 4 86	47.81	39.60	85.43	15
sucrose	5 4 86	54.75	46.09	84.18	16
raffinose	5 4 86	42.08	39.34	80.16	20
ethanol	12 4 86	33.82	33.04	89.43	11
NaCl	4 4 86	40.80	34.24	65.64	34

Experimental data for membrane, Cell3.

Solute	Date of Test	PWP (g/hr)	PR (g/hr)	$\left(\frac{C_{A3}}{C_{A1}}\right)_{expt}$ x 10^2	Solute Separation (%)
PEG 200	6 4 86	12.57	12.41	51.93	48
PEG 200	10 4 86	11.78	11.71	51.82	48
PEG 300	7 4 86	12.46	12.54	45.22	55
PEG 300	10 4 86	11.73	11.71	40.77	59
PEG 400	7 4 86	12.49	12.40	31.88	68
PEG 600	7 4 86	12.51	12.41	27.02	73
PEG 600	11 4 86	11.75	11.69	25.96	74
PEG 1000	8 4 86	11.97	11.81	15.91	84
PEG 1000	11 4 86	11.72	11.65	14.58	85
PEG 2000	8 4 86	11.83	11.73	4.43	96
PEG 2000	11 4 86	11.70	11.63	2.79	97
PEG 3000	8 4 86	11.76	11.70	1.80	98
PEG 3000	12 4 86	11.76	11.69	1.77	98
PEG 4000	9 4 86	11.83	11.77	2.05	98
PEG 6000	9 4 86	11.77	11.73	0.53	99
eth. glycol	10 4 86	11.86	11.75	81.98	18
glycerol	5 4 86	12.42	12.58	76.96	23
erythritol	4 4 86	13.11	12.89	71.82	28
xylitol	4 4 86	13.58	13.05	72.46	28
sorbitol	9 4 86	11.84	11.81	62.94	37
sucrose	5 4 86	13.07	12.49	53.00	47
raffinose	5 4 86	12.63	12.45	47.01	53
ethanol	12 4 86	11.75	11.66	80.75	19
NaCl	4 4 86	13.10	13.26	51.30	49

Experimental data for membrane, Cell4.

Solute	Date of Test	PWP (g/hr)	PR (g/hr)	$\left(\frac{C_{A3}}{C_{A1}}\right)_{expt}$ x 10^2	Solute Separation (%)
PEG 200	6 4 86	16.00	15.83	62.42	38
PEG 200	10 4 86	15.09	15.07	60.50	40
PEG 300	7 4 86	15.85	15.92	53.65	46
PEG 300	10 4 86	15.04	15.01	50.77	49
PEG 400	7 4 86	15.87	15.74	43.44	57
PEG 600	7 4 86	15.98	15.81	33.56	66
PEG 600	11 4 86	15.08	14.97	34.75	65
PEG 1000	8 4 86	15.42	15.15	21.13	79
PEG 1000	11 4 86	15.02	14.94	21.32	79
PEG 2000	8 4 86	15.19	15.10	6.91	93
PEG 2000	11 4 86	15.00	14.90	4.95	95
PEG 3000	8 4 86	15.15	15.02	2.12	98
PEG 3000	12 4 86	15.13	15.01	2.44	98
PEG 4000	9 4 86	15.15	15.06	2.57	97
PEG 6000	9 4 86	15.10	15.01	0.11	100
eth. glycol	10 4 86	15.21	15.07	85.79	14
glycerol	5 4 86	16.06	15.91	78.86	21
erythritol	4 4 86	16.95	16.08	75.92	24
xylitol	4 4 86	16.25	16.32	74.31	26
sorbitol	9 4 86	15.22	15.13	68.86	31
sucrose	5 4 86	15.88	15.89	60.46	40
raffinose	5 4 86	16.65	15.84	53.43	47
ethanol	12 4 86	15.10	14.92	84.41	16
NaCl	4 4 86	16.70	16.51	53.64	46

Experimental data for membrane, Cell5.

Solute	Date of Test	PWP (g/hr)	PR (g/hr)	$\left(\frac{C_{A3}}{C_{A1}}\right)_{expt}$ x 10^2	Solute Separation (%)
PEG 200	6 4 86	25.75	25.49	60.72	39
PEG 200	10 4 86	23.81	23.69	54.99	45
PEG 300	7 4 86	25.49	25.65	49.11	51
PEG 300	10 4 86	23.71	23.67	46.42	54
PEG 400	7 4 86	25.53	25.27	38.43	62
PEG 600	7 4 86	25.63	25.11	29.62	70
PEG 600	11 4 86	23.79	23.59	30.16	70
PEG 1000	8 4 86	24.17	23.78	18.51	81
PEG 1000	11 4 86	23.76	23.50	19.09	81
PEG 2000	8 4 86	23.74	23.59	6.23	94
PEG 2000	11 4 86	23.59	23.45	5.02	95
PEG 3000	8 4 86	23.67	23.55	2.30	98
PEG 3000	12 4 86	23.76	23.54	3.30	97
PEG 4000	9 4 86	23.78	23.66	3.24	97
PEG 6000	9 4 86	23.64	23.50	1.17	99
eth. glycol	10 4 86	23.95	23.78	84.11	16
glycerol	5 4 86	25.89	25.80	78.36	22
erythritol	4 4 86	27.10	26.13	73.92	26
xylitol	4 4 86	26.06	26.47	71.33	29
sorbitol	9 4 86	23.79	23.78	67.68	32
sucrose	5 4 86	25.39	25.66	57.75	42
raffinose	5 4 86	26.49	25.51	50.32	50
ethanol	12 4 86	23.76	23.52	83.91	16
NaCl	4 4 86	26.88	26.81	53.82	46

Experimental data for membrane, Cell6.

Solute	Date of Test	PWP (g/hr)	PR (g/hr)	$\left(\frac{C_{A3}}{C_{A1}}\right)_{expt}$ x 10^2	Solute Separation (%)
PEG 200	6 4 86	53.91	53.21	84.14	16
PEG 200	10 4 86	49.93	49.83	81.59	18
PEG 300	7 4 86	52.71	52.80	79.18	21
PEG 300	10 4 86	49.64	49.48	78.85	21
PEG 400	7 4 86	52.55	52.11	73.11	27
PEG 600	7 4 86	53.15	52.39	66.22	34
PEG 600	11 4 86	49.74	49.17	69.26	31
PEG 1000	8 4 86	51.63	50.53	51.89	48
PEG 1000	11 4 86	49.42	48.88	54.60	45
PEG 2000	8 4 86	50.49	50.05	23.69	76
PEG 2000	11 4 86	49.17	48.82	24.28	76
PEG 3000	8 4 86	50.15	49.04	7.81	92
PEG 3000	12 4 86	49.52	48.95	9.66	90
PEG 4000	9 4 86	50.15	49.80	9.08	91
PEG 6000	9 4 86	49.89	49.58	2.05	98
eth. glycol	10 4 86	50.46	50.02	93.28	7
glycerol	5 4 86	54.82	54.13	90.49	10
erythritol	4 4 86	54.51	55.64	90.73	9
xylitol	4 4 86	56.81	56.81	88.91	11
sorbitol	9 4 86	50.34	50.15	86.09	14
sucrose	5 4 86	54.22	53.75	85.61	14
raffinose	5 4 86	52.07	53.27	81.78	18
ethanol	12 4 86	49.48	48.92	93.75	6
NaCl	4 4 86	58.11	57.41	73.82	26

Experimental data for membrane, Cell7.

Solute	Date of Test	PWP (g/hr)	PR (g/hr)	$\left(\frac{C_{A3}}{C_{A1}}\right)_{expt}$ x 10^2	Solute Separation (%)
PEG 200	6 4 86	29.43	29.06	81.91	18
PEG 200	10 4 86	27.77	27.65	80.50	20
PEG 300	7 4 86	28.94	28.94	78.16	22
PEG 300	10 4 86	27.65	27.53	76.85	23
PEG 400	7 4 86	28.94	28.61	70.90	29
PEG 600	7 4 86	29.06	28.68	61.84	38
PEG 600	11 4 86	27.70	27.36	64.18	36
PEG 1000	8 4 86	28.39	27.94	45.39	55
PEG 1000	11 4 86	27.58	27.36	47.84	52
PEG 2000	8 4 86	27.89	27.60	16.05	84
PEG 2000	11 4 86	27.51	27.27	14.66	85
PEG 3000	8 4 86	27.77	27.33	3.59	96
PEG 3000	12 4 86	27.65	27.39	4.95	95
PEG 4000	9 4 86	27.82	27.60	4.27	96
PEG 6000	9 4 86	27.69	27.48	0.21	100
eth. glycol	10 4 86	27.96	27.72	91.84	8
glycerol	5 4 86	29.55	29.38	89.52	10
erythritol	4 4 86	30.60	29.67	88.78	11
xylitol	4 4 86	30.48	30.12	88.44	12
sorbitol	9 4 86	27.84	27.70	86.02	14
sucrose	5 4 86	29.66	29.18	83.01	17
raffinose	5 4 86	29.86	29.02	80.35	20
ethanol	12 4 86	27.63	27.41	90.32	10
NaCl	4 4 86	30.75	30.53	67.47	33

Experimental data for membrane, Cell8.

Solute	Date of Test	PWP (g/hr)	PR (g/hr)	$\left(\frac{C_{A3}}{C_{A1}}\right)_{expt}$ x 10^2	Solute Separation (%)
PEG 200	6 4 86	23.17	22.90	83.26	17
PEG 200	10 4 86	21.49	21.42	80.85	19
PEG 300	7 4 86	22.31	22.35	78.05	22
PEG 300	10 4 86	21.41	21.39	76.63	23
PEG 400	7 4 86	22.23	22.04	65.65	34
PEG 600	7 4 86	22.41	22.15	56.17	44
PEG 600	11 4 86	21.45	21.28	57.13	43
PEG 1000	8 4 86	21.84	21.65	34.61	65
PEG 1000	11 4 86	21.36	21.21	36.34	64
PEG 2000	8 4 86	21.66	21.45	8.13	92
PEG 2000	11 4 86	21.28	21.10	6.87	93
PEG 3000	8 4 86	21.45	21.37	1.92	98
PEG 3000	12 4 86	21.45	21.23	2.20	98
PEG 4000	9 4 86	21.54	21.42	2.08	98
PEG 6000	9 4 86	21.42	21.31	-0.01	100
eth. glycol	10 4 86	21.66	21.45	91.84	8
glycerol	5 4 86	22.95	23.16	88.79	11
erythritol	4 4 86	22.35	23.38	89.81	10
xylitol	4 4 86	23.76	23.76	93.11	7
sorbitol	9 4 86	21.58	21.50	87.80	12
sucrose	5 4 86	23.06	23.03	83.18	17
raffinose	5 4 86	21.84	22.85	79.86	20
ethanol	12 4 86	21.42	21.19	90.81	9
NaCl	4 4 86	23.92	24.06	68.01	32

Experimental data for membrane, Cell9.

Solute	Date of Test	PWP (g/hr)	PR (g/hr)	$\left(\frac{C_{A3}}{C_{A1}}\right)_{expt}$ x 10^2	Solute Separation (%)
PEG 200	17 4 86	14.46	14.18	58.74	41
PEG 200	24 4 86	13.89	13.78	57.78	42
PEG 300	18 4 86	14.08	13.80	45.27	55
PEG 300	23 4 86	13.76	13.70	47.74	52
PEG 400	17 4 86	14.36	13.94	41.42	59
PEG 400	25 4 86	13.87	13.76	39.38	61
PEG 600	18 4 86	13.99	13.94	29.10	71
PEG 600	23 4 86	13.72	13.80	28.91	71
PEG 1000	18 4 86	14.85	13.70	19.15	81
PEG 1000	24 4 86	14.23	13.74	18.46	82
PEG 2000	21 4 86	14.04	13.85	6.58	93
PEG 3000	21 4 86	13.88	13.74	3.45	97
PEG 4000	21 4 86	13.96	13.66	3.14	97
PEG 6000	22 4 86	13.69	13.66	0.34	100
eth. glycol	23 4 86	13.94	13.78	86.50	14
glycerol	22 4 86	14.00	13.95	79.33	21
erythritol	22 4 86	13.84	13.78	72.58	27
xylitol	15 4 86	14.68	14.26	71.25	29
sorbitol	16 4 86	7.37	14.48	65.31	35
sucrose	15 4 86	14.96	14.59	57.98	42
raffinose	17 4 86	13.88	13.85	48.60	51
ethanol	25 4 86	14.00	13.86	83.84	16
ethanol	25 4 86	13.85	9.81	85.99	14
NaCl	24 4 86	13.91	13.82	60.69	39

Experimental data for membrane, Cell10.

Solute	Date of Test	PWP (g/hr)	PR (g/hr)	$\left(\frac{C_{A3}}{C_{A1}}\right)_{expt}$ x 10^2	Solute Separation (%)
PEG 200	17 4 86	29.11	27.60	87.45	13
PEG 200	24 4 86	26.40	25.51	84.68	15
PEG 300	18 4 86	25.63	25.05	76.42	24
PEG 300	23 4 86	25.11	24.55	80.40	20
PEG 400	17 4 86	28.53	26.74	77.87	22
PEG 400	25 4 86	24.67	24.43	76.57	23
PEG 600	18 4 86	24.99	24.63	63.42	37
PEG 600	23 4 86	25.23	25.05	64.66	35
PEG 1000	18 4 86	24.72	24.36	45.94	54
PEG 1000	24 4 86	25.83	24.45	47.71	52
PEG 2000	21 4 86	25.06	24.79	15.56	84
PEG 3000	21 4 86	25.05	24.62	4.73	95
PEG 4000	21 4 86	24.86	24.19	3.20	97
PEG 6000	22 4 86	24.29	24.19	0.74	99
eth. glycol	23 4 86	24.67	24.62	92.40	8
glycerol	22 4 86	24.84	24.53	90.75	9
erythritol	22 4 86	24.55	24.36	87.55	12
xylitol	15 4 86	29.37	28.34	90.65	9
sorbitol	16 4 86	27.63	31.29	88.98	11
sucrose	15 4 86	30.31	27.89	85.49	15
raffinose	17 4 86	26.54	25.83	81.33	19
ethanol	25 4 86	24.82	24.55	86.77	13
ethanol*	25 4 86	24.63	17.40	96.65	3
NaCl	24 4 86	25.23	25.05	72.76	27

Experimental data for membrane, Cell11.

Solute	Date of Test	PWP (g/hr)	PR (g/hr)	$\left(\frac{C_{A3}}{C_{A1}}\right)_{expt}$ x 10^2	Solute Separation (%)
PEG 200	6 4 86	25.61	30.14	74.41	26
PEG 200	10 4 86	19.58	17.26	56.31	44
PEG 300	7 4 86	20.14	18.24	47.53	52
PEG 300	10 4 86	18.05	17.28	47.58	52
PEG 400	7 4 86	19.03	19.59	41.64	58
PEG 600	7 4 86	19.68	19.08	32.86	67
PEG 600	11 4 86	17.91	17.45	30.26	70
PEG 1000	8 4 86	23.14	17.49	19.74	80
PEG 1000	11 4 86	17.40	16.94	17.80	82
PEG 2000	8 4 86	19.70	19.27	18.22	82
PEG 2000	11 4 86	17.09	16.89	5.11	95
PEG 3000	8 4 86	19.71	18.17	10.59	89
PEG 3000	12 4 86	17.11	17.02	3.97	96
PEG 4000	9 4 86	18.05	17.49	6.75	93
PEG 6000	9 4 86	18.77	19.11	0.55	99
eth. glycol	10 4 86	19.54	18.43	85.45	15
glycerol	5 4 86	20.64	19.05	77.46	23
erythritol	4 4 86	22.75	20.07	74.55	25
xylitol	4 4 86	23.07	20.69	73.34	27
sorbitol	9 4 86	18.41	17.59	65.96	34
sucrose	5 4 86	19.65	19.68	57.45	43
raffinose	5 4 86	25.17	22.77	59.36	41
ethanol	12 4 86	17.26	16.95	83.65	16
NaCl	4 4 86	26.78	21.26	57.99	42

Experimental data for membrane, Cell12.

Solute	Date of Test	PWP (g/hr)	PR (g/hr)	$\left(\frac{C_{A3}}{C_{A1}}\right)_{expt}$ x 10^2	Solute Separation (%)
PEG 200	6 4 86	35.59	34.93	78.80	21
PEG 200	10 4 86	32.15	31.83	76.92	23
PEG 300	7 4 86	33.85	33.66	74.36	26
PEG 300	10 4 86	32.02	31.99	73.32	27
PEG 400	7 4 86	33.57	33.41	66.98	33
PEG 600	7 4 86	34.29	33.69	59.83	40
PEG 600	11 4 86	32.05	31.52	61.11	39
PEG 1000	8 4 86	37.26	32.43	46.68	53
PEG 1000	11 4 86	30.66	31.36	49.19	51
PEG 2000	8 4 86	33.25	33.09	26.65	73
PEG 2000	11 4 86	31.77	31.23	22.98	77
PEG 3000	8 4 86	33.35	32.02	13.34	87
PEG 3000	12 4 86	31.61	31.20	12.72	87
PEG 4000	9 4 86	32.49	31.93	13.17	87
PEG 6000	9 4 86	32.37	31.64	5.63	94
eth. glycol	10 4 86	32.72	32.15	91.80	8
glycerol	5 4 85	35.53	35.94	88.15	12
erythritol	4 4 86	38.31	35.02	88.44	12
xylitol	4 4 86	38.65	35.53	86.28	14
sorbitol	9 4 86	32.37	32.40	84.18	16
sucrose	5 4 86	38.12	36.35	82.93	17
raffinose	5 4 86	38.72	35.49	79.99	20
ethanol	12 4 86	31.83	31.23	90.00	10
NaCl	4 4 86	35.91	36.00	67.83	32

Experimental data for membrane, Cell13.

Solute	Date of Test	PWP (g/hr)	PR (g/hr)	$\left(\frac{C_{A3}}{C_{A1}}\right)_{expt}$ x 10^2	Solute Separation (%)
PEG 200	6 4 86	56.05	55.04	83.53	16
PEG 200	10 4 86	50.34	50.15	81.95	18
PEG 300	7 4 86	54.47	54.22	79.39	21
PEG 300	10 4 86	49.99	49.74	79.20	21
PEG 400	7 4 86	54.19	53.46	73.61	26
PEG 600	7 4 86	54.76	54.13	65.46	35
PEG 600	11 4 86	50.05	49.45	67.82	32
PEG 1000	8 4 86	52.52	51.09	53.73	46
PEG 1000	11 4 86	49.93	49.39	54.98	45
PEG 2000	8 4 86	51.09	50.43	23.37	77
PEG 2000	11 4 86	49.52	49.11	23.70	76
PEG 3000	8 4 86	50.56	50.37	7.14	93
PEG 3000	12 4 86	49.80	49.29	8.58	91
PEG 4000	9 4 86	50.72	50.24	8.12	92
PEG 6000	9 4 86	50.24	49.96	1.67	98
eth. glycol	10 4 86	50.81	50.31	93.07	7
glycerol	5 4 86	58.86	55.80	90.95	9
erythritol	4 4 86	60.95	56.87	92.37	8
xylitol	4 4 86	56.34	57.98	90.83	9
sorbitol	9 4 86	50.75	50.62	89.08	11
sucrose	5 4 86	54.98	55.58	85.26	15
raffinose	5 4 86	56.12	55.20	82.08	18
ethanol	12 4 86	49.77	49.20	92.08	8
NaCl	4 4 86	61.20	57.79	72.01	28

Experimental data for membrane, Cell14.

Solute	Date of Test	PWP (g/hr)	PR (g/hr)	$\left(\frac{C_{A3}}{C_{A1}}\right)_{expt}$ x 10^2	Solute Separation (%)
PEG 200	9 10 85	10.00	9.96	49.45	51
PEG 200	17 10 85	10.11	9.95	45.53	54
PEG 300	17 10 85	8.96	9.95	35.31	65
PEG 300	9 10 85	9.98	9.97	30.87	69
PEG 400	2 10 85	10.11	9.96	36.85	63
PEG 400	17 10 85	9.96	9.93	23.60	76
PEG 600	2 10 85	9.97	9.91	22.31	78
PEG 1000	2 10 85	9.95	9.89	13.17	87
PEG 2000	14 10 85	10.22	10.14	2.00	98
PEG 3000	14 10 85	10.14	10.09	0.88	99
PEG 4000	14 10 85	10.07	10.06	1.15	99
PEG 6000	15 10 85	9.87	9.87	0.42	100
erythritol	5 10 85	10.01	9.96	81.36	19
erythritol	30 10 85	10.44	10.26	67.12	33
xylitol	9 10 85	10.02	10.08	68.78	31
xylitol	30 10 85	10.20	10.14	65.90	34
sucrose	5 10 85	10.19	10.00	49.39	51
sucrose	30 10 85	10.11	10.07	49.93	50
raffinose	5 10 85	10.02	9.99	37.04	63
raffinose	31 10 85	10.12	10.02	50.45	50
ethanol	15 10 85	9.95	9.92	83.87	16
ethanol	31 10 85	10.10	10.05	82.00	18
NaCl	15 10 85	9.93	9.98	52.60	47
NaCl	31 10 85	10.14	10.19	55.51	44

Experimental data for membrane, Cell15.

Solute	Date of Test	PWP (g/hr)	PR (g/hr)	$\left(\frac{C_{A3}}{C_{A1}}\right)_{expt}$ x 10^2	Solute Separation (%)
PEG 200	6 8 85	15.48	15.46	73.35	27
PEG 200	24 9 85	16.09	15.81	66.97	33
PEG 300	6 8 85	14.99	14.93	56.25	44
PEG 300	20 8 85	15.63	15.45	62.59	37
PEG 300	24 9 85	16.32	15.93	61.55	38
PEG 400	25 9 85	15.98	15.94	56.99	43
PEG 600	12 8 85	15.73	15.52	31.60	68
PEG 1000	12 8 85	15.58	15.45	11.16	89
PEG 1000	22 8 85	15.68	15.45	9.32	91
PEG 2000	15 8 85	15.77	15.58	1.43	99
PEG 3000	15 8 85	15.56	15.54	0.06	100
PEG 4000	15 8 85	15.52	15.40	-0.11	100
PEG 6000	20 8 85	15.51	15.44	-0.13	100
eth. glycol	6 8 85	16.31	15.62	90.79	9
eth. glycol	25 9 85	15.48	15.67	89.06	11
sorbitol	19 8 85	15.76	15.61	66.70	33
sucrose	19 8 85	15.54	15.43	59.76	40
raffinose	19 8 85	15.49	15.42	48.81	51
ethanol*	25 9 85	15.25	11.10	92.67	7
NaCl	22 8 85	15.98	15.39	56.20	44
NaCl	24 9 85	16.50	16.34	54.97	45

Experimental data for membrane, Cell16.

Solute	Date of Test	PWP (g/hr)	PR (g/hr)	$\left(\frac{C_{A3}}{C_{A1}}\right)_{expt}$ x 10^2	Solute Separation (%)
PEG 200	6 8 85	13.82	13.64	58.90	41
PEG 200	24 9 85	13.58	13.50	52.20	48
PEG 300	6 8 85	13.57	13.41	44.21	56
PEG 300	20 8 85	13.70	13.33	45.17	55
PEG 300	24 9 85	13.45	13.39	48.88	51
PEG 400	25 9 85	13.34	13.29	39.12	61
PEG 600	12 8 85	14.16	13.93	22.76	77
PEG 1000	12 8 85	14.08	14.02	9.42	91
PEG 1000	22 8 85	13.27	13.13	7.75	92
PEG 2000	15 8 85	14.26	14.18	2.19	98
PEG 3000	15 8 85	14.10	14.08	0.46	100
PEG 4000	15 8 85	14.10	14.03	0.36	100
PEG 6000	20 8 85	13.39	13.22	0.18	100
eth. glycol	6 8 85	14.30	13.93	86.05	14
eth. glycol	25 9 85	13.42	13.35	88.56	11
sorbitol	19 8 85	15.51	14.60	58.43	42
sucrose	19 8 85	14.60	14.00	45.55	54
raffinose	19 8 85	13.67	13.40	36.16	64
ethanol*	25 9 85	13.67	9.14	82.50	18
NaCl	22 8 85	13.14	13.14	50.24	50
NaCl	24 9 85	13.56	13.62	48.58	51

Experimental data for membrane, Cell17.

Solute	Date of Test	PWP (g/hr)	PR (g/hr)	$\left(\frac{C_{A3}}{C_{A1}}\right)_{expt}$ x 10^2	Solute Separation (%)
PEG 200	9 10 85	6.50	6.49	48.63	51
PEG 200	17 10 85	6.56	6.52	36.73	63
PEG 300	17 10 85	6.50	6.48	33.15	67
PEG 300	9 10 85	6.51	6.49	28.33	72
PEG 400	2 10 85	6.46	6.40	32.56	67
PEG 400	17 10 85	6.53	6.47	18.02	82
PEG 600	2 10 85	6.41	6.36	23.58	76
PEG 1000	2 10 85	6.38	6.38	13.49	87
PEG 2000	14 10 85	6.62	6.55	1.39	99
PEG 3000	14 10 85	6.61	6.57	0.30	100
PEG 4000	14 10 85	6.56	6.55	0.54	99
PEG 6000	15 10 85	6.45	6.42	0.43	100
erythritol	5 10 85	6.51	6.49	77.10	23
erythritol	30 10 85	6.76	6.70	60.88	39
xylitol	9 10 85	6.47	6.56	63.52	36
xylitol	30 10 85	6.68	6.60	58.41	42
sucrose	5 10 85	6.57	6.46	47.63	52
sucrose	30 10 85	6.62	6.58	50.76	49
raffinose	5 10 85	6.50	6.50	34.65	65
raffinose	31 10 85	6.66	6.57	58.43	42
ethanol	15 10 85	6.46	6.43	77.61	22
ethanol*	31 10 85	6.61	6.59	81.45	19
NaCl	15 10 85	6.46	6.52	50.14	50
NaCl	31 10 85	6.66	6.67	52.10	48

Experimental data for membrane, Cell18.

Solute	Date of Test	PWP (g/hr)	PR (g/hr)	$\left(\frac{C_{A3}}{C_{A1}}\right)_{expt}$ x 10^2	Solute Separation (%)
PEG 200	9 10 85	8.29	10.27	52.35	48
PEG 200	17 10 85	10.38	10.27	44.36	56
PEG 300	17 10 85	10.28	10.26	35.72	64
PEG 300	9 10 85	9.82	10.27	30.50	70
PEG 400	2 10 85	10.31	10.20	35.58	64
PEG 400	17 10 85	9.75	10.26	24.50	76
PEG 600	2 10 85	10.23	10.17	23.83	76
PEG 1000	2 10 85	9.72	10.17	16.51	83
PEG 2000	14 10 85	10.48	10.44	3.46	97
PEG 3000	14 10 85	10.49	10.41	2.27	98
PEG 4000	14 10 85	9.92	10.38	2.25	98
PEG 6000	15 10 85	9.66	10.16	0.54	99
erythritol	5 10 85	9.77	10.19	68.63	31
erythritol	30 10 85	10.69	10.54	66.31	34
xylitol	9 10 85	10.27	10.33	65.15	35
xylitol	30 10 85	10.49	10.43	62.99	37
sucrose	5 10 85	10.43	10.26	54.02	46
sucrose	30 10 85	9.91	10.36	64.57	35
raffinose	5 10 85	10.31	10.27	46.04	54
raffinose	31 10 85	9.87	10.31	42.37	58
ethanol	15 10 85	10.22	10.19	83.24	17
ethanol	31 10 85	10.33	10.28	81.58	18
NaCl	15 10 85	10.18	10.26	52.27	48
NaCl	31 10 85	10.45	10.48	54.32	46

Experimental data for membrane, Cell19.

Solute	Date of Test	PWP (g/hr)	PR (g/hr)	$\left(\frac{C_{A3}}{C_{A1}}\right)_{expt}$ x 10^2	Solute Separation (%)
PEG 200	9 10 85	7.15	7.14	45.75	54
PEG 200	17 10 85	7.21	7.14	41.71	58
PEG 300	17 10 85	7.12	7.10	32.62	67
PEG 300	9 10 85	7.15	7.13	29.39	71
PEG 400	2 10 85	7.14	7.05	33.38	67
PEG 400	17 10 85	7.13	7.09	21.10	79
PEG 600	2 10 85	7.07	7.00	24.00	76
PEG 1000	2 10 85	7.03	7.03	18.96	81
PEG 2000	14 10 85	7.29	7.25	1.74	98
PEG 3000	14 10 85	7.23	7.22	0.43	100
PEG 4000	14 10 85	7.20	7.20	0.52	99
PEG 6000	15 10 85	7.09	7.07	0.61	99
erythritol	5 10 85	7.12	7.08	62.66	37
erythritol	30 10 85	7.49	7.39	66.63	33
xylitol	9 10 85	7.15	7.19	61.80	38
xylitol	30 10 85	7.31	7.28	65.03	35
sucrose	5 10 85	7.24	7.15	58.00	42
sucrose	30 10 85	7.28	7.25	57.11	43
raffinose	5 10 85	7.12	7.13	37.18	63
raffinose	31 10 85	7.31	7.24	44.55	55
ethanol	15 10 85	7.10	7.09	79.49	21
ethanol	31 10 85	7.27	7.26	80.08	20
NaCl	15 10 85	7.12	7.18	52.11	48
NaCl	31 10 85	7.28	7.42	54.32	46

Experimental data for membrane, Cell20.

Solute	Date of Test	PWP (g/hr)	PR (g/hr)	$\left(\frac{C_{A3}}{C_{A1}}\right)_{expt}$ x 10^2	Solute Separation (%)
PEG 200	9 10 85	10.20	10.18	50.86	49
PEG 200	17 10 85	10.30	10.18	48.08	52
PEG 300	17 10 85	10.15	10.12	35.72	64
PEG 300	9 10 85	10.20	10.15	32.07	68
PEG 400	2 10 85	10.22	10.09	34.53	65
PEG 400	17 10 85	10.14	10.15	26.07	74
PEG 600	2 10 85	10.12	10.06	25.12	75
PEG 1000	2 10 85	10.06	10.06	14.87	85
PEG 2000	14 10 85	10.41	10.34	2.57	97
PEG 3000	14 10 85	10.32	10.30	0.99	99
PEG 4000	14 10 85	10.28	10.22	1.18	99
PEG 6000	15 10 85	10.06	10.06	0.45	100
erythritol	5 10 85	10.16	10.11	67.32	33
erythritol	30 10 85	10.58	10.43	65.50	35
xylitol	9 10 85	10.21	10.26	65.25	35
xylitol	30 10 85	10.35	10.33	62.85	37
sucrose	5 10 85	10.28	10.21	48.51	51
sucrose	30 10 85	10.29	10.27	56.68	43
raffinose	5 10 85	10.18	10.12	61.55	38
raffinose	31 10 85	10.28	10.20	45.65	54
ethanol	15 10 85	10.13	10.11	83.40	17
ethanol	31 10 85	10.29	10.23	81.03	19
NaCl	15 10 85	10.10	10.17	52.27	48
NaCl	31 10 85	10.38	10.38	56.03	44

Experimental data for membrane, Cell21.

Solute	Date of Test	PWP (g/hr)	PR (g/hr)	$\left(\frac{C_{A3}}{C_{A1}}\right)_{expt}$ x 10^2	Solute Separation (%)
PEG 200	6 8 85	11.58	11.47	56.42	44
PEG 200	24 9 85	11.46	11.42	51.30	49
PEG 300	6 8 85	11.36	11.32	40.95	59
PEG 300	20 8 85	11.95	11.24	43.42	57
PEG 300	24 9 85	11.38	11.36	45.54	54
PEG 400	25 9 85	11.33	11.29	35.72	64
PEG 600	12 8 85	12.51	11.78	15.50	85
PEG 1000	12 8 85	11.90	11.84	5.88	94
PEG 1000	22 8 85	11.96	11.32	6.09	94
PEG 2000	15 8 85	12.56	11.96	0.64	99
PEG 3000	15 8 85	11.95	11.95	-0.21	100
PEG 4000	15 8 85	11.91	11.87	-0.77	100
PEG 6000	20 8 85	11.36	11.27	-0.13	100
eth. glycol	6 8 85	12.73	11.71	93.74	6
eth. glycol	25 9 85	11.83	11.29	74.26	26
sorbitol	19 8 85	12.53	11.94	57.27	43
sucrose	19 8 85	11.74	11.62	41.65	58
raffinose	19 8 85	11.58	11.63	31.82	68
ethanol*	25 9 85	11.30	7.69	87.35	13
NaCl	22 8 85	11.42	11.41	48.12	52
NaCl	24 9 85	11.99	11.51	46.30	54

Experimental data for membrane, Cell22.

Solute	Date of Test	PWP (g/hr)	PR (g/hr)	$\left(\frac{C_{A3}}{C_{A1}}\right)_{expt}$ x 10^2	Solute Separation (%)
PEG 200	6 8 85	11.11	11.02	53.50	47
PEG 200	24 9 85	12.51	12.40	43.78	56
PEG 300	6 8 85	10.92	10.97	35.19	65
PEG 300	20 8 85	10.34	10.19	36.52	63
PEG 300	24 9 85	12.65	12.31	30.86	69
PEG 400	25 9 85	14.75	11.96	15.17	85
PEG 600	12 8 85	11.37	11.14	12.33	88
PEG 1000	12 8 85	11.23	11.24	3.84	96
PEG 1000	22 8 85	10.32	10.24	10.31	90
PEG 2000	15 8 85	11.46	11.31	0.23	100
PEG 3000	15 8 85	11.26	11.29	-0.54	100
PEG 4000	15 8 85	11.28	11.21	-0.66	100
PEG 6000	20 8 85	10.32	10.22	-0.13	100
NaCl	22 8 85	10.23	10.25	46.20	54
NaCl	24 9 85	14.47	14.21	47.88	52

Experimental data for membrane, Cell23.

Solute	Date of Test	PWP (g/hr)	PR (g/hr)	$\left(\frac{C_{A3}}{C_{A1}}\right)_{expt}$ x 10^2	Solute Separation (%)
PEG 200	9 10 85	10.09	10.08	53.43	47
PEG 200	17 10 85	10.20	10.09	48.76	51
PEG 300	17 10 85	10.07	10.02	38.48	62
PEG 300	9 10 85	10.11	10.08	32.19	68
PEG 400	2 10 85	10.23	10.09	39.01	61
PEG 400	17 10 85	10.07	10.03	27.14	73
PEG 600	2 10 85	10.08	10.03	29.47	71
PEG 1000	2 10 85	10.06	10.01	15.36	85
PEG 2000	14 10 85	10.34	10.26	2.89	97
PEG 3000	14 10 85	10.21	10.18	0.54	99
PEG 4000	14 10 85	10.18	10.13	0.73	99
PEG 6000	15 10 85	10.01	10.00	0.63	99
erythritol	5 10 85	10.17	10.09	70.43	30
erythritol	30 10 85	10.55	10.35	67.77	32
xylitol	9 10 85	10.15	10.18	67.04	33
xylitol	30 10 85	10.31	10.24	66.79	33
sucrose	5 10 85	10.31	10.16	51.91	48
sucrose	30 10 85	10.23	10.18	53.83	46
raffinose	5 10 85	10.13	10.16	40.95	59
raffinose	31 10 85	10,32	10.16	46.60	53
ethanol	15 10 85	10.05	10.03	84.50	16
ethanol	31 10 85	10.26	10.20	82.68	17
NaCl	15 10 85	10.04	10.12	54.25	46
NaCl	31 10 85	10.27	10.31	56.54	43

Experimental data for membrane, Cell24.

Solute	Date of Test	PWP (g/hr)	PR (g/hr)	$\left(\frac{C_{A3}}{C_{A1}}\right)_{expt}$ x 10^2	Solute Separation (%)
PEG 200	6 8 85	9.70	9.62	58.90	41
PEG 200	24 9 85	8.98	8.93	50.19	50
PEG 300	6 8 85	9.53	9.48	47.92	52
PEG 300	20 8 85	9.04	8.95	47.16	53
PEG 300	24 9 85	8.94	8.88	45.31	55
PEG 400	25 9 85	8.88	8.83	37.90	62
PEG 600	12 8 85	10.04	9.89	21.53	78
PEG 1000	12 8 85	9.97	9.96	8.41	92
PEG 2000	22 8 85	9.03	8.97	7.75	92
PEG 2000	15 8 85	10.11	10.03	1.24	99
PEG 3000	15 8 85	9.98	10.03	-0.32	100
PEG 4000	15 8 85	9.99	9.99	-0.77	100
PEG 6000	20 8 85	8.98	8.93	-0.13	100
eth. glycol	6 8 85	10.06	9.84	85.23	15
eth. glycol	25 9 85	8.92	8.84	93.69	6
sorbitol	19 8 85	9.55	9.51	52.67	47
sucrose	19 8 85	9.49	9.43	50.53	49
raffinose	19 8 85	9.45	9.42	44.10	56
ethanol*	25 9 85	8.67	6.09	83.22	17
NaCl	22 8 85	8.99	9.01	47.80	52
NaCl	24 9 85	9.04	9.04	44.82	55

Experimental data for membrane, Cell25.

Solute	Date of Test	PWP (g/hr)	PR (g/hr)	$\left(\frac{C_{A3}}{C_{A1}}\right)_{expil}$ x 10^2	Solute Separation (%)
PEG 200	9 10 85	15.14	15.03	64.07	36
PEG 200	17 10 85	15.23	15.02	61.51	38
PEG 300	17 10 85	15.06	14.96	56.11	44
PEG 300	9 10 85	15.08	15.02	40.54	59
PEG 400	2 10 85	15.32	15.15	52.35	48
PEG 400	17 10 85	15.04	15.00	43.73	56
PEG 600	2 10 85	15.16	15.04	40.05	60
PEG 1000	2 10 85	15.10	14.99	26.79	73
PEG 2000	14 10 85	15.43	15.29	6.21	94
PEG 3000	14 10 85	15.31	15.19	1.92	98
PEG 4000	14 10 85	15.24	15.12	2.07	98
PEG 6000	15 10 85	14.90	14.87	0.43	100
erythritol	5 10 85	15.12	15.04	76.60	23
erythritol	30 10 85	15.70	15.39	80.29	20
xylitol	9 10 85	15.15	15.18	75.95	24
xylitol	30 10 85	15.36	15.28	73.50	27
sucrose	5 10 85	15.43	15.18	63.49	37
sucrose	30 10 85	15.24	15.19	66.37	34
raffinose	5 10 85	15.18	15.07	78.01	22
raffinose	31 10 85	15.23	15.10	63.07	37
ethanol	15 10 85	15.00	14.94	88.10	12
ethanol	31 10 85	15.24	15.12	86.41	14
NaCl	15 10 85	14.93	15.11	57.56	42
NaCl	31 10 85	15.32	15.35	58.26	42

Experimental data for membrane, Cell26.

Solute	Date of Test	PWP (g/hr)	PR (g/hr)	$\left(\frac{C_{A3}}{C_{A1}}\right)_{expil}$ x 10^2	Solute Separation (%)
PEG 200	6 8 85	9.10	9.02	58.90	41
PEG 200	24 9 85	9.13	9.06	44.82	55
PEG 300	6 8 85	8.93	8.88	35.82	64
PEG 300	20 8 85	9.19	8.98	35.38	65
PEG 300	24 9 85	9.06	8.98	42.04	58
PEG 400	25 9 85	9.02	8.98	31.70	68
PEG 600	12 8 85	9.59	9.39	13.36	87
PEG 1000	12 8 85	9.47	9.42	5.27	95
PEG 1000	22 8 85	9.12	9.02	5.31	95
PEG 2000	15 8 85	9.62	9.51	1.06	99
PEG 3000	15 8 85	9.48	9.48	0.58	99
PEG 4000	15 8 85	9.50	9.45	0.24	100
PEG 6000	20 8 85	9.03	8.94	-0.13	100
eth. glycol	6 8 85	9.48	9.18	89.56	10
eth. glycol	25 9 85	9.04	8.98	75.11	25
sorbitol	19 8 85	9.64	9.51	50.40	50
sucrose	19 8 85	9.53	9.45	37.84	62
raffinose	19 8 85	9.51	9.50	27.63	72
ethanol*	25 9 85	9.71	6.10	85.38	15
NaCl	22 8 85	9.07	9.08	47.48	53
NaCl	24 9 85	9.15	9.14	46.30	54

Experimental data for membrane, Cell27.

Solute	Date of Test	PWP (g/hr)	PR (g/hr)	$\left(\frac{C_{A3}}{C_{A1}}\right)_{expt}$ x 10^2	Solute Separation (%)
PEG 200	6 8 85	12.06	11.96	52.74	47
PEG 200	24 9 85	12.10	11.99	48.23	52
PEG 300	6 8 85	11.81	11.77	37.73	62
PEG 300	20 8 85	12.05	11.88	50.47	50
PEG 300	24 9 85	12.01	11.92	41.12	59
PEG 400	25 9 85	11.90	11.86	39.53	60
PEG 600	12 8 85	12.59	12.33	16.61	83
PEG 1000	12 8 85	12.41	12.38	5.88	94
PEG 1000	22 8 85	12.01	11.92	6.09	94
PEG 2000	15 8 85	12.65	12.56	1.06	99
PEG 3000	15 8 85	12.48	12.50	0.06	100
PEG 4000	15 8 85	12.47	12.41	-0.11	100
PEG 6000	20 8 85	11.93	11.87	-0.13	100
eth. glycol	6 8 85	12.48	12.19	86.05	14
eth. glycol	25 9 85	11.98	11.91	80.88	19
sorbitol	19 8 85	12.44	12.29	50.40	50
sucrose	19 8 85	12.25	12.23	38.78	61
raffinose	19 8 85	12.24	12.21	36.16	64
ethanol*	25 9 85	12.23	8.13	85.14	15
NaCl	22 8 85	11.94	11.92	48.12	52
NaCl	24 9 85	12.12	12.14	46.75	53

Experimental data for membrane, Cell28.

Solute	Date of Test	PWP (g/hr)	PR (g/hr)	$\left(\frac{C_{A3}}{C_{A1}}\right)_{expt}$ x 10^2	Solute Separation (%)
PEG 200	9 10 85	12.47	12.40	52.12	48
PEG 200	17 10 85	12.57	12.42	48.59	51
PEG 300	17 10 85	12.42	12.38	38.06	62
PEG 300	9 10 85	12.48	12.40	30.83	69
PEG 400	2 10 85	12.62	12.41	34.42	66
PEG 400	17 10 85	12.38	12.35	25.54	74
PEG 600	2 10 85	12.42	12.30	23.15	77
PEG 1000	2 10 85	12.37	12.27	13.89	86
PEG 2000	14 10 85	12.73	12.61	2.16	98
PEG 3000	14 10 85	12.65	12.54	0.90	99
PEG 4000	14 10 85	12.56	12.48	1.11	99
PEG 6000	15 10 85	12.30	12.28	0.53	99
erythritol	5 10 85	12.50	12.36	70.10	30
erythritol	30 10 85	13.05	12.79	71.54	28
xylitol	9 10 85	12.50	12.55	68.43	32
xylitol	30 10 85	12.76	12.63	65.32	35
sucrose	5 10 85	12.72	12.49	51.17	49
sucrose	30 10 85	12.66	12.62	55.39	45
raffinose	5 10 85	12.50	12.44	51.00	49
raffinose	31 10 85	12.73	12.62	46.60	53
ethanol	15 10 85	12.37	12.31	84.50	16
ethanol	31 10 85	12.69	12.61	83.37	17
NaCl	15 10 85	12.38	12.47	52.60	47
NaCl	31 10 85	12.73	12.75	54.83	45

Experimental data for membrane, Cell29.

Solute	Date of Test	PWP (g/hr)	PR (g/hr)	$\left(\frac{C_{A3}}{C_{A1}}\right)_{expt}$ x 10^2	Solute Separation (%)
PEG 200	6 8 85	20.81	20.57	79.39	21
PEG 200	24 9 85	19.97	19.85	61.65	38
PEG 300	6 8 85	19.80	20.33	68.54	31
PEG 300	20 8 85	19.81	19.54	59.15	41
PEG 300	24 9 85	19.20	19.67	67.01	33
PEG 400	25 9 85	19.62	19.60	64.27	36
PEG 600	12 8 85	21.12	20.68	58.80	41
PEG 1000	12 8 85	20.86	20.77	39.47	61
PEG 1000	22 8 85	19.69	19.43	42.04	58
PEG 2000	15 8 85	21.04	20.77	14.63	85
PEG 3000	15 8 85	20.80	20.66	4.26	96
PEG 4000	15 8 85	20.11	20.51	4.42	96
PEG 6000	20 8 85	19.62	19.54	0.38	100
eth. glycol	6 8 85	21.70	21.07	91.99	8
eth. glycol	25 9 85	19.70	19.57	83.21	17
sorbitol	19 8 85	20.44	20.15	71.52	28
sucrose	19 8 85	20.15	20.00	66.06	34
raffinose	19 8 85	19.46	20.11	62.34	38
ethanol*	25 9 85	41.45	13.43	90.61	9
NaCl	22 8 85	19.57	19.58	57.97	42
NaCl	24 9 85	20.02	20.00	55.81	44

Experimental data for membrane, Cell30.

Solute	Date of Test	PWP (g/hr)	PR (g/hr)	$\left(\frac{C_{A3}}{C_{A1}}\right)_{expt}$ x 10^2	Solute Separation (%)
PEG 200	9 10 85	10.04	9.99	49.06	51
PEG 200	17 10 85	10.13	10.01	41.38	59
PEG 300	17 10 85	10.03	9.97	37.23	63
PEG 300	9 10 85	10.04	9.99	30.23	70
PEG 400	2 10 85	10.04	9.90	37.93	62
PEG 400	17 10 85	10.03	10.01	22.46	78
PEG 600	2 10 85	9.89	9.85	23.92	76
PEG 1000	2 10 85	9.93	9.84	14.87	85
PEG 2000	14 10 85	10.28	10.19	3.12	97
PEG 3000	14 10 85	10.18	10.14	1.87	98
PEG 4000	14 10 85	10.15	10.09	1.68	98
PEG 6000	15 10 85	9.91	9.91	0.61	99
erythritol	5 10 85	9.98	9.91	62.98	37
erythritol	30 10 85	10.45	10.26	73.20	27
xylitol	9 10 85	10.06	10.07	60.97	39
xylitol	30 10 85	10.21	10.18	62.41	38
sucrose	5 10 85	10.13	10.00	45.90	54
sucrose	30 10 85	10.16	10.12	47.87	52
raffinose	5 10 85	10.00	10.01	41.98	58
raffinose	31 10 85	10.15	10.06	42.68	57
ethanol	15 10 85	9.95	9.93	81.05	19
ethanol	31 10 85	10.11	10.05	80.90	19
NaCl	15 10 85	9.95	10.00	53.26	47
NaCl	31 10 85	10.20	10.24	54.83	45

Experimental data for membrane, Cell31.

Solute	Date of Test	PWP (g/hr)	PR (g/hr)	$\left(\frac{C_{A3}}{C_{A1}}\right)_{expt}$ x 10^2	Solute Separation (%)
PEG 200	6 8 85	22.79	22.46	79.39	21
PEG 200	24 9 85	22.05	21.88	73.93	26
PEG 300	6 8 85	21.88	21.71	70.61	29
PEG 300	20 8 85	22.17	21.79	77.52	22
PEG 300	24 9 85	21.89	21.73	71.54	28
PEG 400	25 9 85	21.63	21.57	72.12	28
PEG 600	12 8 85	22.80	22.38	59.52	40
PEG 1000	12 8 85	22.52	22.39	37.72	62
PEG 1000	22 8 85	21.91	21.64	40.86	59
PEG 2000	15 8 85	22.67	22.37	11.21	89
PEG 3000	15 8 85	22.38	22.34	2.32	98
PEG 4000	15 8 85	22.34	22.17	2.13	98
PEG 6000	20 8 85	21.96	21.74	0.38	100
eth. glycol	6 8 85	23.46	22.71	93.74	6
eth. glycol	25 9 85	21.77	21.60	91.09	9
sorbitol	19 8 85	22.65	22.42	73.95	26
sucrose	19 8 85	22.38	22.21	67.12	33
raffinose	19 8 85	22.26	22.26	72.61	27
ethanol*	25 9 85	21.57	14.92	90.10	10
NaCl	22 8 85	21.78	21.68	58.87	41
NaCl	24 9 85	22.16	22.24	58.72	41

Experimental data for membrane, Cell32.

Solute	Date of Test	PWP (g/hr)	PR (g/hr)	$\left(\frac{C_{A3}}{C_{A1}}\right)_{expt}$ x 10^2	Solute Separation (%)
PEG 200	6 8 85	13.17	12.89	61.23	39
PEG 200	24 9 85	14.59	14.09	54.14	46
PEG 300	6 8 85	12.81	12.66	43.95	56
PEG 300	20 8 85	15.24	15.85	49.52	50
PEG 300	24 9 85	14.20	13.77	48.88	51
PEG 400	25 9 85	13.81	13.84	35.62	64
PEG 600	12 8 85	13.45	13.28	16.83	83
PEG 1000	12 8 85	13.35	13.36	6.52	93
PEG 1000	22 8 85	14.82	14.33	6.09	94
PEG 2000	15 8 85	13.61	13.44	0.46	100
PEG 3000	15 8 85	13.39	13.39	-0.43	100
PEG 4000	15 8 85	13.42	13.31	-0.56	100
PEG 6000	20 8 85	19.07	16.01	-0.13	100
eth. glycol	6 8 85	13.92	13.30	86.05	14
eth. glycol	25 9 85	13.86	13.91	81.81	18
sorbitol	19 8 85	13.56	13.42	54.96	45
sucrose	19 8 85	13.41	13.34	41.65	58
raffinose	19 8 85	13.37	13.35	32.89	67
ethanol*	25 9 85	13.90	9.24	88.34	12
NaCl	22 8 85	14.11	13.55	51.07	49
NaCl	24 9 85	14.80	14.21	51.71	48

Experimental data for membrane, Cell33.

Solute	Date of Test	PWP (g/hr)	PR (g/hr)	$\left(\frac{C_{A3}}{C_{A1}}\right)_{expt}$ x 10^2	Solute Separation (%)
PEG 200	9 10 85	8.90	8.89	43.81	56
PEG 200	17 10 85	8.92	8.84	36.73	63
PEG 300	17 10 85	8.82	8.80	28.58	71
PEG 300	9 10 85	8.92	8.84	27.68	72
PEG 400	2 10 85	8.91	8.81	30.83	69
PEG 400	17 10 85	8.82	8.78	17.00	83
PEG 600	2 10 85	8.82	8.79	20.24	80
PEG 1000	2 10 85	8.82	8.77	12.05	88
PEG 2000	14 10 85	9.04	9.01	2.13	98
PEG 3000	14 10 85	8.98	8.98	1.03	99
PEG 4000	14 10 85	8.93	8.88	1.27	99
PEG 6000	15 10 85	8.77	8.77	0.63	99
erythritol	5 10 85	8.91	8.86	67.16	33
erythritol	30 10 85	9.26	9.09	61.36	39
xylitol	9 10 85	8.83	8.94	57.60	42
xylitol	30 10 85	9.07	9.01	57.00	43
sucrose	5 10 85	8.98	8.92	43.19	57
sucrose	30 10 85	9.00	8.92	46.11	54
raffinose	5 10 85	8.89	8.88	42.72	57
raffinose	31 10 85	9.06	8.95	37.08	63
ethanol	15 10 85	8.82	8.81	80.90	19
ethanol	31 10 85	9.03	8.96	79.26	21
NaCl	15 10 85	8.79	8.86	51.78	48
NaCl	31 10 85	9.04	9.10	52.44	48

Experimental data for membrane, Cell34.

Solute	Date of Test	PWP (g/hr)	PR (g/hr)	$\left(\frac{C_{A3}}{C_{A1}}\right)_{expt}$ x 10^2	Solute Separation (%)
PEG 200	6 8 85	29.68	27.62	80.98	19
PEG 200	24 9 85	28.58	26.05	70.93	29
PEG 300	6 8 85	26.65	24.98	65.11	35
PEG 300	20 8 85	27.80	26.67	62.59	37
PEG 300	24 9 85	25.76	25.20	69.93	30
PEG 400	25 9 85	26.35	25.05	59.53	40
PEG 600	12 8 85	26.89	24.22	45.69	54
PEG 1000	12 8 85	26.60	24.90	23.51	76
PEG 1000	22 8 85	24.63	23.98	29.26	71
PEG 2000	15 8 85	26.77	25.08	6.73	93
PEG 3000	15 8 85	25.89	25.05	4.12	96
PEG 4000	15 8 85	24.63	24.32	1.93	98
PEG 6000	20 8 85	26.23	25.35	0.89	99
eth. glycol	6 8 85	33.13	30.73	91.54	8
eth. glycol	25 9 85	27.43	26.64	84.16	16
sorbitol	19 8 85	27.60	25.67	73.95	26
sucrose	19 8 85	25.25	24.46	62.90	37
raffinose	19 8 85	24.44	24.32	57.33	43
ethanol*	25 9 85	24.12	17.90	91.12	9
NaCl	22 8 85	24.03	24.12	57.97	42
NaCl	24 9 85	27.03	28.01	61.91	38

Experimental data for membrane, Cell35.

Solute	Date of Test	PWP (g/hr)	PR (g/hr)	$\left(\frac{C_{A3}}{C_{A1}}\right)_{expt}$ x 10^2	Solute Separation (%)
PEG 200	9 10 85	11.29	11.29	47.59	52
PEG 200	17 10 85	11.42	11.27	50.84	49
PEG 300	17 10 85	11.23	11.21	33.95	66
PEG 300	9 10 85	11.28	11.25	31.07	69
PEG 400	2 10 85	11.37	11.18	37.17	63
PEG 400	17 10 85	11.20	11.20	23.34	77
PEG 600	2 10 85	11.23	11.13	25.29	75
PEG 1000	2 10 85	11.16	11.11	14.78	85
PEG 2000	14 10 85	11.54	11.43	2.38	98
PEG 3000	14 10 85	11.43	11.38	0.74	99
PEG 4000	14 10 85	11.36	11.33	1.06	99
PEG 6000	15 10 85	11.13	11.15	0.42	100
erythritol	5 10 85	11.28	11.24	67.00	33
erythritol	30 10 85	11.81	11.60	68.91	31
xylitol	9 10 85	11.30	11.37	64.36	36
xylitol	30 10 85	11.56	11.47	68.26	32
sucrose	5 10 85	11.50	11.36	47.34	53
sucrose	30 10 85	11.44	11.41	51.17	49
raffinose	5 10 85	11.29	11.29	45.89	54
raffinose	31 10 85	11.51	11.41	53.74	46
ethanol	15 10 85	11.20	11.18	82.46	18
ethanol	31 10 85	11.49	11.45	81.72	18
NaCl	15 10 85	11.21	11.25	52.11	48
NaCl	31 10 85	11.53	11.54	52.61	47

Experimental data for membrane, Cell36.

Solute	Date of Test	PWP (g/hr)	PR (g/hr)	$\left(\frac{C_{A3}}{C_{A1}}\right)_{expt}$ x 10^2	Solute Separation (%)
PEG 200	9 10 85	13.10	13.05	58.30	42
PEG 200	17 10 85	13.68	13.03	52.93	47
PEG 300	17 10 85	13.06	13.02	44.47	56
PEG 300	9 10 85	13.07	13.07	35.23	65
PEG 400	2 10 85	13.70	13.05	42.34	58
PEG 400	17 10 85	13.02	13.03	32.42	68
PEG 600	2 10 85	13.07	13.00	30.11	70
PEG 1000	2 10 85	13.02	13.00	20.25	80
PEG 2000	14 10 85	13.84	13.26	2.86	97
PEG 3000	14 10 85	13.30	13.19	1.14	99
PEG 4000	14 10 85	13.19	13.16	1.20	99
PEG 6000	15 10 85	12.92	12.93	0.63	99
erythritol	5 10 85	13.09	13.00	71.75	28
erythritol	30 10 85	14.06	13.36	71.54	28
xylitol	9 10 85	13.58	13.13	70.73	29
xylitol	30 10 85	13.25	13.27	67.97	32
sucrose	5 10 85	13.80	13.15	56.76	43
sucrose	30 10 85	13.17	13.16	58.55	41
raffinose	5 10 85	13.12	13.09	46.65	53
raffinose	31 10 85	13.17	13.06	52.58	47
ethanol	15 10 85	12.99	12.97	85.75	14
ethanol	31 10 85	13.61	13.05	84.75	15
NaCl	15 10 85	13.44	13.07	54.58	45
NaCl	31 10 85	13.24	13.30	55.86	44

Experimental data for membrane, Cell37.

Solute	Date of Test	PWP (g/hr)	PR (g/hr)	$\left(\frac{C_{A3}}{C_{A1}}\right)_{expt}$ x 10^2	Solute Separation (%)
PEG 200	6 8 85	10.59	10.47	62.79	37
PEG 200	24 9 85	10.55	10.47	53.34	47
PEG 300	6 8 85	10.36	10.35	42.90	57
PEG 300	20 8 85	10.58	10.47	56.96	43
PEG 300	24 9 85	10.44	10.41	47.32	53
PEG 400	25 9 85	10.34	10.34	47.60	52
PEG 600	12 8 85	10.89	10.73	26.04	74
PEG 1000	12 8 85	10.81	10.80	10.47	90
PEG 1000	22 8 85	10.53	10.44	7.75	92
PEG 2000	15 8 85	10.97	10.87	2.33	98
PEG 3000	15 8 85	10.83	10.85	0.01	100
PEG 4000	15 8 85	10.82	10.77	-0.22	100
PEG 6000	20 8 85	10.55	10.48	-0.13	100
eth. glycol	6 8 85	10.96	10.69	80.13	20
eth. glycol	25 9 85	10.42	10.33	75.98	24
sorbitol	19 8 85	10.88	10.81	69.10	31
sucrose	19 8 85	10.78	10.69	51.54	48
raffinose	19 8 85	10.73	10.68	40.65	59
ethanol*	25 9 85	10.29	7.12	79.93	20
NaCl	22 8 85	10.53	10.48	50.24	50
NaCl	24 9 85	10.55	10.58	47.36	53

Experimental data for membrane, Cell38.

Solute	Date of Test	PWP (g/hr)	PR (g/hr)	$\left(\frac{C_{A3}}{C_{A1}}\right)_{expt}$ x 10^2	Solute Separation (%)
PEG 200	17 4 86	21.53	21.30	82.55	17
PEG 200	24 4 86	21.19	21.00	81.34	19
PEG 300	18 4 86	21.38	21.14	70.84	29
PEG 300	23 4 86	20.95	20.84	74.15	26
PEG 400	17 4 86	21.52	21.22	66.35	34
PEG 400	25 4 86	21.13	20.93	65.22	35
PEG 600	18 4 86	21.20	20.93	43.59	56
PEG 600	23 4 86	20.87	20.96	46.12	54
PEG 1000	18 4 86	20.98	20.84	21.06	79
PEG 1000	24 4 86	21.18	20.89	21.95	78
PEG 2000	21 4 86	21.58	21.35	3.26	97
PEG 3000	21 4 86	21.38	21.16	1.13	99
PEG 4000	21 4 86	21.19	21.01	0.92	99
PEG 6000	22 4 86	20.84	20.87	0.39	100
eth. glycol	23 4 86	21.22	20.96	93.83	6
glycerol	22 4 86	21.30	21.04	90.04	10
erythritol	22 4 86	21.02	20.88	87.70	12
xylitol	15 4 86	21.79	21.56	87.39	13
sorbitol	16 4 86	13.22	21.70	86.57	13
sucrose	15 4 86	21.92	21.66	80.60	19
raffinose	17 4 86	21.30	21.08	73.75	26
ethanol	25 4 86	21.26	21.06	90.55	9
ethanol*	25 4 86	21.08	14.86	91.77	8
NaCl	24 4 86	21.16	21.02	71.58	28

Experimental data for membrane, Cell39.

Solute	Date of Test	PWP (g/hr)	PR (g/hr)	$\left(\frac{C_{A3}}{C_{A1}}\right)_{expt}$ x 10^2	Solute Separation (%)
PEG 200	17 4 86	20.12	19.93	80.22	20
PEG 200	24 4 86	19.84	19.70	81.69	18
PEG 300	18 4 86	19.99	19.74	73.94	26
PEG 300	23 4 86	19.66	19.54	77.20	23
PEG 400	17 4 86	20.11	19.86	73.69	26
PEG 400	25 4 86	19.78	19.62	71.35	29
PEG 600	18 4 86	19.73	19.46	55.10	45
PEG 600	23 4 86	19.57	19.68	63.14	37
PEG 1000	18 4 86	19.48	19.33	48.95	51
PEG 1000	24 4 86	19.84	19.60	50.84	49
PEG 2000	21 4 86	20.09	19.87	22.87	77
PEG 3000	21 4 86	19.90	19.63	7.35	93
PEG 4000	21 4 86	19.68	19.48	6.88	93
PEG 6000	22 4 86	19.55	19.46	-0.27	100
eth. glycol	23 4 86	19.88	19.70	90.75	9
glycerol	22 4 86	19.87	19.72	89.49	11
erythritol	22 4 86	19.67	19.56	86.57	13
xylitol	15 4 86	20.66	21.65	95.88	4
sorbitol	16 4 86	12.32	20.30	82.41	18
sucrose	15 4 86	20.80	20.53	83.36	17
raffinose	17 4 86	19.85	19.68	79.77	20
ethanol	25 4 86	19.93	19.75	87.92	12
ethanol*	25 4 86	19.55	13.94	84.02	16
NaCl	24 4 86	19.82	19.74	70.57	29

Experimental data for membrane, Cell40.

Solute	Date of Test	PWP (g/hr)	PR (g/hr)	$\left(\frac{C_{A3}}{C_{A1}}\right)_{expt}$ x 10^2	Solute Separation (%)
PEG 200	17 4 86	22.66	22.43	77.79	22
PEG 200	24 4 86	22.39	22.19	78.32	22
PEG 300	18 4 86	22.54	22.15	68.35	32
PEG 300	23 4 86	22.10	22.02	71.24	29
PEG 400	17 4 86	22.64	22.34	66.27	34
PEG 400	25 4 86	22.33	22.10	63.45	37
PEG 600	18 4 86	22.28	21.98	49.68	50
PEG 600	23 4 86	22.06	22.19	52.15	48
PEG 1000	18 4 86	22.07	21.90	35.45	65
PEG 1000	24 4 86	22.42	22.07	36.26	64
PEG 2000	21 4 86	22.68	22.42	12.54	87
PEG 3000	21 4 86	22.49	22.19	3.78	96
PEG 4000	21 4 86	22.28	22.04	3.68	96
PEG 6000	22 4 86	22.08	22.04	1.31	99
eth. glycol	23 4 86	22.44	22.24	91.07	9
glycerol	22 4 86	22.46	22.25	88.06	12
erythritol	22 4 86	22.21	22.09	84.49	16
xylitol	15 4 86	23.03	22.79	85.24	15
sorbitol	16 4 86	13.88	22.81	80.91	19
sucrose	15 4 86	23.20	22.38	78.18	22
raffinose	17 4 86	22.39	22.20	71.57	28
ethanol	25 4 86	22.50	22.25	83.52	16
ethanol*	25 4 86	22.25	15.77	85.77	14
NaCl	24 4 86	22.34	22.24	68.71	31

Experimental data for membrane, Cell41.

Solute	Date of Test	PWP (g/hr)	PR (g/hr)	$\left(\frac{C_{A3}}{C_{A1}}\right)_{expt}$ x 10^2	Solute Separation (%)
PEG 200	17 4 86	25.70	25.64	87.11	13
PEG 200	24 4 86	23.54	23.34	85.13	15
PEG 300	18 4 86	24.04	23.48	79.81	20
PEG 300	23 4 86	23.16	23.10	81.91	18
PEG 400	17 4 86	25.66	25.84	79.22	21
PEG 400	25 4 86	23.88	23.62	78.75	21
PEG 600	18 4 86	23.44	23.14	63.59	36
PEG 600	23 4 86	23.04	23.18	66.28	3[illegible]
PEG 1000	18 4 86	23.20	22.92	50.28	50
PEG 1000	24 4 86	24.80	23.02	51.33	49
PEG 2000	21 4 86	23.88	23.62	23.94	76
PEG 3000	21 4 86	23.70	23.38	9.30	91
PEG 4000	21 4 86	23.60	23.12	8.81	91
PEG 6000	22 4 86	23.46	23.34	3.09	97
eth. glycol	23 4 86	23.52	23.28	94.07	6
glycerol	22 4 86	23.60	23.24	92.00	8
erythritol	22 4 86	23.24	23.38	89.14	11
xylitol	15 4 86	30.44	28.62	92.23	8
sorbitol	16 4 86	30.78	29.34	89.42	11
sucrose	15 4 86	30.90	28.46	90.41	10
raffinose	17 4 86	25.66	23.74	81.26	19
ethanol	25 4 86	24.02	23.70	92.90	7
ethanol*	25 4 86	23.90	16.70	98.01	2
NaCl	24 4 86	23.48	23.38	74.10	26

Experimental data for membrane, Cell42.

Solute	Date of Test	PWP (g/hr)	PR (g/hr)	$\left(\frac{C_{A3}}{C_{A1}}\right)_{expt}$ x 10^2	Solute Separation (%)
PEG 200	17 4 86	24.93	24.68	85.20	15
PEG 200	24 4 86	24.68	24.45	85.39	15
PEG 300	18 4 86	24.81	24.55	80.04	20
PEG 300	23 4 86	24.39	24.23	82.07	18
PEG 400	17 4 86	24.88	24.53	79.35	21
PEG 400	25 4 86	24.57	24.35	76.66	23
PEG 600	18 4 86	24.49	24.11	67.45	33
PEG 600	23 4 86	24.31	24.41	70.02	30
PEG 1000	18 4 86	24.17	23.97	57.30	43
PEG 1000	24 4 86	25.20	24.28	59.05	41
PEG 2000	21 4 86	24.93	24.57	31.17	69
PEG 3000	21 4 86	24.59	24.23	12.44	88
PEG 4000	21 4 86	24.35	24.04	12.02	88
PEG 6000	22 4 86	24.25	24.07	0.90	99
eth. glycol	23 4 86	24.68	24.45	94.47	6
glycerol	22 4 86	24.63	24.45	90.97	9
erythritol	22 4 86	24.36	24.27	88.84	11
xylitol	15 4 86	25.27	24.97	90.14	10
sorbitol	16 4 86	16.93	25.15	85.67	14
sucrose	15 4 86	25.37	25.08	86.17	14
raffinose	17 4 86	24.63	24.36	81.97	18
ethanol	25 4 86	24.77	24.49	90.39	10
ethanol*	25 4 86	24.52	17.31	92.35	8
NaCl	24 4 86	24.61	24.52	73.77	26

Experimental data for membrane, Cell43.

Solute	Date of Test	PWP (g/hr)	PR (g/hr)	$\left(\frac{C_{A3}}{C_{A1}}\right)_{expt}$ x 10^2	Solute Separation (%)
PEG 200	17 4 86	14.45	14.32	60.08	40
PEG 200	24 4 86	14.20	13.75	57.42	43
PEG 300	18 4 86	14.14	14.00	47.85	52
PEG 300	23 4 86	13.78	13.76	47.74	52
PEG 400	17 4 86	14.45	14.23	42.33	58
PEG 400	25 4 86	13.87	13.73	47.59	52
PEG 600	18 4 86	14.03	13.85	28.44	72
PEG 600	23 4 86	13.68	13.92	29.15	71
PEG 1000	18 4 86	13.88	13.72	17.90	82
PEG 1000	24 4 86	13.38	13.75	17.55	82
PEG 2000	21 4 86	14.10	13.97	5.84	94
PEG 3000	21 4 86	13.99	13.86	2.38	98
PEG 4000	21 4 86	13.88	13.78	2.45	98
PEG 6000	22 4 86	13.70	13.73	0.48	100
eth. glycol	23 4 86	13.92	13.81	84.22	16
glycerol	22 4 86	13.94	13.81	79.22	21
erythritol	22 4 86	13.76	13.70	71.46	29
xylitol	15 4 86	15.24	14.82	71.99	28
sorbitol	16 4 86	9.49	15.25	69.01	31
sucrose	15 4 86	15.65	15.29	61.00	39
raffinose	17 4 86	14.27	14.17	48.70	51
ethanol	25 4 86	13.98	13.81	82.26	18
ethanol*	25 4 86	13.84	9.76	80.67	19
NaCl	24 4 86	14.11	14.15	60.18	40

Experimental data for membrane, Cell44.

Solute	Date of Test	PWP (g/hr)	PR (g/hr)	$\left(\frac{C_{A3}}{C_{A1}}\right)_{expt}$ x 10^2	Solute Separation (%)
PEG 200	6 4 86	11.36	11.21	58.47	42
PEG 200	10 4 86	10.66	10.62	54.52	45
PEG 300	7 4 86	11.30	11.36	49.87	50
PEG 300	10 4 86	10.62	10.61	47.28	53
PEG 400	7 4 86	11.33	11.23	40.22	60
PEG 600	7 4 86	11.33	11.21	32.83	67
PEG 600	11 4 86	10.67	10.57	32.93	67
PEG 1000	8 4 86	10.87	10.72	20.59	79
PEG 1000	11 4 86	10.61	10.56	21.25	79
PEG 2000	8 4 86	10.75	10.66	5.36	95
PEG 2000	11 4 86	10.61	10.54	3.97	96
PEG 3000	8 4 86	10.68	10.65	0.76	99
PEG 3000	12 4 86	10.65	10.57	1.57	98
PEG 4000	9 4 86	10.95	11.29	1.89	98
PEG 6000	9 4 86	10.83	11.24	-0.13	100
eth. glycol	10 4 86	10.71	10.62	83.18	17
glycerol	5 4 86	11.53	11.30	77.21	23
erythritol	4 4 86	11.92	11.72	72.98	27
xylitol	4 4 86	12.15	11.85	69.12	31
sorbitol	9 4 86	10.80	10.73	66.39	34
sucrose	5 4 86	11.57	11.25	58.72	41
raffinose	5 4 86	11.37	11.18	52.14	48
ethanol	12 4 86	10.66	10.58	82.16	18
NaCl	4 4 86	12.30	12.06	53.46	47

Experimental data for membrane, Cell45.

Solute	Date of Test	PWP (g/hr)	PR (g/hr)	$\left(\frac{C_{A3}}{C_{A1}}\right)_{expt}$ x 10^2	Solute Separation (%)
PEG 200	17 4 86	30.31	30.02	81.74	18
PEG 200	24 4 86	30.05	29.79	79.60	20
PEG 300	18 4 86	30.07	29.73	72.79	27
PEG 300	23 4 86	29.62	29.49	75.72	24
PEG 400	17 4 86	30.27	29.88	69.20	31
PEG 400	25 4 86	29.93	29.66	68.76	31
PEG 600	18 4 86	29.71	29.28	56.65	43
PEG 600	23 4 86	29.50	29.76	58.80	41
PEG 1000	18 4 86	29.35	29.16	46.95	53
PEG 1000	24 4 86	30.38	29.62	47.81	52
PEG 2000	21 4 86	30.21	29.81	23.57	76
PEG 3000	21 4 86	29.88	29.52	9.01	91
PEG 4000	21 4 86	29.59	29.23	8.49	92
PEG 6000	22 4 86	29.47	29.35	1.31	99
eth. glycol	23 4 86	29.95	29.81	93.31	7
glycerol	22 4 86	29.88	29.74	90.10	10
erythritol	22 4 86	29.61	29.50	87.37	13
xylitol	15 4 86	30.63	30.38	87.09	13
sorbitol	16 4 86	26.38	30.50	83.15	17
sucrose	15 4 86	30.81	30.50	80.65	19
raffinose	17 4 86	29.97	29.64	75.01	25
ethanol	25 4 86	30.15	29.86	87.80	12
ethanol*	25 4 86	29.88	21.33	89.19	11
NaCl	24 4 86	29.98	29.78	70.90	29

Experimental data for membrane, Cell46.

Solute	Date of Test	PWP (g/hr)	PR (g/hr)	$\left(\frac{C_{A3}}{C_{A1}}\right)_{expt}$ x 10^2	Solute Separation (%)
PEG 200	17 4 86	25.25	24.99	79.71	20
PEG 200	24 4 86	24.86	24.70	77.79	22
PEG 300	18 4 86	24.94	24.62	71.30	29
PEG 300	23 4 86	24.60	24.45	72.28	28
PEG 400	17 4 86	25.69	25.86	68.46	32
PEG 400	25 4 86	24.76	24.57	67.63	32
PEG 600	18 4 86	24.58	24.23	54.05	46
PEG 600	23 4 86	24.49	24.68	57.14	43
PEG 1000	18 4 86	24.23	24.11	42.71	57
PEG 1000	24 4 86	24.58	24.58	44.97	55
PEG 2000	21 4 86	24.99	24.70	21.66	78
PEG 3000	21 4 86	24.68	24.41	8.72	91
PEG 4000	21 4 86	24.44	24.24	8.30	92
PEG 6000	22 4 86	24.49	24.31	0.81	99
eth. glycol	23 4 86	24.83	24.63	90.82	9
glycerol	22 4 86	24.76	24.86	90.63	9
erythritol	22 4 86	24.75	24.65	84.50	16
xylitol	15 4 86	28.10	27.47	86.01	14
sorbitol	16 4 86	21.34	25.91	83.01	17
sucrose	15 4 86	27.97	27.94	80.80	19
raffinose	17 4 86	25.99	24.62	72.38	28
ethanol	25 4 86	25.02	24.75	90.39	10
ethanol*	25 4 86	24.75	17.68	95.70	4
NaCl	24 4 86	24.84	24.73	69.38	31

Experimental data for membrane, Cell47.

Solute	Date of Test	PWP (g/hr)	PR (g/hr)	$\left(\frac{C_{A3}}{C_{A1}}\right)_{expt}$ x 10^2	Solute Separation (%)
PEG 200	17 4 86	35.04	32.12	92.94	7
PEG 200	24 4 86	23.16	18.96	83.79	16
PEG 300	18 4 86	22.20	22.02	80.98	19
PEG 300	23 4 86	23.58	27.30	85.60	14
PEG 400	17 4 86	35.48	30.80	87.22	13
PEG 400	25 4 86	22.96	21.78	81.43	19
PEG 600	18 4 86	25.94	25.60	76.25	24
PEG 600	23 4 86	26.34	24.06	76.83	23
PEG 1000	18 4 86	24.08	21.26	65.97	34
PEG 1000	24 4 86	19.96	19.68	66.54	33
PEG 2000	21 4 86	27.22	21.24	52.85	47
PEG 3000	21 4 86	23.20	20.12	44.87	55
PEG 4000	21 4 86	26.74	21.10	47.71	52
PEG 6000	22 4 86	20.06	26.20	30.91	69
eth. glycol	23 4 86	24.78	24.14	94.21	6
glycerol	22 4 86	28.62	22.14	92.46	8
erythritol	22 4 86	25.26	20.74	88.79	11
xylitol	15 4 86	52.64	47.96	96.58	3
sorbitol	16 4 86	50.40	45.64	87.99	12
sucrose	15 4 86	72.92	49.84	94.62	5
raffinose	17 4 86	33.00	27.12	87.25	13
ethanol	25 4 86	21.82	19.90	85.72	14
ethanol*	25 4 86	22.12	14.10	89.46	11
NaCl	24 4 86	26.40	23.44	79.93	20

Experimental data for membrane, Cell48.

Solute	Date of Test	PWP (g/hr)	PR (g/hr)	$\left(\frac{C_{A3}}{C_{A1}}\right)_{expt}$ x 10^2	Solute Separation (%)
PEG 200	15 02 86	18.39	18.05	79.76	20
PEG 200	16 03 86	18.26	18.01	85.75	14
PEG 300	15 02 86	18.14	17.89	75.39	25
PEG 300	19 03 86	17.71	17.89	75.72	24
PEG 400	15 02 86	17.98	17.82	71.03	29
PEG 400	19 03 86	18.40	17.71	71.59	28
PEG 600	19 03 86	18.07	17.59	64.30	36
PEG 600	27 02 86	18.68	18.38	64.18	36
PEG 1000	10 03 86	18.25	17.92	55.26	45
PEG 1000	27 02 86	18.44	18.14	52.69	47
PEG 2000	10 03 86	18.03	17.73	29.30	71
PEG 3000	18 03 86	18.05	17.68	9.92	90
PEG 4000	18 03 86	17.99	17.66	12.55	87
PEG 6000	18 03 86	17.88	17.59	1.50	99
ethanol	25 3 86	18.16	17.95	90.81	9
NaCl	25 3 86	18.31	18.00	80.78	19

Experimental data for membrane, Cell49.

Solute	Date of Test	PWP (g/hr)	PR (g/hr)	$\left(\frac{C_{A3}}{C_{A1}}\right)_{expt}$ x 10^2	Solute Separation (%)
PEG 200	15 02 86	24.01	23.40	80.97	19
PEG 200	16 03 86	23.89	23.44	86.63	13
PEG 300	15 02 86	23.56	23.33	77.58	22
PEG 300	19 03 86	23.05	23.27	76.27	22
PEG 400	15 02 86	23.40	23.12	72.64	27
PEG 400	19 03 86	23.31	23.08	73.27	27
PEG 600	19 03 86	22.39	22.88	69.53	30
PEG 600	27 02 86	24.48	24.17	67.63	32
PEG 1000	10 03 86	23.92	23.47	56.24	44
PEG 1000	27 02 86	24.08	23.79	54.90	45
PEG 2000	10 03 86	23.65	23.24	26.00	74
PEG 3000	18 03 86	23.56	23.07	8.44	92
PEG 4000	18 03 86	23.45	23.04	10.97	89
PEG 6000	18 03 86	23.36	22.93	1.39	99
ethanol	25 3 86	23.63	23.39	92.54	8
NaCl	25 3 86	24.63	23.96	82.24	18

Experimental data for membrane, Cell50.

Solute	Date of Test	PWP (g/hr)	PR (g/hr)	$\left(\frac{C_{A3}}{C_{A1}}\right)_{expt}$ x 10^2	Solute Separation (%)
PEG 200	15 02 86	4.85	4.75	54.40	46
PEG 200	16 03 86	4.94	4.83	64.21	36
PEG 300	15 02 86	4.77	4.71	44.92	55
PEG 300	19 03 86	4.49	4.83	46.13	54
PEG 400	15 [illegible] 86	4.76	4.69	37.25	63
PEG 400	19 03 86	5.09	4.79	38.04	62
PEG 600	19 03 86	5.03	4.75	28.68	71
PEG 600	27 02 86	4.99	4.93	30.46	70
PEG 1000	10 03 86	4.93	4.85	18.99	81
PEG 1000	27 02 86	4.95	4.89	17.69	82
PEG 2000	10 03 86	4.87	4.80	6.82	93
PEG 3000	18 03 86	4.91	4.78	2.48	98
PEG 4000	18 03 86	4.84	4.79	2.72	97
PEG 6000	18 03 86	4.84	4.77	0.81	99
ethanol	25 3 86	4.91	4.83	77.60	22
NaCl	25 3 86	4.96	4 85	56.97	43

Experimental data for membrane, Cell51.

Solute	Date of Test	PWP (g/hr)	PR (g/hr)	$\left(\frac{C_{A3}}{C_{A1}}\right)_{expt}$ x 10^2	Solute Separation (%)
PEG 200	15 02 86	9.97	9.79	58.31	42
PEG 200	16 03 86	9.83	9.68	66.35	34
PEG 300	15 02 86	9.85	9.77	50.86	49
PEG 300	19 03 86	9.25	9.62	51.56	48
PEG 400	15 02 86	9.83	9.71	44.16	56
PEG 400	19 03 86	10.29	9.53	44.03	56
PEG 600	19 03 86	10.51	9.49	36.35	64
PEG 600	27 02 86	10.03	9.93	36.98	63
PEG 1000	10 03 86	9.88	9.71	26.32	74
PEG 1000	27 02 86	9.91	9.82	26.26	74
PEG 2000	10 03 86	9.75	9.64	10.00	90
PEG 3000	18 03 86	9.72	9.54	3.46	97
PEG 4000	18 03 86	9.68	9.55	5.84	94
PEG 6000	18 03 86	9.64	9.52	2.49	98
ethanol	25 3 86	9.76	9.66	80.41	20
NaCl	25 3 86	10.36	10.18	56.95	43

Experimental data for membrane, Cell52.

Solute	Date of Test	PWP (g/hr)	PR (g/hr)	$\left(\frac{C_{A3}}{C_{A1}}\right)_{expt}$ x 10^2	Solute Separation (%)
PEG 200	15 02 86	10.73	10.52	53.53	46
PEG 200	16 03 86	10.71	10.55	61.98	38
PEG 300	15 02 86	10.65	10.54	43.06	57
PEG 300	19 03 86	10.37	10.49	43.44	57
PEG 400	15 02 86	10.59	10.54	35.70	64
PEG 400	19 03 86	10.26	10.41	36.94	63
PEG 600	19 03 86	11.04	10.35	27.10	73
PEG 600	27 02 86	10.84	10.72	26.14	74
PEG 1000	10 03 86	10.73	10.55	16.54	83
PEG 1000	27 02 86	10.72	10.59	15.69	84
PEG 2000	10 03 86	10.62	10.47	5.56	94
PEG 3000	18 03 86	10.59	10.42	2.14	98
PEG 4000	18 03 86	10.53	10.40	3.04	97
PEG 6000	18 03 86	10.50	10.37	2.20	98
ethanol	25 3 86	10.67	10.54	79.61	20
NaCl	25 3 86	11.01	10.79	49.75	50

Experimental data for membrane, Cell53.

Solute	Date of Test	PWP (g/hr)	PR (g/hr)	$\left(\frac{C_{A3}}{C_{A1}}\right)_{expt}$ x 10^2	Solute Separation (%)
PEG 200	15 02 86	7.80	7.42	56.39	44
PEG 200	16 03 86	7.77	7.63	65.13	35
PEG 300	15 02 86	7.72	7.65	48.92	51
PEG 300	19 03 86	8.11	7.61	48.37	52
PEG 400	15 02 86	7.67	7.60	40.94	59
PEG 400	19 03 86	7.38	7.53	40.45	60
PEG 600	19 03 86	7.70	7.50	32.46	68
PEG 600	27 02 86	7.91	7.79	33.18	67
PEG 1000	10 03 86	7.79	7.64	23.84	76
PEG 1000	27 02 86	7.79	7.70	22.99	77
PEG 2000	10 03 86	7.69	7.59	9.96	90
PEG 3000	18 03 86	7.66	7.53	3.26	97
PEG 4000	18 03 86	7.64	7.53	4.92	95
PEG 6000	18 03 86	7.59	7.49	2.00	98
ethanol	25 3 86	7.73	7.63	81.67	18
NaCl	25 3 86	8.13	7.94	54.36	46

Experimental data for membrane, Cell54.

Solute	Date of Test	PWP (g/hr)	PR (g/hr)	$\left(\frac{C_{A3}}{C_{A1}}\right)_{expt}$ x 10^2	Solute Separation (%)
PEG 200	15 02 86	16.31	16.02	74.15	26
PEG 200	16 03 86	16.28	16.00	84.27	16
PEG 300	15 02 86	16.12	15.96	67.92	32
PEG 300	19 03 86	16.03	15.90	69.86	30
PEG 400	15 02 86	16.04	15.81	60.76	39
PEG 400	19 03 86	15.87	15.74	61.46	39
PEG 600	19 03 86	16.73	15.65	50.09	50
PEG 600	27 02 86	16.74	16.46	51.75	48
PEG 1000	10 03 86	16.35	16.03	37.06	63
PEG 1000	27 02 86	16.51	16.26	36.55	63
PEG 2000	10 03 86	16.16	15.87	13.67	86
PEG 3000	18 03 86	16.10	15.77	3.46	97
PEG 4000	18 03 86	16.00	15.76	4.68	95
PEG 6000	18 03 86	15.90	15.68	1.89	98
ethanol	25 3 86	16.17	15.96	86.61	13
NaCl	25 3 86	16.78	16.33	73.36	27

Experimental data for membrane, Cell55.

Solute	Date of Test	PWP (g/hr)	PR (g/hr)	$\left(\frac{C_{A3}}{C_{A1}}\right)_{expt}$ x 10^2	Solute Separation (%)
PEG 200	15 02 86	11.67	11.45	59.53	40
PEG 200	16 03 86	11.42	11.25	66.63	33
PEG 300	15 02 86	11.49	11.45	50.14	50
PEG 300	19 03 86	11.66	11.20	51.10	49
PEG 400	15 02 86	11.45	11.37	43.48	57
PEG 400	19 03 86	11.28	11.12	42.94	57
PEG 600	19 03 86	11.41	11.05	33.70	66
PEG 600	27 02 86	11.65	11.51	40.41	60
PEG 1000	10 03 86	11.49	11.31	23.34	77
PEG 1000	27 02 86	11.49	11.36	23.47	77
PEG 2000	10 03 86	11.39	11.23	7.20	93
PEG 3000	18 03 86	11.33	11.17	1.90	98
PEG 4000	18 03 86	11.27	11.13	2.50	98
PEG 6000	18 03 86	11.21	11.08	0.92	99
ethanol	25 3 86	11.34	11.25	79.74	20
NaCl	25 3 86	12.00	11.75	56.67	43

Experimental data for membrane, Cell56.

Solute	Date of Test	PWP (g/hr)	PR (g/hr)	$\left(\frac{C_{A3}}{C_{A1}}\right)_{expt}$ x 10^2	Solute Separation (%)
PEG 200	15 02 86	16.59	15.35	74.04	26
PEG 200	16 03 86	15.30	15.03	79.98	20
PEG 300	15 02 86	15.42	15.21	67.73	32
PEG 300	19 03 86	15.95	14.92	69.37	31
PEG 400	15 02 86	15.28	15.14	62.28	38
PEG 400	19 03 86	14.78	14.80	60.80	39
PEG 600	19 03 86	15.17	14.71	52.86	47
PEG 600	27 02 86	15.77	15.54	54.61	45
PEG 1000	10 03 86	15.36	15.04	42.93	57
PEG 1000	27 02 86	15.58	15.35	43.21	57
PEG 2000	10 03 86	15.17	14.92	20.05	80
PEG 3000	18 03 86	15.10	14.77	6.99	93
PEG 4000	18 03 86	15.12	14.77	8.80	91
PEG 6000	18 03 86	14.95	14.73	2.19	98
ethanol	25 3 86	15.20	15.01	86.10	14
NaCl	25 3 86	17.03	15.65	73.66	26

Experimental data for membrane, Cell57.

Solute	Date of Test	PWP (g/hr)	PR (g/hr)	$\left(\frac{C_{A3}}{C_{A1}}\right)_{expt}$ x 10^2	Solute Separation (%)
PEG 200	15 02 86	18.66	18.28	80.92	19
PEG 200	16 03 86	18.39	18.05	84.88	15
PEG 300	15 02 86	18.34	18.16	76.50	24
PEG 300	19 03 86	18.21	17.93	78.06	22
PEG 400	15 02 86	18.21	18.07	71.23	29
PEG 400	19 03 86	18.24	17.77	74.00	26
PEG 600	19 03 86	18.12	17.62	64.02	36
PEG 600	27 02 86	18.92	18.65	64.02	36
PEG 1000	10 03 86	18.55	18.19	52.16	48
PEG 1000	27 02 86	18.68	18.25	54.37	46
PEG 2000	10 03 86	18.31	18.01	26.38	74
PEG 3000	18 03 86	18.19	17.80	8.78	91
PEG 4000	18 03 86	18.05	17.74	9.94	90
PEG 6000	18 03 86	17.97	17.66	0.92	99
ethanol	25 3 86	18.25	18.02	89.47	11
NaCl	25 3 86	19.15	18.64	81.67	18

Experimental data for membrane, Cell58.

Solute	Date of Test	PWP (g/hr)	PR (g/hr)	$\left(\frac{C_{A3}}{C_{A1}}\right)_{expt}$ x 10^2	Solute Separation (%)
PEG 200	14 12 86	18.64	21.15	62.27	38
PEG 200	18 12 86	18.44	17.68	62.85	37
PEG 300	18 12 86	18.29	17.60	48.51	51
PEG 400	06 01 87	19.13	18.66	41.16	59
PEG 400	14 12 86	24.75	24.55	39.99	60
PEG 600	06 01 87	19.04	18.59	30.44	70
PEG 600	16 12 86	20.70	20.17	29.04	71
PEG 1000	14 12 86	21.50	24.00	18.94	81
PEG 1000	18 12 86	17.64	17.76	17.89	82
PEG 2000	05 01 87	19.80	19.36	8.18	92
PEG 2000	16 12 86	22.96	25.71	4.05	96
PEG 3000	05 01 87	19.15	18.51	2.30	98
PEG 3000	16 12 86	22.19	24.44	4.36	96
PEG 4000	05 01 87	18.33	18.80	4.75	95
PEG 6000	06 01 87	18.64	18.54	1.20	99
eth. glycol	07 01 87	18.96	18.61	97.22	3
glycerol	02 01 87	18.65	18.45	86.79	13
erythritol	30 12 86	18.98	18.36	76.00	24
xylitol	30 12 86	18.35	18.07	73.75	26
sorbitol	30 12 86	20.36	19.06	71.10	29
sucrose	02 01 87	20.66	18.69	57.41	43
raffinose	02 01 87	18.76	18.67	48.14	52
ethanol	07 01 87	18.71	18.44	87.27	13
NaCl	12 12 86	25.29	21.55	54.61	45

Experimental data for membrane, Cell59.

Solute	Date of Test	PWP (g/hr)	PR (g/hr)	$\left(\frac{C_{A3}}{C_{A1}}\right)_{expt}$ x 10^2	Solute Separation (%)
PEG 200	14 12 86	15.85	17.09	67.60	32
PEG 200	18 12 86	14.86	14.19	68.63	31
PEG 300	18 12 86	14.23	13.83	57.02	43
PEG 400	06 01 87	14.66	14.39	53.95	46
PEG 400	14 12 86	18.61	20.98	51.11	49
PEG 600	06 01 87	14.47	14.33	46.15	54
PEG 600	16 12 86	17.13	17.43	43.70	56
PEG 1000	14 12 86	18.30	20.00	34.86	65
PEG 1000	18 12 86	14.30	13.74	35.35	65
PEG 2000	05 01 87	14.66	14.62	25.20	75
PEG 2000	16 12 86	18.30	20.56	15.43	85
PEG 3000	05 01 87	14.39	14.04	17.76	82
PEG 3000	16 12 86	18.09	19.59	16.23	84
PEG 4000	05 01 87	14.41	14.10	19.68	80
PEG 6000	06 01 87	14.40	13.71	10.92	89
eth. glycol	07 01 87	14.37	14.21	86.80	13
glycerol	02 01 87	14.49	14.36	88.68	11
erythritol	30 12 86	14.57	14.30	79.82	20
xylitol	30 12 86	14.37	14.21	77.78	22
sorbitol	30 12 86	14.79	14.63	73.60	26
sucrose	02 01 87	16.18	14.68	66.71	33
raffinose	02 01 87	14.70	14.39	60.83	39
ethanol	07 01 87	14.30	14.25	88.47	12
NaCl	12 12 86	16.67	20.24	61.72	38

Experimental data for membrane, Cell60.

Solute	Date of Test	PWP (g/hr)	PR (g/hr)	$\left(\frac{C_{A3}}{C_{A1}}\right)_{expt}$ x 10^2	Solute Separation (%)
PEG 200	14 12 86	84.11	80.78	81.02	19
PEG 200	18 12 86	58.53	52.91	81.32	19
PEG 300	18 12 86	55.25	50.78	72.00	28
PEG 400	06 01 87	50.02	46.20	62.96	37
PEG 400	14 12 86	89.02	83.35	68.70	31
PEG 600	06 01 87	46.80	43.47	53.63	46
PEG 600	16 12 86	80.29	68.89	61.11	39
PEG 1000	14 12 86	85.47	78.49	52.20	48
PEG 1000	18 12 86	53.45	48.65	51.49	49
PEG 2000	05 01 87	52.96	50.18	37.52	62
PEG 2000	16 12 86	76.36	75.44	29.44	71
PEG 3000	05 01 87	50.51	45.65	30.16	70
PEG 3000	16 12 86	72.33	71.51	36.19	64
PEG 4000	05 01 87	48.00	44.84	31.22	69
PEG 6000	06 01 87	44.73	42.33	25.27	75
eth. glycol	07 01 87	46.47	45.22	91.33	9
glycerol	02 01 87	50.73	46.85	96.67	3
erythritol	30 12 86	57.55	50.78	86.58	13
xylitol	30 12 86	54.71	49.80	84.18	16
sorbitol	30 12 86	68.56	57.05	85.15	15
sucrose	02 01 87	62.18	51.49	76.99	23
raffinose	02 01 87	53.62	48.05	69.85	30
ethanol	07 01 87	44.78	43.53	93.94	6
NaCl	12 12 86	78.90	82.65	79.57	20

Experimental data for membrane, Cell61.

Solute	Date of Test	PWP (g/hr)	PR (g/hr)	$\left(\frac{C_{A3}}{C_{A1}}\right)_{expt}$ x 10^2	Solute Separation (%)
PEG 200	14 12 86	3.67	3.96	43.20	57
PEG 200	18 12 86	3.30	3.27	44.99	55
PEG 300	18 12 86	3.31	3.26	33.30	67
PEG 400	06 01 87	3.36	3.34	27.05	73
PEG 400	14 12 86	4.27	4.85	25.50	75
PEG 600	06 01 87	3.35	3.33	19.45	81
PEG 600	16 12 86	3.87	4.09	20.32	80
PEG 1000	14 12 86	4.22	4.67	12.15	88
PEG 1000	18 12 86	3.30	3.30	11.80	88
PEG 2000	05 01 87	3.34	3.35	3.24	97
PEG 2000	16 12 86	4.32	4.88	2.63	97
PEG 3000	05 01 87	3.34	3.30	1.24	99
PEG 4000	05 01 87	3.33	3.29	1.22	99
PEG 6000	06 01 87	3.34	3.32	0.49	100
eth. glycol	07 01 87	3.32	3.32	72.87	27
glycerol	02 01 87	3.35	3.31	71.56	28
erythritol	30 12 86	3.33	3.29	60.20	40
xylitol	30 12 86	3.31	3.30	56.50	44
sorbitol	30 12 86	3.38	3.35	51.25	49
sucrose	02 01 87	3.35	3.33	40.77	59
raffinose	02 01 87	3.32	3.31	34.57	65
ethanol	07 01 87	3.34	3.30	76.87	23
NaCl	12 12 86	3.85	4.72	50.38	50

Experimental data for membrane, Cell62.

Solute	Date of Test	PWP (g/hr)	PR (g/hr)	$\left(\frac{C_{A3}}{C_{A1}}\right)_{expt}$ x 10^2	Solute Separation (%)
PEG 200	06 02 87	25.44	25.19	76.10	24
PEG 200	26 01 87	26.23	25.82	74.52	25
PEG 300	06 02 87	25.22	25.01	62.83	37
PEG 300	29 01 87	25.98	25.63	74.07	26
PEG 400	06 02 87	25.14	24.96	66.00	34
PEG 400	26 01 87	25.79	25.46	69.74	30
PEG 600	11 02 87	25.42	25.18	57.91	42
PEG 600	29 01 87	25.43	25.37	60.42	40
PEG 1000	11 02 87	25.27	24.97	44.42	56
PEG 1000	26 01 87	25.57	25.32	32.74	67
PEG 2000	25 01 87	25.70	25.38	12.29	88
PEG 2000	29 01 87	25.22	25.21	14.62	85
PEG 3000	02 02 87	25.60	25.34	5.07	95
PEG 4000	05 02 87	25.50	25.27	4.25	96
PEG 6000	05 02 87	25.32	25.09	2.88	97
eth. glycol	02 02 87	25.98	25.61	92.69	7
eth. glycol	11 02 87	25.73	25.22	90.53	9
glycerol	02 02 87	25.69	25.50	84.34	16
glycerol	08 02 87	25.14	24.62	87.16	13
erythritol	25 01 87	26.22	25.69	83.89	16
erythritol	13 02 87	25.10	24.79	88.63	11
xylitol	25 01 87	25.80	25.51	84.36	16
xylitol	08 02 87	25.19	24.91	89.80	10
sorbitol	08 02 87	25.38	24.97	85.28	15
sorbitol	23 01 87	26.32	17.17	85.05	15
sucrose	13 02 87	25.34	24.96	81.00	19
sucrose	23 01 87	3.97	1.12	4.75	95
raffinose	13 02 87	25.20	24.92	75.78	24
raffinose	23 01 87	25.90	25.45	74.10	26
ethanol	05 02 87	25.74	25.45	93.39	7
ethanol	16 02 87	25.52	25.02	92.39	8
NaCl	16 02 87	25.12	24.97	60.74	39

Experimental data for membrane, Cell63.

Solute	Date of Test	PWP (g/hr)	PR (g/hr)	$\left(\frac{C_{A3}}{C_{A1}}\right)_{expt}$ x 10^2	Solute Separation (%)
PEG 200	06 02 87	5.24	5.27	55.11	45
PEG 200	26 01 87	5.47	5.53	56.39	44
PEG 300	06 02 87	5.30	5.21	44.85	55
PEG 300	29 01 87	5.32	5.34	51.11	49
PEG 400	06 02 87	5.26	5.21	43.62	56
PEG 400	26 01 87	5.49	5.24	41.15	59
PEG 600	11 02 87	5.25	5.21	33.71	66
PEG 600	29 01 87	5.35	5.32	36.18	64
PEG 1000	11 02 87	5.23	5.19	24.00	76
PEG 1000	26 01 87	5.32	5.11	15.75	84
PEG 2000	25 01 87	5.45	5.32	9.83	90
PEG 2000	29 01 87	5.30	5.19	11.00	89
PEG 3000	02 02 87	5.20	5.20	5.87	94
PEG 4000	05 02 87	5.23	5.21	6.97	93
PEG 6000	05 02 87	5.32	5.20	4.92	95
eth. glycol	02 02 87	5.31	5.23	81.21	19
eth. glycol	11 02 87	5.30	5.22	83.31	17
glycerol	02 02 87	5.27	5.27	75.02	25
glycerol	08 02 87	5.19	5.15	74.57	25
erythritol	25 01 87	5.65	5.37	68.88	31
erythritol	13 02 87	5.21	5.18	74.04	26
xylitol	25 01 87	5.59	5.33	69.19	31
xylitol	08 02 87	5.20	5.16	74.59	25
sorbitol	08 02 87	5.25	5.19	67.34	33
sorbitol	23 01 87	5.63	5.41	67.59	32
sucrose	13 02 87	5.23	5.19	59.03	41
sucrose	23 01 87	5.54	5.47	58.02	42
raffinose	13 02 87	5.24	5.20	52.62	47
raffinose	23 01 87	5.69	5.33	48.74	51
ethanol	05 02 87	5.27	5.22	83.39	17
ethanol	16 02 87	5.31	5.23	83.85	16
NaCl	16 02 87	5.27	5.23	56.84	43

Experimental data for membrane, Cell64.

Solute	Date of Test	PWP (g/hr)	PR (g/hr)	$\left(\frac{C_{A3}}{C_{A1}}\right)_{expt}$ x 10^2	Solute Separation (%)
PEG 200	06 02 87	11.61	11.52	68.36	32
PEG 200	26 01 87	11.79	11.51	67.08	33
PEG 300	06 02 87	11.55	11.47	52.75	47
PEG 300	29 01 87	11.69	11.55	58.06	42
PEG 400	06 02 87	11.50	11.45	54.12	46
PEG 400	26 01 87	11.53	11.37	55.12	45
PEG 600	11 02 87	11.63	11.55	48.03	52
PEG 600	29 01 87	11.47	11.46	45.97	54
PEG 1000	11 02 87	11.57	11.48	42.44	58
PEG 1000	26 01 87	11.45	11.38	37.65	62
PEG 2000	25 01 87	11.66	11.49	31.63	68
PEG 2000	29 01 87	11.41	11.37	32.78	67
PEG 3000	02 02 87	11.54	11.42	28.74	71
PEG 4000	05 02 87	11.55	11.43	29.06	71
PEG 6000	05 02 87	11.52	11.21	25.05	75
eth. glycol	02 02 87	11.79	11.62	95.02	5
eth. glycol	11 02 87	11.77	11.57	92.47	8
glycerol	02 02 87	11.58	11.54	86.86	13
glycerol	08 02 87	11.50	11.42	87.28	13
erythritol	25 01 87	11.86	11.71	80.22	20
erythritol	13 02 87	11.55	11.43	87.96	12
xylitol	25 01 87	11.99	11.59	81.92	18
xylitol	08 02 87	11.51	11.43	85.10	15
sorbitol	08 02 87	11.57	11.44	80.85	19
sorbitol	23 01 87	14.56	11.66	79.57	20
sucrose	13 02 87	11.68	11.49	68.59	31
sucrose	23 01 87	11.70	11.56	66.89	33
raffinose	13 02 87	11.58	11.47	60.94	39
raffinose	23 01 87	11.71	11.58	55.92	44
ethanol	05 02 87	11.66	11.50	93.12	7
ethanol	16 02 87	11.75	11.55	92.85	7
NaCl	16 02 87	11.64	11.56	72.47	27

Experimental data for membrane, Cell65.

Solute	Date of Test	PWP (g/hr)	PR (g/hr)	$\left(\frac{C_{A3}}{C_{A1}}\right)_{expt}$ x 10^2	Solute Separation (%)
PEG 200	06 02 87	3.25	3.24	45.01	55
PEG 200	26 01 87	3.27	3.27	43.00	57
PEG 300	06 02 87	3.25	3.24	37.78	62
PEG 300	29 01 87	3.28	3.28	36.77	63
PEG 400	06 02 87	3.25	3.24	36.16	64
PEG 400	26 01 87	3.26	3.25	32.72	67
PEG 600	11 02 87	3.29	3.28	30.44	70
PEG 600	29 01 87	3.26	3.27	30.60	69
PEG 1000	11 02 87	3.28	3.25	20.59	79
PEG 1000	26 01 87	3.25	3.24	15.77	84
PEG 2000	25 01 87	3.31	3.27	5.07	95
PEG 2000	29 01 87	3.23	3.22	6.42	94
PEG 3000	02 02 87	3.27	3.23	2.78	97
PEG 4000	05 02 87	3.27	3.23	7.00	93
PEG 6000	05 02 87	3.25	3.24	2.00	98
eth. glycol	02 02 87	3.30	3.26	79.26	21
eth. glycol	11 02 87	3.32	3.29	76.56	23
glycerol	02 02 87	3.28	3.27	66.15	34
glycerol	08 02 87	3.25	3.25	67.61	32
erythritol	25 01 87	3.33	3.30	58.48	42
erythritol	13 02 87	3.24	3.25	64.05	36
xylitol	25 01 87	3.29	3.31	57.90	42
xylitol	08 02 87	3.27	3.26	61.79	38
sorbitol	08 02 87	3.26	3.24	54.00	46
sorbitol	23 01 87	3.31	3.29	56.51	43
sucrose	13 02 87	3.27	3.25	47.54	52
sucrose	23 01 87	3.29	3.30	45.90	54
raffinose	13 02 87	3.25	3.25	44.20	56
raffinose	23 01 87	3.32	3.30	40.72	59
ethanol	05 02 87	3.26	3.27	76.66	23
ethanol	16 02 87	3.29	3.27	77.80	22
NaCl	16 02 87	3.27	3.24	44.22	56

Experimental data for membrane, Cell66.

Solute	Date of Test	PWP (g/hr)	PR (g/hr)	$\left(\frac{C_{A3}}{C_{A1}}\right)_{expt}$ x 10^2	Solute Separation (%)
PEG 200	06 02 87	12.17	12.05	69.92	30
PEG 200	26 01 87	12.24	12.07	66.10	34
PEG 300	06 02 87	12.09	12.03	53.64	46
PEG 300	29 01 87	12.23	12.10	59.59	40
PEG 400	06 02 87	12.07	12.03	49.09	51
PEG 400	26 01 87	12.07	11.97	48.83	51
PEG 600	11 02 87	12.44	12.30	41.16	59
PEG 600	29 01 87	11.99	12.01	39.76	60
PEG 1000	11 02 87	12.34	12.20	31.59	68
PEG 1000	26 01 87	12.04	11.93	25.52	74
PEG 2000	25 01 87	12.05	11.90	15.07	85
PEG 2000	29 01 87	11.93	11.95	18.01	82
PEG 3000	02 02 87	12.16	12.05	13.29	87
PEG 4000	05 02 87	12.17	12.03	13.86	86
PEG 6000	05 02 87	12.11	11.89	7.67	92
eth. glycol	02 02 87	12.36	12.19	92.87	7
eth. glycol	11 02 87	12.99	12.43	93.16	7
glycerol	02 02 87	12.17	12.13	88.68	11
glycerol	08 02 87	12.07	12.01	87.41	13
erythritol	25 01 87	12.31	12.06	80.77	19
erythritol	13 02 87	12.24	12.08	85.96	14
xylitol	25 01 87	12.10	12.00	82.44	18
xylitol	08 02 87	12.11	12.05	85.60	14
sorbitol	08 02 87	12.18	12.05	78.89	21
sorbitol	23 01 87	12.69	12.17	79.13	21
sucrose	13 02 87	12.51	12.28	67.57	32
sucrose	23 01 87	12.25	12.09	65.93	34
raffinose	13 02 87	12.34	12.20	57.94	42
raffinose	23 01 87	12.29	12.00	52.68	47
ethanol	05 02 87	12.35	12.20	93.12	7
ethanol	16 02 87	12.37	12.17	93.42	7
NaCl	16 02 87	12.22	12.15	64.47	36

Experimental data for membrane, Cell67.

Solute	Date of Test	PWP (g/hr)	PR (g/hr)	$\left(\frac{C_{A3}}{C_{A1}}\right)_{expt}$ x 10^2	Solute Separation (%)
PEG 200	06 02 87	17.20	16.99	68.29	32
PEG 200	26 01 87	17.34	17.00	66.42	34
PEG 300	06 02 87	17.34	17.07	55.63	44
PEG 300	29 01 87	17.87	17.33	62.46	38
PEG 400	06 02 87	17.35	17.08	53.43	47
PEG 400	26 01 87	17.73	16.89	54.14	46
PEG 600	11 02 87	17.05	16.95	43.80	56
PEG 600	29 01 87	18.16	17.19	45.89	54
PEG 1000	11 02 87	16.93	16.84	31.11	69
PEG 1000	26 01 87	17.69	17.02	27.86	72
PEG 2000	25 01 87	17.30	16.84	10.89	89
PEG 2000	29 01 87	16.97	17.06	14.77	85
PEG 3000	02 02 87	17.07	17.44	8.53	91
PEG 4000	05 02 87	17.25	16.95	7.60	92
PEG 6000	05 02 87	17.07	16.72	3.28	97
eth. glycol	02 02 87	17.62	17.02	93.99	6
eth. glycol	11 02 87	17.37	17.05	87.84	12
glycerol	02 02 87	17.89	17.22	82.91	17
glycerol	08 02 87	16.98	16.77	81.34	19
erythritol	25 01 87	18.50	17.31	76.90	23
erythritol	13 02 87	16.81	16.60	81.51	18
xylitol	25 01 87	17.54	17.16	80.24	20
xylitol	08 02 87	17.13	16.74	83.54	16
sorbitol	08 02 87	17.49	16.88	76.29	24
sorbitol	23 01 87	21.15	18.79	78.97	21
sucrose	13 02 87	17.19	16.81	71.22	29
sucrose	23 01 87	19.18	17.92	70.94	29
raffinose	13 02 87	16.88	16.70	62.72	37
raffinose	23 01 87	19.06	17.13	59.43	41
ethanol	05 02 87	17.58	17.18	90.93	9
ethanol	16 02 87	17.08	16.75	88.54	11
NaCl	16 02 87	16.83	16.70	56.66	43

Experimental data for membrane, Cell68.

Solute	Date of Test	PWP (g/hr)	PR (g/hr)	$\left(\frac{C_{A3}}{C_{A1}}\right)_{expt}$ x 10^2	Solute Separation (%)
PEG 200	06 02 87	19.88	19.27	71.26	29
PEG 200	26 01 87	20.14	19.63	68.45	32
PEG 300	06 02 87	19.55	19.00	58.72	41
PEG 300	29 01 87	18.80	18.86	62.37	38
PEG 400	06 02 87	19.03	18.20	52.90	47
PEG 400	26 01 87	19.62	18.67	54.62	45
PEG 600	11 02 87	18.86	18.90	46.92	53
PEG 600	29 01 87	18.43	18.71	45.98	54
PEG 1000	11 02 87	19.50	18.02	30.90	69
PEG 1000	26 01 87	18.53	18.67	28.60	71
PEG 2000	25 01 87	18.00	17.72	10.82	89
PEG 2000	29 01 87	18.06	17.75	12.42	88
PEG 3000	02 02 87	18.85	18.59	11.14	89
PEG 4000	05 02 87	19.36	18.95	12.88	87
PEG 6000	05 02 87	19.91	18.97	13.18	87
eth. glycol	02 02 87	18.96	18.49	90.60	9
eth. glycol	11 02 87	20.03	19.15	90.46	10
glycerol	02 02 87	19.22	18.61	83.25	17
glycerol	08 02 87	18.28	18.05	82.98	17
erythritol	25 01 87	18.32	17.94	81.05	19
erythritol	13 02 87	17.78	17.50	82.10	18
xylitol	25 01 87	18.26	17.65	79.62	20
xylitol	08 02 87	18.48	17.92	83.31	17
sorbitol	08 02 87	19.43	18.80	76.63	23
sorbitol	23 01 87	19.36	18.25	77.26	23
sucrose	13 02 87	18.38	17.96	70.92	29
sucrose	23 01 87	18.02	17.72	67.64	32
raffinose	13 02 87	18.05	17.71	62.60	37
raffinose	23 01 87	18.11	17.64	58.51	41
ethanol	05 02 87	19.15	19.12	90.02	10
ethanol	16 02 87	17.77	17.50	87.45	13
NaCl	16 02 87	17.81	17.33	57.92	42

Experimental data for membrane, Cell69.

Solute	Date of Test	PWP (g/hr)	PR (g/hr)	$\left(\frac{C_{A3}}{C_{A1}}\right)_{expt}$ x 10^2	Solute Separation (%)
PEG 200	06 02 87	22.20	22.00	74.40	26
PEG 200	26 01 87	22.62	22.22	71.47	29
PEG 300	06 02 87	22.01	21.89	62.33	38
PEG 300	29 01 87	22.54	22.19	69.25	31
PEG 400	06 02 87	21.98	21.82	59.82	40
PEG 400	26 01 87	22.21	21.98	61.51	38
PEG 600	11 02 87	22.10	21.92	50.33	50
PEG 600	29 01 87	22.08	21.94	51.53	48
PEG 1000	11 02 87	22.04	21.79	35.23	65
PEG 1000	26 01 87	22.14	21.90	30.09	70
PEG 2000	25 01 87	22.30	21.95	9.87	90
PEG 2000	29 01 87	21.92	21.85	11.05	89
PEG 3000	02 02 87	22.16	22.01	3.34	97
PEG 4000	05 02 87	22.19	22.03	4.23	96
PEG 6000	05 02 87	22.14	21.90	2.32	98
eth. glycol	02 02 87	22.64	22.24	90.96	9
eth. glycol	11 02 87	22.54	22.12	91.44	9
glycerol	02 02 87	22.24	22.06	89.62	10
glycerol	08 02 87	21.84	21.70	84.54	15
erythritol	25 01 87	22.70	22.19	84.49	16
erythritol	13 02 87	21.92	21.65	87.37	13
xylitol	25 01 87	22.25	22.10	84.39	16
xylitol	08 02 87	22.00	21.71	87.03	13
sorbitol	08 02 87	22.20	21.84	80.47	20
sorbitol	23 01 87	22.78	22.31	82.24	18
sucrose	13 02 87	22.22	21.84	76.45	24
sucrose	23 01 87	22.21	22.16	75.81	24
raffinose	13 02 87	21.90	21.74	70.47	30
raffinose	23 01 87	22.49	22.04	67.27	33
ethanol	05 02 87	22.48	22.25	92.21	8
ethanol	16 02 87	22.36	21.91	90.21	10
NaCl	16 02 87	22.06	21.86	58.44	42

Experimental data for membrane, Cell70.

Solute	Date of Test	PWP (g/hr)	PR (g/hr)	$\left(\frac{C_{A3}}{C_{A1}}\right)_{expt}$ x 10^2	Solute Separation (%)
PEG 200	06 02 87	14.71	13.58	68.01	32
PEG 200	26 01 87	13.38	13.35	73.74	26
PEG 300	06 02 87	13.31	13.09	59.67	40
PEG 300	29 01 87	13.32	12.85	61.07	39
PEG 400	06 02 87	13.19	12.53	51.36	49
PEG 400	26 01 87	14.07	12.55	52.17	48
PEG 600	11 02 87	13.80	13.06	43.04	57
PEG 600	29 01 87	13.41	13.01	44.71	55
PEG 1000	11 02 87	12.84	12.[illegible]	27.89	72
PEG 1000	26 01 87	12.77	12.84	24.55	75
PEG 2000	25 01 87	12.33	12.17	8.27	92
PEG 2000	29 01 87	13.21	12.50	11.93	88
PEG 3000	02 02 87	13.16	12.98	9.91	90
PEG 4000	05 02 87	13.64	13.37	12.03	88
PEG 6000	05 02 87	13.18	12.99	10.04	90
eth. glycol	02 02 87	12.99	13.03	90.13	10
eth. glycol	11 02 87	12.75	13.03	90.97	9
glycerol	02 02 87	13.33	12.88	86.00	14
glycerol	08 02 87	12.62	12.25	82.86	17
erythritol	25 01 87	12.57	12.25	80.05	20
erythritol	13 02 87	12.96	12.74	83.11	17
xylitol	25 01 87	12.64	12.17	80.69	19
xylitol	08 02 87	12.89	12.44	80.71	19
sorbitol	08 02 87	12.89	12.34	75.47	25
sorbitol	23 01 87	13.52	12.57	77.00	23
sucrose	13 02 87	13.18	12.88	70.59	29
sucrose	23 01 87	12.82	12.39	68.15	32
raffinose	13 02 87	12.82	12.81	61.74	38
raffinose	23 01 87	12.79	12.17	58.72	41
ethanol	05 02 87	13.18	12.96	86.46	14
ethanol	16 02 87	12.84	12.57	86.06	14
NaCl	16 02 87	12.61	12.60	54.35	46